12-14-2015

The Role of Ovarian Function in the Progression of Cachexia in the $APC^{MIN/+}$ Mouse

Kimbell Louise Hetzler
University of South Carolina - Columbia

THE ROLE OF OVARIAN FUNCTION IN THE PROGRESSION OF CACHEXIA IN THE *APC*$^{Min/+}$ MOUSE

by

Kimbell Louise Hetzler

Bachelor of Science
Clemson University, 2010

Submitted in Partial Fulfillment of the Requirements

For the Degree of Doctor of Philosophy in

Exercise Science

The Norman J. Arnold School of Public Health

University of South Carolina

2015

Accepted by:

James A. Carson, Major Professor

J. Larry Durstine, Committee Member

J. Mark Davis, Committee Member

E. Angela Murphy, Committee Member

Lacy Ford, Senior Vice Provost and Dean of Graduate Studies

ACKNOWLEDGEMENTS

The body of work represented in this dissertation would have been impossible to achieve without the love and support of my fiancé, Brian Bell, and my parents, Dale and Susan Hetzler. I am indebted to them for standing by me through the figurative and literal blood, sweat, and tears over the past five years.

I am also indebted to my advisor, Dr. James Carson, who has guided me through this journey with patience and understanding; and who has pushed me to do work of a higher caliber and quality than I believed possible.

I would also like to thank my dissertation committee: Dr. J. Larry Durstine, Dr. E. Angela Murphy, and Dr. J. Mark Davis. Each has given willingly of their time, effort, and wisdom in order to help guide me through this process.

Aside from these key people, making it to this point in my doctorate career would have been impossible without help from the USC Counseling and Human Development Center, motivation and further counseling from my former swimming coach Pat Murphy, Hi-Caf Teas, Immaculate Consumption's "Motivator™," and the soothing sounds of Pandora's Stevie Nicks Radio.

And of course, the hundreds of mice that have sacrificed their lives and tissues for this work.

ABSTRACT

Cachexia is a devastating a life-threatening condition that occurs secondary to underlying disease including cancer, AIDS, COPD and comprises severe loss of muscle and fat mass. Muscle mass atrophy and wasting with cachexia is especially dire, as skeletal muscle mass is associated with quality of life, functionality, and ability to respond to chemotherapeutics. While much investigation has been done in the male animal to elucidate the inflammatory pathways and muscle signaling underlying cachexia, very little work has occurred in the female. The overall purpose of this study is to determine if ovarian function can alter cachexia progression in the female $Apc^{Min/+}$ mouse through IL-6 signaling and the regulation of skeletal muscle metabolism. Specific aim #1 sought to determine the relationship between circulating IL-6 and cancer cachexia progression in the female $Apc^{Min/+}$ mouse. We found that the canonical IL-6 signaling pathway that is a key point of regulation in the male $Apc^{Min/+}$ is dysregulated in the female, and that IL-6 levels do not correlate with body weight loss and severity as they do in the male. Specific aim #2 sought to determine whether ovarian function loss or dysfunction could influence IL-6 regulation of cancer cachexia progression in the female $Apc^{Min/+}$ mouse. The loss of ovarian function due to disease did cause an increase in Il-6-related and other inflammation, while ovariectomy (OVX) alleviated much of the cachexia-related inflammation. Specific aim #3 sought to determine whether cachexia-induced skeletal muscle metabolic dysfunction is regulated by ovarian function in the female $Apc^{Min/+}$ mouse. As expected, measures of protein degradation and mitochondrial

dysregulation increased with increasing cachexia severity; however, OVX brought these measures back towards baseline. These findings provide insight into the intricate regulation of cachectic pathways by ovarian endocrine function, and will provide potential targets for therapeutics interventions for cancer cachexia.

TABLE OF CONTENTS

LIST OF TABLES

LIST OF FIGURES

LIST OF ABBREVIATIONS

AIDS ..... Acquired Immunodeficiency Syndrome

Apc$^{Min/+}$ ..... *Adenomatous polyposis coli* heterozygote (Multiple intestinal neoplasms)

B6 ..... Black-6 mouse strain

C26 ..... Colon-26 Carcinoma

C57BL/6 ..... Black-6 mouse strain

cDNA ..... Complementary DNA

CMV ..... Cytomegalovirus

COPD ..... Chronic Obstructive Pulmonary Disease

CRP ..... C-reactive protein

DEPC ..... Active Cas

DNA ..... Deoxyriboonucleic Acid

EGFR ..... EGF Receptor

ELISA ..... Enzyme-Linked Immunosorbent Assay

ERK ..... Extracellular Receptor Kinase

FDA ..... Food and Drug Administration

GAPDH ..... Glyceraldehyde-3-phosphate dehydrogenase

Gp130 ..... Glycoprotein-130

Gp80 ..... Glycoprotein-80

IL-6 ..... Interleukin-6

IL-6r ..... IL-6 receptor

JAK ..... Janus Kinase

kDa ..... Kilodaltons

LLC ..... Lewis Lung Carcinoma

mIL-6r ..... Membrane-bound IL-6 receptor

mRNA ..... Messenger RNA

ms ..... Millisecond

n ..... Number (of samples)

NfκB ..... Nuclear factor-kappa B

p ..... Probability

p38 ..... 38-kilodalton protein

PCR ..... Polymerase chain reaction

R^2 ..... Correlation

RNA ..... Ribonucleic Acid

RT-PCR ..... Real-time PCR

SOCS3 ..... Suppressor of Cytokine Signaling-3

STAT3 ..... Signal transducer and activator of transcription-3

TNFα ..... Tumor necrosis factor-alpha

ul ..... Microliters

V ..... Volts

CHAPTER 1

INTRODUCTION

Cachexia is a devastating condition that occurs secondary to several chronic diseases, including AIDS, COPD, chronic renal failure, and many forms of cancer [1]. There is no cure or FDA-approved treatment for cachexia, though it occurs in 30-50% of cancers [1-3] and has an annual mortality rate of 80% [1], underlining the necessity of investigation into its etiology and progression. The most recent definition of cachexia includes an unintentional weight loss of 5% or more secondary to a chronic condition in addition to other symptoms including anemia, fatigue, muscle weakness, increased inflammatory markers and plasma triglycerides, and insulin resistance [1]. Cachexia comprises a severe loss of adipose and skeletal muscle mass, the latter of which has serious implications for quality of life, function, wound healing, and ability to respond to chemotherapeutic treatments. The loss of both lean and fat mass is largely mediated by inflammatory cytokines, including IL-1β, IL-6, and TNFα [2]. The $Apc^{Min/+}$ mouse is an established model of colon cancer and cachexia [4-6] that has been widely used by our lab and others. The mouse has a nonsense mutation in the adenomatous polyposis coli (*Apc*) gene, a tumor suppressor gene [7] which is also mutated in the majority of human colon cancer cases [8] as well as familial adenomatous polyposis (FAP), a congenital disease leading to about 15% of human colorectal cancer cases [9]. *Apc* encodes the APC protein, which regulates cell proliferation via a direct interaction with, and leading to ubiquitin-mediated destruction of, β-catenin, a protein regulating multiple proto-oncogenes [9]. The $Apc^{Min/+}$ mouse develops a large number of intestinal neoplasms beginning at 4 weeks of age and plateauing by 12 weeks, after which cachexia develops over the next several weeks [4, 10].

IL-6 is a pro-inflammatory cytokines closely involved with cancer cachexia progression in many animal models, as well as the human condition [11, 12], including the *Apc*$^{Min/+}$ mouse. Our laboratory has previously shown that overexpression of IL-6 in a male *Apc*$^{Min/+}$ mouse can induce [13] and aggravate [14] cachexia progression; inversely, global IL-6 knockout (KO) in a male *Apc*$^{Min/+}$ alleviates tumor burden and severity of cachexia symptoms [13, 14]. The role of IL-6 during cachexia progression is less clear in the female, however. While our lab has begun to elucidate the differences in IL-6-related signaling that occur during cachexia in the female [15], many gaps remain in our knowledge of the true etiology of cachexia in the female, as well as the exact role of IL-6 in the female. Plasma levels of IL-6 do not correlate with weight loss in the female [15] as they do in the male [13], and overexpression experiments in the female ([15], unpublished data) have shown no abrogation of cachexia severity.

Dysregulation of muscle metabolism leading to muscle wasting with cachexia is regulated by a number of pro-inflammatory and pro-apoptotic factors. Four major pathways exist that are involved in proteolysis due to various wasting conditions [3]; the major pathway at work during cancer cachexia is the ubiquitin-proteasome system (UPS), which is an ATP-dependent mechanism that involves tagging (ubiquitinating) proteins for breakdown by the 26s proteasome [16]. This process is regulated upstream by inflammatory factors including IL-6, STAT3, ERK, and p38 MAPK [17]. Many of the pathways are redundant.

Though cachexia has been well-characterized in the male by our lab and others [4-6, 10, 18-24], almost no research into the condition has taken place in the female. It had long been assumed that the male and female underwent the same pathophysiology

leading to cachexia; however, data from our laboratory has shown differences in the response of the male and female [15]. Though both sexes undergo cachexia, data from our lab has shown that the female loses less body weight than the male, and seems to have a differential response to IL-6 from the male [20]. Cachectic male and female *Apc*$^{Min/+}$ mice have similar plasma IL-6 levels [15]; however, induced overexpression of IL-6 in the male abrogates the cachectic response [5, 6, 20], but has no effect in the female. There is no increase in STAT3 signaling in the female *Apc*$^{Min/+}$ mouse with overexpression of IL-6 [15], indicating a differential regulation of this pathway. Importantly, it has been shown that estrogen, specifically 17β-estradiol, can block transcription of IL-6 [25, 26] and signaling downstream of STAT3 [27]. IL-6 is a major putative regulatory point in the pathophysiology of cancer cachexia as it is increased in most cachexia models [11] and activates several pathways leading to eventual muscle wasting [11, 28].

Ovarian function plays a major role in the health and disease outcomes of females. The role of estrogen, in particular, in the health of both males and females has come into focus in the past decade. Body composition is regulated in part by estrogen signaling, and it has been shown that the ablation of such has a significant deleterious impact on regulation of muscle and fat mass [29-32]; this dysregulation has potentially dire consequences when coupled with the innate dysregulation of cachexia. Estrogen has well-documented benefits against inflammation [33-35], particularly IL-6 [36, 37], that may provide some benefit to the female during the onset and progression of cancer cachexia. In addition, the relatively recent discovery of estrogen receptors α and β in skeletal muscle has led to new insight into estrogen's benefits to skeletal muscle mass

and strength [30, 38, 39]. Specifically, estrogen is necessary for recovery from atrophy [29, 40]. Preliminary data from our lab shows that estrous cycling, which normally occurs in the C57BL/6 mouse until around 14 months of age [41], ceases during the progression of cancer cachexia in the female *Apc*$^{Min/+}$ mouse, which indicates interplay between the ovary and cachexia. Apart from estrogen, the other major ovarian hormone progesterone and its analogs show potential for cachexia therapeutics; progestins including megestrol acetate (MA) and medroxyprogesterone acetate (MPA) have been shown to improve caloric intake and and anorexia symptoms in cachexia patients [3]. IL-6 plays a role in the normal cyclic signaling of the ovary [42], but its dysregulation is also linked to ovarian pathology [42, 43]. This supports the hypothesis that there is interplay between ovarian function and IL-6. This, together with the gaps in understanding of the mechanisms underlying cachexia-related muscle wasting in the female provides the rationale for this study. The novelty of this study arises from it being, to our knowledge, the first study to specifically look at mechanisms of cachexia in the female *Apc*$^{Min/+}$ mouse, as well as the first study to investigate a potential role of ovarian endocrine function.

Purpose & Specific Aims

The *overall goal* of this proposal is to determine if ovarian function can alter cachexia progression in the female *Apc*$^{Min/+}$ mouse through IL-6 signaling and the regulation of skeletal muscle metabolism. The *central hypothesis* of the proposed study is that loss of ovarian function in the female *Apc*$^{Min/+}$ mouse causes abrogated progression of cachexia through altered IL-6 sensitivity, which increases skeletal muscle metabolic dysfunction and leads to increased skeletal muscle loss. Outcomes related to the specific aims of the

study include body composition, in vivo functional capacity, abnormal blood biochemistry, tissue IL-6 signaling, and disrupted skeletal muscle metabolism.

In order to prove the proposed study's overall hypothesis three specific aims are proposed.

Specific Aim #1 will determine the relationship between of circulating IL-6 to cancer cachexia progression in the female *Apc*$^{Min/+}$ mouse (revised 4/23/15)

Specific Aim #2 will determine if IL-6 regulation of cachexia progression is regulated by ovarian function in the female *Apc*$^{Min/+}$ mouse.

Specific Aim #3 will determine whether cachexia-induced skeletal muscle metabolic dysfunction is regulated by ovarian function in the female *Apc*$^{Min/+}$ mouse.

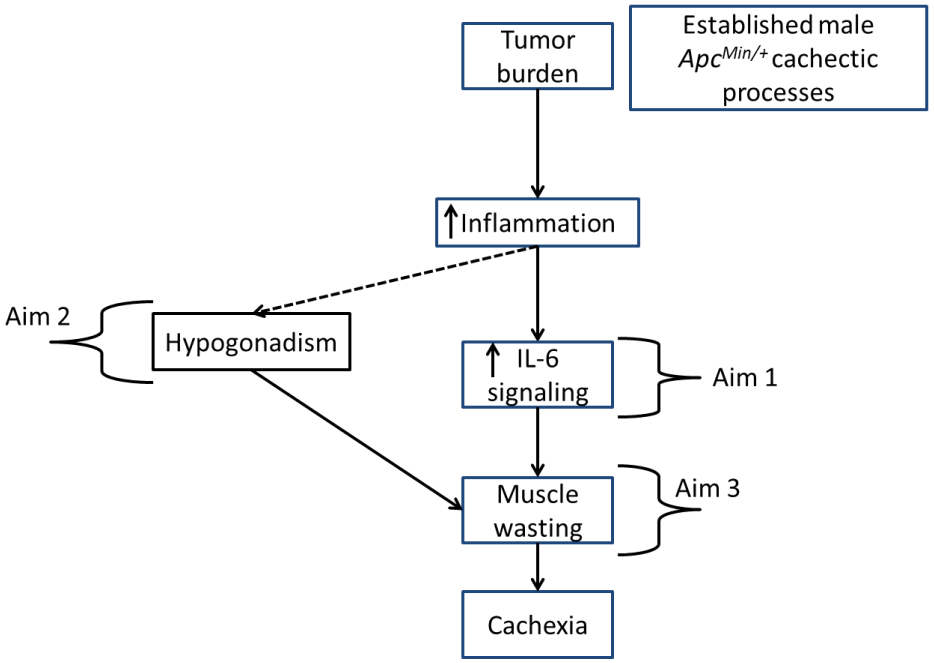

Figure 1.1 Overall Working Model**:** Working model of the focus of each of the three specific aims. First, the proposal will examine sex differences in the role of IL-6 signaling during cancer cachexia progression in *Apc*$^{Min/+}$ mice (AIM 1). Second, the proposal will examine the role of loss of ovarian function (or ovariectomy) and its effect on inflammatory signaling during cancer cachexia progression in the female *Apc*$^{Min/+}$ mouse. Hypogonadism has an established role in cachexia progression of the male *Apc*$^{Min/+}$ mouse, but has not been investigated in the female (AIM 2). Finally, this proposal will

examine the effect of cachexia severity and ovarian function on muscle metabolic dysregulation during cachexia in the female *Apc*$^{Min/+}$ mouse (AIM 3). Dysregulation of muscle signaling has been closely examined in the male *Apc*$^{Min/+}$ mouse but has not been elucidated in the female.

CHAPTER 2

REVIEW OF LITERATURE

2.1 Colon Cancer

Colorectal cancer is one of the leading forms of cancer in both men and women [7]. The *adenomatous polyposis coli* (*Apc*) gene is a tumor suppressor gene that accounts for one of the highest rates of loss-of-function in human colon cancer [7]. The *Apc* gene lies on 5q21 and includes 15 exons; the translated protein is fairly large at 309 kilodaltons [9]. Some studies have shown that obesity affects men's risk of colon cancer more so than women's; other studies have shown no effect [44]. Sporadic colon cancer accounts for 85% of cases, whereas familial adenomatous polyposis accounts for the other 15% [9]. This syndrome causes the development of thousands of intestinal and rectal adenomas in the second decade of life and is due to a germline mutation of the *Apc* gene [9]. In fact, most colon cancers involve loss-of-function mutations in *Apc* [8]. Cancer cachexia frequently occurs secondary to colon cancer and accounts for 30-50% of deaths due to gastrointestinal cancers [45]. In cancer it is unclear whether cytokines are produced by tumor cells or inflammatory cells in response to tumor burden [3].

2.2 Cancer cachexia

Cachexia develops secondary to many chronic disease, including AIDS, COPD, chronic renal disease, and cancer [1]. Gastrointestinal cancer patients are particularly susceptible to cancer cachexia [20]. Estimates of prevalence in cancer patients range from 28-57% [1, 2], with an annual mortality rate of 80% [1] and contributing to 20% of cancer-related deaths [2, 4]. This translates to over two million cancer-related cachexia deaths per year [1]. The most recent definition of cachexia includes an unintentional weight loss, secondary to underlying disease, of greater than 5% in 12 months, as well as additional

symptoms including anemia, fatigue, anorexia, decreased muscle strength, and increased inflammatory markers [1]. During experimental cachexia, fat stores are mobilized prior to muscle catabolism [2]. With some cancers, patients show high levels of TNFα, IL-1β, and IL-6, which roughly correlate with tumor progression [3]. Antibodies against each of these factors have been used with some success, but none has completely attenuated cachexia progression [3]. IL-6 is an important mediator of cachexia [20].

Cachexia is essentially an inflammatory process. Several inflammatory cytokines are known to play roles in the etiology and progression of cachexia. TNFα leads to extensive apoptosis of skeletal muscle cells during cachexia [2]. IL-1β and IL-6 promote TNFα-mediated cachexia, which then leads to an increase in FoxO1 signaling [3] as well as NfκB signaling through TNFR1[2]. IL-1β and IL-6 also contribute to the loss of lean body mass during cachexia [46]. Inactive NfκB is suppressed by the IKB family of proteins; when stimulated by TNFα, the IKB kinase complex (IKK) degrades IKB, which releases and thereby activates NfκB [2]. NfκB plays a major role in the upregulation of inflammation during cachexia [3]. Toll-like receptors (TLRs) are pathogen-recognizing receptors present on immune cells, tumor cells, and muscle cells that play a role not only in pathogen-related inflammation, but cachexia-related inflammation as well [46]. TLR2 and TLR4 are expressed in skeletal muscle and lead to further increases of cytokine production (including IL-1β, IL-6, and TNFα) when stimulated [46]. The transforming growth factor (TGF) family of proteins is yet another inflammatory system capable of regulating cachexia-induced muscle wasting; TGFβ is the major player, signaling through SMAD 2/3 and leading to increased lean mass loss through proteolysis [47].

2.3 *Apc*$^{Min/+}$ mouse model

The *Apc*$^{Min/+}$ mouse has a nonsense mutation in codon 850 of the *Adenomatous polyposis coli* gene, (*Apc*) causing it to spontaneously develop colon polyps [4]. This model is especially relevant, as the *Apc* gene is mutated in the majority of human colorectal cancers [9]. *Apc* is a tumor-suppressor gene that regulates cell proliferation through physical interaction with β-catenin, which leads to the ubiquitination and proteasomal degradation of β-catenin [9]. When *Apc* heterozygosity and expression is lost, activation of β-catenin by Wnt signaling is increased, leading to increased transcription of β-catenin target genes including several proto-oncogenes [9]. Min/+ mice lose heterozygosity of *Apc* in some cells, which leads to overexpression of β-catenin and eventually causes tumors [24]. Min/+ mice generally have tumors in the small intestine and not the colon, unlike humans; however, the loss of both *Apc* and estrogen receptor beta (ERβ) in tumor cells make it a good model for the human disease [24]. Polyp number plateaus by 12 weeks of age, but tumor size continues to increase as cachexia develops, up to 20 weeks of age [4].

2.4 Cachexia and Skeletal Muscle

Hypermetabolism due to cancer cachexia results in accelerated breakdown of adipose tissue and skeletal muscle in order to provide energy substrates to the tumor and host organism [16]. Skeletal muscle atrophy due to cachexia can lead to disability, weakness, lessened wound healing, and decreased response to chemotherapeutic agents [16].

Skeletal muscle is highly affected by cancer cachexia, though all fiber types do not undergo wasting uniformly [16, 20]. Fast-twitch (type II) muscle fibers are more susceptible to wasting with cancer cachexia than slow-twitch (type I) fibers, as the oxidative phenotype is protective against cachexia [2, 20]. Initiation of muscle mass loss with cachexia occurs as myonuclei undergo caspase-3-mediated apoptosis, decreasing the size of the myonuclear domain [2]. Additionally, dysregulated protein synthesis and myofiber regeneration [48], in addition to increased protein degradation, contribute to net muscle wasting with cachexia.

There are four major proteolytic pathways involved in the loss of skeletal muscle mass during cancer cachexia: Calcium-dependent (calpain/calpastatin-dependent), lysosomal, caspase-dependent, and ubiquitin/proteasome [2, 3]. The calpain and calpastatin proteolytic systems disrupt myofibrillar proteins and lead to eventual ubiquitination and proteasomal degradation of such [2]. Lysosomal proteases play only a small role in cachexia [2]. The ubiquitin/proteasome pathway is the major proteolytic player during cachexia [16], and is regulated by FoxO3 [3]. The other major proteolytic system involved in cachexia-related muscle wasting is autophagy; this mechanism is also regulated largely by FoxO3 [17]. FoxO3 is generally phosphorylated, and therefore inactivated and excluded from the nucleus of the cell, by PI3K/Akt [3]. When activated, FoxO3 translocates to the nucleus, where it acts as a transcription factors for skeletal muscle-specific E3 ligases including muscle ring finger (MuRF)1 and atrogin-1/MAFbx [3], which are highly activated with cachexia [16]. Upstream of PI3K/Akt, the pathway is regulated by reactive oxygen species (ROS), TNFα, PGC1α, and IGF-1[3]. Independent of FoxO3, UPS signaling can also be induced by oxidative stress and p38

MAPK signaling [17]. The UPS is an ATP-dependent process, and can therefore contribute to lower efficiency and further dysregulation of mitochondrial energy synthesis [16].

In recent years, it has become apparent that mitochondrial dysfunction plays a major role in the etiology of cachexia and directly leads to many of the metabolic abnormalities and overall atrophy of skeletal muscle due to cachexia. Indeed, it is thought that mitochondria are the site of energy waste in skeletal muscle that leads to the degradation of protein and overall wasting [49]. Oxygen consumption in mitochondria isolated from cachectic muscle is lower than in healthy mitochondria [16]. Initial cachexia does not affect mitochondrial content, though PGC1α and Mfn1, mitochondrial proteins, are decreased at this stage [50]. As cachexia progresses, these changes become more apparent and mitochondrial content decreases [50]. Cytochrome C oxidase (COX) IV protein levels [14] and activity decrease with cachexia; the latter of which is correlated with decreased oxygen consumption in mitochondria [16]. Higher levels of uncoupling protein-3 (UCP3) have been noted in wasting muscle cells [49]. It has been proposed that this decrease in mitochondrial content leads to an increase in reactive oxygen species (ROS), which leads to an increase in oxidative stress, energy stress, and apoptosis susceptibility leading to AMPK and FoxO1 activation [50]. However, *Apc* $^{min/+}$ mice show these metabolic changes independent of oxidative stress [50].

2.5 Role of IL-6 in tumorigenesis and cachexia

Interleukin-6 (IL-6) is a pro-inflammatory cytokine secreted by many types of immune cells [51]; this process is mediated by IL-1β, TNFα, and interferons [52]. Chronically

elevated IL-6 is associated with many pathophysiological conditions including cachexia and insulin resistance [51]. IL-6 suppresses insulin signal transduction via SOCS1 [2]. In humans, IL-6 and c-reactive protein (CRP) plasma levels correlate with insulin resistance [53]. IL-6 has further been shown to inhibit hepatic insulin signaling *in vitro* and *in vivo*, though it does not affect insulin receptor signal transduction in skeletal muscle [53].

Classic IL-6 signaling involves IL-6 binding to its membrane-bound receptor comprising IL6Rα, the ligand-binding domain, and gp130, the signal-transducing domain [54, 55]. The membrane-bound IL-6 receptor has limited tissue expression, including hepatocytes, immune cells, and skeletal muscle cells [55]. The alternative signaling paradigm is known as *trans* IL-6 signaling, and is thought to be responsible for many of the pro-inflammatory effects of IL-6 during cancer cachexia [56]. Inflammatory responses are largely mediated by endothelial cells, which lack mIL-6r and therefore rely on trans signaling [56]. *Trans* IL-6 signaling involves binding of the soluble IL-6 receptor-IL-6 complex to the ubiquitously-expressed gp130 receptor [55], allowing for IL-6 signaling in nontraditional tissues. Soluble IL-6 receptor (sIL6r) is found in many body fluids. Structurally identical to membrane-bound IL-6r and with the same affinity for IL-6 as the membrane-bound receptor [56], it can be formed by alternative mRNA splicing of the IL-6r gene (*IL6ra*) (10% of sIL-6r protein), or by shedding of the membrane-bound protein by metalloproteinase ADAM17 (90%) [52]. The cleaved protein can then dimerize and bind IL-6 in circulation, thereby increasing its half-life [57]. This complex formed can then bind to gp130 which is ubiquitously expressed on cell membranes, thereby allowing IL-6 signaling to occur in tissues where it normally

would not [42]. Cancer patients have higher levels of plasma sIL-6r compared with healthy controls [56].

Activation of the membrane-bound IL-6 receptor or gp130 receptor activates signal transducer and activator of transcription 3 (STAT3), which causes many of IL-6's downstream deleterious effects [27]. Further, STAT3 is essential for gp130-mediated cell survival, cell cycle phase transition, cell movement, and cell differentiation [58]. Suppressor of cytokine signaling-3 (SOCS3) is the major negative regulator of STAT3, and exerts its effects on STAT3 signaling by binding simultaneously to gp130, JAK1, and JAK2 on the gp130/IL-6r/JAK/STAT3 complex [59]. SOCS3 can thereby inhibit IL-6-induced STAT3 signaling and further aggravation of this pro-inflammatory pathway. However, when the epidermal growth factor (EGF) receptor (EGFR) is active and present, STAT3 can be re-phosphorylated by a second influx of IL-6 despite the continued presence of SOCS3 [59]. In muscle, IL-6 can also act as a mitogen, activating satellite cell and myocyte proliferation [51]. In addition to the STAT3 pathway, IL-6 can activate AMPK, p38 MAPK, and NfκB signaling [11, 60]. Muscle contraction, functional overload, and recovery from disuse all increase IL-6 secretion from muscle [51]. When IL-6 is knocked out in mice, IGF-1 signaling decreases 80% [51].

Cells secrete proteins, a process known as "shedding," by releasing extracellular vesicles [61]. Cancer cells shed more proteins, including IL-6, than normal cells, thus providing a means by which tumors secrete IL-6 [61]. IL-6 causes high levels of hepatocellular proliferation, eventually to hepatocellular carcinoma (HCC), the most common form of liver cancer [25]. Experimental ablation of IL-6 in mice abolished sex differences in occurrence of this cancer [25].

Phosphorylated (activated) STAT3 is higher in 22-week old male *Apc*$^{Min/+}$ mice than in 13-week old mice, indicating that IL-6 signaling is involved in the development of cachexia [20]. *Fbxo32* (Atrogin-1) mRNA and protein are also increased by 18-22 weeks of age in male mice, and correlate with the decrease seen in gastrocnemius muscle weight [20]. When IL-6 was overexpressed in male *Apc*$^{Min/+}$ mice for two weeks, the cross-sectional area of type IIB muscle fibers decreased by 11% in the gastrocnemius muscle, indicating that IL-6 is involved in the skeletal muscle wasting seen with cachexia in the male [20]. However, overexpression of IL-6 in wildtype mice did not have the same effect, indicating the IL-6 is not sufficient to induce muscle wasting [20]. Conversely, administration of an IL-6 receptor antibody (IL-6ra) to cachectic *Apc*$^{Min/+}$ mice attenuated further cachexia progression as well as loss of mitochondria and changes in mitochondrial dynamics [50].

2.6 Sex differences with Cancer and Cachexia

Sex differences have been noted with muscle mass and strength in cancer and other forms of cachexia [62-64]; however, the vast majority of mechanistic work in cancer cachexia has been performed in the male. In healthy mice, there are no differences in intermuscular amino acid kinetics. In the postabsorptive state, however, there are significant differences in amino acid turnover between the sexes. Additionally, men have a higher overall protein turnover rate than women, which also may play a factor in the sex differences seen in cachexia. Interestingly, differences between the sexes in cachexia have been seen on the molecular level as well. After 14 days of synergist ablation in male and female (Atrogin-1) MAFbx-KO rats, male rats were able to induce muscle hypertrophy, while females were not [65]. This points to the possibility that many

classical cachectic pathways are differentially regulated by the sexes. Interestingly, our lab has shown that hypogonadism play a major role in the etiology of cachexia progression in the male [66], however, it is unknown if a similar effect happens in females. Leptin is a molecule that reports the organism's overall energy status to the brain, Leptin levels are lower in cachectic cancer patients than in healthy controls [67]; interestingly, women's leptin levels tend to be higher than men's when matched for body fat [68]. Sex differences have long been seen in immune function; men generally have lower immune responses than women do to a stimulus [69]. Men also have naturally higher plasma levels of proinflammatory cytokines including TNFα and IL-6, two key cytokines involved in the progression of cachexia. Hepatocellular carcinoma (HCC) is the most common liver cancer; however, it occurs three to five times more often in men than in women [25]. This cancer is caused by high levels of IL-6, which are abolished in women by circulating estrogen [25]. Interestingly, several single-nucleotide polymorphisms (SNPs) along the IL-6 gene promoter that affect outcome in IL-6-related conditions have sex-related differences in frequency [70].

2.7 Ovarian Function

The ovary comprises oocytes in various stages of maturity, surrounded by granulosa and theca cells, which produce estrogen and progesterone, respectively, among other secreted hormones and cytokines. These functional units of the ovary are known as follicles [71].

The hypothalamic-pituitary-gonadal (HPG) axis is similar across all animals, and almost all mammals have similarities between their ovarian function [72]. Ovarian

function in rodents can be monitored outwardly via the estrus cycle [73]. The estrus cycle lasts 4-5 days and consists of four stages based on relative estrogen levels and cell population present. Stages include diestrus, in which estrogen levels are lowest; proestrus, featuring rising estrogen levels; estrus, during which estrogen levels are highest and ovulation occurs, and metestrus, during which estrogen levels fall [73]. The cycle is very regular and is not disrupted by stresses commonly found in animal facility settings [73]. Similar to humans, the estrogen spike is caused by a surge in LH and FSH. At the antral (early) stage of follicle development, the majority of follicles undergo atresia and die, unless they are stimulated to be ovulated [74]. Antral follicles produce Anti-Müllerian hormone (AMH), which is used as a marker of ovarian reserve [71]. As woman approach menopuase, FSH levels rise as inhibin, a negative feedback molecule, levels decrease [72]. At the time of menopause, Inhibins A, B, and C each decrease before there is a noticeable decrease in estrogen levels. Eventually, there are very low levels of estrogen, progesterone, and AMH, and ovulation stops [72].

Ovariectomized mice have increased body fat, which can be reversed by estrogen replacement [32]. Along with higher body fat, ovariectomized mice have higher blood glucose, higher insulin, a higher insulin resistance index, higher cholesterol, and higher TNFα levels [32]. Before menopause, the incidence of type II diabetes is lower in women than in men. After menopause, insulin sensitivity decreases, coinciding with a rise in inflammatory factors and a decrease in proper glucose metabolism [75]. Kidneys of ovariectomized mice show decreases in estrogens receptors α and β, as well as adiponectin; as the kidney is estrogen-sensitive, this indicates a shift in proper kidney function with ovariectomy [32].

OVX mice also have lower levels of energy expenditure and higher levels of energy intake [76]. These animals also have a chronically activated inflammatory response in adipose tissue [76]; this suggests that ovarian hormones ate involved in the modulation of inflammation.

Estrogen is an ovarian steroid hormone that typically works through a genomic pathway; that is, it binds to estrogen-response elements (EREs) on promoter sequences of target genes to activate transcription [77]. However, the estrogen/receptor complex can also work nongenomically by directly activating targets such as phosphatidylinositol-3-kinase (PI3K) and mitogen-activated protein kinase (MAPK), which have roles in cell proliferation, protection against oxidative stress, and survival [77-80]. This is the mechanism by which estrogen conveys its osteoporosis-preventing effects in osteocytes, degeneration-preventing effects in neurons, and protective effects in many other cell types [77, 79-81]. Estrogen prevents apoptosis in many cells types by upregulating Bcl-2, an anti-apoptotic mitochondrial protein, and by activating PI3K [81, 82]. Women have improved outcomes after ischemia/reperfusion injury to cardiomyocytes, largely due to estrogen's effects in the cardiovascular system; specifically, estrogen activates the PI3K/Akt pathway in cardiomyocytes, leading to less inflammation, oxidative stress and apoptosis than men [33, 83].

Estrogen has significant effects on metabolism. In a healthy animal muscle cell, insulin signals for upregulation of GLUT4 at the cell membrane through the PI3K pathway [38]. Estrogen receptor α-knockout mice have very reduced GLUT4 signaling, indicating that estrogen is an important modulator of insulin sensitivity [38]. The kidney is estrogen-sensitive; estrogen deficiency causes improper handling of energy substrates

by the kidney, leading to metabolic imbalances [32]. In fact, estrogen receptor α-knockout mice show many of the symptoms of the metabolic syndrome, including glucose intolerance, insulin resistance, and adiposity [32]. It has been shown that overexpression of estrogen sulfotransferase (EST), an enzyme responsible for the deactivation of estrogens, causes inhibitions of insulin signaling, indicating that a certain level of active estrogen is necessary to maintain proper insulin signaling [31]. Estrogen receptor β activation has been shown to increase PGC-1, thereby modulating lipid metabolism [31]. Estrogen receptors α and β have further been implicated in the maintenance of body composition. Experimentally, estrogen receptor α has been shown to increase hormone-sensitive lipase (HSL) in adipose tissue, which causes conversion of triglycerides to free fatty acids, and increases AMPK expression in skeletal muscle [31]. Estrogen receptor β has been shown to keep body weight stable in high fat diet (HFD)-fed mice [31]. Because it plays such a major role in glucose and lipid metabolism, estrogen receptor β has become a target of great potential for metabolic disease [31].

Estrogen's effects in skeletal muscle are not well-studied, though estrogen receptors α and β are both present [84]. It is thought that many of estrogen's beneficial effects in skeletal muscle are due to its antioxidant capacity and anti-inflammatory properties. It has been hypothesized that estrogen stabilizes the cell membrane, protecting muscle cells from damage [84]. Though more study is needed, it has been shown in various animal muscle atrophy models that estrogen is necessary for recovery of muscle size and fiber cross-sectional area [40, 84]. Estrogen receptor α-knockout mice have lower contractile strength than wildtype mice, indicating that estrogen has important estrogen receptor α-mediated effects on muscular strength [84]. Additionally,

perimenopause in women is associated with a decrease in muscle mass and strength, though hormone replacement therapy (HRT) has been shown to increase both variables [85].

Exposing skeletal muscle cells to estrogen before damaging stimuli protects them from apoptosis, as has been seen in many other cell types [86]. Estrogen regulates myoblast proliferation and differentiation [86]. In skeletal muscle, estrogen increases PPARδ and FoxO1, both of which are involved in the genesis of type I muscle fibers [87]. Ovariectomized mice showed significant decreases in genes associated with type I muscle fibers including PPARδ, FoxO1, myogenin, myosin light chain, and troponin C, and significant increases in genes associated with type II muscle fibers including MyoD [87]. However, ovariectomized mice also showed decreases in atrogin-1 and MuRF1 expression, which may indicate less muscle wasting [87].

The rate of colon cancer in men is 35% higher than in women [88, 89], and some part of this is due to the beneficial effects of estrogen. In fact, hormone replacement therapy (HRT) is associated with a 30-40% reduction of risk of colorectal cancer [24]. Population studies have shown menopause is associated with obesity and colon cancer [44]. The effects of estrogen on colon epithelium are numerous and lead to overall lower rates of colon cancer. Hormone replacement therapy is associated with a 30-40% reduction in colon cancer risk Estrogen reduces plasma IGF-1, a risk factor for tumor development [90], and increases insulin sensitivity [91]. Insulin and IGF-1 are mitogenic to colon cancer cells, and epidemiologic studies have shown a correlation between colorectal cancer and insulin levels [91]. Interestingly, however, the loss of estrogen in ovariectomized mice has no effect on tumor number [24]; it is possible that it only keeps

colonocytes from transforming into malignancies. [24, 88, 91]. Estrogen reduces growth in colonocytes via ERβ-mediated effects, including higher rates of apoptosis in pre-malignant cells [44, 88]. The first sign of colon tumors are often aberrant crypt foci (ACFs); mice treated with estrogen had fewer ACFs than untreated mice, though this effect is ablated in ERβKO mice [88].

The effects of ERβ on colon epithelium have been well-established. Estrogen can reduce the incidence of chemically-induced polyps in ERαKO mice, but not ERβKO mice, indicating that this receptor mediates the effects [88]. ERβ controls cell cycling in colon epithelium [89-91], and expression is frequently lost in colon tumors [24, 89, 91]. In fact, ERβ expression is inversely related to tumor differentiation in colon epithelium [91]This effect occurs via estrogen responsive element (ERE)-binding dependent transcription, as well as through activator protein 1 (AP1) and SP1 [90]. ERαKO and ERβKO mice have increased colon tumor numbers and abnormal colon histology [24]. It has been found that injecting mice with SW480 (colon cancer) cells as well as an ERβ construct decreases size of tumors compared to mice injected with only SW480 cells [90]. Contrary to the effects of ERβ in colon epithelium, ERα expression has been associated with increased incidence of cancer cell proliferation [44]. This follows with the general functions of the ERs: ERα induces proliferation and ERβ suppresses proliferation [44].

Conversion of androgen into estrogens is favored in pro-inflammatory environments [92]. Bacterial lipopolysaccharide (LPS; endotoxin) induces multiple pro-inflammatory factors including TNFα and NfκB, leading to apoptosis; these are inhibited by Akt-mediated 17β-estradiol and ERα signaling [35]. Endotoxin, interleukins 1 and 6

(IL-1β; IL-6) and tumor necrosis factor alpha (TNFα), all pro-inflammatory inflammatory factors, are able to activate the hypothalamic-pituitary-adrenal (HPA) axis. Estrogen modulates the HPA axis response, but has different modulatory effects on HPA responses to endotoxin and IL-1 [37]. HPA responses to estrogen are attenuated by ovariectomy [37]. Estrogen inhibits NfκB, which activates monocyte chemoattractant protein-1 (MCP1) [26], and along with other co-factors is involved in the transcription of IL-6, thereby blocking pro-inflammatory responses [26]. In fact, estrogen and NfκB have a mutually inhibitory relationship [33].

Many of estrogen's anti-inflammatory properties have been most thoroughly investigated in the context of ischemia-reperfusion (I-R) injury of myocardial cells. Estrogen has been shown to decrease p38 MAPK-mediated inflammation following I-R [33]; this protection is ablated in ovariectomized female rodents. Indeed, OVX was shown to increase phosphorylated p38, IL-1β, IL-6, TNFα, and caspase-3 cleavage in the myocardium [33].

Menopause is associated with an increase in inflammatory factors, including TNFα, IL-6, and plasminogen activator inhibitor-1 (PAI-1) [75], indicating that estrogen regulates levels of these factors in the pre-menopausal state.

2.8 Ovarian Function and IL-6

Granulosa cells of the ovary secrete IL-6 and other cytokines throughout the menstrual or estrous cycle. Granulosa cells present both mIL-6r and gp130 [93]. Increasing amounts of IL-6 inhibit estrogen production by these cells, regardless of the stimulating presence of FSH [93]. During ovulation, rat ovaries produce a large amount

of IL-6 [58, 94]. TGFβ and IL-6 are involved in the post-ovulation healing process of the ovary [95]. In humans, during the follicular phase of the menstrual cycle (during which estrogen is high), IL-6 levels do not change but TNFα levels increase [57]. TNFα levels as well as sIL-6r levels increase during the luteal phase, during which there are low estrogen levels [57]. Across the whole menstrual cycle, women have higher TNFα and sIL-6r plasma levels than males [57]. Levels of IL-6 mRNA are increased in ovarian epithelial cells and cancer cells that have been stimulated with luteinizing hormone (LH) and follicle-stimulating hormone (FSH) [58]. Gonadotropins including LH and FSH have been shown to be more potent than sex steroids at stimulating IL-6 production [58].

Circulating IL-6 increases after menopause [92]. IL-6 levels have been shown to increase in younger women who undergo oophorectomy, but this is abolished by hormone replacement therapy [92]. Additionally, the hypogonadism seen with menopause is associated with increased plasma levels of IL-6, and more negative outcomes associated with IL-6 [85]. Hormone replacement therapy after menopause is associated with increases in ovarian cancer rates [58]. Interestingly, postmenopausal women have increased plasma levels of soluble gp130 and soluble IL-6 receptor [85]. IL-6 has been implicated in the pathogenesis of polycystic ovarian syndrome (PCOS) [42]. Women with PCOS had higher serum gp130 concentrations than women without PCOS; women with PCOS have significantly lower sIL6r concentrations than women without, indicating that IL-6 signaling is occurring via a different mechanism in this syndrome [42]. Serum gp130 is related to SHBG levels [42].

Elite female gymnasts who had not reached menarche have increased IL-6 and TNFα expression in leukocyte compared to athletes who had reached menarche and therefore

had estrogen levels that were 200% of those athletes who had not yet reached menarche [96].

In intact mice, it has been shown that both androgens and estrogens are able to inhibit IL-6 production [37]. Estrogen directly inhibits IL-6 synthesis and release from bone marrow cells through ERα-mediated gene transcription [37, 58]. Estrogen has been reported to increase IL-6 expression in circulating mononuclear cells, but to inhibit IL-6 synthesis in other cell types including osteoblasts [58]. Estrogen prevents necessary transcription factors, including NfκB, C/EBPβ [25], and p65 [26] from binding to the IL-6 promoter, thereby inhibiting transcription [97]. The estrogen receptor α (ERα) also blocks NfκB from binding to the MCP-1 promoter and blocks TNFα from inducing high levels of MCP-1[26]. Ovariectomized mice show higher plasma IL-6 levels than intact mice, but estrogen replacement attenuates this increase [37]. Further, estrogen upregulates SOCS3 in hepatocytes [25]. Administration of estrogen has been shown to decrease plasma levels of IL-6, IL-1β, and TNFα [85]. In mice given diethylnitrosamine (DEN) to induce hepatocellular carcinoma (HCC), a form of liver cancer, estrogen abolishes IL-6 secretion from hepatic Kupffer cells by inhibiting IKKβ and Myd88, protecting the female from IL-6-induced tumorigenesis [25]. Estrogen can block downstream signaling of STAT3 [27]; further, estrogen can upregulate SOCS3 (a downstream negative inhibition molecule which inhibits STAT3 signaling) in hepatocytes [98]. Administration of estrogen to males and ovariectomized females protected them as well as intact females [25]. It was found that STAT3 was being activated by IL-6 in the males, but not the females, leading to an important finding about the mechanism of estrogen's effect on IL-6 signaling [25].

IL-6 inhibits cilia activity in fallopian tubes; gp130 and IL-6r are also present in fallopian tubes [54]. In the uterus, estrogen can both positively and negatively regulate IL-6 [54]. Interestingly, estrogen induces a time-dependent decrease in IL-6r expression; this can be blocked by inhibiting ERα [54].

In multiple myeloma cells, 17β-estradiol completely abolishes IL-6-inducible cell proliferation and STAT3 DNA binding [27]. Importantly, estrogen does not inhibit STAT3 activation by IL-6; it blocks downstream activity of STAT3 [27].

In breast cancer cells, IL-6 is a key factor in the secretion of estrogen. It strongly synergizes with estrogen to activate aromatase and steroid sulphatase in order to further stimulate production [99]. Further, IL-6 activates transcriptional activity of ERα via estrogen response elements (EREs) [99].

2.9 Ovarian Function and Cancer

Hypogonadism is apparent in 40-90% of male cancer patients [66]. Though this has not yet been proven in females, the hypogonadism seen with menopause negatively affects the metabolism of multiple organ systems including skeletal muscle and the immune system [85]. Sex hormone binding globulin (SHBG) is increased in cancer patients, leaving less unbound (biologically active) hormone available [66]. Progestins, including megestrol acetate (MA) and medroxyprogesterone acetate (MPA), have been shown to decrease anorexia seen with cachexia, and possibly inhibiting IL-6 and TNFα [3]. Unfortunately, it is very difficult to study the role of ovarian function with cancer, as most chemotherapeutic agents ablate ovarian function, making most women who undergo cancer treatment sterile [100]. A great number of childhood cancer survivors live to

adulthood; however, women tend to have fewer primordial and antral (growing, healthy) follicles in their ovaries than age-matched controls, generally due to the ionizing effects of radiation or chemotherapy [101].

2.10 Ovarian Function and Skeletal Muscle

OVX mice have significant decreases in gene expression of PPARδ, FoxO1, PDK4, and UCP2 in skeletal muscle [87]. PPARδ and FoxO1 affect muscle fiber type; both tend to shift towards type I [87]. In addition, OVX mice have decreased myosin light chain and troponin C proteins, both of which are prevalent in type I fibers [87]. Interestingly, these mice also have more MyoD than sham mice, which drives development of type II fibers [87]. OVX mice also have decreased atrogin-1 and MuRF1 [87], two essential skeletal muscle-specific E3 ligases involved in the degradation of skeletal muscle protein with cancer cachexia. Metabolically, OVX is associated with increased adiposity due to upregulation of genes involved with lipid storage including lipoprotein lipase (LPL), acetyl-CoA carboxylase-1 (ACC-1), fatty acid synthase (FAS), and others; supplementation of estrogen downregulated these genes [102].

Estrogen has multiple mechanisms by which it can enhance skeletal muscle function and quality, including antioxidant properties, stabilizing myofiber membranes by intercalation, and downstream gene expression [103]. After muscle damage or unaccustomed exercise, estrogen plays a role in stimulating muscle repair and regeneration, in part by activating satellite cells [103]. Due to membrane rupture, damaged skeletal muscle cells release creatine kinase (CK) and myoglobin after damage or unaccustomed exercise; though there is a great amount of variability in the release of

CK, women do tend to have lower levels in circulation which is directly attributable to estrogen [103].

In C2C12 mouse myoblast culture, exposing cells to 17β-estradiol before exposure to apoptotic stimuli including hydrogen peroxide (H2O2) protects them from damage [86]. One of the protective mechanisms of estrogen on skeletal muscle is increased expression of heat-shock proteins (HSPs), which control cell homeostasis by acting as protein-folding chaperones and protecting protein structure from physiological stresses [86]. Expression of HSPs 25, 27, 70, and 90 is directly modulated by estrogen [86].

Estrogen causes lower skeletal muscle mass in ovaries-intact mice or estrogen-replete mice compared to OVX mice; this is at least in part attributable to the effects of ubiquitin-specific peptidase 19 (USP19), which is upregulated by estrogen receptor alpha (ERα) and during muscle atrophy [104]. The promoter of USP19 contains estrogen response elements (EREs), to which ERα binds in female mice and male mice given estrogen; this does not occur in OVX female mice or control male mice [104].

2.11 Conclusion

Though much work has been done in the areas of ovarian function, largely including estrogen's roles, in cancer and skeletal muscle, it is clear that many gaps remain in our knowledge. Very little is known of ovarian function's effects on muscle outside of what we have learned from menopausal women or from animal studies of estrogen's direct effects on muscle. Additionally, beyond estrogen's effects in cancer, there is a paucity of research on ovarian function as a whole and how it contributes to cancer formation or

progression. As far as cachexia, there is an embarrassing lack of research regarding the roles of either ovarian function or estrogen in the treatment or role in the etiology of cachexia. Going forward, it is intended that the present studies will fill some of these gaps and begin to fill in the picture of how ovarian function contributes to the etiology and progression of cachexia.

CHAPTER 3

SEX DIFFERENCES IN THE RELATIONSHIP OF IL-6 SIGNALING TO CANCER CACHEXIA PROGRESSION[1]

[1]Hetzler KL, Hardee JP, Puppa MJ, Narsale AA, Sato S, Davis JM, Carson JA. 2015. *Biochimica et Biophysica Acta*1825: 816-25.
Reprinted here with permission of publisher.

3.1 Abstract

A devastating aspect of cancer cachexia is severe loss of muscle and fat mass. Though cachexia occurs in both sexes, it is not well-defined in the female. The *Apc* $^{Min/+}$ mouse is genetically predisposed to develop intestinal tumors; circulating IL-6 is a critical regulator of cancer cachexia in the male *Apc* $^{Min/+}$ mouse. The purpose of this study was to examine the relationship between IL-6 signaling and cachexia progression in the female *Apc* $^{Min/+}$ mouse. Male and female *Apc* $^{Min/+}$ mice were examined during the initiation and progression of cachexia. Another group of females had IL-6 overexpressed between 12-14 weeks or 15-18 weeks of age to determine whether IL-6 could induce cachexia. Cachectic female *Apc* $^{Min/+}$ mice lost body weight, muscle mass, and fat mass; increased muscle IL-6 mRNA expression was associated with these changes, but circulating IL-6 levels were not. Circulating IL-6 levels did not correlate with downstream signaling in muscle in the female. Muscle IL-6r mRNA expression and SOCS3 mRNA expression as well as muscle IL-6r protein and STAT3 phosphorylation increased with severe cachexia in both sexes. Muscle SOCS3 protein increased in cachectic females but decreased in cachectic males. IL-6 overexpression did not affect cachexia progression in female *Apc* $^{Min/+}$ mice. Our results indicate that female *Apc* $^{Min/+}$ mice undergo cachexia progression that is at least initially IL-6-independent. Future studies in the female will need to determine mechanisms underlying regulation of IL-6 response and cachexia induction.

Key Words: IL-6r, STAT3, SOCS3, skeletal muscle, *Apc* $^{Min/+}$

3.2 Introduction

Cachexia is a devastating condition that occurs secondary to several chronic diseases, including AIDS, COPD, chronic renal failure, and many forms of cancer [1]. There is no FDA-approved treatment for cachexia, though it occurs in 30-50% of cancers [1-3] and has an annual mortality rate of 80% [1]; the investigation into its etiology and progression is therefore essential. The most recent definition of cachexia includes an unintentional 5% weight loss over twelve months, comprising the loss of muscle and fat [1]. Other abnormalities associated with cachexia include anemia, fatigue, muscle weakness, increased plasma triglycerides and inflammatory markers, and insulin resistance [1]. There has been considerable improvement in our understanding of the regulation of cancer cachexia progression due to research employing male mouse models [5, 14, 21, 105, 106]. However, there is evidence that sex differences exist in the development of cachexia in rodents [107]. Additionally, sex differences have been observed in the loss of muscle strength associated with cachexia severity in humans [108]. Although there is clear evidence that cachexia occurs in both males and females, the fundamental differences in the pathophysiology due to sex and underlying mechanisms are unknown.

Systemic inflammation related to cancer is thought to be a mediator of cachexia, as several pro-inflammatory pathways are enhanced during the progression of cachexia [109, 110]. Sex hormones can modulate the inflammatory response to a variety of stimuli [33, 37, 111]. Specifically, estrogen is known to inhibit NfκB and tumor necrosis factor α (TNFα) signaling [35, 111], C-reactive protein (CRP)-induced interleukin-6 (IL-6) production [36], and signal transducer and activator of transcription-3 (STAT3) signaling

downstream of IL-6 [27]. In several rodent models of cachexia and some human cancers, IL-6 is associated with the development of muscle wasting and body weight loss [5, 13, 14, 112, 113]. Classical IL-6 signaling involves binding of the cytokine to the membrane-bound IL-6 receptor (mIL-6r) on target tissues, which include hepatocytes, immune cells, and skeletal muscle [42, 55, 114]. mIL-6r is a heterodimer comprising the ligand-specific gp80 unit and the signal-transducing gp130 unit [54]. Activation of mIL-6r induces downstream activation of many signaling pathways, including JAK/STAT, p38, and ERK [11, 55, 115, 116]. Several of these pathways have been implicated in the regulation of muscle mass loss during cancer cachexia [11, 28].

The $Apc^{Min/+}$ mouse is genetically predisposed to develop intestinal tumors and becomes cachectic secondary to the tumor burden [20, 105]. Our lab initially characterized cachexia in retired female $Apc^{Min/+}$ breeders [18]; however, the progression and etiology of cachexia in the female $Apc^{Min/+}$ mouse has not been described. Development of cachexia in the male $Apc^{Min/+}$mouse has an established IL-6 dependence [4-6, 14, 20, 22, 106]. Administration of an IL-6 receptor antibody to cachectic male $Apc^{Min/+}$ mice can attenuate further cachexia progression [106]. When IL-6 is systemically overexpressed in the male, more body weight is lost and cachexia is more severe, indicating a causative role [5, 11, 14]. However, the response of female $Apc^{Min/+}$ mice to IL-6 overexpression has not been examined. Sex differences have been noted in the inflammatory milieu of humans [68, 69] and mice [25, 33] under multiple pathological circumstances. Additionally, estrogen has been shown to inhibit IL-6 transcription and signaling in several tissues [25, 27, 36, 92, 97], which may also lead to sex differences in IL-6 response during cancer cachexia progression. Therefore, the

purpose of the present study was to examine the relationship of circulating IL-6 to cancer cachexia progression in the female *Apc*$^{Min/+}$ mouse. Our hypothesis is that cachexia progression in the female *Apc*$^{Min/+}$ mouse would not be associated with increased circulating IL-6 levels as has been reported in the male. This hypothesis was tested through three experiments. The first experiment followed a cohort of female and male *Apc*$^{Min/+}$ mice to 18 weeks of age, at which point the association between cachexia severity and circulating IL-6 level was determined. In the second experiment, 12-week old female *Apc*$^{Min/+}$ mice had IL-6 systemically overexpressed for two weeks (until 14 weeks of age) to determine if supraphysiological IL-6 levels could induce cachexia as we have previously shown in the male [5, 6, 60]. In the third experiment, 15-week old female *Apc*$^{Min/+}$ mice had IL-6 systemically overexpressed for three weeks (until 18 weeks of age) to determine if supraphysiological IL-6 levels could accelerate cachexia progression as we have previously shown in the male [20].

3.3 Methods

Animals

Female *Apc*$^{Min/+}$mice (N=32), male *Apc*$^{Min/+}$ mice (N=12), female C57BL/6 mice (N=6), and male C57BL/6 mice (N=6) were bred and maintained at the University of South Carolina Animal Resource Facility. *Apc*$^{Min/+}$ mice used were offspring from breeders originally purchased from Jackson Labs (Bar Harbor, ME, USA). Male and female mice were taken during the three-month period from a standing inbred *Apc*$^{Min/+}$ breeding colony. *Apc*$^{Min/+}$ mice used were on a C57BL/6 background. Mice were kept on a 12:12h light/dark cycle beginning at 7:00 AM and were given unrestricted access to standard

rodent chow (Harlan Teklad Rodent Diet, #8604). Mice were weighed weekly. Blood was collected by retro-orbital eye bleed at 12, 14, 16, 18, and 20 weeks for IL-6 analysis. All experiments were approved by the University of South Carolina's Institutional Animal Care and Use Committee.

Procedures

Three experiments were performed. *Experiment 1* examined the progression of cachexia. Female $Apc^{Min/+}$mice (n=18) were sacrificed at 18 weeks of age. Male $Apc^{Min/+}$ mice were sacrificed at 18-20 weeks of age. Female (n=6) and male (n=6) C57BL/6 (B6) were sacrificed at 18 weeks of age as non-cancer controls. Prior to sacrifice, blood was taken for analysis of IL-6 levels. *Experiment 2* examined 2 weeks of IL-6 over-expression in 12 week-old, weight stable female $Apc^{Min/+}$ mice as we have previously completed in the male [60]. Female $Apc^{Min/+}$ mice were electroporated with a control plasmid or with an IL-6 overexpression plasmid (n=4 per group) at 12 weeks and were sacrificed at 14 weeks. Blood was taken at sacrifice (post-treatment) to determine plasma IL-6 levels. Mice from this experiment were not used for any other analysis. *Experiment 3* examined IL-6 over-expression in 15-week-old female $Apc^{Min/+}$ mice corresponding with the initiation of cachexia, a time course we have previously examined in the male [20]. At 15 weeks of age mice were randomly separated into IL-6 over-expression (n=6), control plasmid (N=3), or non-electroporated control (n=3) treatment groups. All female $Apc^{Min/+}$ mice were sacrificed at 18 weeks of age. Blood was taken at sacrifice (post-treatment) for determination of plasma IL-6 levels. No differences were found in body weight (p=0.78) or muscle mass (p=0.36) between control plasmid and non-electroporated mice. Therefore, the control plasmid and non-electroporated

female *Apc*$^{Min/+}$ mice were then pooled for analysis. Additionally, these 6 mice are in the cohort of 18 female *Apc*$^{Min/+}$ mice related to Experiment 1. In all experiments, blood, inguinal fat, hindlimb muscles, and spleen were removed at the time of sacrifice. Hindlimb muscle mass measurements comprise the sum of left soleus, plantaris, gastrocnemius, tibialis anterior, extensor digitalis longus, and quadriceps masses.

IL-6 overexpression by electroporation

In vivo intramuscular electroporation of an IL-6 plasmid was used to increase circulating IL-6 levels in mice as previously described [117]. The right quadriceps muscle was used to synthesize and secrete exogenous IL-6 into circulation from the injected expression plasmid, and was not used for any analyses in the study. The gastrocnemius muscle used in the study was not subjected to electroporation. Briefly, mice were injected with 50 μg of IL-6 plasmid driven by the CMV promoter, or control plasmid (pV1J), into the right quadriceps muscle. Mice were anesthetized with a 2% mixture of isoflurane (IsoSol, VEDCO, St. Joseph, MO, USA) and oxygen (1 L/min). The leg was shaved, and a small incision was made over the quadriceps muscle. Fat was dissected away from the muscle, and the plasmid was injected in a 50 μl volume of sterile phosphate-buffered saline (PBS). A series of eight 50 ms, 100 V pulses was used to promote uptake of the plasmid into myonuclei, and the incision was closed with a wound clip. In Experiment 2, electroporation was performed at 12 weeks and mice were sacrificed at 14 weeks of age. In Experiment 3, electroporation was performed at 15 weeks and mice were sacrificed at 18 weeks of age.

RNA isolation and RT-PCR

RNA isolation, cDNA synthesis, and real-time PCR were performed as previously described [118]. Reagents from Applied Biosystems (Foster City, CA, USA) were used. Briefly, proximal gastrocnemius muscle was homogenized in TRIzol (Life Technologies, Grand Island, NY, USA) and mixed with chloroform, then centrifuged. The RNA phase was removed and washed several times with ethanol in DEPC-treated water. cDNA was synthesized using 1 μg of RNA. RT-PCR was performed on an Applied Biosystems 7300 thermocycler. A Taqman gene expression assay was used to determine IL-6 mRNA expression (Life Technologies). IL-6 receptor (forward, 5'-CTGCCAGTATTCTCAGCAGCTG-3', and reverse, 5'-CCTGTGTGGGGTTCCAGAGGAT-3'); SOCS3 (forward, 5'-TGCAGGAGAGCTGATTCTAC-3', and reverse, 5'-TGACGCTCAACGTGAAGAAG-3'); gp130 and GAPDH primer sequences have been published elsewhere [119].

Western blotting

Western blots were performed as described previously [106, 120]. Briefly, gastrocnemius muscle samples were run on 6-8% acrylamide gels and transferred overnight to PVDF membrane (Thermo Scientific, Waltham, MA, USA). After transfer, Ponceau stains were imaged to verify equal loading. The membrane was blocked for 1 hour in 5% milk-TBS-Tween 20, and incubated with primary antibodies at 1:2000 dilution overnight at 4^0C. After several washes, membranes were incubated with secondary antibodies at 1:2000 dilution for 1 hour. Blots were visualized with WesternBright ECL (BioExpress, Kaysville, UT, USA). SOCS3 antibody was obtained

from Abcam (Cambridge, MA, USA). STAT3, phopho-STAT3 (Y705), anti-mouse IgG, and anti-rabbit IgG antibodies were obtained from Cell Signaling (Danvers, MA, USA).

Grip strength measurement

Grip strength measurements were determined as previously described [5]. Mice underwent 2 sets of 5 grip strength trials. The first mouse was removed from its cage, held firmly by the base of the tail, and allowed to grasp the top of the grate attached to the force gauge (Chatillon, Largo, FL, USA) with its paws. The mouse was firmly pulled down the grate, and grip strength was recorded in Newtons. The mouse completed the 5 trials of the first set and was returned to its cage. Each mouse tested went through the same procedure for its first trial, and mice were cycled through in the same order for the second trial.

Fasting glucose

Mice were fasted for five hours prior to blood glucose measurements. Blood glucose measurements were performed using a handheld glucometer (Bayer CONTOUR®, Whippany, NJ, USA) according to the manufacture's instructions.

IL-6 Enzyme-linked immunosorbent assay

Plasma IL-6 concentrations were determined as previously described [5]. A commercial IL-6 ELISA kit was obtained from Invitrogen (Fredrick, MD, USA) and the manufacturer's protocol was followed. Briefly, blood was centrifuged after sacrifice; plasma was removed and stored at -80°C until analysis. A Costar clear 96-well plate (Corning, NY, USA) was coated with IL-6 capture antibody and allowed to incubate overnight. The next morning, the plate was blocked with assay diluent buffer. The plate was washed; plasma samples and IL-6 standards were diluted with assay diluent buffer

and added in duplicate to the plate. The plate was again washed and sAV-HRP reagent was added to wells. After several washes, TMB substrate was added to wells and color was allowed to develop. The reaction was stopped with sulfuric acid and absorbance was read in a BioRad iMark plate reader (Hercules, CA, USA) at 450 nm.

IL-6R Enzyme-linked immunosorbent assay

Muscle IL-6R protein levels were determined using a DuoSet ELISA kit (R&D Systems, Minneapolis, MN, USA) as previously described [121]. Briefly, gastrocnemius muscle tissue was homogenized in buffer containing 50mM HEPES, 4mM EGTA, 10mM EDTA, 15mM $Na_4P_2O_7$, 100mM β-glycerophosphate, 25mM NaF, 5mM $NaVO_4$, 0.1% Triton-X, and 0.1% protease inhibitor cocktail (Sigma-Aldrich, St. Louis, MO, USA). A Costar 96-well plate (Corning) was coated with IL-6r capture antibody and allowed to incubate overnight. The next morning, the plate was blocked with assay diluent. After washing, IL-6r standards and 50-500 µg protein of samples were added to wells in duplicate. The plate was again washed and detection antibody was added. Another wash was performed and streptavidin-HRP was added to the plate. After a final wash, substrate solution was added to the plate and color was allowed to develop before the addition of stop solution. Absorbance was read at 450 and 570 nm in a BioRad iMark plate reader (BioRad). Standard and sample concentration was determined using a third-order polynomial curve.

Intestinal polyp quantification

Quantification of intestinal polyps was determined as previously described [19]. Briefly, intestinal sections were fixed in formalin at time of sacrifice. At time of analysis,

sections were rinsed in deionized water and dipped briefly in 0.1% methylene blue. Polyps from segment 4 were counted under a dissecting microscope; it has been determined that tumor number in segment 4 is representative of total tumor number [122].

Statistical analysis

All results are reported as means ± SEM. Differences between degrees of cachexia severity were analyzed by one-way ANOVA using Tukey *post hoc* test where appropriate. Differences between sexes and genotypes were determined by two-way ANOVA with Student-Newman-Keuls *post hoc* test where appropriate. Correlations were determined by Pearson's test for correlation. Differences between 12-14 week and 15-18 week IL-6 treatment groups were determined by Student's t-test. Level of significance was set at 0.05.

3.4 Results

Differential cachexia progression in male and female $Apc^{Min/+}$ *mice (Experiment 1)*

Both male and female $Apc^{Min/+}$ mice undergo varying degrees of cachexia; however, efforts to characterize progression have focused overwhelmingly on the male. Our lab has previously described the male [5, 13, 106], but limited data has been presented related to the female response [23]. Both male (n=12) and female (n=18) $Apc^{Min/+}$ mice lost a significant amount of body weight from their peak weight (Figure 1A); however, males lost a greater percentage of body weight than females ($p<0.0001$). $Apc^{Min/+}$ mice generally have the greatest density of tumors in segment 4 of the small intestine, and the number of tumors in this segment correlates with total tumor number

[122]. The number of tumors in male and female *Apc*$^{Min/+}$ mice, though significantly higher than male and female B6 mice ($p<0.0001$), did not differ (Figure 1B), indicating that the differences in body weight loss were not due to tumor burden. Regardless of sex, *Apc*$^{Min/+}$ mice had significantly higher circulating IL-6 levels than B6 mice ($p<0.0001$). Despite the consistency in tumor burden, male *Apc*$^{Min/+}$ mice had higher circulating IL-6 levels than females ($p<0.0001$) (Figure 1C). Both male and female *Apc*$^{Min/+}$ mice had significantly larger spleens than B6 mice of the same sex ($p<0.0001$), indicating a higher level of systemic inflammation (Figure 1D); however, male *Apc*$^{Min/+}$ had larger spleens than females ($p=0.03$).

Progression of cachexia in female Apc$^{Min/+}$ *mice (Experiment 1)*

To determine the changes seen with progression of cachexia in the female *Apc*$^{Min/+}$ mouse, a cohort of 18 week old female *Apc*$^{Min/+}$ mice (n=18) were stratified based on body weight change from peak (Table 1). The cohort was divided based on body weight loss; "Weight Stable" comprises mice with less than 2% body weight loss from peak weight (n=6), "Initial Cachexia" comprises mice with 2-9% body weight loss (n=6), and "Cachexia" comprises mice with greater than 10% body weight loss (n=6). Body weight loss ranged from 0% to -15.8%; ~30% of the mice were classified as "cachectic," with severe body weight loss, fat and muscle mass loss, and decreased muscle strength (Table 1). As expected, body weight change from peak weight was significantly different between all groups (Table 1). Spleen weight did not differ between weight stable and the initiation of cachexia. Cachectic female *Apc*$^{Min/+}$ mice had significantly larger spleens than either of the other groups ($p=0.01$) (Table 1). Segment 4 tumor count did not differ between weight stable and the initiation of cachexia. Cachectic

Apc$^{Min/+}$ mice had significantly more tumors than either of the other groups (p=0.002) (Table 1). This indicates a relationship between tumor burden and cachexia development in the female that has also been reported in the male [105]. Hindlimb muscle mass and inguinal fat mass did not differ between weight stable and initiation of cachexia. Cachectic *Apc*$^{Min/+}$ females had significantly less hindlimb muscle mass and inguinal fat mass than weight stable or the initial cachexia groups (Table 1). Importantly, there were no differences in circulating IL-6 levels between any of the groups (Table 1). Cachectic *Apc*$^{Min/+}$ females had significantly lower voluntary forelimb grip strength than either of the other groups, though this difference was eliminated when normalized to body weight (Table 1).

All female *Apc*$^{Min/+}$ mice continued to gain weight until 16 weeks of age; differences in body weight between groups are only seen after this point (Figure 2A; p=0.016). Across all female *Apc*$^{Min/+}$ mice, there was a significant relationship between hindlimb muscle mass and body weight loss (Figure 2B; p<0.0001, R^2=0.64). Inguinal fat mass demonstrated a curvilinear relationship (p=0.0002, R^2=0.58) with body weight loss, with fat mass having the most direct relationship with body loss during the initiation of cachexia (Figure 2C). Taken together, this indicates that during the progression of cachexia in the female *Apc*$^{Min/+}$ mouse the loss of inguinal fat mass occurs early, while muscle mass loss demonstrates a consistent decline over time.

Muscle IL-6 signaling-associated mRNA expression in male and female Apc$^{Min/+}$ *mice (Experiment 1)*

The levels of circulating IL-6 in female *Apc*$^{Min/+}$ mice were not associated with body weight loss, hindlimb muscle mass, or inguinal fat mass (Table 2). However,

muscle mRNA expression of IL-6 was significantly correlated with both body weight loss and hindlimb muscle mass (Table 2). There was a main effect of cachexia independent of sex to increase muscle IL-6 receptor mRNA expression (p=0.043; Figure 3A). In female *Apc*$^{Min/+}$ mice, muscle IL-6 receptor mRNA expression was significantly correlated with muscle gp130 mRNA and SOCS3 mRNA expression (Table 2). Neither sex nor cachexia had a significant effect on muscle gp130 mRNA expression (Figure 3B). Although gp130 mRNA expression was not associated with body weight loss in female *Apc*$^{Min/+}$ mice, it was significantly associated with muscle SOCS3 mRNA expression (Table 2). Cachexia increased muscle SOCS3 mRNA expression independent of sex (p=0.01; Figure 3C). However, muscle SOCS3 mRNA expression was not correlated with body weight loss in female *Apc*$^{Min/+}$ mice (Table 2).

Muscle IL-6 signaling-associated protein expression in male and female Apc$^{Min/+}$ *mice (Experiment 1)*

Muscle IL-6 receptor protein expression was examined in gastrocnemius muscle of male and female B6 and *Apc*$^{Min/+}$ mice. Interestingly, male B6 mice have significantly higher levels of muscle IL-6r than female B6 mice (Figure 4A; p=0.006). In female *Apc*$^{Min/+}$ mice, muscle IL-6r increases with cachexia severity (Figure 4B; p=0.002); however, cachectic male Apc$^{Min/+}$ mice have significantly higher expression than cachectic females (Figure 4B; p=0.02).

Muscle STAT3 phosphorylation was examined during the progression of cachexia in female *Apc*$^{Min/+}$ mice (Figure 4C). Muscle STAT3 phosphorylation (Y705) was normalized to female B6 levels of phosphorylation. Total STAT3 muscle expression did

not change with the progression of cachexia (B6: 1 ± 0.05; Weight stable: 1.03 ± 0.03; Cachexia: 1.02 ± 0.07). Muscle STAT3 phosphorylation was significantly different across groups (p=0.010). Muscle STAT3 phosphorylation significantly increased in cachectic muscle when compared to the initially cachectic female *Apc*$^{Min/+}$ mice (p=0.049). The induction of STAT3 phosphorylation had a strong trend towards correlation with body weight loss in female *Apc*$^{Min/+}$ mice, but there was no association with circulating IL-6 levels (Table 2). There was no difference in muscle STAT3 phosphorylation between female and male cachectic muscle (Figure 4C). These results demonstrate that muscle STAT3 phosphorylation is not related to circulating IL-6 level during the progression of cachexia in female *Apc*$^{Min/+}$ mice.

SOCS3 protein expression was examined in muscle of male and female B6 and cachectic *Apc*$^{Min/+}$ mice. As with the IL-6 receptor, male B6 mice had significantly higher levels of SOCS3 protein than female B6 mice (Figure 4D; p=0.015). However, cachexia had differential effects on SOCS3 protein expression between the sexes. SOCS3 protein expression was significantly higher in female *Apc*$^{Min/+}$ mice than female B6 (Figure 4D; p=0.03); however, there was a strong trend towards a decrease in SOCS3 protein with cachexia in the male versus the B6 male (Figure 4D; p=0.053).

Effect of IL-6 overexpression on cachexia initiation in Apc$^{Min/+}$ *females (Experiment 2)*

We have previously shown that IL-6 overexpression in male *Apc*$^{Min/+}$ mice is sufficient to initiate or accelerate cachexia progression [5, 20]. To determine the effect of IL-6 on the initiation of cachexia in the female *Apc*$^{Min/+}$ mouse, we overexpressed IL-6 from 12-14 weeks of age, when tumor burden is fully present but cachexia has not been

initiated. Plasma IL-6 levels were significantly higher in mice treated with the IL-6 overexpression vector (Table 3). There were no differences in body weight between treatments groups at the initiation of IL-6 overexpression, and IL-6 treatment did not alter body weights after two weeks (Table 3). In spite of IL-6 overexpression, 12-14 week-old female *Apc*$^{Min/+}$ mice continued to grow (Table 3). Inguinal fat mass and hindlimb muscle mass did not significantly change in response to IL-6 overexpression (Table 3). Tumor number was quantified at the end of the study. Although tumor numbers were variable, there were no significant differences between treatment groups (not shown).

Effect of IL-6 overexpression on cachexia progression in Apc$^{Min/+}$ *females (Experiment 3)*

To determine the effect of IL-6 on cachexia progression in the female *Apc*$^{Min/+}$ mouse, we overexpressed IL-6 between 15 and 18 weeks of age, which generally corresponds with the development of cachexia. Plasma IL-6 levels were significantly higher in mice overexpressing IL-6 ($p=0.002$, Figure 5A), though it is important to note that the control mice had significantly higher levels of IL-6 than B6 females ($p=0.01$, data not shown). IL-6 overexpression above this cancer-induced increase did not induce an acceleration of body weight loss in female *Apc*$^{Min/+}$ mice that had initiated cachexia (Table 3, Figure 5B). It is unlikely that tumor counts would have been affected by IL-6 overexpression, as polyp number stabilizes at approximately 12 weeks of age [4]. Tumor number was highly variable, but there were no differences between treatment groups in the number of intestine segment 4 tumors (not shown). Spleen weight was not further increased with IL-6 overexpression (Table 3). Hindlimb muscle mass and inguinal fat mass loss were not accelerated by IL-6 overexpression in 18 week female *Apc*$^{Min/+}$ mice (Figure 5B, Table 3). Importantly, muscle STAT3 phosphorylation was not increased by systemic IL-

6 overexpression (Figure 5D). These results are in direct contrast to previous work by our lab with the male *Apc*$^{Min/+}$ mouse, which showed decreases in body weight and muscle mass, and an increase in spleen weight as a result of IL-6 overexpression in addition to the cancer-induced levels between 16 and 18 weeks [20].

3.5 Discussion

Circulating IL-6 has been demonstrated to be a regulator of cancer cachexia progression in male *Apc*$^{Min/+}$ mice. Circulating IL-6 is a known cachectic factor in human cancer populations as well [113, 123-125]. Treatments for cancer cachexia that target IL-6 signaling are currently being examined [12, 126]. However, it is known that sex differences exist in inflammatory responses [33, 111, 127, 128], and sex differences have been reported in cancer cachexia progression in both rodents and humans [107, 108, 115]. We therefore sought to determine the relationship between circulating IL-6 and cachexia progression the female *Apc*$^{Min/+}$ mouse. We have demonstrated for the first time that circulating IL-6 level is not associated with the degree of cachexia in the female *Apc*$^{Min/+}$ mouse, as IL-6 levels were similar between weight stable and cachectic mice. We also report that, unlike the male [5, 20], IL-6 overexpression above cancer-induced levels does not induce or accelerate cachexia progression in female *Apc*$^{Min/+}$ mice. Additionally, we report that sex alters muscle IL-6 transcription during cachexia. Female muscle IL-6 mRNA expression increased with cachexia severity, which contrasts with male cachexia progression [20, 106]. We found that the female muscle may become more sensitive to circulating IL-6 levels during the progression of cachexia, since muscle IL-6r protein and phosphorylated STAT3 increased with severe cachexia. Though the female *Apc*$^{Min/+}$ mouse loses both muscle and fat with the progression of cachexia, the development of

this loss occurs differently from that reported in the male [106]. The male *Apc*$^{Min/+}$ mouse initiates cachexia with the rapid loss of both muscle and fat [106]. We provide evidence that the initiation of cachexia in the female *Apc*$^{Min/+}$ mouse involves a rapid loss of fat mass, while the loss of muscle mass occurs later in the development of cachexia. These data clearly show that sex influences the regulation of cachexia progression in the *Apc*$^{Min/+}$ mouse.

As therapies targeting IL-6 for the treatment of cancer cachexia are gaining traction [12, 126], it is of utmost importance that basic research support this modality. The majority of investigations into human cancer cachexia do not separately analyze men and women [123-125, 129], which does not allow for the determination of sex differences in IL-6 levels. Recent investigation into single nucleotide polymorphisms (SNPs) in the IL-6 and IL-6 receptor promoter sequences has shown that certain SNPs affect levels of circulating IL-6 and soluble IL-6r; however, there are no differences between the sexes in allele frequency, indicating that sex differences do not likely occur at the transcriptional level [130]. While we have consistently found that cachexia development in the male *Apc*$^{Min/+}$ mouse is directly related to tumor burden and the level of circulating IL-6 [5, 6, 13, 14, 20, 60, 131], this relationship has not been firmly established in the female. Though we found that male and female *Apc*$^{Min/+}$ mice had similar tumor burdens, females had significantly lower levels of circulating IL-6 than males, even when weight loss was comparable. However, the female also appears to have a differential cachectic response to IL-6 that is independent of circulating level. Specifically, plasma IL-6 did not increase as cachexia progressed, while muscle IL-6 mRNA expression and STAT3 phosphorylation were increased. Additionally, systemic overexpression of circulating IL-6 did not

accelerate the progression of cachexia, indicating that higher circulating IL-6 levels are not sufficient to induce cachexia in the female *Apc*$^{Min/+}$ mouse. We also found that circulating IL-6 levels were not correlated with increased muscle IL-6r mRNA expression. Though the C26 and *Apc*$^{Min/+}$ models of cancer cachexia are IL-6 dependent in the male [11, 28, 131], sex differences have been found in the C26 model of cachexia, providing evidence that this is not a singular phenomenon related to the *Apc*$^{Min/+}$ mouse [107]. Importantly, estrogen inhibits IL-6 transcription and signaling in many tissues [25, 27, 36, 92, 97]; however, IL-6 is a known mediator of diseases in females including polycystic ovarian syndrome, ovarian cancer, and osteoporosis [56, 58, 97], indicating that females are susceptible to the pathophysiological effects of IL-6 under multiple circumstances regardless of estrogen status. The overall inflammatory environment related to the underlying disease may also alter IL-6 action. The circulating levels of IL-10, IL-4, and interferon-α (IFNα) have been shown to influence IL-6 action [124, 132]. Interestingly, sex differences in inflammation have been reported in IL-10 knockout mice [110]. Further investigation is required to determine if the systemic inflammatory environment, particularly the presence of estrogen, is differentially regulating IL-6 function in female *Apc*$^{Min/+}$ mice.

A key factor that determines tissue response to the inflammatory environment is receptor expression. IL-6 initiates intracellular signaling through binding with mIL-6r, which interacts with the signal-transducing gp130 [133]. The importance of muscle IL-6 signaling through mIL-6r and gp130 in the development of cachexia has been clearly demonstrated in many tumor models [6, 56, 115, 134]. Signaling through gp130 activates many signaling pathways, including JAK/STAT, p38 MAPK, and ERK [11, 55,

115, 116]. We have previously demonstrated that LLC-induced cachexia in males suppresses muscle gp130 expression [109]. However, alterations in the expression level of gp130 or IL-6r during cachexia progression in *Apc*$^{Min/+}$ mice have not been previously reported. Interestingly, cachectic muscle from both male and female *Apc*$^{Min/+}$ mice demonstrated an induction of muscle *IL6ra* mRNA expression and protein expression, without a significant change in muscle *gp130* mRNA expression. The novel observation that male C57BL/6 mice have significantly higher muscle IL-6r protein level than females may explain why males have a more robust response to IL-6 than females. As IL-6 signaling has been linked to the induction of muscle protein degradation [11, 106], it remains to be determined why this signal is being amplified in cachectic muscle of both sexes at both the mRNA and protein levels. It also appears unlikely that differential muscle gp130 and IL-6r expression can account for differential sex responses to circulating IL-6 in *Apc*$^{Min/+}$ mice.

In addition to IL-6 interaction with its receptor complex, downstream regulators have the potential to alter IL-6 signaling in muscle [135-137]. STAT3 is activated by phosphorylation at Y705 by Janus kinases downstream of the IL-6r/ gp130 complex [11]. Activation of JAK/STAT signaling in cachectic muscle is associated with ubiquitin/proteasome and autophagy-mediated protein degradation [11, 106]. SOCS3 has the capacity to directly bind to gp130, inhibiting IL-6 signaling [137]. Cachexia increased muscle *SOCS3* mRNA expression in *Apc*$^{Min/+}$ mice of both sexes. However, the observation that SOCS3 protein has a differential sex response both in B6 and cachectic *Apc*$^{Min/+}$ mice may have implications for differential control of STAT3 expression and downstream signaling between the sexes. The pattern of increased *SOCS3* mRNA and

decreased SOCS3 protein that we report in the male *Apc*$^{Min/+}$ has been previously noted with cachexia in the C26 tumor-bearing model; it has been shown that phosphorylation of SOCS3 by Jak can destabilize SOCS3 and lead to its proteasome-mediated degradation [28]. Further, there is evidence that a second chronological activation of STAT3 signaling may occur even in the presence of SOCS3 binding; this activation is induced by binding of the epidermal growth factor receptor (EGFR) to IL-6r in the continued presence of IL-6, though it is unknown if sex differences exist [59]. We demonstrate a strong trend towards increased STAT3 phosphorylation during cachexia progression in female *Apc*$^{Min/+}$ mice, as previously seen in the male [106]. This also corresponds with female muscle becoming more sensitive to inflammatory signaling with the progression of cachexia, and may represent the loss of a protective mechanism present in female muscle that suppresses inflammatory signaling. However, IL-6 signaling is only one of many inflammatory pathways involved in the progression of cachexia, and other inflammatory factors may regulate cachexia development in the female *Apc*$^{Min/+}$ mouse. Further work is needed to determine the regulation of JAK/STAT signaling during the progression of cachexia in female muscle and its relationship to wasting.

We have shown that female *Apc*$^{Min/+}$ mice undergo cachexia that is, at least initially, independent of IL-6 regulation. This finding has important ramifications, particularly as IL-6 has garnered interest as a potential therapeutic target for cancer cachexia. We report for the first time levels of IL-6r, gp130, and SOCS3 mRNA and protein expression in the muscle of male and female *Apc*$^{Min/+}$ mice. We also report the novel finding that there is differential expression of muscle IL-6r protein in male and female mice. Further, we have reported a difference in the timing of muscle and fat loss

between the sexes that may have important ramifications for metabolism and cytokine signaling during the progression of cachexia. It appears that factors involved in the regulation of cancer cachexia progression are subject to differential sex regulation, and more work is needed to mechanistically understand these differences. In addition, future work will need to determine the mechanisms in skeletal muscle during the progression of cachexia related to protein turnover, oxidative metabolism, and apoptosis that undergo differential regulation in the female.

3.6 Acknowledgements

This work was supported by National Institutes of Health grant # NCI-R01CA121249A501 (JAC), National Institutes of Health Grant P20 RR-017698 from the National Center for Research, and by the USC Behavioral-Biomedical Interface Program, which is a NIGMS/NIH-T32 supported program. Contents of this publication are solely the responsibility of the authors and do not necessarily represent the official views of the NIGMS or NIH. The authors would like to acknowledge Tia Davis and Dr. M. Marjorie Peña for assistance with mouse breeding and IL-6 overexpression experiments. The authors declare no competing interests.

Table 3.1: Characteristics of female *Apc*$^{Min/+}$ mice (Experiment 1). Weight change (%): Percent weight change from peak body weight to weight at sacrifice [(weight at sacrifice-peak weight)/peak weight]. Hindlimb muscle mass comprises left soleus, plantaris, gastrocnemius, tibialis anterior, extensor digitalis longus, and quadriceps mass. n, number. seg 4, segment 4 of the small intestine. mg, milligrams. pg, picograms. ml, milliliters. N, Newtons. * indicates significantly different from weight stable ($p<0.05$). † indicates significantly different from initial cachexia ($p<0.05$).

	Female *Apc* $^{Min/+}$ mice		
	Weight stable	**Initial Cachexia**	**Cachexia**
n	**6**	**6**	**6**
Weight change (%)	**-1.1 ± 0.5%**	**-4.2 ± 0.4%***	**-11.0 ± 1.3%*†**
Spleen weight (mg)	**250.5 ± 50.2**	**310.5 ± 64.4**	**485.7 ± 37.7*†**
Tumor count (seg 4)	**7.8 ± 2.2**	**6.8 ± 3.0**	**26.3 ± 1.0*†**
Hindlimb muscle mass (mg)	**300.2 ± 9.9**	**299.7 ± 18.9**	**226.8 ± 13.4*†**
Inguinal fat mass (mg)	**224.0 ± 34.7**	**153.8 ± 35.2**	**14.8 ± 6.6*†**
Plasma IL-6 (pg/ml)	**17.6 ± 6.7**	**34.4 ± 18.9**	**39.3 ± 13.1**
Grip strength (N)	**1.9 ± 0.2**	**1.9 ± 0.1**	**1.6 ± 0.1*†**
Grip strength/Body weight (N/g)	**0.092 ± 0.008**	**0.098 ± 0.006**	**0.084 ± 0.003**

Table 3.2: Relationships between circulating IL-6 and skeletal muscle signaling during cachexia development (Experiment 1). Correlations calculated in 18-week female *Apc*$^{Min/+}$ mice of varying degrees of cachexia (n=18). R^2, coefficient of determination; p, p-value. Correlations determined by Pearson's correlation. mRNA levels are expressed as fold change from female C57BL/6 mice. * indicates significant correlation between factors ($p<0.05$).

Muscle mRNA expression correlations

Factor 1	Factor 2	R^2	p
Circulating plasma IL-6 (pg/ml)	Body weight loss	0.004	0.802
	Hindlimb muscle mass	0.070	0.289
	Inguinal fat mass	0.004	0.797
	IL-6 mRNA	0.041	0.436
	IL-6 receptor mRNA	0.038	0.468
	gp130 mRNA	0.014	0.701
	SOCS3 mRNA	0.045	0.428
Muscle IL-6 mRNA expression	Body weight loss	0.380	**0.008***
	Hindlimb muscle mass	0.315	**0.019***
	Inguinal fat mass	0.151	0.124
	IL-6 receptor mRNA	0.183	0.112
	gp130 mRNA	0.000	0.981
	SOCS3 mRNA	0.224	0.075
Muscle IL-6 receptor mRNA expression	Body weight loss	0.189	0.092
	Hindlimb muscle mass	0.142	0.150
	Inguinal fat mass	0.218	0.068
	IL-6 receptor protein	0.246	0.060
	gp130 mRNA	0.769	**0.000***
	SOCS3 mRNA	0.913	**0.000***
Muscle gp130 mRNA expression	Body weight loss	0.200	0.125
	Hindlimb muscle mass	0.130	0.226
	Inguinal fat mass	0.151	0.190
	SOCS3 mRNA	0.757	**0.000***
Muscle SOCS3 mRNA expression	Body weight loss	0.212	0.110
	Hindlimb muscle mass	0.124	0.181
	Inguinal fat mass	0.045	0.428

Muscle protein expression correlations

Factor 1	Factor 2	R^2	p
Circulating plasma IL-6 (pg/ml)	IL-6 receptor protein	0.098	0.221
	STAT3 phosphorylation/STAT3	0.008	0.728
	Body weight loss	0.005	0.795
Muscle IL-6 receptor protein (pg/ug)	Hindlimb muscle mass	0.007	0.745
	Inguinal fat mass	0.001	0.913
	STAT3 phosphorylation/STAT3	0.001	0.912
Muscle pSTAT3/STAT3	Body weight loss	0.205	0.059
	Hindlimb muscle mass	0.385	**0.006***
	Inguinal fat mass	0.034	0.465

Table 3.3: Characteristics of 14-week and 18-week female *Apc* $^{Min/+}$ mice with IL-6 overexpression (Experiments 2 and 3). Female *Apc* $^{Min/+}$ mice had the right quadriceps muscle electroporated with control plasmid or IL-6 overexpression plasmid. G, grams; mg, milligrams; dl, deciliter; pg, picograms; ml, milliliters; seg 4, segment 4 of the small intestine; N, Newtons. * denotes significant difference from control group ($p<0.05$).

Female *Apc* $^{Min/+}$ mice			
IL-6 overexpression	-	+	
12-14 week treatment			**p-value**
n	**4**	**4**	
12-week body weight (g)	**20.0 ± 0.7**	**19.0 ± 0.7**	**0.38**
14-week body weight (g)	**20.3 ± 0.6**	**19.5 ± 0.7**	**0.49**
Spleen weight (mg)	**312.3 ± 35.0**	**336.5 ± 22.3**	**0.59**
Fasting Glucose (mg/dl)	**140.7 ± 1.3**	**171.0 ± 28.0**	**0.34**
Plasma IL-6 (pg/ml)	**1.5 ± 1.5**	**65.0 ± 18.1***	**0.02**
Grip strength (N)	**2.1 ± 0.1**	**2.0 ± 0.1**	**0.67**
15-18 week treatment			
n	**6**	**6**	
Peak body weight (g)	**20.4 ± 0.3**	**19.4 ± 0.6**	**0.21**
15-week body weight (g)	**19.6 ± 0.3**	**18.8 ± 0.7**	**0.41**
18-week body weight (g)	**19.3 ± 0.3**	**17.9 ± 0.6**	**0.06**
Inguinal fat mass (mg)	**130.3 ± 39.9**	**65.5 ± 36.3**	**0.27**
Spleen weight (mg)	**318.7 ± 77.6**	**367.3 ± 75.7**	**0.68**
Fasting Glucose (mg/dl)	**119.3 ± 6.8**	**111.3 ± 4.7**	**0.37**
Grip strength (N)	**1.9 ± 0.1**	**1.9 ± 0.1**	**0.89**

3.7 Figure Legends

Figure 3.1: Characteristics of male and female *Apc*$^{Min/+}$ mice (Experiment 1): A) Average body weight change from peak weight in male and female *Apc*$^{Min/+}$ mice (n=12 males, n=18 females). Male *Apc*$^{Min/+}$ mice had more body weight loss than female *Apc*$^{Min/+}$ mice. B) There is no difference in the average number of tumors in segment 4 of the small intestine between male and female *Apc*$^{Min/+}$ mice. C) Average level of plasma IL-6 (pg/ml). D) Average spleen weight in male and female *Apc*$^{Min/+}$ mice. Male *Apc*$^{Min/+}$ mice had larger spleens than female *Apc*$^{Min/+}$ mice. * indicates significantly different from B6 mice of the same sex ($p<0.05$); † indicates significant difference from male *Apc*$^{Min/+}$ ($p<0.05$).

Figure 3.2: Cachexia progression in female *Apc*$^{Min/+}$ mice (Experiment 1): A) Average body weight from 10-18 weeks for weight stable, initial cachexia, and cachexia groups (n=6 per group). Groups are significantly different at 18 weeks of age ($p=0.016$, repeated measures ANOVA). B) Hindlimb muscle mass has a negative correlation with body weight loss during cachexia in the female *Apc*$^{Min/+}$ mouse (Pearson's correlation, $p<0.0001$). C) Inguinal fat mass has a negative correlation with body weight loss during cachexia in the female *Apc*$^{Min/+}$ mouse (Pearson's correlation, $p=0.0002$). Horizontal dotted lines in B and C show average B6 muscle and fat masses. Dotted line at -5% body weight loss intended to show the contrast between fat and muscle loss before and after 5% body weight loss. * indicates significant differences between groups ($p<0.05$).

Figure 3.3: Muscle IL-6 signaling-associated mRNA levels (Experiment 1): A) IL-6 receptor mRNA expression is significantly higher in male and female *Apc*$^{Min/+}$ mice than B6 mice. B) There is no difference in gp130 mRNA expression between male or female *Apc*$^{Min/+}$ mice or B6 mice. C) SOCS3 mRNA expression is higher in male and female *Apc*$^{Min/+}$ mice than B6 mice. All differences were analyzed by two-way ANOVA. # indicates main effect of *Apc*$^{Min/+}$ ($p<0.05$).

Figure 3.4: Muscle IL-6 signaling-associated protein levels (Experiment 1): A) Muscle IL-6 receptor levels (pg/ug total protein) are significantly higher in male B6 than in female B6 mice (0.28 ± 0.04 vs 0.07 ± 0.04, $p=0.01$, Student's t-test) B) Muscle IL-6 receptor levels (pg/ug total protein) increases with cachexia severity in female *Apc*$^{Min/+}$ mice (one-way ANOVA, $p<0.0001$). Cachectic levels were different from all other groups ($p<0.05$, Tukey *post hoc*). IL-6 receptor levels are significantly higher in male cachexia than female cachexia (0.78 ± 0.11 vs. 0.42 ± 0.09, $p=0.02$, Student's t-test). C) Upper: Representative blots shown. All samples per group were run on a gel with all weight stable samples, and then normalized during analysis. Lower: Quantification of pSTAT3/STAT3 blots. The ratio of phosphorylated STAT3 (Y705)/STAT3 increases with cachexia severity in the female *Apc*$^{Min/+}$ mouse (one-way ANOVA, $p=0.01$). There is no difference in phosphorylation of STAT3 (Y705) between cachectic females and cachectic males ($p=0.154$, Student's t-test). No differences were seen between groups in total

STAT3. D) Upper: Representative blots shown. All $Apc^{Min/+}$ samples were run on a gel with male B6 samples for normalization. Lower: Quantification of SOCS3 blots. There is a significant interaction of sex by genotype in muscle SOCS3 protein expression (p=0.006, two-way ANOVA). Female B6 mice had significantly lower SOCS3 expression than male B6 mice (p=0.015, Student-Newman-Keuls *post hoc*). Female $Apc^{Min/+}$ mice had significantly higher SOCS3 expression than female B6 (p=0.029, Student-Newman-Keuls *post hoc*), while male $Apc^{Min/+}$ mice showed a strong trend towards lower SOCS3 expression than male B6 (p=0.053, Student-Newman-Keuls *post hoc*). $ indicates significant difference from initial cachexia (p=0.005, Tukey *post hoc*); * indicates significantly different from same-sex B6; # indicates significant difference from male B6; † indicates significantly different from female. Dotted lines on graphs indicate B6 levels.

Figure 3.5: Effect of IL-6 overexpression in 18 week-old female *Apc* $^{Min/+}$ mice (Experiment 3): A) Female *Apc* $^{Min/+}$ mice that had IL-6 systemically overexpressed from 15-18 weeks of age had higher circulating plasma IL-6 than control mice (p=0.002). B) There is no difference in body weight change from peak body weight (%) between female *Apc* $^{Min/+}$ mice that have had IL-6 systemically overexpressed from 15-18 weeks of age and control female *Apc* $^{Min/+}$ mice at 18 weeks of age. C) There is no difference in hindlimb muscle mass between female *Apc* $^{Min/+}$ mice that have had IL-6 systemically overexpressed from 15-18 weeks of age and control female *Apc* $^{Min/+}$ mice at 18 weeks of age. D) There is no difference in the ratio of phosphorylation of STAT3/STAT3 between female *Apc* $^{Min/+}$ mice that have had IL-6 systemically overexpressed from 15-18 weeks of age and control female *Apc* $^{Min/+}$ mice at 18 weeks of age (p=0.662, Student's t-test). Upper: Representative blots showing pSTAT3 and STAT3 expression. Dashed line indicates that samples were run on same gel, but separated by other samples. Lower: Quantification of pSTAT3/STAT3 expression. Dotted line on graph indicates female B6 level of phosphorylation/total STAT3. * indicates pSTAT3/STAT3 levels were significantly higher than B6 (p=0.008).

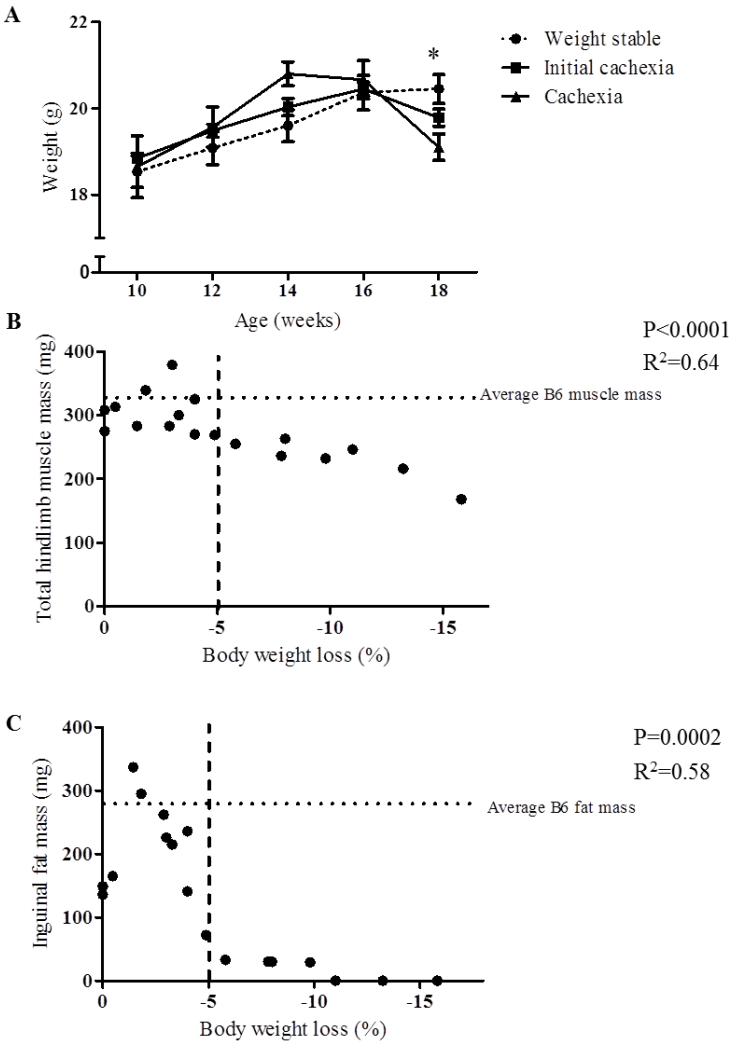

Figure 3.1: Characteristics of male and female *Apc*$^{Min/+}$ mice (Experiment 1): A) Average body weight change from peak weight in male and female *Apc*$^{Min/+}$ mice (n=12 males, n=18 females). Male *Apc*$^{Min/+}$ mice had more body weight loss than female *Apc*$^{Min/+}$ mice. B) There is no difference in the average number of tumors in segment 4 of the small intestine between male and female *Apc*$^{Min/+}$ mice. C) Average level of plasma IL-6 (pg/ml). D) Average spleen weight in male and female *Apc*$^{Min/+}$ mice. Male *Apc*$^{Min/+}$ mice had larger spleens than female *Apc*$^{Min/+}$ mice. * indicates significantly different from B6 mice of the same sex ($p<0.05$); † indicates significant difference from male *Apc*$^{Min/+}$ ($p<0.05$).

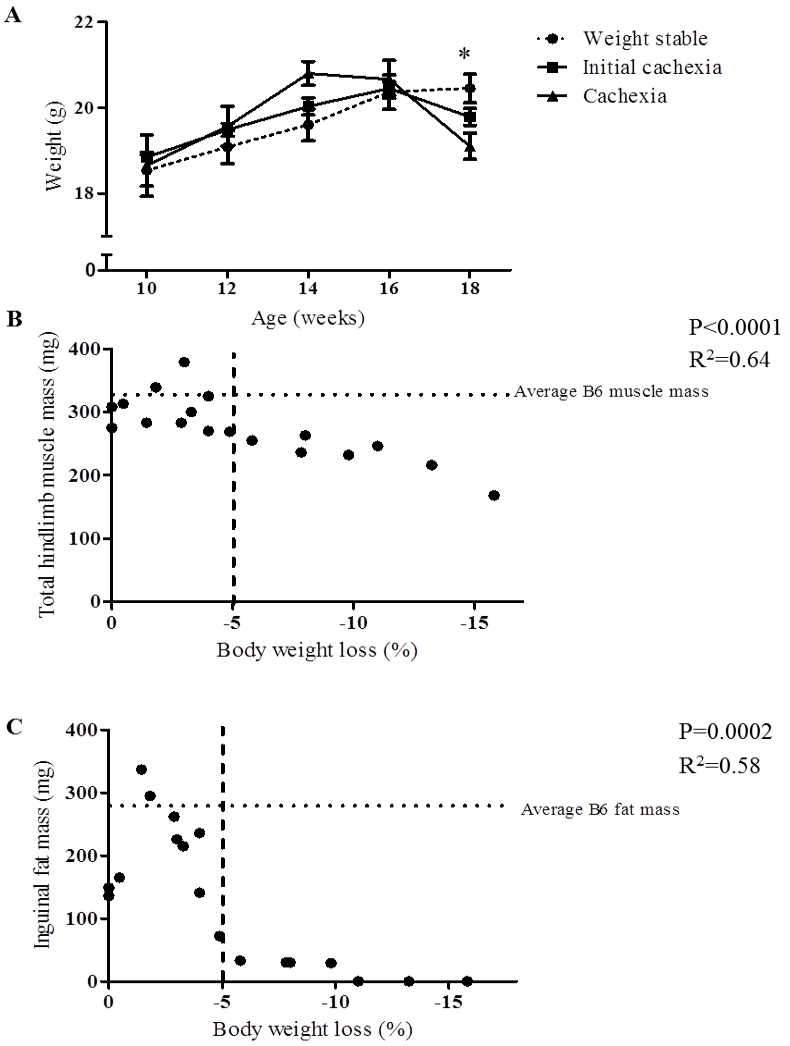

Figure 3.2: Cachexia progression in female *Apc*$^{Min/+}$ mice (Experiment 1): A) Average body weight from 10-18 weeks for weight stable, initial cachexia, and cachexia groups (n=6 per group). Groups are significantly different at 18 weeks of age (p=0.016, repeated measures ANOVA). B) Hindlimb muscle mass has a negative correlation with body weight loss during cachexia in the female *Apc*$^{Min/+}$ mouse (Pearson's correlation, p<0.0001). C) Inguinal fat mass has a negative correlation with body weight loss during cachexia in the female *Apc*$^{Min/+}$ mouse (Pearson's correlation, p=0.0002). Horizontal dotted lines in B and C show average B6 muscle and fat masses. Dotted line at -5% body weight loss intended to show the contrast between fat and muscle loss before and after 5% body weight loss. * indicates significant differences between groups (p<0.05).

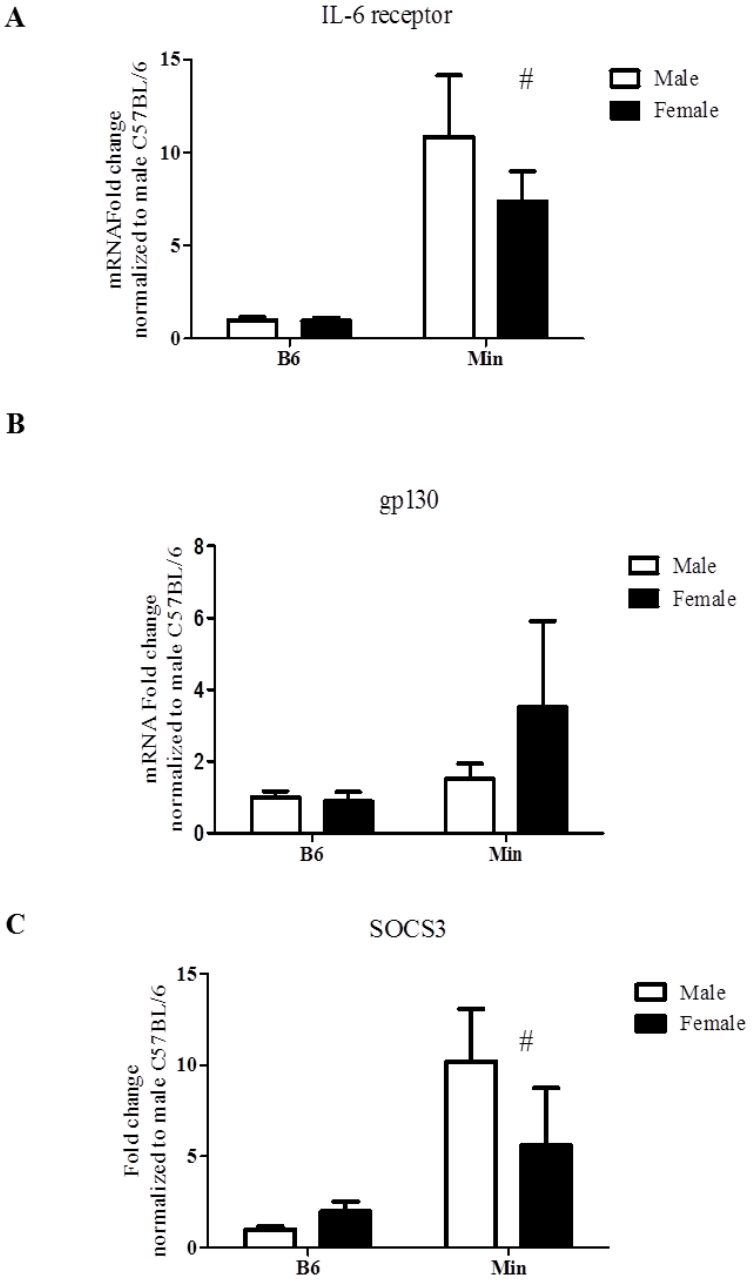

Figure 3.3: Muscle IL-6 signaling-associated mRNA levels (Experiment 1): A) IL-6 receptor mRNA expression is significantly higher in male and female *Apc* $^{Min/+}$ mice than B6 mice. B) There is no difference in gp130 mRNA expression between male or female *Apc* $^{Min/+}$ mice or B6 mice. C) SOCS3 mRNA expression is higher in male and female *Apc* $^{Min/+}$ mice than B6 mice. All differences were analyzed by two-way ANOVA. # indicates main effect of *Apc* $^{Min/+}$ ($p<0.05$).

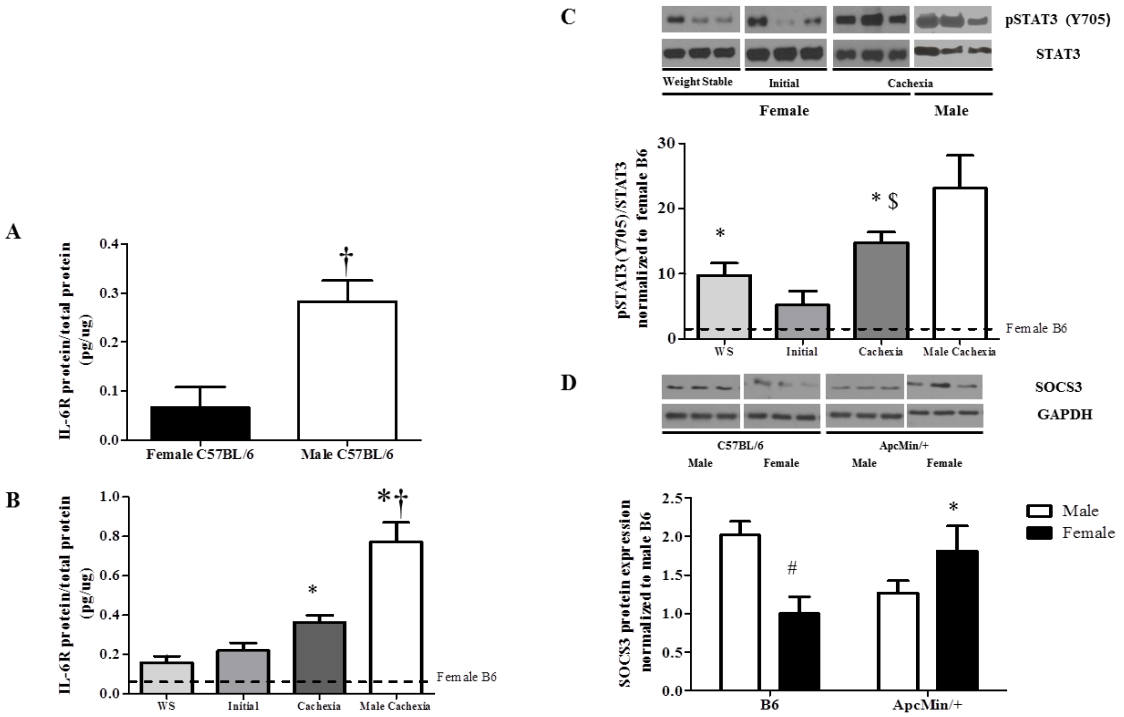

Figure 3.4: Muscle IL-6 signaling-associated protein levels (Experiment 1): A) Muscle IL-6 receptor levels (pg/ug total protein) are significantly higher in male B6 than in female B6 mice (0.28 ± 0.04 vs 0.07 ± 0.04, p=0.01, Student's t-test) B) Muscle IL-6 receptor levels (pg/ug total protein) increases with cachexia severity in female *Apc*$^{Min/+}$ mice (one-way ANOVA, p<0.0001). Cachectic levels were different from all other groups (p<0.05, Tukey *post hoc*). IL-6 receptor levels are significantly higher in male cachexia than female cachexia (0.78 ± 0.11 vs. 0.42 ± 0.09, p=0.02, Student's t-test). C) Upper: Representative blots shown. All samples per group were run on a gel with all weight stable samples, and then normalized during analysis. Lower: Quantification of pSTAT3/STAT3 blots. The ratio of phosphorylated STAT3 (Y705)/STAT3 increases with cachexia severity in the female *Apc*$^{Min/+}$ mouse (one-way ANOVA, p=0.01). There is no difference in phosphorylation of STAT3 (Y705) between cachectic females and cachectic males (p=0.154, Student's t-test). No differences were seen between groups in total STAT3. D) Upper: Representative blots shown. All *Apc*$^{Min/+}$ samples were run on a gel with male B6 samples for normalization. Lower: Quantification of SOCS3 blots. There is a significant interaction of sex by genotype in muscle SOCS3 protein expression (p=0.006, two-way ANOVA). Female B6 mice had significantly lower SOCS3 expression than male B6 mice (p=0.015, Student-Newman-Keuls *post hoc*). Female *Apc*$^{Min/+}$ mice had significantly higher SOCS3 expression than female B6 (p=0.029, Student-Newman-Keuls *post hoc*), while male *Apc*$^{Min/+}$ mice showed a strong trend towards lower SOCS3 expression than male B6 (p=0.053, Student-Newman-Keuls *post hoc*). $ indicates significant difference from initial cachexia (p=0.005, Tukey *post hoc*); * indicates significantly different from same-sex B6; # indicates significant difference from male B6; † indicates significantly different from female. Dotted lines on graphs indicate B6 levels.

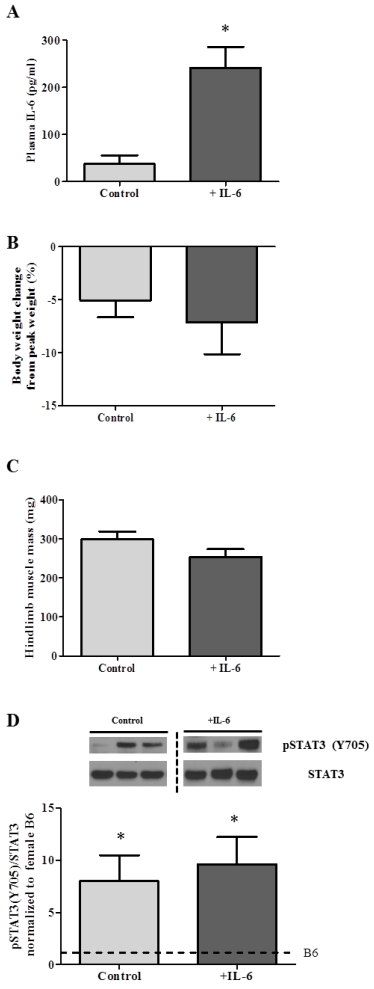

Figure 3.5: Effect of IL-6 overexpression in 18 week-old female *Apc*$^{Min/+}$ mice (Experiment 3): A) Female *Apc*$^{Min/+}$ mice that had IL-6 systemically overexpressed from 15-18 weeks of age had higher circulating plasma IL-6 than control mice (p=0.002). B) There is no difference in body weight change from peak body weight (%) between female *Apc*$^{Min/+}$ mice that have had IL-6 systemically overexpressed from 15-18 weeks of age and control female *Apc*$^{Min/+}$ mice at 18 weeks of age. C) There is no difference in hindlimb muscle mass between female *Apc*$^{Min/+}$ mice that have had IL-6 systemically overexpressed from 15-18 weeks of age and control female *Apc*$^{Min/+}$ mice at 18 weeks of age. D) There is no difference in the ratio of phosphorylation of STAT3/STAT3 between female *Apc*$^{Min/+}$ mice that have had IL-6 systemically overexpressed from 15-18 weeks of age and control female *Apc*$^{Min/+}$ mice at 18 weeks of age (p=0.662, Student's t-test). Upper: Representative blots showing pSTAT3 and STAT3 expression. Dashed line indicates that samples were run on same gel, but separated by other samples. Lower: Quantification of pSTAT3/STAT3 expression. Dotted line on graph indicates female B6 level of phosphorylation/total STAT3. * indicates pSTAT3/STAT3 levels were significantly higher than B6 (p=0.008).

CHAPTER 4

THE ROLE OF OVARIAN FUNCTION IN IL-6 REGULATION OF INFLAMMATION DURING CANCER CACHEXIA PROGRESSION[1]

[1]HETZLER KL, HARDEE JP, LAVOIE HA, MURPHY EA, CARSON JA. TO BE SUBMITTED FOR PUBLICATION.

4.1 Abstract

Cancer cachexia is a debilitating condition that occurs secondary to chronic disease including cancer; our research has shown that some effects of cachexia are affected by sex. The *Apc* $^{Min/+}$ mouse is genetically predisposed to develop intestinal tumors; hypogonadism is strongly associated with cachexia severity in the male, though the relationship in the female is uncertain. Ovarian endocrine functions have a variety of targets including inflammation, and it is likely that there is cross-talk between the female gonads (ovaries) and inflammatory signaling during cancer cachexia progression; however, it is unknown how ovarian endocrine function affects the chronic inflammation seen with cancer cachexia. The purpose of this study is to examine the relationship of inflammation, ovarian endocrine function, and cancer cachexia progression in the female *Apc* $^{Min/+}$ mouse. Ovarian function, determined by estrus cycle tracking, was monitored from 10 to 18 weeks of age in female *Apc* $^{Min/+}$ mice. Natural cessation of estrus cycling secondary to disease progression was seen in ~30% of mice and was associated with severe cachexia, including greater body weight loss, higher fatigue, lower cage activity, and enhanced inflammatory signaling. In contrast, ovariectomy ameliorated body weight loss and rescued muscle mass and function. Our results indicate that loss of ovarian function secondary to disease is different than surgical ablation of ovarian function, possibly indicating that the non-cycling ovary still has some function that is injurious during cachexia progression. Future studies in the female will need to determine the precise mechanisms of this change.

Key Words: inflammation, estrogen, ovariectomy, *Apc* $^{Min/+}$

4.2 Introduction

Cachexia, the progressive wasting of muscle and adipose tissue secondary to chronic disease, represents a significant clinical burden; cancer-related cachexia alone causes two million deaths a year [1]. Occurring in one-third to one-half of cancer patients [1, 3], and leading to nearly one-third of cancer deaths [2], the need for targeted and effective therapies is urgent. Unintentional weight loss, a hallmark of cachexia, is associated with a systemic increase of inflammatory cytokines [45], hypermetabolism, fatigue, and muscle weakness [117]. Both men and women undergo decreases in muscle mass and strength due to cachexia; however, men see a relationship between these deficits and cancer-related fatigue while women do not [63]. Though both sexes experience the functional and metabolic declines associated with cachexia, the etiology and presentation differs between sexes [15]. A dichotomy has been seen between male and female animals with cancer cachexia as well [15, 107]. Despite these observations, the differential mechanisms related to the female response are not yet understood.

It is known that inflammatory processes related to the host's immune system and possibly tumor microenvironment [3] play a role in the etiology of cancer cachexia. Specifically, inflammatory cytokines including IL-1β, TNFα, NfκB, and IL-6 are associated with wasting processes during cachexia progression [2, 3, 20, 138, 139]. Several of these factors cross-regulate one another during cancer cachexia; for example, IL-1β and IL-6 promote TNFα, while TNFα and NfκB promote IL-6 transcription [2]. Additionally, macrophages secrete IL-6 during inflammation in response to toll-like

receptor (TLR) activity [52]. Increased systemic inflammation related to signal transducer and activator of transcription-3 (STAT3) activation, of which IL-6 is a major regulator, plays a major role in muscle wasting [5, 14, 20]. The *Apc* $^{Min/+}$ mouse has a nonsense mutation in the *Apc* gene, leading to intestinal adenomas and cachexia secondary to the tumor burden [20, 105]; we have previously shown that this model develops an IL-6-dependent cachexia [6, 14, 60]. Despite attention to IL-6's role in the etiology of cancer cachexia, our lab has shown that the relationship is not straightforward in the female as in the male [15]. Menopause causes an increase in overall systemic inflammation [85, 140], including the IL-6 pathway and C-reactive protein, an index of overall inflammation [68, 92]. Menopause is also associated with increases in leptin, a cytokine associated with adipose tissue regulation. Interestingly, a link has been shown between IL-6 and leptin levels; however, the mechanism is unknown [68]. Interestingly, SOCS3, a key negative regulator of IL-6/STAT3 signaling, also binds directly to the leptin receptor to regulate leptin sensitivity [98]. Likewise, ovariectomy in mice as well as humans has been shown to cause increased inflammation and metabolic dysregulation [32, 92]. Despite the association between loss of ovarian function and increased inflammation, it is unknown whether inflammation levels are increased *per se*, or whether the body becomes more susceptible to the effects of inflammation without a direct increase in circulating factors.

It is likely that there is crosstalk between sex hormones and the inflammatory milieu during cachexia progression in the female *Apc*$^{Min/+}$ mouse, as we have previously shown in the male [22]. Ovarian endocrine function regulates countless processes throughout the body, including inflammation. Estrogen has been shown to abolish IL-6 secretion in

the liver [25], inhibit NfκB activation of IL-6 [26], and block p38 MAPK-induced activation of TNFα [33]. It is therefore plausible that ovarian endocrine function could modulate the chronic inflammation seen with cachexia. The ovary itself secretes IL-6 during the normal menstrual cycle [94, 141]; this is regulated by FSH (follicle-stimulating hormone, a gonadotropin) [58], in addition to its role of regulating the pre-ovulatory estrogen spike in concert with luteinizing hormone (LH). Interestingly, FSH and IL-6 cross-regulate one another; IL-6 reduces FSH binding to granulosa cells [95], while FSH induces soluble IL-6 receptor (sIL-6r) synthesis [142], a key mediator of the *trans* IL-6 pathway [55, 56]. Ovarian cancer patients have increased levels of plasma sIL-6r compared to non-cancer controls [56], and cachectic women have lower FSH levels than non-cachectic women [62]; these examples may point to a role for IL-6-FSH crosstalk during cachexia progression. Anti-Müllerian hormone (AMH) is secreted by early primordial follicles in the ovary and is used as an index of fertility in women [71, 143]. Interestingly, AMH is a member of the TGFβ superfamily [144, 145], several members of which have established roles in cachexia progression [47, 146, 147]; however, it is unknown whether ovarian AMH plays a role in the etiology. Another factor regulating ovarian hormone levels is leptin, an adipokine [141]; estrogen and particularly progesterone can regulate leptin levels, as well. Leptin levels are closely regulated with adipose tissue mass [148], and both are known to decrease with cachexia progression [148]. Interestingly, leptin levels are inversely associated with IL-6 levels in both male and female cancer patients [148]. IL-6 is known to have physiological [58, 95, 149] and pathophysiological [42, 56, 142] roles in the ovary, indicating that the ovary is sensitive to systemic inflammatory signaling. Additionally, estrogen has been shown to

inhibit IL-6 transcription and signaling in several cell lines and tissues [25-27, 36, 92, 97]. Interestingly, progesterone analogs including megestrol acetate and medroxyprogesterone acetate have been shown to improve caloric intake during cachexia [3]; lending further evidence that the loss of ovarian function could have deleterious effects during cachexia progression.

Our lab has previously characterized the male *Apc* $^{Min/+}$ mouse as a hypogonadism model related to cachexia development [22]; this has not been investigated in the female, though it is likely that there is crosstalk between sex hormones and the inflammatory milieu in the female as well as the male. It is of interest that ovarian granulosa cells bear the IL6r/gp130 complex; as IL-6 signaling increases, estrogen production is inhibited in these cells. It is unknown if the increase in IL-6 with cancer causes ovarian dysfunction through this mechanism [93]. Additionally, though we have shown that the female *Apc*$^{Min/+}$ mouse does not have the same IL-6 response during cachexia progression as the male [15], it is unknown whether ovarian function mediates this difference. Therefore, the purpose of this study is to examine the relationship of inflammation, ovarian endocrine function, and cancer cachexia progression in the female *Apc* $^{Min/+}$ mouse. A second purpose was to determine whether IL-6 mediates changes in ovarian endocrine function. This purpose was investigated through a series of experiments. The first experiment followed ovarian function (determined by presence of estrus cycling) in a cohort of female *Apc* $^{Min/+}$ mice from 10 weeks until 18 weeks of age, at which point the mice were stratified based on body weight change from 15 weeks to 18 weeks of age and presence or absence of estrus cycling. In the second experiment, female *Apc*$^{Min/+}$ mice were ovariectomized (OVX) at 11 weeks of age and followed until 18 weeks of age. A

third experiment investigated whether IL-6 overexpression caused ovarian dysfunction, and whether it affected the changes seen in ovariectomized mice.

4.3 Methods

Animals

Female *Apc* $^{Min/+}$mice (n=75) and female C57BL/6 mice (n=12) were bred and maintained at the University of South Carolina Animal Resource Facility. *Apc*$^{Min/+}$ mice used were on a C57BL/6 background and were offspring from breeders originally purchased from Jackson Labs (Bar Harbor, ME, USA). Mice were kept on a 12:12h light/dark cycle beginning at 7:00 AM and were given unrestricted access to standard rodent chow (Harlan Teklad Rodent Diet, #8604, Harlan, Indianapolis, IN, USA). Mice were weighed weekly. Food intake was measured at 12 and 18 weeks of age. All experiments were approved by the University of South Carolina's Institutional Animal Care and Use Committee.

Experimental Design

Three experiments were performed. *Experiment 1* examined the ovarian progression during the progression of cachexia. Female *Apc* $^{Min/+}$mice (n=24) had estrus cycling measured daily from 10-18 weeks of age for determination of ovarian function. Mice were sacrificed at 18 weeks of age and stratified based on weight change between 15 and 18 weeks of age as well as by presence or absence of ovarian function (estrus cycle). In *Experiment 2*, a cohort (n=10) of female *Apc* $^{Min/+}$ mice were ovariectomized (OVX) at 11 weeks of age and were monitored until sacrifice at 18 weeks of age. *Experiment 3* examined the interaction between ovarian function and inflammation during the initiation

of cachexia. Female *Apc* $^{Min/+}$ mice underwent OVX or sham surgery at 11 weeks of age, followed by overexpression of IL-6 or an empty vector at 13 weeks of age, before sacrifice at 15 weeks of age, for four treatment groups: sham-OVX + vector (n=13), sham-OVX + IL-6 (n=10), OVX + vector (n=10), and OVX + IL-6 (n=8). In all experiments, blood, inguinal fat, hindlimb muscles, ovaries, uterus, and spleen were removed at the time of sacrifice. Hindlimb muscle mass measurements comprise the sum of left soleus, plantaris, gastrocnemius, tibialis anterior, extensor digitalis longus, and quadriceps masses.

Determination of estrus cycling and stage of cycle

Female *Apc* $^{Min/+}$ and C57BL/6 mice had estrus cycling tracked from 10 weeks of age until sacrifice at 18 weeks of age. A sterile cotton swab was dipped in sterile 0.9% saline. The mouse was grasped by the base of the tail, and the cotton swab was gently inserted 0.5 cm into the vagina to collect cells. Cells collected were smeared onto a glass slide (VWR, Radnor, PA, USA) and allowed to dry. Slides were dipped for 5-10 minutes in hematoxylin (Ricca Chemical Company, Arlington, TX, USA), rinsed in deionized water, and allowed to dry. Cell populations were visualized with an Olympus BX41 microscope (Tokyo, Japan) at 100x, and estrus cycle presence and stage were classified based on the observations of Caligoni [73].

Ovariectomy

Female *Apc* $^{Min/+}$ and C57BL/6 mice were ovariectomized at 11 weeks of age. Mice were anesthetized by ketamine/acepromazine/xylazine. Once anesthetized, the mouse was placed in a prone position on a sterile absorbent pad. The back was shaved from the

caudal edge of the ribcage to the base of the tail. The shaved region was then sterilized with betadine (PDI, Orangeburg, NY, USA) and rubbing alcohol (PDI). A 2-cm dorsal midline incision was made with sterile scissors halfway between the caudal edge of the ribcage and the base of the tail. Fascia was the cleared away by blunt dissection. As second 1-cm long incision was made into the muscle wall. The ovary and surrounding fat pad were extracted through the incision with forceps. A hemostat was closed around the distal oviduct/uterine horn to terminate blood supply to the ovary. Non-absorbable suture (AD Surgical, Sunnyvale, CA) was used to tie off the oviduct, and the ovary was removed. The uterine horn was returned to the peritoneal cavity, and absorbable suture (AD Surgical) was used to close the muscle incision. Wound clips were used to close the skin incision, and the process was repeated on the contralateral side. Mice were given 0.01 mg/kg buprenorphine (Burprenex ©, Reckitt Benckiser Pharmaceuticals, Pendergrass, GA, USA) for pain. Wound clips were removed 7 days after surgery.

IL-6 overexpression by electroporation

In vivo intramuscular electroporation of an IL-6 plasmid was used to increase circulating IL-6 levels in mice as previously described [117]. The right quadriceps muscle was used to synthesize and secrete exogenous IL-6 into circulation from the injected expression plasmid, and was not used for any analyses in the study. The gastrocnemius muscle used in the study was not subjected to electroporation. Briefly, mice were injected with 50 μg of IL-6 plasmid driven by the CMV promoter, or control plasmid (pV1J), into the right quadriceps muscle. Mice were anesthetized with a 2% mixture of isoflurane (IsoSol, VEDCO, St. Joseph, MO, USA) and oxygen (1 L/min). The leg was shaved, and a small incision was made over the quadriceps muscle. Fat was dissected away from the muscle,

and the plasmid was injected in a 50 µl volume of sterile phosphate-buffered saline (PBS). A series of eight 50 ms, 100 V pulses was used to promote uptake of the plasmid into myonuclei, and the incision was closed with a wound clip.

Run to Fatigue

At 12, 15, and 18 weeks of age, mice were subjected to a run-to-fatigue treadmill protocol. After 5 minutes of acclimation at 5 meters/minute and 5 minutes of warm-up at 10 m/m, the clock was started when speed was increased to 15 m/m. The treadmill protocol was as follows: 20 minutes at 15 m/m, 20 minutes at 18 m/m, 30 minutes at 20m/m, 30 minutes at 25 m/m, and 28 m/m until all mice stopped. A mouse was considered "fatigued" when it refused to run or could not keep up with the treadmill despite gentle nudging for 1 minute. Time and distance to fatigue were recorded.

Voluntary Cage Activity

At 12, 15, and 18 weeks, mice were single-housed and placed in an activity monitor (Opto-M3 Activity Meter, Columbus Instruments, Columbus, OH) as previously described [5]. Briefly, activity was measured for 12h during the dark cycle (7PM-7AM), and the number of beams crossed on the X-Y plane was recorded for 3 nights. Food consumption was recorded during this same period of single-housing.

RNA isolation and RT-PCR

RNA isolation, cDNA synthesis, and real-time PCR were performed as previously described [118]. cDNA synthesis reagents from Applied Biosystems (Foster City, CA, USA) were used. Bio-Rad SsoAdvanced Universal Probes Supermix and SYBR Green Supermix were used for RT-PCR reactions (Hercules, CA). Briefly, proximal gastrocnemius muscle was homogenized in TRIzol (Life Technologies, Grand Island,

NY, USA) and mixed with chloroform, then centrifuged. The RNA phase was removed and washed several times with ethanol in DEPC-treated water. cDNA was synthesized using 1 μg of RNA. RT-PCR was performed on an Applied Biosystems 7300 thermocycler. Taqman gene expression assay was used to determine IL-6 and TGFβ mRNA expression (Life Technologies). Primers for AMH, TNFa, TLR4, IL-6r, and GAPDH were obtained from IDT (Coralville, IA, USA). Primer sequences are as follows.

AMH (F): 5'TTGCTGAAGTTCCAAGAGCCTCCA-3' (R): 5'-GAAACAGCGGGAATCAGAGCCAAA-3';

TNFa (F): 5'-CCCAGACCCTCACACTCAGAT-3' (R): 5'-TTGTCCCTTGAAGAGAACCTG-3';

TLR4 (F): 5'GGAAGGACTATGTGATGTGAC-3' (R): 5'-GCTCTTCTAGACCCATGAAATTGG-3'.

IL-6r and GAPDH primer sequences have been published elsewhere [15, 119].

Western blotting

Western blots were performed as described previously [106, 120]. Briefly, gastrocnemius muscle samples were run on 6-8% acrylamide gels and transferred overnight to PVDF membrane (Thermo Scientific, Waltham, MA, USA). After transfer, Ponceau stains were imaged to verify equal loading. The membrane was blocked for 1 hour in 5% milk-TBS-Tween 20, and incubated with primary antibodies at 1:2000 dilution overnight at 4^0C. After several washes, membranes were incubated with secondary antibodies at 1:2000 dilution for 1 hour. Blots were visualized with WesternBright ECL (BioExpress, Kaysville, UT, USA). IL-6r antibody was obtained from Santa Cruz Biotech (Santa Cruz, CA). STAT3, phopho-STAT3 (Y705), anti-mouse

IgG, and anti-rabbit IgG antibodies were obtained from Cell Signaling (Danvers, MA, USA).

IL-6 Enzyme-linked immunosorbent assay

A mouse IL-6 ELISA kit was obtained from Life Technologies (Frederick, MD), and manufacturer's protocol was followed. Briefly, 100 µl of samples and standards were added in duplicate to the 96-well plate. Plate was incubated for 2 hours at room temperature, followed by 4 washes. 100 µl IL-6 biotin conjugate was added to wells and incubated for 30 minutes at room temperature. Plate was washed 4 times. 100 µl Streptavidin-HRP was added to wells and allowed to incubate for 30 minute at room temperature. Plate was then washed 4 times. 100 µl stabilized chromogen was added to wells and incubated for 30 minutes in the dark until color developed. 100 µl Stop Solution was added to wells and the plate was read at 450nm in a Bio Rad iMark plate reader (Carlsbad, CA).

Soluble IL-6R Enzyme-linked immunosorbent assay

Soluble IL-6r (sIL-6r) ELISA kit was obtained from MyBioSource (City, State) and manufacturer's protocol was followed. Briefly, 100 µl of standards and samples were added to wells. 50 µl of conjugate was added to sample in each well, and plate was incubated for 1 hour at 37°C. Plate was washed five times. 50 µl each of Substrate A and B were added to wells. Plate was again incubated at 37°C for 15 minutes until color developed. 50 µl Stop Solution was added to wells, and the plate was immediately read at 450nm on a BioRad iMark plate reader (Carlsbad, CA).

Leptin Enzyme-linked immunosorbent assay

A commercial mouse leptin ELISA was obtained (Quantikine, R&D Systems, Minneapolis, MN) and manufacturer's instructions were followed. Briefly, standards and samples were added to the pre-coated plate and allowed to incubate for two hours at room temperature. The plate was washed five times and leptin conjugate was added to wells. Plate was allowed to incubate for two hours at room temperature. Again, the plate was washed five times. Substrate Solution was added to wells, and plate was incubated in the dark for thirty minutes at room temperature. Stop Solution was added to wells, and the plate was read at 450 nm on a BioRad iMark plate reader.

Intestinal polyp quantification

Quantification of intestinal polyps was determined as previously described [19]. Briefly, intestinal sections were fixed in formalin at time of sacrifice. At time of analysis, sections were rinsed in deionized water and dipped briefly in 0.1% methylene blue. Polyps from segment 4 were counted under a dissecting microscope; it has been determined that tumor number in segment 4 is representative of total tumor number [122].

Ovarian Histology

Ovaries were excised from B6, Cycle Present, and Cycle Absent mice and immediately transferred to 4% PFA. Ovaries were mounted in paraffin, sectioned, and stained by hematoxylin and eosin by the University of South Carolina School of Medicine Instrument Resource Facility. Pictures were taken using a Nikon E600 microscope (Nikon, Tokyo, Japan) at 400x and 1000x.

Statistical analysis

All results are reported as means ± SEM. Differences between B6, Cycle Present, and Cycle Absent were analyzed by one-way ANOVA using Tukey *post hoc* where appropriate. Differences between timepoints and ovarian status, were determined by two-way repeated measures ANOVA with Sidak's multiple comparisons test where appropriate. Differences between genotype and ovarian status were determined by two-way ANOVA with Tukey *post hoc* where appropriate. Differences between Cycle Absent and OVX mice were determined by Student's t-test. Differences between Cycle Present, Cycle Absent, and OVX mice were determined by one-way ANOVA with Tukey *post hoc* where appropriate. Differences between Sham + vector, Sham + IL-6, OVX + vector, and OVX + IL-6 mice were determined by two-way ANOVA with Tukey *post hoc* where appropriate. Level of significance was set at 0.05.

4.4 Results

Estrus cycle cessation with cachexia

Female *Apc* $^{Min/+}$ mice (n=24) and female C57BL/6 (B6) mice (n=7) had estrus cycles tracked by vaginal cytology daily until sacrifice; this was measured as an index of ovarian reproductive function though it does not account for ovarian endocrine function. All B6 mice continued cycling normally (data not shown). Nine of the 24 female *Apc* $^{Min/+}$ mice (37.5%) ceased estrus cycling before 16 weeks of age (Figure 1A). Estrus cycling was tracked in Experiment 3 as well; while 4/13 (~31%) of control 15-week *Apc*$^{Min/+}$ mice ceased estrus cycling, IL-6 overexpression did not induce cessation of estrus cycling in female *Apc*$^{Min/+}$ mice (data not shown). To further investigate differences

between mice that had continued estrus cycling through sacrifice at 18 weeks ("Cycle Present") and mice who had ceased estrus cycling before sacrifice ("Cycle Absent"), ovarian histology was performed. Figure 1B shows representative images at 400x and 1000x of ovaries taken from B6, Cycle Present, and Cycle Absent mice. Ovaries of Cycle Absent mice show more dying, or atretic, follicles (indicated by arrows) than the ovaries of either B6 or Cycle Present mice. We further attempted to characterize the difference between Cycle Present and Cycle Absent ovaries through gene expression of Anti-Müllerian hormone (AMH), a hormone secreted by primordial ovarian follicles that is often used as a marker of the size of the follicular pool, or as a proxy for fertility in women. Interestingly, AMH expression in Cycle Absent ovaries increased 3-fold over B6 levels ($p<0.0001$, Tukey *post hoc*), while there was little difference between B6 and Cycle Present (1 vs. 1.287). AMH gene expression in Cycle Absent ovaries was significantly higher than in the Cycle Present group, as well ($p<0.0001$, Tukey *post hoc*). Interestingly, uterine weight was significantly lower than B6 uterine not only in Cycle Absent $Apc^{Min/+}$ mice, but in Cycle Present $Apc^{Min/+}$ mice as well (Figure 1D). All three groups differed from one another, with Cycle Absent having the lowest average uterine weight ($p<0.001$ for each comparison, Tukey post hoc).

Morphological and functional changes with ovarian dysfunction due to cachexia

After sacrifice at 18 weeks of age, female $Apc^{Min/+}$ mice were stratified into Cycle Present and Cycle Absent groups for all other analysis in order to determine the effect of loss of ovarian function on cachexia-related outcomes. A main effect of age and an interaction of age x cycle presence were determined by two-way repeated measures ANOVA (Figure 2A). Cycle Present and Cycle Absent female $Apc^{Min/+}$ mice had similar

body weights at 12 and 15 weeks of age (12 weeks: Cycle Present 18.3 ± 0.3g, Cycle Absent 18.6 ± 0.5g; 15 weeks: Cycle Present 19.1 ± 0.3g, Cycle Absent 19.3 ± 0.5g; Figure 2A). Importantly, the two groups were of similar weight at the age at which the Cycle Absent group ceased estrus cycling. However, body weights between the two groups were significantly different at sacrifice (Cycle Present 19.6 ± 0.2g, Cycle Absent 17.4 ± 0.6g; Table 1, Figure 2A) ($p<0.01$, Sidak's multiple comparisons test). Similarly, main effects of age, cycle presence, and an interaction of the two were determined by two-way repeated measures ANOVA. Cycle Present and Cycle Absent mice had no difference in body fat percentage at 12 or 15 weeks of age (12 weeks: Cycle Present 12.9 ± 0.6%, Cycle Absent 12.9 ± 0.1%; 15 weeks: Cycle Present 11.5 ± 0.3%, Cycle Absent 9.7 ± 0.7%), but Cycle Absent mice had significantly lower percentage body fat at sacrifice (Cycle Present 11.8 ± 0.5%, Cycle Absent 7.4 ± 0.2%; Figure 2B) ($p<0.01$, Sidak's multiple comparisons test). At sacrifice, inguinal fat mass differed between B6, Cycle Present, and Cycle Absent mice ($p<0.05$, one-way ANOVA); Cycle Absent mice had significantly less fat than either of the other groups ($p<0.05$ for each comparison, Tukey *post hoc*) (Table 1). Similar to inguinal fat mass, hindlimb muscle mass at sacrifice differed between B6, Cycle Present, and Cycle Absent mice ($p<0.05$, one-way ANOVA); Cycle Absent mice had significantly less muscle mass than the other groups ($p<0.05$, Tukey *post hoc*) (Table 1). Spleen weight was different between each of the three groups ($p<0.05$, one-way ANOVA and Tukey *post hoc*), indicating that inflammation increased over B6 levels in the female $Apc^{Min/+}$, and that inflammation was further increased in the Cycle Absent group (Table 1). There was a significant difference between the three groups in heart weight, with the Cycle Absent group having

significantly heavier hearts than either of the other two groups ($p<0.05$, one-way ANOVA and Tukey *post hoc*).

Functional measurements were taken at 12, 15, and 18 weeks of age in B6, Cycle Present, and Cycle Absent female $Apc^{Min/+}$ mice. Voluntary cage activity decreased over time in both Cycle Present and Cycle Absent groups. Main effects of age ($p=0.0015$) and cycle presence (0.045) were determined by two-way repeated measures ANOVA. Cycle Present and Cycle Absent groups trended towards difference at 18 weeks ($p=0.056$, pre-planned Student's t-test) (Figure 2C). No differences in distance run by Cycle Present and Cycle Absent female $Apc^{Min/+}$ mice at 18 weeks were seen (Table 1). No differences in food intake (Table 1) or food intake/body weight (data not shown) were seen at any age across the groups; this is an important point when considering the severe weight loss in the Cycle Absent group. Overall, Cycle Absent female $Apc^{Min/+}$ mice present with much more severe cachexia at 18 weeks of age than Cycle Present female $Apc^{Min/+}$ mice.

Morphological and functional changes with ovariectomy

Female B6 and $Apc^{Min/+}$ mice were ovariectomized (OVX) at 11 weeks of age (Figure 3A) to determine the effects of loss of ovarian function on cachexia progression. Regardless of genotype, OVX increased body weight at sacrifice (Table 2). Ovaries-intact (Intact) $Apc^{Min/+}$ females weighed significantly less than intact B6 females, but OVX maintained body weight at levels similar to B6 mice (Table 2). Though OVX caused an increase in body weight over intact mice, no differences were seen in weight of the inguinal fat pad (Table 2). Among $Apc^{Min/+}$ mice, OVX caused significantly greater hindlimb muscle mass compared to intact mice (Table 2). Importantly, uterine weight decreased significantly with OVX regardless of genotype, indicating success of the

procedure (Table 2). Among *Apc*$^{Min/+}$ females, OVX mice were compared directly to Cycle Absent mice in order to compare phenotypes of mice who had lost ovarian function by different means. While Cycle Absent mice lost weight between 11 and 18 weeks of age, OVX mice gained nearly 15% body weight (Figure 3B). Importantly, *Apc*$^{Min/+}$ mice continue to grow until 14-15 weeks of age, so this comparison does not reflect weight loss from peak weight. OVX mice had significantly greater percentage of body fat than Cycle Absent mice (Figure 3C), while there was no difference in lean mass (Figure 3D). Functionally, OVX mice significantly outperformed Cycle Absent mice in run to fatigue (Figure 3E) and voluntary cage activity (Figure 3F). Importantly, however, there was no difference in food intake between the two groups (Figure 3G), despite striking differences in morphology and function. These differences between Cycle Absent and OVX mice are key, as they indicate that the ovarian pathology found in intact, Cycle Absent *Apc*$^{Min/+}$ females is not simply early ovarian failure.

Morphological changes with ovariectomy and IL-6 overexpression

Female *Apc*$^{Min/+}$ underwent OVX or sham surgery at 11 weeks of age, IL-6 overexpression or vector electroporation at 13 weeks of age, and were sacrificed at 15 weeks of age (Figure 4A). Body weight change from 11-15 weeks of age was analyzed to determine effects of treatment. Main effects of OVX ($p=0.0012$) and IL-6 overexpression ($p=0.017$) were determined by two-way ANOVA. Interestingly, the OVX + vector group gained significantly more weight than the OVX+IL-6 group ($p<0.05$, preplanned Student's t-test), indicating that the addition of IL-6 to an OVX female stunted growth. No differences were seen among groups in change in body fat from 11-15 weeks of age. Interestingly, lean mass change from 11-15 weeks followed

the same pattern as body weight change (Figure 4D); an interaction between OVX and IL-6 overexpression was determined by two-way ANOVA (p=0.009). OVX+vector group gained significantly more muscle mass than control and OVX+IL-6 groups, indicating that the addition of IL-6 to an OVX animal may specifically inhibit muscle growth. Taken together with the lack of change in fat mass, it follows that the differences in body weight change from 11-15 weeks are due to growth of muscle mass more so than fat mass.

Effect of loss of ovarian function and ovariectomy on tumor burden and circulating factors

Cycle Present, Cycle Absent, and OVX female $Apc^{Min/+}$ mice were directly compared to one another to determine differences in circulating factors that may provide insight into the etiology of estrus cycle cessation. Tumor numbers from the entirety of the small intestine and colon were significantly different among groups (p=0.0002, one-way ANOVA); Cycle Absent had significantly more tumors than Cycle Present or OVX ($p<0.01$ for each comparison, Tukey post hoc) (Figure 5A). It has been shown that tumor burden is correlated with weight loss and cachexia severity [13]; however, the association with ovarian dysfunction is novel. No differences between groups were found for plasma IL-6 levels (Figure 5C); however, Cycle Absent had significantly higher plasma IL-6 levels than OVX (p=0.0003; pre-planned Student's t-test). Interestingly, there were no changes among groups for soluble IL-6r (Figure 5E); sIL-6r is thought to be a key component of the *trans* IL-6 pathway, and has been shown to increase in cachectic males (unpublished data). Further, a significant decrease in sIL-6r was found in Cycle Absent mice compared to Cycle Present mice by pre-planned Student's t-test (p=0.050). Among 15-week mice that had undergone either ovariectomy, IL-6 overexpression, or both,

interesting trends were seen in these same factors. There was a main effect of OVX to decrease tumor burden, though it has been shown that ovariectomy should not affect tumor number (Figure 5B). As expected, there was a main effect of IL-6 to increase plasma IL-6 levels (Figure 5D). Interestingly, there was a main effect of IL-6 overexpression to decrease sIL-6r (Figure 5F) (two-way ANOVA: $p<0.05$).

Effect of loss of ovarian function on circulating inflammatory factors

Several circulating inflammatory factors were examined to determine whether the loss of ovarian function by disease or by ovariectomy affected systemic inflammation. Plasma leptin differed across B6, Cycle Present, Cycle Absent, and OVX groups ($p=0.005$, one-way ANOVA); Cycle Absent mice had significantly lower leptin levels than C57BL/6 ($p<0.05$, Tukey *post hoc*) (Figure 6A). Plasma Interferon-gamma (IFNγ) decreased in both control and OVX $Apc^{Min/+}$ mice compared to B6 (Figure 6B). Surprisingly, plasma MCP-1 decreased in both control and OVX $Apc^{Min/+}$ mice compared to B6 (Figure 6C). Plasma RANTES increased in Cycle Present mice over B6 levels, but was significantly lower in Cycle Absent mice (Figure 6D). Plasma IL-10, an anti-inflammatory cytokine, decreased significantly from B6 levels in both control and OVX $Apc^{Min/+}$ mice. Interestingly, within the control $Apc^{Min/+}$ mice, IL-10 levels were significantly higher in Cycle Absent than Cycle Present mice (Figure 6E). Plasma M-CSF increased above B6 levels in control $Apc^{Min/+}$ mice, but this effect was attenuated by OVX, which brought levels down significantly. Among control $Apc^{Min/+}$ mice, Cycle Absent had significantly lower levels than Cycle Present mice (Figure 6F). IL-1β, IL-17, LIF, TNFα, and VEGF showed no changes across groups (Table 3).

Changes in muscle inflammatory signaling with loss of ovarian function and IL-6 overexpression

IL-6 and other cachexia-related inflammatory markers were examined in muscle, a cachexia-sensitive tissue, in order to determine the effect of ovarian dysfunction or loss of function on inflammatory signaling. Despite the lack of difference between Cycle Present and Cycle Absent plasma IL-6 levels (Figure 4B), Cycle Absent muscle IL-6 mRNA was significantly higher, despite a large amount of variability, than B6, Cycle Present or OVX (Figure 7A)(one-way ANOVA: $p=0.014$; $p<0.05$ for each comparison, Tukey *post hoc*). Additionally, TNFα followed the same trend ($p=0.005$, one-way ANOVA; Cycle Absent differs from Cycle Present ($p<0.05$) and OVX ($p<0.01$), Tukey *post hoc*) (Figure 7E). Interestingly, TGFβ did not follow this same trend. Although significant differences were found between groups ($p=0.0448$, one-way ANOVA), OVX expression was significantly higher than Cycle Present ($p<0.05$, Tukey *post hoc*) (Figure 7C). Among 15-week $Apc^{Min/+}$ mice that had undergone ovariectomy, IL-6 overexpression, or both, no changes were seen across groups for any of these inflammatory cytokines (Figure 7B,D,F).

Changes in muscle inflammatory receptors with loss of ovarian function and IL-6 overexpression

Expression of two critical inflammatory receptors to the development of cachexia was examined in both cohorts of mice. IL-6 receptor mRNA was different across groups with varying ovarian statuses (determined by one-way ANOVA, $p<0.0001$). Cycle Absent mice had 30-fold higher expression than any of the other groups (Figure 8A). The same trend was seen for TLR4 expression in these same mice, with Cycle Absent mice having 15-fold higher expression than any of the other groups ($p<0.0001$, one-way

ANOVA; $p<0.0001$ for each multiple comparison, Tukey *post hoc*). Among 15-week $Apc^{Min/+}$ mice that had undergone ovariectomy, IL-6 overexpression, or both, there was an interaction of the two treatments to influence IL-6r expression. However, the Tukey *post hoc* revealed no differences between individual groups (Figure 8B). There were no differences among groups for TLR4 expression (Figure 8D).

4.5 Discussion

The purpose of this study was to examine the relationship of inflammation, ovarian function, and cachexia progression in the female $Apc^{Min/+}$ mouse. To this end, we saw no differences in circulating inflammatory factors including plasma IL-6 (Figure 5C), and soluble IL-6 receptor (Figure 5E). However, we saw a large induction of cytokine and receptor mRNA in the cycle absent group (Figures 6 and 7), potentially indicating that this inflammation is not induced by IL-6. However, OVX returned many cytokine levels to B6 or Cycle Present levels. Therefore, we postulate that ovarian dysfunction does not directly increase inflammation. However, we did see an increase in gene expression of inflammatory receptors including IL-6r, gp130, and TLR4 in muscle (Figure 8), indicating that ovarian dysfunction may cause an increase in *susceptibility* to systemic inflammation. Further evidence for this hypothesis comes from Experiment 3, in which female $Apc^{Min/+}$ mice underwent overexpression of IL-6 in addition to OVX. While OVX+vector mice gained the most weight during this experiment, OVX+IL-6 mice did not gain weight, indicating that loss of ovarian function increases the animal's susceptibility to induced inflammation (Figure 4B). Interestingly, the weight gained during this time by OVX+vector mice consisted largely of muscle mass, and the overexpression of IL-6 blocked this muscle mas increase (Figure 4D). Importantly, there

were no differences between control *Apc*$^{Min/+}$ mice and IL-6+ sham-OVX mice in body weight or muscle mass change. An especially interesting finding is the lack of increase in sIL-6r expression in female *Apc*$^{Min/+}$ mice over C57BL/6 levels, and especially in the more severely cachectic Cycle Absent mice. This differs from we have seen previously in male *Apc*$^{Min/+}$ mice (unpublished data), and may indicate that *trans* IL-6 signaling does not play a role in the etiology of cachexia progression in the female as it does in the male [119].

The most striking finding from this study is that, across all measures, the cessation of estrus cycling does not equate with ovariectomy. Whereas ovariectomy led to improvement in female *Apc*$^{Min/+}$ mice body composition (Figure 3B,C), function (Figure 3E,F), circulating plasma IL-6 (Figure 5A), and muscle inflammatory signaling (Figure 7); mice who had ceased estrus cycling (Cycle Absent) fared worse on every outcome than their Cycle Present littermates. Importantly, while hypogonadism is apparent in Cycle Absent mice, this appears to be an effect rather than a cause of cachexia. An unknown factor leading to increased severity in the female appears to cause cessation of estrus cycling, possibly secondary to fat loss (Table 4.1, Figure 4.2B). Tumor burden was significantly higher in Cycle Absent mice than Cycle Present (Figure 5A), which provides valuable insight into the potential etiology of increased inflammation and more severe cachexia in Cycle Absent mice. While OVX mice had significantly fewer tumors than Cycle Absent (Figure 5A), it is extremely important to note that previous reports have indicated that OVX does not affect tumor number in *Apc*$^{Min/+}$ mice [24]. Further, while we have seen in two separate cohorts of ovaries-intact female *Apc*$^{Min/+}$ mice, both in the present study and in a previous report [15], that approximately 30%

become severely cachectic, none of the OVX female *Apc*$^{Min/+}$ mice became severely cachectic. We propose that this is a sufficient sample size to indicate that OVX does protect the female *Apc*$^{Min/+}$ mouse from cachexia.

While we originally hypothesized that Cycle Absent mice and OVX mice would be similar in phenotype, the two groups show vast differences. It is therefore clear that female *Apc*$^{Min/+}$ mice who cease estrus cycling are not simply losing ovarian function, but are undergoing a complex ovarian dysfunction syndrome due to underlying disease. Ovarian histology indicated an increased number of atretic (dead or dying) ovarian follicles in Cycle Absent mice (Figure 1B), which can induce a number of endocrine change in the ovary, including inhibition of ovarian steroidogenesis [150]. Atresia of follicles generally occurs due to caspase-induced apoptosis regulated by BCL-2 [150]. Additionally, we found a significant increase in ovarian gene expression of Anti-Mullerian hormone (AMH) (Figure 1C). While menopausal women have an almost complete loss of AMH expression [145], the increase we see is more similar to that which is seen with polycystic ovarian syndrome (PCOS) [145]. Importantly, atretic follicles do not express AMH [145], so the increases we see in both atretic follicles and AMH are not directly related. Interestingly, the similarities with PCOS continue, as women with PCOS have lower serum sIL-6r than women without PCOS; in the current study we saw that serum sIL-6r was significantly lower in Cycle Absent mice than Cycle Preset mice (Figure 4C). The lower levels of plasma leptin seen in Cycle Absent mice (Figure 6A) provide a potential mechanistic link between disease and loss of ovarian function; leptin levels are lower in human cachexia patients than healthy controls [67]. Leptin is a major regulator of ovarian steroidogenesis and is regulated in turn by estrogen and particularly

progesterone [141]. Hypoleptinemia, furthermore, is commonly seen in women with hypothalamic amenorrhea and is caused by energy deficiency [151].

A final potential explanation for differences seen between Cycle Absent mice and OVX mice is the dysregulation of the gonadotropins LH and FSH. While OVX mice, as in menopausal humans or animals, have higher circulating LH or FSH than cycling females [152, 153], it is likely that the dysfunctional ovaries of Cycle Absent mice feedback centrally to cause dysregulation of the secretion of these hormones. The release of both hormones is controlled by the pulsatile release of gonadotropin-releasing hormone (GnRH), which is secreted from the hypothalamus and whose pulsatile pattern can influence the ratio of and to what extent LH and FSH are released [154]. Given the importance of the pattern of GnRH secretion, it is highly likely that Cycle Absent mice enter a feedback cycle of greater and greater dysfunction with regards to LH and FSH; however, this hypothesis needs to be tested in future studies. In human cases of primary ovarian insufficiency (POI), where ovarian function fails before age 40 and at a mean age of 17 years [155], a key marker of the syndrome is consistently high levels of FSH (40 IU/L), similar to menopausal women [152, 156]. However, women with POI also have low levels of AMH [156], contrary to what we see in Cycle Absent mice. Functional hypothalamic amenorrhea occurs secondary to several systemic stresses, including chronic disease, and is mediated by cortisol or corticotropin-releasing hormone (CRH) inhibition of GnRH [157]. This mechanism is a distinct possibility in Cycle Absent mice; however, it will require further investigation. Interestingly, another leading cause of secondary amenorrhea in humans is traumatic brain injury, lending further evidence to a central role in the pathophysiology of premature cycle cessation [157].

Morphologically, striking differences were seen among Cycle Present, Cycle Absent, and OVX female *Apc*$^{Min/+}$ mice. While it is clear that Cycle Absent mice were much more severely cachectic than Cycle Present mice, it is not clear why Cycle Absent mice stopped estrus cycling. Tumor burden was much higher in Cycle Absent mice (Figure 4A), and it is known that tumor burden is directly related to cachexia severity (CITE). However, it is unsure what the direct link is between tumor burden and cessation of estrus cycling. One hypothesis is that since loss of white adipose tissue (WAT) is one of the first tissues to be depleted during cachexia progression [158], the reproductive system would shut down in response. However, we show in the present study that at 15 weeks of age, the average age at which Cycle Absent mice stop cycling, there is no difference in body fat percentage (Figure 2B). However, there was a significant drop in body fat within Cycle Absent animals between 12 and 15 weeks of age (Figure 2B), so perhaps there is an intra-animal threshold for minimum body fat for reproductive function.

While tumor burden might explain the differences between Cycle Present and Cycle Absent animals, it is unclear how ovariectomy caused female *Apc*$^{Min/+}$ mice to gain body weight (Figure 3B), gain muscle mass (Table 2), and improve running endurance (Figure 3E) without a change in food intake (Table 2, Figure 3G). It is known that estrogen modulates energy intake and substrate utilization [102], so these findings went against our original hypothesis. However, several reports have noted relationships between ovariectomy and autophagy; it is possible that the increased autophagy seen in several tissues with OVX [159] allows for increased turnover of damaged proteins in muscle and systemically, allowing for healthier muscle and greater function.

This study aimed to determine the relationship between inflammation, ovarian function, and cancer cachexia progression. It appears that the advent of ovarian dysfunction (Cycle Absent mice) does not increase circulating inflammation *per se*, but induces higher sensitivity to baseline inflammation at the tissue level. OVX seems to decrease systemic inflammation, which is in contrast to our original hypothesis. Further work must be done in order to elucidate remaining questions surrounding the cessation of estrus cycling with disease and the beneficial effects of OVX.

4.6 Acknowledgements

The authors would like to acknowledge Dr. Udai Singh and Mr. Benny Davidson from the USC School of Medicine's Instrument Resource Facility for assistance with ovarian histology, microscopy, and use of their equipment. This work was supported by National Institutes of Health grant # NCI-R01CA121249A501 (JAC), National Institutes of Health Grant P20 RR-017698 from the National Center for Research, and by the USC Behavioral-Biomedical Interface Program, which is a NIGMS/NIH-T32 supported program. Contents of this publication are solely the responsibility of the authors and do not necessarily represent the official views of the NIGMS or NIH.

Table 4.1: Characteristics of 18-week female *Apc*$^{Min/+}$ mice stratified by ovarian status. Hindlimb muscle mass comprises right gastrocnemius, plantaris, soleus, tibialis anterior, extensor digitorum longus, and quadricep. N, number; g, grams; BW, body weight; pg, picograms; ml, milliliters; mg, milligrams; mm, millimeters. Measurements with superscript lowercase letters indicate significant difference between all groups found by one-way ANOVA; groups with same letters are significantly different from one another for that measurement (Tukey *post hoc*). Significance set at $p<0.05$ for all comparisons.

		Apc$^{Min/+}$	
	B6	**Cycle Present**	**Cycle Absent**
N	7	15	9
BW at 18w (g)	20.2 ± 0.3^{a}	19.6 ± 0.2^{b}	17.4 ± 0.6^{ab}
Tibia length (mm)	16.5 ± 0.1	16.3 ± 0.1	16.2 ± 0.1
Inguinal fat (mg)	116 ± 10^{a}	170 ± 18^{b}	3 ± 2^{ab}
Hindlimb Muscle Mass (mg)	298 ± 13^{a}	271 ± 8^{b}	194 ± 11^{ab}
Hindlimb muscle mass/Tibia length	18.1 ± 0.8^{a}	16.7 ± 0.6^{b}	12.0 ± 0.7^{ab}
Estrus cycle present (%)	100%	100%	0%
% of animals cachectic	0%	0%	89%
Spleen (mg)	87 ± 6^{ab}	243 ± 28^{ac}	372 ± 35^{bc}
Heart (mg)	91 ± 4^{a}	96 ± 2^{b}	121 ± 6^{ab}
Heart/BW	4.5 ± 0.2^{a}	4.9 ± 0.1^{b}	7.0 ± 0.4^{ab}
Food intake (g/day) 12 w	3.7 ± 0.1	3.5 ± 0.2	3.5 ± 0.2
Food intake (g/day) 18w	3.5 ± 0.2	3.4 ± 0.2	3.1 ± 0.3
Distance run to fatigue (m) 12 w	1354 ± 173	1155 ± 175	1239 ± 250
Distance run to fatigue (m) 18w	1669 ± 243^{ab}	955 ± 127^{a}	383 ± 204^{b}

Table 4.2: Characteristics of 18-week female C57BL/6 and *Apc*$^{Min/+}$ mice with ovaries intact or treated by ovariectomy. Mice were ovariectomized at 11 weeks and sacrificed at 18 weeks. OVX, ovariectomy; IL-6, interleukin-6; N, number; 15w, 15 weeks of age; BW, body weight; g, grams; mm, millimeters; mg, milligrams; TL, tibia length. * indicates main effect of OVX; # indicates main effect of genotype; & indicates interaction of OVX x genotype (determined by two-way ANOVA). Means with same superscript lowercase letters indicates significant difference between columns (Tukey *post hoc*, $p<0.05$). ^ indicates significant difference between *Apc*$^{Min/+}$ intact and OVX groups ($p<0.05$, Student's t-test).

	B6		*Apc*$^{Min/+}$		
	Intact	**OVX**	**Intact**	**OVX**	
N	7	5	24	10	
BW at 18w (g)	20.2 ± 0.3	21.9 ± 0.7	18.8 ± 0.3	21.0 ± 0.3^	*#
Inguinal fat (mg)	116 ± 10	168 ± 18	108 ± 20	111 ± 9	
Tibia length (mm)	16.5 ± 0.1	16.6 ± 0.2	16.3 ± 0.1	16.6 ± 0.1^	
Hindlimb muscle mass (mg)	298 ± 13	277 ± 10	242 ± 10	278 ± 10^	
HMM/Tibia length	18.1 ± 0.8	16.7 ± 0.6	14.9 ± 0.6	16.8 ± 0.5	
% mice estrus cycle present	100%	0%	64%	0%	
Spleen (mg)	87 ± 6	90 ± 9	291 ± 25	223 ± 23	#
Uterus (mg)	100 ± 9^{abc}	36 ± 7^{b}	45 ± 4^{a}	28 ± 2^{c}^	*#&
Heart (mg)	91 ± 4	114 ± 5	106 ± 4	108 ± 3	*
Heart/BW	4.5 ± 0.2	5.2 ± 0.1	5.7 ± 0.3	5.2 ± 0.2	
Food intake 18w	3.1 ± 0.2	4.5 ± 0.4	3.3 ± 0.3	3.5 ± 0.1	*#

Table 4.3: Circulating levels of cytokines in female B6 and *Apc*$^{Min/+}$ mice with differing ovarian function statuses. Mice from Experiment 1 cohort as well as additional Cycle Present and Cycle Absent mice were used for this assay (*Experiment 1*). All measurements shown are pg/ml. IL-1β, interleukin-1β; IL-10, interleukin-10; IL-17, interleukin-17; IFN-γ, interferon γ; MCP-1, monocyte chemoattractant protein-1; RANTES, regulated on activation, normal T expressed and secreted / CCL5; LIF, Leukemia-inhibiting factor; TNFα, tumor necrosis factor α; M-CSF, macrophage colony stimulating factor. P-value determined by one-way ANOVA. Groups within the same row with same superscript lowercase letters indicate significant difference between groups, determined by Tukey *post hoc*. Significance was set at $p<0.05$ for all comparisons.

		ApcMin/+			
	B6	**Cycle Present**	**Cycle Absent**	**OVX**	**p-value**
N	5	11	14	7	
IL-1b	281.3 ± 5.9 pg/ml	313.9 ± 46.1 pg/ml	232.2 ± 22.6 pg/ml	227.8 ± 5.5 pg/ml	0.177
IL-17	21.4 ± 0.7 pg/ml	21.2 ± 5.7 pg/ml	17.6 ± 1.9 pg/ml	14.5 ± 0.8 pg/ml	0.603
LIF	3.2 ± 0.6 pg/ml	4.7 ± 1.3 pg/ml	8.3 ± 4.2 pg/ml	13.7 ± 12.0 pg/ml	0.757
TNFa	116.2 ± 37.1 pg/ml	368.4 ± 157.7 pg/ml	173.3 ± 116.7 pg/ml	17.99 ± 12.0 pg/ml	0.314
VEGF	33.7 ± 3.3 pg/ml	53.3 ± 16.2 pg/ml	39.4 ± 11.8 pg/ml	32.9 ± 20.1 pg/ml	0.816

Table 4.4: Descriptive characteristics of female ApcMin/+ mice treated by ovariectomy, IL-6 overexpression, or both. Mice were ovariectomized at 11 weeks, electroporated with IL-6 overexpression vector at 13 weeks, and sacrificed at 15 weeks. OVX, ovariectomy; IL-6, interleukin-6; N, number; 15w, 15 weeks of age; BW, body weight; g, grams; mm, millimeters; mg, milligrams; TL, tibia length. * indicates main effect of OVX; # indicates main effect of IL-6; & indicates interaction of OVX x IL-6 (determined by two-way ANOVA). Means with same superscript lowercase letters indicates significant difference between columns (Tukey *post hoc*, $p<0.05$)

	***Apc*$^{Min/+}$**				
	Control	**+IL6**	**OVX**	**OVX + IL-6**	
N	**13**	**10**	**10**	**8**	
15w BW (g)	18.3 ± 0.6^{a}	17.6 ± 0.4^{b}	$21.4 \pm 0.5^{a,b,c}$	18.5 ± 0.9^{c}	*#&
Tibia length (mm)	16.2 ± 0.1	15.9 ± 0.2	16.6 ± 0.1	16.3 ± 0.1	*#
Inguinal fat (mg)	120 ± 29	49 ± 24	85 ± 15	63 ± 21	
Hindlimb muscle mass (mg)	221 ± 15	199 ± 10	248 ± 8	206 ± 17	#
HMM/TL	13.6 ± 0.9	12.5 ± 0.6	14.9 ± 0.5	12.6 ± 1.0	#
% mice estrus cycle present	70%	100%	0%	0%	
Spleen (mg)	197 ± 38	393 ± 47	216 ± 29	304 ± 34	#
Uterus (mg)	$46 \pm 5^{a,b,c}$	29 ± 4^{a}	28 ± 3^{b}	27 ± 3^{c}	*#&
Heart (mg)	93 ± 3	102 ± 6	108 ± 2	109 ± 6	*
Heart/BW	5.2 ± 0.4	5.8 ± 0.4	5.1 ± 0.1	6.1 ± 0.6	#

4.7 Figure Legends

Figure 4.1: Estrus cycle cessation with cachexia (Experiment 1): A) Survival curve showing age of cycle cessation in Cycle Absent mice. At 18 weeks, n=9 mice were classified as "Cycle Absent" and n=15 mice were classified as "Cycle Present" B) Hematoxylin and eosin staining of ovaries taken from B6, Cycle Present, and Cycle Absent mice; shown at 400x and 1000x. Black arrows point to atretic (dead/dying) follicles in Cycle Absent ovary. C) Anti-Müllerian Hormone (AMH) gene expression in ovaries of B6 and $Apc^{Min/+}$ mice stratified into "Cycle Present" and "Cycle Absent." Significant differences between groups were determined by one-way ANOVA ($p<0.0001$). Cycle Absent significantly differed from both B6 and Cycle Present (Tukey *post hoc*, $p<0.0001$ for each comparison). D) Uterine weight of B6, Cycle Present, and Cycle Absent mice. Significant differences between groups were determined by one-way ANOVA ($p<0.0001$). All groups were significantly different from one another ($p<0.001$ for each comparison, Tukey post hoc). * indicates significant difference from B6; $ indicates significant difference from Cycle Present; # indicates significant difference from Cycle Absent; significance for all measures was set at $p<0.05$.

Figure 4.2: Morphological and functional changes with disease-related cessation of ovarian function (Experiment 1): A) Body weights (grams) at 12, 15, and 18 weeks in female $Apc^{Min/+}$ mice stratified into Cycle Present and Cycle Absent groups. Main effect of age ($p<0.0001$) and interaction of age x cycle presence ($p<0.0001$) determined by two-way repeated measures ANOVA. All Cycle Absent timepoints differ; all Cycle Present timepoints differ (Sidak's Multiple Comparisons test; $p<0.01$ for each comparison). B) Body fat percentages at 12, 15, and 18 weeks of age in Cycle Present and Cycle Absent female $Apc^{Min/+}$ mice . Main effect of age ($p=0.0002$), main effect of cycle presence ($p=0.0006$), and interaction of age x cycle presence ($p=0.0067$) determined by two-way repeated measures ANOVA. Cycle Absent-12 differs from Cycle Absent-15 ($p<0.05$, Sidak's multiple comparison test). Cycle Absent-12 differs from Cycle Absent-18 ($p<0.001$, Sidak's multiple comparison test). Cycle Present-18 and Cycle Absent-18 significantly differ ($p<0.001$, Sidak's multiple comparisons test). C) Voluntary cage activity at 12, 15, and 18 weeks of age in Cycle Present and Cycle Absent female $Apc^{Min/+}$ mice. Main effect of age ($p=0.0015$) and cycle presence (0.045) determined by two-way repeated measures ANOVA. Cycle Present and Cycle Absent groups trended towards difference at 18 weeks ($p=0.056$), determined by pre-planned Student's t-test. Dotted line represents average week of estrus cycle cessation. + indicates significant difference between all cycle absent timepoints; % indicates significant difference between all cycle present timepoints; $ indicates significant difference between 12-week cycle absent and 15-week cycle; # indicates significant difference between 12-week cycle absent and 18-week cycle absent; Significance was set at $p<0.05$ for all measures.

Figure 4.3: Morphological and functional changes with ovariectomy (Experiment 2): A) Timeline of experimental procedures for Experiment 2. Mice were ovariectomized at 11 weeks of age and followed until sacrifice at 18 weeks of age. B) Percentage body weight change in Cycle Absent and OVX female $Apc^{Min/+}$ mice from 11-18 weeks of age. Cycle Absent and OVX female $Apc^{Min/+}$ mice groups significantly differ ($p<0.05$,

Student's t-test). C) Percent body fat at 18 weeks of age in Cycle Absent and OVX female *Apc*$^{Min/+}$ mice. Cycle Absent and OVX female *Apc*$^{Min/+}$ mice groups significantly differ ($p<0.05$, Student's t-test). D) Lean mass change (grams) from 12-18 weeks of age in Cycle Absent and OVX female *Apc*$^{Min/+}$ mice. P=0.65 between groups. E) Distance run to fatigue (meters) in Cycle Absent and OVX female *Apc*$^{Min/+}$ mice. Cycle Absent and OVX female *Apc*$^{Min/+}$ mice groups significantly differ ($p<0.05$, Student's t-test). F) Voluntary cage activity at 18 weeks of age in Cycle Absent and OVX female *Apc*$^{Min/+}$ mice. Cycle Absent and OVX female *Apc*$^{Min/+}$ mice groups significantly differ ($p<0.05$, Student's t-test). G) Food intake (grams/day) at 18 weeks of age in Cycle Absent and OVX female *Apc*$^{Min/+}$ mice. Horizontal dotted lines indicate average B6 measurement. * indicates significant difference between Cycle Absent and OVX groups ($p<0.05$), determined by Student's t-test. Significance was set at $p<0.05$ for all measures.

Figure 4.4: Morphological and functional changes with ovariectomy and IL-6 overexpression (Experiment 3): A) Timeline of experimental procedures for Experiment 3. B) Percentage body weight change between 11-15 weeks of age in female *Apc*$^{Min/+}$ mice treated with OVX, IL-6 overexpression, or both. A main effect of OVX ($p=0.0012$) and a main effect of IL-6 overexpression ($p=0.017$) were determined by two-way ANOVA. OVX +vector group was significantly different from all other groups ($p<0.05$), determined by pre-planned Student's t-test. C) Percentage body fat between 11-15 weeks of age in female *Apc*$^{Min/+}$ mice. No differences between groups were determined by two-way ANOVA. D) Lean mass change (grams) from 11-15 weeks of age in female *Apc*$^{Min/+}$ mice treated with OVX, IL-6 overexpression, or both. A trend for a main effect of IL-6 ($p=0.052$) and an interaction between OVX and IL-6 ($p=0.0093$) were detected by two-way ANOVA. OVX group significantly differed from control *Apc*$^{Min/+}$ and OVX+ IL-6 groups ($p<0.05$), determined by Tukey *post hoc.* * indicates difference from control ApcMin/+ group; ^ indicates significant difference from sham + IL-6 group; $ indicates significant difference from OVX+IL-6 group. Significance was set at $p<0.05$ for all measures.

Figure 4.5: **Effect of loss of ovarian function and IL-6 overexpression on tumor burden and circulating IL-6 signaling:** A) Number of tumors in the small intestine and colon of estrus cycle present, estrus cycle absent, and OVX female *Apc*$^{Min/+}$ mice. Significant difference between groups ($p=0.0002$) determined by one-way ANOVA. Estrus cycle absent is significantly different from estrus cycle present ($p<0.001$) and from OVX ($p<0.01$) determined by Tukey *post hoc*. All groups differ significantly from B6, determined by Student's t-test ($p<0.05$ for each comparison). B) Number of tumors in the small intestine and colon of control, OVX, IL-6 overexpression, and OVX+IL-6 female *Apc*$^{Min/+}$ mice. Main effect of OVX was determined by two-way ANOVA ($p=0.0492$). C) Plasma IL-6 levels (pg/ml) in estrus cycle present, estrus cycle absent, and OVX female *Apc*$^{Min/+}$ mice. One-way ANOVA detected no difference between groups ($p=0.091$). Estrus cycle absent significantly differs from OVX ($p=0.0003$), determined by pre-planned Student's t-test. All groups differ significantly from B6, determined by Student's t-test ($p<0.05$ for each comparison). D) Plasma IL-6 levels (pg/ml) in control, OVX, IL-6 overexpression, and OVX+IL-6 female *Apc*$^{Min/+}$ mice. A main effect of IL-6 overexpression was determined by two-way ANOVA ($p<0.01$). E) Soluble IL-6 receptor plasma levels (ng/ml) in estrus cycle present, estrus cycle absent, and OVX female

Apc$^{Min/+}$ mice. No differences were determined by one-way ANOVA; however, Cycle Absent levels are significantly lower than Cycle Present levels by pre-planned Student's t-test (p=0.050). F) Soluble IL-6 receptor plasma levels (ng/ml) in control, OVX, IL-6 overexpression, and OVX+IL-6 female *Apc*$^{Min/+}$ mice. A main effect of IL-6 overexpression was determined by two-way ANOVA ($p<0.05$). * indicates significant difference from estrus cycle present; # indicates significant difference from OVX; & indicates significant difference from B6. Level of significance was set at $p<0.05$ for all measures.

Figure 4.6: Effect of Cachexia and Loss of Ovarian Function on Circulating Inflammatory Cytokines: A) Plasma leptin levels (pg/ml) in Cycle present, Cycle absent, and OVX *ApcMin/*+ mice. Significant difference between groups was indicated by one-way ANOVA (p=0.005); Cycle Absent was significantly lower than B6 ($p<0.05$, Tukey post hoc). B) Plasma Interferon-gamma (IFNγ) levels (pg/ml) in C57BL/6 (B6), female *ApcMin/*+, and OVX *ApcMin/*+ mice. Significant difference between groups was determined by one way ANOVA (p=0.0012). *ApcMin/*+ and OVX *ApcMin/*+ mice both differ from B6 ($p<0.001$ and $p<0.05$, respectively, Tukey *post hoc*). C) Plasma monocyte chemoattractant protein-1 (MCP-1) levels (pg/ml) in C57BL/6 (B6), female *ApcMin/*+, and OVX *ApcMin/*+ mice. Significant differences between groups were determined by one-way ANOVA (p=0.0002). *ApcMin/*+ and OVX *ApcMin/*+ groups both differ from B6 ($p<0.001$ and $p<0.01$, respectively, Tukey *post hoc*). D) Plasma "Regulated on Activation, Normal T Expressed and Secreted" (RANTES) levels (pg/ml) in Cycle Present and Cycle Absent *ApcMin/*+ mice. A significant difference between the two was determined by Student's t-test (p=0.017). E) (left) Plasma interleukin-10 (IL-10) levels (pg/ml) in C57BL/6 (B6), female *ApcMin/*+, and OVX *ApcMin/*+ mice. Significant differences between groups were determined by one-way ANOVA (p=0.0046). *ApcMin/*+ and OVX *ApcMin/*+ each differ from B6 level ($p<0.05$ and $p<0.01$, respectively, Tukey *post hoc*). (right) Plasma IL-10 levels (pg/ml) in Cycle Present and Cycle Absent *ApcMin/*+ mice. A significant difference between the two was determined by Student's t-test (p=0.010) F) (left) Plasma macrophage colony stimulating factor (M-CSF) levels (pg/ml) in C57BL/6 (B6), female *ApcMin/*+, and OVX *ApcMin/*+ mice. Significant difference between groups were determined by one-way ANOVA (p=0.037). OVX *ApcMin/*+ differed significantly from control *ApcMin/*+ ($p<0.05$, Tukey *post hoc*). (right) Plasma M-CSF levels (pg/ml) in Cycle Present and Cycle Absent ApcMin/+ mice. A significant difference was determined by Student's t-test (p=0.023). & indicates significant difference from B6; * indicates significant difference from Cycle Present; # indicates significant difference from control *ApcMin/*+. Significance was set at $p<0.05$ for all measures.

Figure 4.7: Changes in inflammatory signaling with loss of ovarian signaling and IL-6 overexpression: A) Muscle IL-6 mRNA in Cycle Present, Cycle Absent, and OVX female *Apc*$^{Min/+}$ mice. A significant difference between groups was determined by one-way ANOVA (p=0.0138). Cycle Absent is significantly different from all other groups ($p<0.05$ for each comparison, Tukey *post hoc*) B) Muscle IL-6 mRNA in control, OVX, IL-6 overexpression, and OVX+IL-6 female *Apc*$^{Min/+}$ mice. No differences were determined by two-way ANOVA. C) Muscle TGFβ mRNA in Cycle Present, Cycle Absent, and OVX groups. A significant difference between groups was determined by

one-way ANOVA ($p=0.0448$). OVX significantly differs from Cycle Present ($p<0.05$, Tukey *post hoc*). D) Muscle TGFβ mRNA in control, OVX, IL-6 overexpression, and OVX+IL-6 groups. No differences were determined by two-way ANOVA. E) Muscle TNFα mRNA in Cycle Present, Cycle Absent, and OVX groups. A significant difference between groups was determined by one-way ANOVA ($p=0.005$). Cycle Absent is significantly different from Cycle Present and OVX ($p<0.05$ and $p<0.01$, respectively, Tukey *post hoc*). F) Muscle TNFα mRNA in control, OVX, IL-6 overexpression, and OVX+IL-6 groups. No differences were determined by two-way ANOVA. *indicates significant difference from Cycle Present; # indicates significant difference from OVX; $ indicates significant difference from C57BL/6 ($p<0.05$).

Figure 4.8: Changes in muscle inflammatory receptors with loss of ovarian function and IL-6 overexpression: A) Muscle IL-6r mRNA in Cycle Present, Cycle Absent, and OVX groups. A significant difference between groups was determined by one-way ANOVA ($p<0.0001$). Cycle Absent is significantly different from all other groups ($p<0.001$ for each comparison; Tukey *post hoc*). B) Muscle IL-6r mRNA in control, OVX, IL-6 overexpression, and OVX+IL-6 groups. An interaction of OVX x IL-6 was determined by two-way ANOVA ($p=0.0459$). No differences between individual groups were determined by Tukey *post hoc*. C) Muscle TLR4 mRNA in Cycle Present, Cycle Absent, and OVX groups. A significant difference between groups was determined by one-way ANOVA ($p<0.0001$). Cycle Absent is significantly different from all other groups ($p<0.001$ for each comparison; Tukey *post hoc*). D) Muscle TLR4 mRNA in control, OVX, IL-6 overexpression, and OVX+IL-6 groups. No differences were determined by two-way ANOVA. * indicates significant difference from Cycle Present; # indicates significant difference from OVX; $ indicates significant difference from B6. Significance was set at $p<0.05$ for all measures.

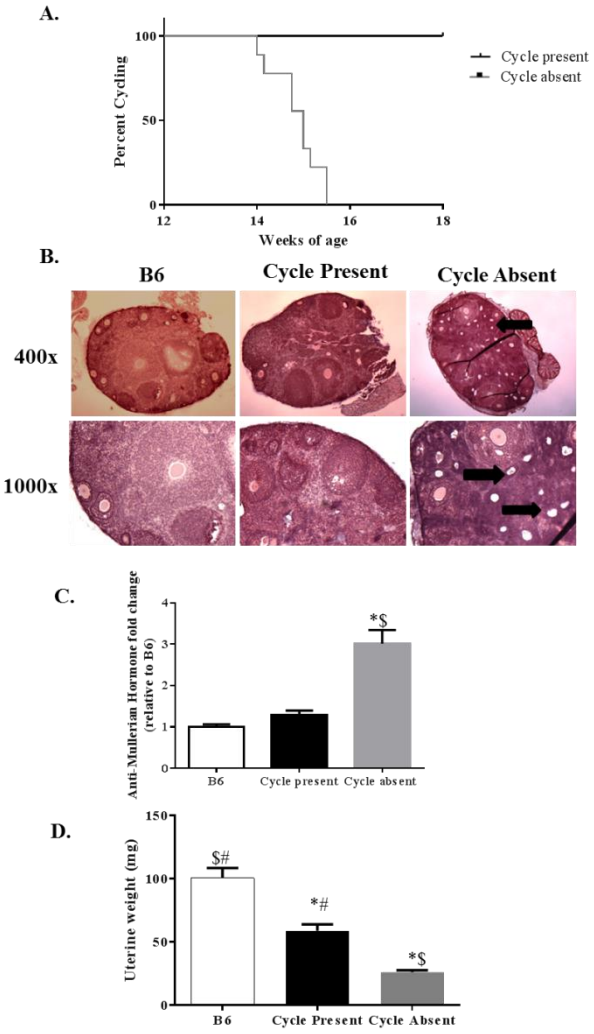

Figure 4.1: Estrus cycle cessation with cachexia (Experiment 1): A) Survival curve showing age of cycle cessation in Cycle Absent mice. At 18 weeks, n=9 mice were classified as "Cycle Absent" and n=15 mice were classified as "Cycle Present" B) Hematoxylin and eosin staining of ovaries taken from B6, Cycle Present, and Cycle Absent mice; shown at 400x and 1000x. Black arrows point to atretic (dead/dying) follicles in Cycle Absent ovary. C) Anti-Müllerian Hormone (AMH) gene expression in ovaries of B6 and $Apc^{Min/+}$ mice stratified into "Cycle Present" and "Cycle Absent." Significant differences between groups were determined by one-way ANOVA ($p<0.0001$). Cycle Absent significantly differed from both B6 and Cycle Present (Tukey *post hoc*, $p<0.0001$ for each comparison). D) Uterine weight of B6, Cycle Present, and Cycle Absent mice. Significant differences between groups were determined by one-way ANOVA ($p<0.0001$). All groups were significantly different from one another ($p<0.001$ for each comparison, Tukey post hoc). * indicates significant difference from B6; $ indicates significant difference from Cycle Present; # indicates significant difference from Cycle Absent; significance for all measures was set at $p<0.05$.

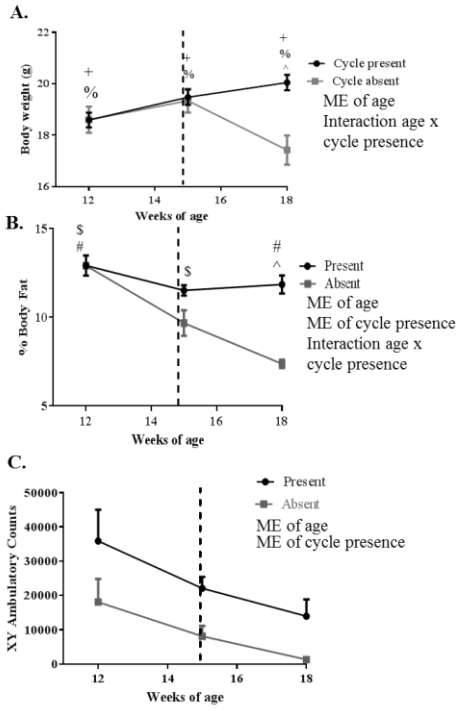

Figure 4.2: Morphological and functional changes with disease-related cessation of ovarian function (Experiment 1): A) Body weights (grams) at 12, 15, and 18 weeks in female *Apc*$^{Min/+}$ mice stratified into Cycle Present and Cycle Absent groups. Main effect of age ($p<0.0001$) and interaction of age x cycle presence ($p<0.0001$) determined by two-way repeated measures ANOVA. All Cycle Absent timepoints differ; all Cycle Present timepoints differ (Sidak's Multiple Comparisons test; $p<0.01$ for each comparison). B) Body fat percentages at 12, 15, and 18 weeks of age in Cycle Present and Cycle Absent female *Apc*$^{Min/+}$ mice . Main effect of age ($p=0.0002$), main effect of cycle presence ($p=0.0006$), and interaction of age x cycle presence ($p=0.0067$) determined by two-way repeated measures ANOVA. Cycle Absent-12 differs from Cycle Absent-15 ($p<0.05$, Sidak's multiple comparison test). Cycle Absent-12 differs from Cycle Absent-18 ($p<0.001$, Sidak's multiple comparison test). Cycle Present-18 and Cycle Absent-18 significantly differ ($p<0.001$, Sidak's multiple comparisons test). C) Voluntary cage activity at 12, 15, and 18 weeks of age in Cycle Present and Cycle Absent female *Apc*$^{Min/+}$ mice. Main effect of age ($p=0.0015$) and cycle presence (0.045) determined by two-way repeated measures ANOVA. Cycle Present and Cycle Absent groups trended towards difference at 18 weeks ($p=0.056$), determined by pre-planned Student's t-test. Dotted line represents average week of estrus cycle cessation. + indicates significant difference between all cycle absent timepoints; % indicates significant difference between all cycle present timepoints; $ indicates significant difference between 12-week cycle absent and 15-week cycle; # indicates significant difference between 12-week cycle absent and 18-week cycle absent; Significance was set at $p<0.05$ for all measures.

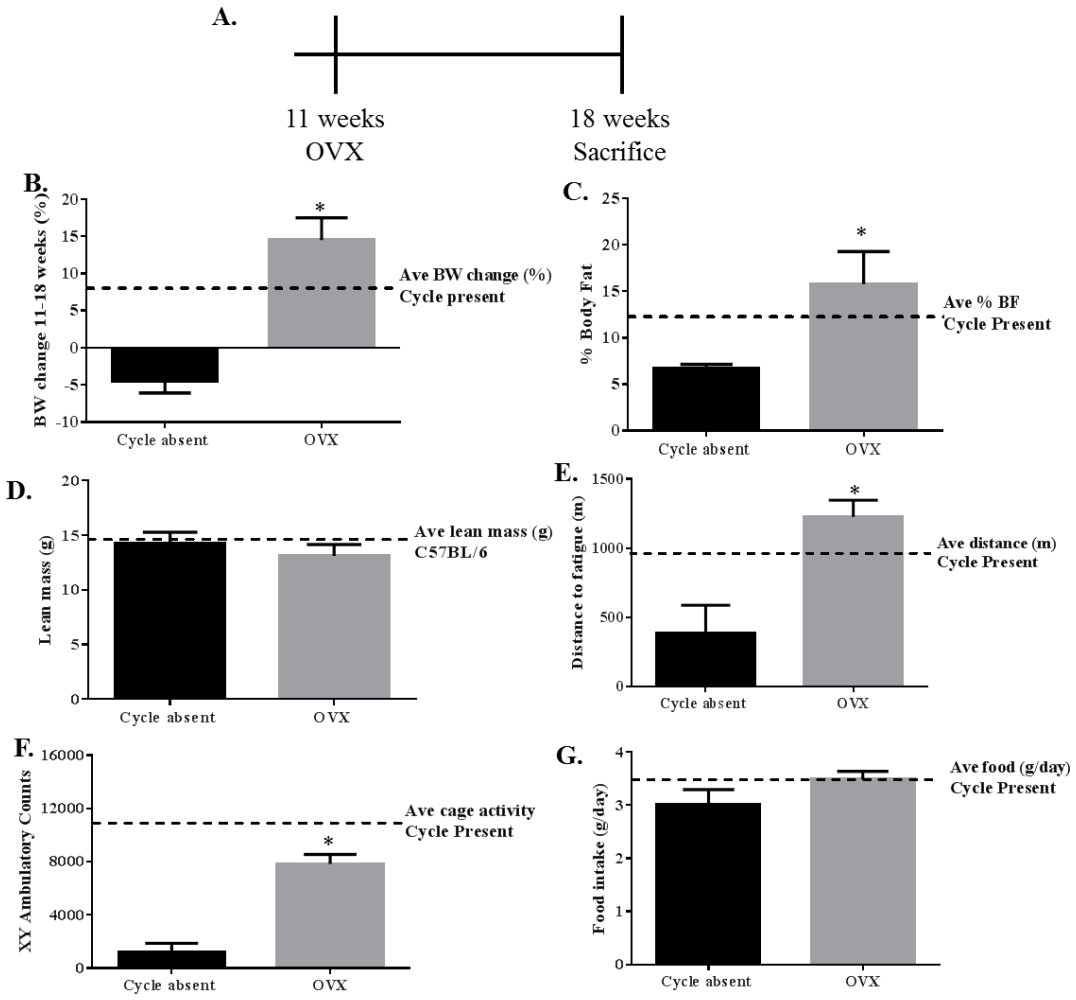

Figure 4.3: Morphological and functional changes with ovariectomy (Experiment 2): A) Timeline of experimental procedures for Experiment 2. Mice were ovariectomized at 11 weeks of age and followed until sacrifice at 18 weeks of age. B) Percentage body weight change in Cycle Absent and OVX female *Apc*$^{Min/+}$ mice from 11-18 weeks of age. Cycle Absent and OVX female *Apc*$^{Min/+}$ mice groups significantly differ ($p<0.05$, Student's t-test). C) Percent body fat at 18 weeks of age in Cycle Absent and OVX female *Apc*$^{Min/+}$ mice. Cycle Absent and OVX female *Apc*$^{Min/+}$ mice groups significantly differ ($p<0.05$, Student's t-test). D) Lean mass change (grams) from 12-18 weeks of age in Cycle Absent and OVX female *Apc*$^{Min/+}$ mice. P=0.65 between groups. E) Distance run to fatigue (meters) in Cycle Absent and OVX female *Apc*$^{Min/+}$ mice. Cycle Absent and OVX female *Apc*$^{Min/+}$ mice groups significantly differ ($p<0.05$, Student's t-test). F) Voluntary cage activity at 18 weeks of age in Cycle Absent and OVX female *Apc*$^{Min/+}$ mice. Cycle Absent and OVX female *Apc*$^{Min/+}$ mice groups significantly differ ($p<0.05$, Student's t-test). G) Food intake (grams/day) at 18 weeks of age in Cycle Absent and OVX female *Apc*$^{Min/+}$ mice. Horizontal dotted lines indicate average B6 measurement. * indicates significant difference between Cycle Absent and OVX groups ($p<0.05$), determined by Student's t-test. Significance was set at $p<0.05$ for all measures.

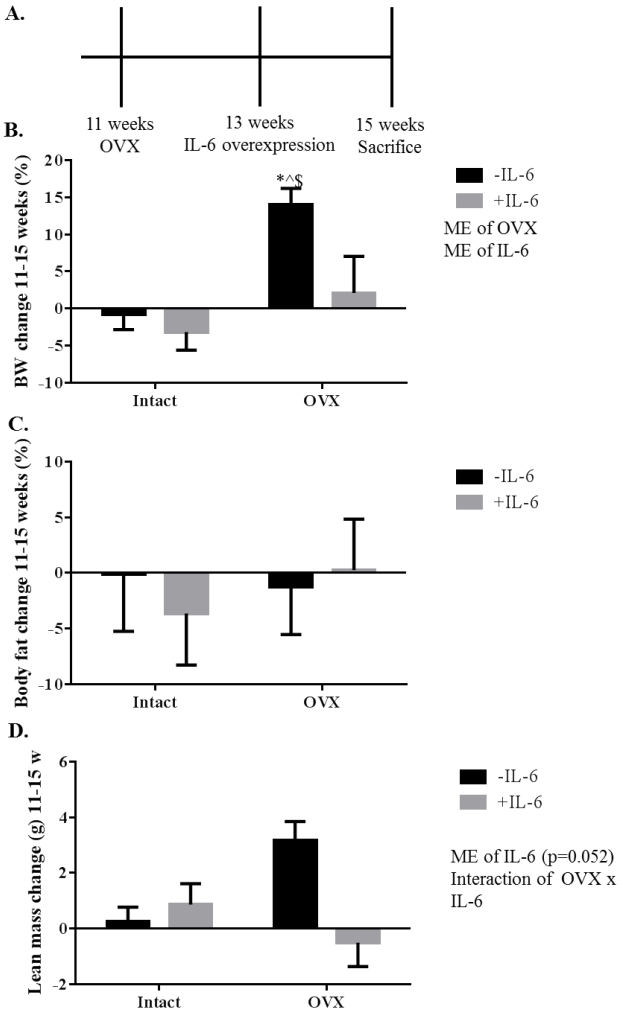

Figure 4.4: Morphological and functional changes with ovariectomy and IL-6 overexpression (Experiment 3): A) Timeline of experimental procedures for Experiment 3. B) Percentage body weight change between 11-15 weeks of age in female *Apc*$^{Min/+}$ mice treated with OVX, IL-6 overexpression, or both. A main effect of OVX ($p=0.0012$) and a main effect of IL-6 overexpression ($p=0.017$) were determined by two-way ANOVA. OVX +vector group was significantly different from all other groups ($p<0.05$), determined by pre-planned Student's t-test. C) Percentage body fat between 11-15 weeks of age in female *Apc*$^{Min/+}$ mice. No differences between groups were determined by two-way ANOVA. D) Lean mass change (grams) from 11-15 weeks of age in female *Apc*$^{Min/+}$ mice treated with OVX, IL-6 overexpression, or both. A trend for a main effect of IL-6 ($p=0.052$) and an interaction between OVX and IL-6 ($p=0.0093$) were detected by two-way ANOVA. OVX group significantly differed from control *Apc*$^{Min/+}$ and OVX+ IL-6 groups ($p<0.05$), determined by Tukey *post hoc.* * indicates difference from control ApcMin/+ group; ^ indicates significant difference from sham + IL-6 group; $ indicates significant difference from OVX+IL-6 group. Significance was set at $p<0.05$ for all measures.

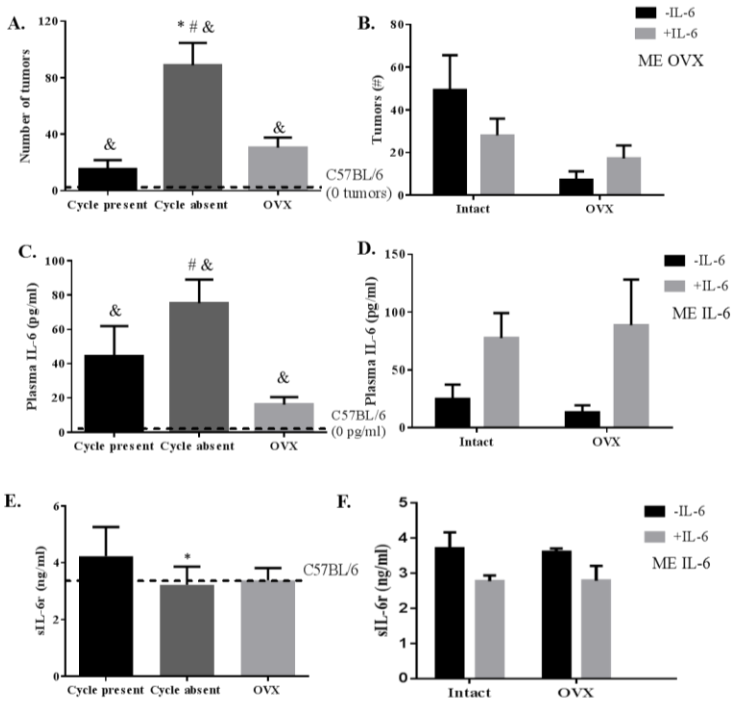

Figure 4.5: **Effect of loss of ovarian function and IL-6 overexpression on tumor burden and circulating IL-6 signaling:** A) Number of tumors in the small intestine and colon of estrus cycle present, estrus cycle absent, and OVX female $Apc^{Min/+}$ mice. Significant difference between groups (p=0.0002) determined by one-way ANOVA. Estrus cycle absent is significantly different from estrus cycle present (p<0.001) and from OVX (p<0.01) determined by Tukey *post hoc*. All groups differ significantly from B6, determined by Student's t-test (p<0.05 for each comparison). B) Number of tumors in the small intestine and colon of control, OVX, IL-6 overexpression, and OVX+IL-6 female $Apc^{Min/+}$ mice. Main effect of OVX was determined by two-way ANOVA (p=0.0492). C) Plasma IL-6 levels (pg/ml) in estrus cycle present, estrus cycle absent, and OVX female $Apc^{Min/+}$ mice. One-way ANOVA detected no difference between groups (p=0.091). Estrus cycle absent significantly differs from OVX (p=0.0003), determined by pre-planned Student's t-test. All groups differ significantly from B6, determined by Student's t-test (p<0.05 for each comparison). D) Plasma IL-6 levels (pg/ml) in control, OVX, IL-6 overexpression, and OVX+IL-6 female $Apc^{Min/+}$ mice. A main effect of IL-6 overexpression was determined by two-way ANOVA (p<0.01). E) Soluble IL-6 receptor plasma levels (ng/ml) in estrus cycle present, estrus cycle absent, and OVX female $Apc^{Min/+}$ mice. No differences were determined by one-way ANOVA; however, Cycle Absent levels are significantly lower than Cycle Present levels by pre-planned Student's t-test (p=0.050). F) Soluble IL-6 receptor plasma levels (ng/ml) in control, OVX, IL-6 overexpression, and OVX+IL-6 female $Apc^{Min/+}$ mice. A main effect of IL-6 overexpression was determined by two-way ANOVA (p<0.05). * indicates significant difference from estrus cycle present; # indicates significant difference from OVX; & indicates significant difference from B6. Level of significance was set at p<0.05 for all measures.

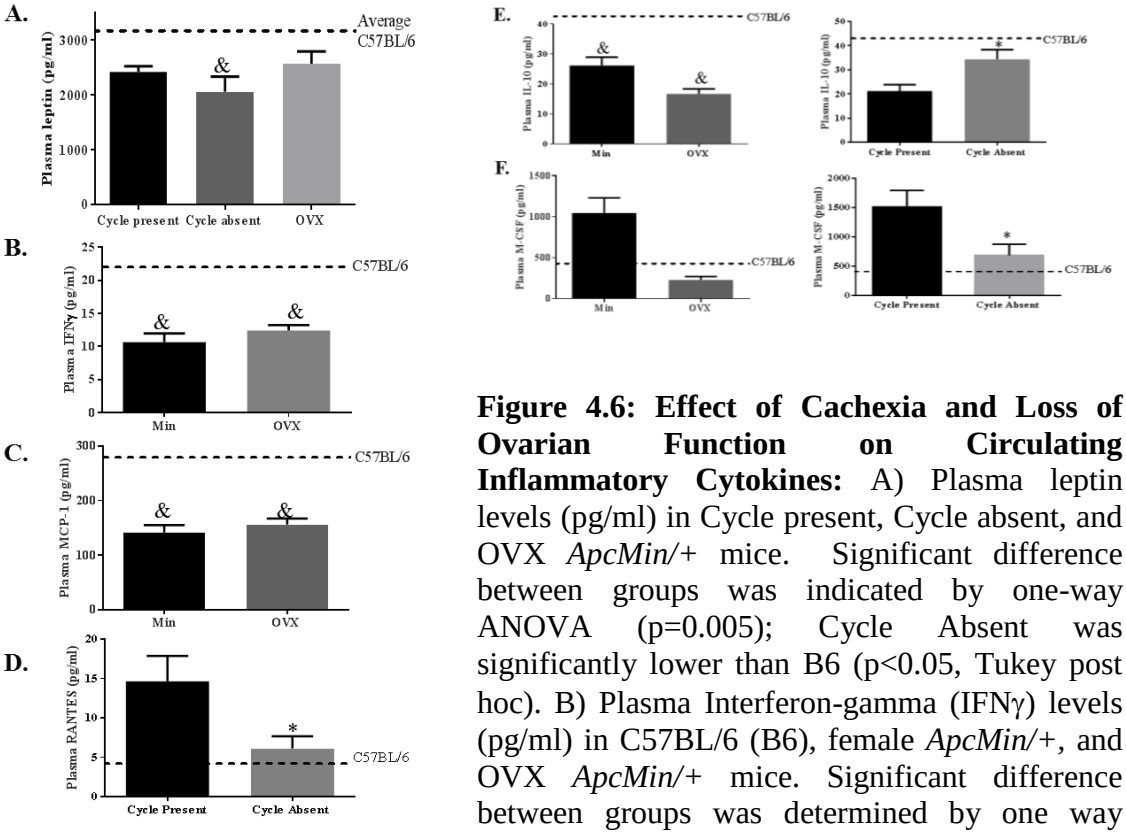

Figure 4.6: Effect of Cachexia and Loss of Ovarian Function on Circulating Inflammatory Cytokines: A) Plasma leptin levels (pg/ml) in Cycle present, Cycle absent, and OVX *ApcMin/*+ mice. Significant difference between groups was indicated by one-way ANOVA (p=0.005); Cycle Absent was significantly lower than B6 (p<0.05, Tukey post hoc). B) Plasma Interferon-gamma (IFNγ) levels (pg/ml) in C57BL/6 (B6), female *ApcMin/*+, and OVX *ApcMin/*+ mice. Significant difference between groups was determined by one way ANOVA (p=0.0012). *ApcMin/*+ and OVX *ApcMin/*+ mice both differ from B6 (p<0.001 and p<0.05, respectively, Tukey *post hoc*). C) Plasma monocyte chemoattractant protein-1 (MCP-1) levels (pg/ml) in C57BL/6 (B6), female *ApcMin/*+, and OVX *ApcMin/*+ mice. Significant differences between groups were determined by one-way ANOVA (p=0.0002). *ApcMin/*+ and OVX *ApcMin/*+ groups both differ from B6 (p<0.001 and p<0.01, respectively, Tukey *post hoc*). D) Plasma "Regulated on Activation, Normal T Expressed and Secreted" (RANTES) levels (pg/ml) in Cycle Present and Cycle Absent *ApcMin/*+ mice. A significant difference between the two was determined by Student's t-test (p=0.017). E) (left) Plasma interleukin-10 (IL-10) levels (pg/ml) in C57BL/6 (B6), female *ApcMin/*+, and OVX *ApcMin/*+ mice. Significant differences between groups were determined by one-way ANOVA (p=0.0046). *ApcMin/*+ and OVX *ApcMin/*+ each differ from B6 level (p<0.05 and p<0.01, respectively, Tukey *post hoc*). (right) Plasma IL-10 levels (pg/ml) in Cycle Present and Cycle Absent *ApcMin/*+ mice. A significant difference between the two was determined by Student's t-test (p=0.010) F) (left) Plasma macrophage colony stimulating factor (M-CSF) levels (pg/ml) in C57BL/6 (B6), female *ApcMin/*+, and OVX *ApcMin/*+ mice. Significant difference between groups were determined by one-way ANOVA (p=0.037). OVX *ApcMin/*+ differed significantly from control *ApcMin/*+ (p<0.05, Tukey *post hoc*). (right) Plasma M-CSF levels (pg/ml) in Cycle Present and Cycle Absent ApcMin/+ mice. A significant difference was determined by Student's t-test (p=0.023). & indicates significant difference from B6; * indicates significant difference from Cycle Present; # indicates significant difference from control *ApcMin/*+. Significance was set at p<0.05 for all measures.

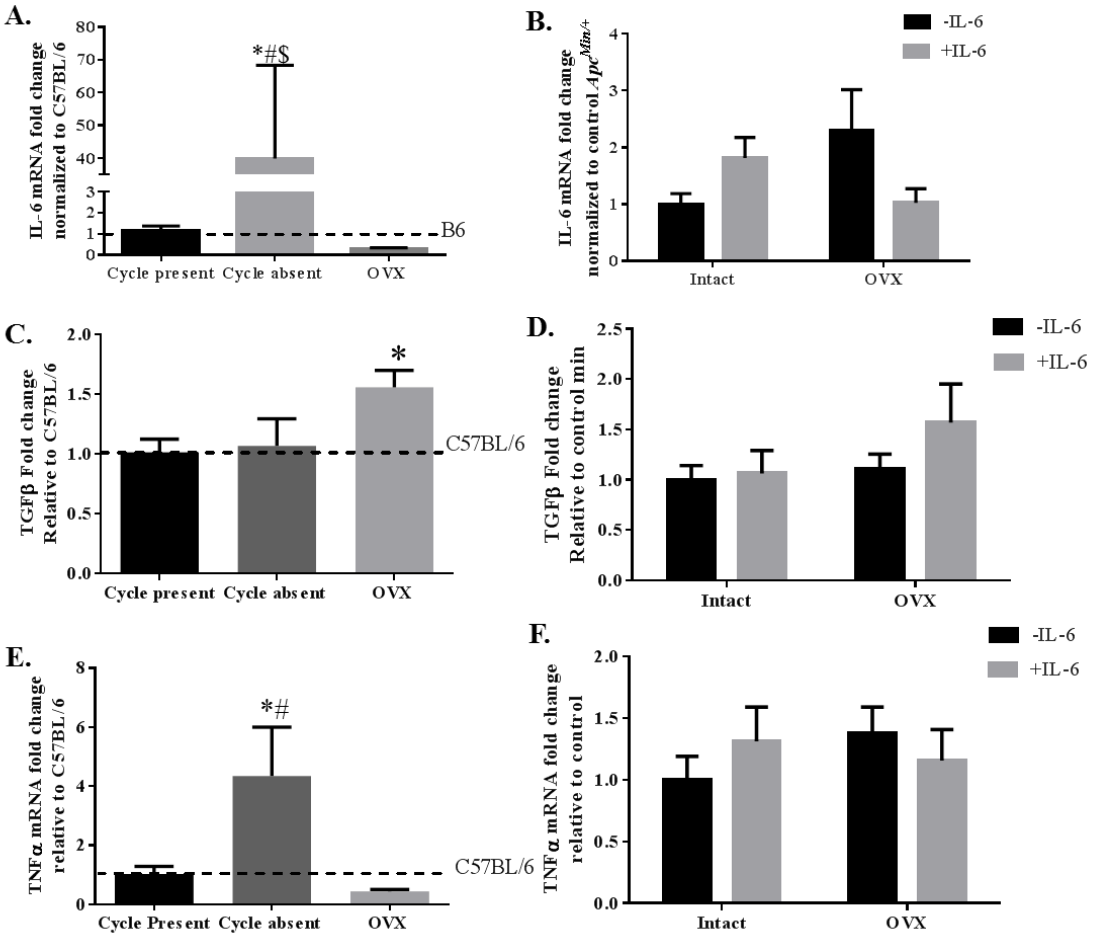

Figure 4.7: Changes in inflammatory signaling with loss of ovarian signaling and IL-6 overexpression: A) Muscle IL-6 mRNA in Cycle Present, Cycle Absent, and OVX female $Apc^{Min/+}$ mice. A significant difference between groups was determined by one-way ANOVA ($p=0.0138$). Cycle Absent is significantly different from all other groups ($p<0.05$ for each comparison, Tukey *post hoc*) B) Muscle IL-6 mRNA in control, OVX, IL-6 overexpression, and OVX+IL-6 female $Apc^{Min/+}$ mice. No differences were determined by two-way ANOVA. C) Muscle TGFβ mRNA in Cycle Present, Cycle Absent, and OVX groups. A significant difference between groups was determined by one-way ANOVA ($p=0.0448$). OVX significantly differs from Cycle Present ($p<0.05$, Tukey *post hoc*). D) Muscle TGFβ mRNA in control, OVX, IL-6 overexpression, and OVX+IL-6 groups. No differences were determined by two-way ANOVA. E) Muscle TNFα mRNA in Cycle Present, Cycle Absent, and OVX groups. A significant difference between groups was determined by one-way ANOVA ($p=0.005$). Cycle Absent is significantly different from Cycle Present and OVX ($p<0.05$ and $p<0.01$, respectively, Tukey *post hoc*). F) Muscle TNFα mRNA in control, OVX, IL-6 overexpression, and OVX+IL-6 groups. No differences were determined by two-way ANOVA. *indicates significant difference from Cycle Present; # indicates significant difference from OVX; $ indicates significant difference from C57BL/6 ($p<0.05$).

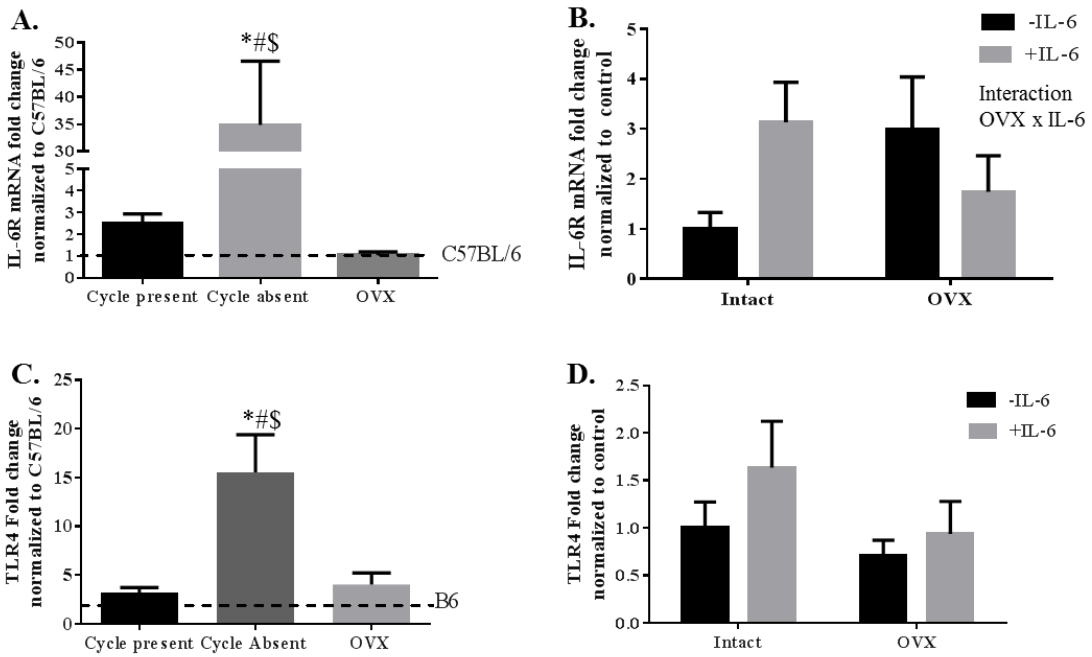

Figure 4.8: Changes in muscle inflammatory receptors with loss of ovarian function and IL-6 overexpression: A) Muscle IL-6r mRNA in Cycle Present, Cycle Absent, and OVX groups. A significant difference between groups was determined by one-way ANOVA ($p<0.0001$). Cycle Absent is significantly different from all other groups ($p<0.001$ for each comparison; Tukey *post hoc*). B) Muscle IL-6r mRNA in control, OVX, IL-6 overexpression, and OVX+IL-6 groups. An interaction of OVX x IL-6 was determined by two-way ANOVA ($p=0.0459$). No differences between individual groups were determined by Tukey *post hoc*. C) Muscle TLR4 mRNA in Cycle Present, Cycle Absent, and OVX groups. A significant difference between groups was determined by one-way ANOVA ($p<0.0001$). Cycle Absent is significantly different from all other groups ($p<0.001$ for each comparison; Tukey *post hoc*). D) Muscle TLR4 mRNA in control, OVX, IL-6 overexpression, and OVX+IL-6 groups. No differences were determined by two-way ANOVA. * indicates significant difference from Cycle Present; # indicates significant difference from OVX; $ indicates significant difference from B6. Significance was set at $p<0.05$ for all measures.

CHAPTER 5

CACHEXIA-INDUCED MUSCLE METABOLIC DYSREGULATION IN THE FEMALE[1]

[1]Hetzler KL, Fix DK, Hardee JP, Durstine JL, Carson JA. To be submitted for publication.

5.1 Abstract

Cachexia occurs secondary to chronic conditions including cancer and causes debilitating muscle wasting due to severe dysfunction in muscle metabolism and protein balance. While muscle metabolic dysfunction and protein imbalance has been characterized in the male, the processes underlying muscle wasting in the female have not been identified. The *Apc*$^{Min/+}$ mouse is genetically predisposed to develop intestinal tumors; hypogonadism is strongly associated with cachexia severity in the male, though the relationship in the female is uncertain. Ovarian endocrine functions are known to impact muscle quality and mitochondrial function; it is therefore likely that the loss of ovarian function plays a role in the etiology of female muscle wasting. The purpose of this study is to examine the relationship of ovarian function, cachexia-related pathways in the muscle, mitochondrial dysfunction, and muscle wasting during cancer cachexia progression in the female *Apc*$^{Min/+}$ mouse. Female *Apc*$^{Min/+}$ mice were tracked functionally until sacrifice at 18 weeks of age. A subset of female *Apc*$^{Min/+}$ mice were ovariectomized at 11 weeks of age and sacrificed at 18 weeks of age. A second experiment examined the effect of ovariectomy on IL-6 overexpression in female *Apc*$^{Min/+}$ mice initiating cachexia. Markers of IL-6 signaling, canonical cachexia pathways, and mitochondrial biogenesis and dynamics were examined in ovaries-intact mice of varying cachexia severity and ovariectomized mice. Several markers of canonical cachexia signaling and IL-6 signaling were increased in severely cachectic female *Apc*$^{Min/+}$ mice. Surprisingly, mitochondrial dysfunction does not seem to play a large role in cachexia in the female. In contrast, ovariectomy ameliorated much of the dysregulated signaling in female *Apc*$^{Min/+}$ mice. Ovariectomy and IL-6 overexpression

upregulated IL-6 signaling, but had little effect on mitochondrial function in initially cachectic female *Apc*$^{Min/+}$ mice. Our results indicate that loss of ovarian function has direct effects on muscle metabolism during cachexia progression that may alleviate some cachexia-associated muscle wasting. Future studies in the female will need to determine the precise mechanisms of this change.

Key Words: muscle metabolism, estrogen, ovariectomy, *Apc*$^{Min/+}$

5.2 Introduction

Cachexia is a devastating loss of muscle and fat mass that accompanies many chronic disease states [1]. Symptoms include an unintentional >5% decline in body weight as well as decreased muscle strength, fatigue, and abnormal biochemistry [105]. The muscle wasting associated with cachexia leads to weakness, loss of function, and decreased ability to heal [16]. The *Apc*$^{Min/+}$ mouse model develops intestinal polyps beginning at four weeks of age and cachexia secondary to the tumor burden [10, 20]; it has been widely used by our lab and others to study cachexia [4, 105, 117]. Cachexia is an inflammatory condition, and several inflammatory factors play roles in muscle wasting, including IL-6, TNFα, and NfKB [2].

Muscle wasting can occur by one of several protein degradation pathways; the major pathway seen in cachexia is the ubiquitin-proteasome system (UPS) [3, 16, 17, 48]. IL-6 is increased in most models of cachexia [11] and activates several downstream pathways leading to muscle wasting, including JAK/STAT3, ERK, and PI3K/Akt/FOXO3 [11]. STAT3 has been shown to be both sufficient and necessary for muscle fiber atrophy [11]; we have previously shown that this pathway is subject to sex

differences with cachexia [15]. FOXO3, usually phosphorylated and hence inactivated by PI3K/Akt, is a key regulator of the UPS [3, 17, 48]. When activated, it is able to enter the nucleus and enhance transcription of the E3 ligases MuRF1 and MAFbx/Atrogin1 [3]. These particular E3 ligases are highly associated with cancer cachexia [16, 48]; in particular, increased circulating IL-6 with cachexia can induce high levels of Atrogin-1[20]. Sex differences have been shown in MAFbx/Atrogin1 knockout rats; female muscle was unable to hypertrophy after fourteen days of functional overload, in contrast to male muscle [65]. Independent of FOXO3, p38 MAPK, putatively induced by IL-6, can also activate the UPS [17]. There are baseline difference between males and females with respect to contractile protein regulation and substrate metabolism [160]; additionally, males have higher baseline muscle protein turnover than females [161]. It is therefore probable that differences exist during muscle wasting, as well. 5'-adenosine monophosphate-activated protein kinase (AMPK) is considered a major cellular energy sensor, and has been shown to be induced with severe body weight loss during cachexia progression [14]. This provides a functional link between body weight loss, muscle mass loss, and mitochondrial function, as AMPK can activate MuRF1, Atrogin-1 [14], and induce mitochondrial biogenesis and substrate uptake [162]

In addition to protein degradation, it has been recognized over the past several years that mitochondrial dysfunction plays a major role in muscle wasting with cancer cachexia. It has previously been shown in $Apc^{Min/+}$ mice that early in cachexia progression, mitochondrial biogenesis and dynamics are dysregulated, leading to a reduction in mitochondrial content as cachexia progresses [6, 14]. PGC1α, associated with mitochondrial biogenesis, is reduced in several tumor implantation models as well

as the *Apc*$^{Min/+}$ mouse [14]. Fission and fusion, dynamic mitochondrial network processes, are induced by stimuli including exercise training, and can be pathologically dysregulated during cachexia progression, leading to fragmented and dysfunctional mitochondrial networks [14]. Mitochondrial dysfunction can lead to activation of AMPK and FOXO3, which leads to further muscle protein degradation [6]. The UPS is an ATP-dependent process; high energy demand causes lower efficiency of ATP synthesis; it is therefore thought that mitochondria are a site of energy wasting with cachexia, leading to further dysregulation of metabolism [16]. It has been shown that mitochondria isolated from cachectic muscle have decreased cytochrome c oxidase (COX) IV protein [14] and activity [16] than mitochondria from healthy muscle.

Ovarian endocrine function, particularly estrogen, has major effects on muscle metabolism and implications for muscle wasting. Estrogen can directly inhibit transcription of IL-6 [37], as well as signaling downstream of STAT3 [27]. Additionally, estrogen decreases p38 MAPK-mediated inflammation in myocytes [33]. Interestingly, and of interest to our current model, decreases in muscle expression of MuRF1 and Atrogin1 have been seen in ovariectomized (OVX) mice [87]. OVX is also associated with a dysregulation of substrate metabolism in muscle, including a downregulation of genes associated with lipid storage and lipogenesis [102]. Estrogen activates AMPK through estrogen receptor alpha (ERα) [163]; and OVX mice show a decrease in AMPK [102].

While the processes accompanying muscle wasting with cachexia have been well-characterized in male animals, a paucity of research exists in the muscle of female animals with cachexia. However, it is clear that there are differences in the etiology and

progression of cachexia between males and females [15]. The purpose for this study is to determine whether cachexia-induced skeletal muscle metabolic dysfunction is regulated by ovarian function in the female *Apc*$^{Min/+}$ mouse. The hypothesis for this study is that loss of ovarian function will increase metabolic dysregulation, leading to aggravated muscle wasting. Further, the loss of ovarian function will disinhibit IL-6 signaling, allowing for increased downstream signaling and further muscle wasting.

5.3 Methods

Animals

Female *Apc* $^{Min/+}$mice (n=75) and female C57BL/6 mice (n=12) were bred and maintained at the University of South Carolina Animal Resource Facility. *Apc*$^{Min/+}$ mice used were on a C57BL/6 background and were offspring from breeders originally purchased from Jackson Labs (Bar Harbor, ME, USA). Mice were kept on a 12:12h light/dark cycle beginning at 7:00 AM and were given unrestricted access to standard rodent chow (Harlan Teklad Rodent Diet, #8604, Harlan, Indianapolis, IN, USA). Mice were weighed weekly. Food intake was measured at 12 and 18 weeks of age. All experiments were approved by the University of South Carolina's Institutional Animal Care and Use Committee.

Experimental Design

Two experiments were performed. *Experiment 1* examined the ovarian progression during the progression of cachexia. Female *Apc*$^{Min/+}$mice (n=24) had estrus cycling measured daily from 10-18 weeks of age for determination of ovarian function. Mice were sacrificed at 18 weeks of age and stratified based on weight change between 15 and

18 weeks of age and were classified as "weight stable" (<1% body weight loss), "moderately cachectic" (1-100% body weight loss), or "severely cachectic (>10% body weight loss). In addition, a cohort (n=10) of female *Apc*$^{Min/+}$ mice were ovariectomized (OVX) at 11 weeks of age and were monitored until sacrifice at 18 weeks of age. In addition, 7 B6 females and 5 B6 females ovariectomized at 11 week of age were sacrificed at 18 weeks to act as controls. *Experiment 2* examined the interaction between ovarian function and inflammation during the initiation of cachexia. Female *Apc*$^{Min/+}$ mice underwent OVX or sham surgery at 11 weeks of age, followed by overexpression of IL-6 or an empty vector at 13 weeks of age, before sacrifice at 15 weeks of age, for four treatment groups: sham-OVX + vector (n=13), sham-OVX + IL-6 (n=10), OVX + vector (n=10), and OVX + IL-6 (n=8). In all experiments, blood, inguinal fat, hindlimb muscles, ovaries, uterus, and spleen were removed at the time of sacrifice. Hindlimb muscle mass measurements comprise the sum of left soleus, plantaris, gastrocnemius, tibialis anterior, extensor digitalis longus, and quadriceps masses.

Ovariectomy

Female *Apc*$^{Min/+}$ and C57BL/6 mice were ovariectomized at 11 weeks of age. Mice were anesthetized by ketamine/acepromazine/xylazine. Once anesthetized, the mouse was placed in a prone position on a sterile absorbent pad. The back was shaved from the caudal edge of the ribcage to the base of the tail. The shaved region was then sterilized with betadine (PDI, Orangeburg, NY, USA) and rubbing alcohol (PDI). A 2-cm dorsal midline incision was made with sterile scissors halfway between the caudal edge of the ribcage and the base of the tail. Fascia was the cleared away by blunt dissection. As second 1-cm long incision was made into the muscle wall. The ovary and surrounding fat

pad were extracted through the incision with forceps. A hemostat was closed around the distal oviduct/uterine horn to terminate blood supply to the ovary. Non-absorbable suture (AD Surgical, Sunnyvale, CA) was used to tie off the oviduct, and the ovary was removed. The uterine horn was returned to the peritoneal cavity, and absorbable suture (AD Surgical) was used to close the muscle incision. Wound clips were used to close the skin incision, and the process was repeated on the contralateral side. Mice were given 0.01 mg/kg buprenorphine (Burprenex ©, Reckitt Benckiser Pharmaceuticals, Pendergrass, GA, USA) for pain. Wound clips were removed 7 days after surgery.

IL-6 overexpression by electroporation

In vivo intramuscular electroporation of an IL-6 plasmid was used to increase circulating IL-6 levels in mice as previously described [117]. The right quadriceps muscle was used to synthesize and secrete exogenous IL-6 into circulation from the injected expression plasmid, and was not used for any analyses in the study. The gastrocnemius muscle used in the study was not subjected to electroporation. Briefly, mice were injected with 50 μg of IL-6 plasmid driven by the CMV promoter, or control plasmid (pV1J), into the right quadriceps muscle. Mice were anesthetized with a 2% mixture of isoflurane (IsoSol, VEDCO, St. Joseph, MO, USA) and oxygen (1 L/min). The leg was shaved, and a small incision was made over the quadriceps muscle. Fat was dissected away from the muscle, and the plasmid was injected in a 50 μl volume of sterile phosphate-buffered saline (PBS). A series of eight 50 ms, 100 V pulses was used to promote uptake of the plasmid into myonuclei, and the incision was closed with a wound clip.

RNA isolation and RT-PCR

RNA isolation, cDNA synthesis, and real-time PCR were performed as previously described [15, 118]. cDNA synthesis reagents from Applied Biosystems (Foster City, CA, USA) were used. Bio-Rad SsoAdvanced Universal Probes Supermix and SYBR Green Supermix were used for RT-PCR reactions (Hercules, CA). Briefly, proximal gastrocnemius muscle was homogenized in TRIzol (Life Technologies, Grand Island, NY, USA) and mixed with chloroform, then centrifuged. The RNA phase was removed and washed several times with ethanol in DEPC-treated water. cDNA was synthesized using 1 μg of RNA. RT-PCR was performed on an Applied Biosystems 7300 thermocycler. Taqman gene expression assay was used to determine Fbxo32 (Atrogin-1), Mfn1, and Fis1 mRNA expression (Life Technologies). Primer sequences are as follows:

MuRF1 (F): 5'-ATGAACTTCACGGTGGGTTT-3' (R): 5'-GGGATTGCCACAGAGGATTA-3';

PGC1a (F): 5'-GACCACAAACGATGACCCTCC-3' (R): 5'-CCTGAGAGAGACTTTGGAGGC-3'.

PGC1a IL-6r, SOCS3, gp130, and GAPDH primer sequences have been published elsewhere [15, 119].

Western blotting

Western blots were performed as described previously [106, 120]. Briefly, gastrocnemius muscle samples were run on 6-8% acrylamide gels and transferred overnight to PVDF membrane (Thermo Scientific, Waltham, MA, USA). After transfer, Ponceau stains were imaged to verify equal loading. The membrane was blocked for 1 hour in 5% milk-TBS-Tween 20, and incubated with primary antibodies at 1:2000 dilution overnight at 4^0C. After several washes, membranes were incubated with

secondary antibodies at 1:2000 dilution for 1 hour. Blots were visualized with WesternBright ECL (BioExpress, Kaysville, UT, USA). IL-6r antibody was obtained from Santa Cruz Biotech (Santa Cruz, CA). STAT3, phopho-STAT3 (Y705), anti-mouse IgG, and anti-rabbit IgG antibodies were obtained from Cell Signaling (Danvers, MA, USA).

IL-6R ELISA

Muscle IL-6r protein content was determined using a commercial IL-6Ra ELISA (DuoSet, R&D Systems, Minneapolis, MN) as previously described. Briefly, Capture Antibody was used to coat wells of a clear 96-well EIA plate (Costar, Corning, Corning, NY) and allowed to incubate overnight. The second day, plate was blocked for one hour using Reagent Diluent. Plate was washed three times. Standards and samples were added and allowed to incubate for two hours. After washes were repeated, Detection Antibody was added to wells and allowed to incubate for two hours. Washes were repeated and Streptavidin-HRP was added to wells and allowed to incubate for twenty minutes. After washes were repeated, Substrate Solution was added to wells and color was allowed to develop for twenty minutes. Stop Solution was added and plate was read at 450 nm on a BioRad iMark plate reader (Carlsbad, CA).

Statistical analysis

All results are reported as means ± SEM. Differences between B6, Weight stable, Severe, and OVX mice were determined by one-way ANOVA with Tukey *post hoc* where appropriate. Differences between Sham + vector, Sham + IL-6, OVX + vector, and OVX + IL-6 mice were determined by two-way ANOVA with Tukey *post hoc* where appropriate. Level of significance was set at 0.05 for all comparisons.

5.4 Results

Canonical cachexia-related signaling with loss of ovarian function in female $Apc^{Min/+}$ mice

Female B6 and $Apc^{Min/+}$ mice were tracked until sacrifice at 18 weeks of age; a subset of mice from each genotype underwent ovariectomy (OVX) at 11 weeks of age. Ovaries-intact $Apc^{Min/+}$ mice were classified based on body weight loss as weight stable (<1% body weight loss), moderately cachectic (1-10% body weight loss) or severely cachectic (>10% body weight loss). These mice have previously been characterized (Chapter 4). Gastrocnemius muscle weight was significantly lower in severely cachectic female $Apc^{Min/+}$ mice (>10% body weight loss) than in their weight stable (<1% body weight loss) counterparts (p=0.0006, Student's t-test) (Figure 1A), indicating that muscle wasting is a key factor in weight loss with cachexia in the female. Across ovaries-intact and OVX B6 and $Apc^{Min/+}$ females, there was a strong trend for $Apc^{Min/+}$ mice to have lower gastrocnemius mass than B6 (p=0.058, two-way ANOVA) (Figure 1A). Additionally, a pre-planned Student's t-test determined that intact $Apc^{Min/+}$ mice have lower gastrocnemius mass than intact B6 females (p=0.016) (Figure 1A). E3 ligases MuRF1 and Atrogin-1 are closely associated with cachexia-related muscle wasting [20]; these were next examined. Severely cachectic $Apc^{Min/+}$ mice had nearly a five-fold induction of *MuRF1* gene expression compared to weight stable mice (p=0.0039) (Figure 1B). However, no differences were seen across intact and OVX B6 and $Apc^{Min/+}$ mice by two-way ANOVA (Figure 1B). A pre-planned t-test between control $Apc^{Min/+}$ mice and OVX mice revealed a significantly lower expression in OVX mice (p=0.033, Student's t-test). Severely cachectic $Apc^{Min/+}$ mice also trended towards an increase in *Fbxo32* (Atrogin-1) gene expression compared to weight stable counterparts (p=0.1064) (Figure

1C), while there was a strong trend towards an effect of genotype to increase *Fbxo32* gene expression in *Apc*$^{Min/+}$ mice compared to B6 mice across intact and OVX mice (p=0.068) (Figure 1C).

Canonical cachexia-related pathways with overexpression of IL-6 in ovariectomized female Apc$^{Min/+}$ *mice*

A second set of *Apc*$^{Min/+}$ females underwent OVX and/or IL-6 overexpression to determine the effect of the interaction of ovarian function and induced IL-6 signaling on cachexia induction; these mice were sacrificed at 15 weeks and have been previously described (Chapter 4). There was a main effect of IL-6 overexpression to decrease gastrocnemius muscle mass across ovaries-intact and OVX *Apc*$^{Min/+}$ mice (p=0.044) (Figure 2A). *MuRF1* and *Fbxo32* (Atrogin-1) gene expression were examined in these mice; however, there were no differences across any of the groups for these markers (Figure 2B, C).

IL-6 receptor expression with loss of ovarian function in female Apc$^{Min/+}$ *mice*

We have previously shown IL-6 signaling in 18 week-old female *Apc*$^{Min/+}$ mice to be dysregulated (compared to the *Apc*$^{Min/+}$ male) during cachexia progression (Chapter 3) [15]. Here, we sought to determine whether this dysregulation is due to the influence of ovarian signaling. In agreement with the previous cohort of 18-week females, here we found that *IL6ra* gene expression was highly induced compared to weight stable mice (p=0.0387) (Figure 3A) [15]. No differences were seen across B6 and *Apc*$^{Min/+}$ intact and OVX mice, however; this was likely due to the wide variation across *Apc*$^{Min/+}$ mice (Figure 3A). IL-6r protein was examined in intact and OVX *Apc*$^{Min/+}$ females as well as B6 controls. There was a significant difference across groups (p=0.0003, one-way

ANOVA); severely cachectic *Apc*$^{Min/+}$ had significantly higher expression than all other groups ($p<0.01$ for each comparison, Tukey *post hoc*) (Figure 3B). Concurrently, there was a trend towards higher muscle *gp130* gene expression in severe *Apc*$^{Min/+}$ mice compared to weight stable ($p=0.085$) (Figure 3C). No differences were seen across intact and OVX B6 and *Apc*$^{Min/+}$ mice (Figure 3C). Muscle gp130 protein significantly differed between B6, weight stable, severe, and OVX mice ($p=0.022$, one-way ANOVA); however, a *post hoc* test showed no differences between specific groups (Figure 3D).

IL-6-related downstream signaling with loss of ovarian function in female $^{ApcMin/+}$ *mice*

Signaling downstream of the IL-6 receptor was analyzed to determine whether pathways activated by IL-6 were affected by ovarian function. Downstream of the receptor, protein expression of phosphorylated/total STAT3 (T389) was increased in severe $^{ApcMin/+}$ mice compared to B6 and weight stable (one-way ANOVA: $p=0.002$; $p<0.01$ for B6 and weight stable comparisons, Tukey *post hoc*); interestingly, severe *Apc*$^{Min/+}$ mice did not differ from OVX (Figure 4A). *SOCS3* gene expression, a negative regulator of JAK/STAT3 signaling, is very highly induced in severe *Apc*$^{Min/+}$ females compared to weight stable ($p=0.022$) (Figure 4B), similar to what we have seen previously [15]. There was no difference across intact and OVX B6 and *Apc*$^{Min/+}$ mice, likely due to wide variation across the intact *Apc*$^{Min/+}$ mice (Figure 4B). Phosphorylated AMPK (T172)/total AMPK, a downstream effector of IL-6 [60] that mediates energy partitioning and regulates mitochondrial biogenesis, showed no differences across groups, though there was wide variation within the severe group (one-way ANOVA) (Figure 4C).

IL-6 receptor expression and related downstream signaling with overexpression of IL-6 in ovariectomized female $Apc^{Min/+}$ mice

Gene expression of *IL-6ra* has been previously reported in the cohort of female $Apc^{Min/+}$ mice having undergone OVX and/or IL-6 overexpression (Chapter 4) [15]. *Gp130* gene expression strongly trended towards an effect of IL-6 overexpression to increase across intact and OVX groups (p=0.056) as well as a trend towards an interaction of OVX x IL-6 (p=0.064) (Figure 5A). Additionally, a pre-planned Student's t-test revealed a sharp increase in *gp130* gene expression in sham+IL-6 mice compared to control $Apc^{Min/+}$ (p=0.043) (Figure 5A). Gp130 protein expression was similar, with main effects of both IL-6 overexpression and OVX (p=0.0012 and 0.0003, respectively, two-way ANOVA). Interestingly, pSTAT3/STAT3 (T389) showed a main effect of OVX to decrease STAT3 phosphorylation (p=0.006) (Figure 5C); this could have major implications for cachexia progression as STAT3 is a key point of regulation for several downstream effectors that lead to muscle wasting. SOCS3 gene expression showed a strong trend towards an interaction of IL-6 x OVX (p=0.0553) (Figure 5D).

Mitochondrial biogenesis, dynamics, and function with loss of ovarian function in female $Apc^{Min/+}$ mice

Mitochondrial function has been recognized over the past several years to be a key point of regulation in muscle wasting associated with several disease states including cachexia. *PGC1α*, a key regulator of mitochondrial biogenesis, showed no change between severe and weight stable $Apc^{Min/+}$ mice, or between intact and OVX B6 and $Apc^{Min/+}$ mice (Figure 6A). No differences were found between severe and weight stable, or between intact and OVX B6 and $Apc^{Min/+}$ mice in *Mfn1* and *Fis1* gene expression (Figure 6B, C). Cytochrome c oxidase (COX) activity did not differ between weight

stable and severe *Apc*$^{Min/+}$ mice (Figure 6D); among intact and OVX B6 and *Apc*$^{Min/+}$ mice, a main effect of OVX ($p<0.0001$), a main effect of genotype ($p<0.0001$), and an interaction between the two ($p=0.0002$) were determined by two-way ANOVA (Figure 6D). B6 OVX mice had significantly higher activity than all other groups ($p<0.0001$ per comparison, Tukey *post hoc*); and *Apc*$^{Min/+}$ mice had significantly lower activity than B6 mice ($p<0.05$) (Figure 6D).

Mitochondrial biogenesis, dynamics, and function with overexpression of IL-6 in ovariectomized female Apc$^{Min/+}$ *mice*

Among 15-week old female *Apc*$^{Min/+}$ mice, there was no effect of IL-6 or OVX on *PGC1α* gene expression (Figure 7A). There was a main effect of IL-6 overexpression to decrease *Mfn1* gene expression among both intact and OVX *Apc*$^{Min/+}$ mice ($p=0.0297$) (Figure 7B). There were no differences among groups on *Fis1* gene expression (Figure 7C).

5.5 Discussion

This series of experiments has shown that the loss of ovarian function by ovariectomy has drastic consequences on muscle metabolism during cancer cachexia progression in the female. The purpose of this study was to determine whether ovarian function regulated muscle signaling during cachexia; we had hypothesized that the loss of ovarian function during cancer cachexia would be akin to opening the metaphorical floodgates and allowing cachectic factors that would normally be inhibited by estrogen or other ovarian products or signaling to run their course, as in the male. Our results, however, were striking. OVX, when compared to intact *Apc*$^{Min/+}$ females, seemed to alleviate many of the cachectic markers that lead to muscle wasting. Importantly, OVX *Apc*$^{Min/+}$ mice

did not only maintain muscle mass; they actually gained muscle mass despite a similar tumor burden to intact *Apc*$^{Min/+}$ mice (Table 1, Table 2). OVX mice, in addition, had 3-fold lower *MuRF1* gene expression than intact *Apc*$^{Min/+}$ mice (Figure 1B), indicating one point of muscle wasting regulation that was attenuated by OVX. This is in contrast to a previous report which saw an increase in *MuRF1* with OVX [87]. Interestingly, this downregulation of *Murf1* by OVX is not seen at 15 weeks (Figure 2B). It is possible that, as 15 weeks is "early cachexia," the E3 ligases may not yet have assumed their roles in muscle wasting; this may not occur until later in cachexia, which we see at 18 week. This is supported by the expression pattern of MuRF1's co-conspirer, Atrogin-1. At 15 weeks, we see no change across groups, while at 18 weeks we see a drastic upregulation of *Fbxo32* (Atrogin-1) gene expression in *Apc*$^{Min/+}$ mice. Another area where OVX has an effect is in the mitochondria. While there were few changes in markers of mitochondrial biogenesis or dynamics, COX activity showed a main effect of OVX to increase activity (Figure 6D). This is striking, as COX activity is a measure of mitochondrial function. Going a step further, this increase in COX activity despite cachexia progression may indicate a true alleviation of mitochondrial dysregulation by OVX. As COX is a subunit of complex IV in the electron transport chain, this is an indication that mitochondria of OVX mice may be better able to meet energy demands, and this may contribute to the overall healthier muscle phenotype seen in OVX mice.

A second hypothesis of this study was that loss of ovarian function would disinhibit IL-6 signaling, allowing IL-6 signaling to progress cachexia development as in the male. Our results to this end show some intriguing relationships between ovarian function, Il-6, and IL-6 signaling. OVX's effect on IL-6 signaling went against our original hypothesis,

but has raised some interesting questions and uncovered some new relationships between these factors. IL-6R protein was lower in OVX mice than in severely cachectic *Apc*$^{Min/+}$ mice (Figure 3B), despite similar IL-6 circulating levels (data not shown) (Chapter 4). As further evidence that OVX can downregulate IL-6 signaling, there was a main effect of OVX to decrease gp130 protein levels, even when IL-6 levels are maintained at a high level (Figure 5B). Interestingly, STAT3 activation did not differ between severe mice and OVX mice at 18 weeks of age (Figure 4A), leading to speculation that another factor may be activating the pathway in OVX mice. However, in our 15-week experiment, there was a main effect of OVX to decrease STAT3 activation. It is interesting to postulate the mechanisms at play here- perhaps in early cachexia, OVX is sufficient to suppress IL-6 signaling, but in later stages of cachexia, other cachectic factors are able to activate STAT3 despite OVX's effect on IL-6 signaling.

Some of the most interesting findings emerged from the comparison between OVX *Apc*$^{Min/+}$ mice and OVX+IL-6 *Apc*$^{Min/+}$ mice, further complicating the interaction between these two factors. For some measures, such as gp130 protein (Figure 5B), OVX+IL-6 was able to rescue expression where OVX alone had downregulated it compared to the control *Apc*$^{Min/+}$. Though a comparison between OVX and OVX+IL-6 with regard to AMPK activation did not reach significance due to a high amount of variation in the latter group, it seems that OVX and IL-6 have a synergistic effect to increase AMPK activation, while all other groups, including the sham + IL-6 geoups, showed no increase over the control *Apc*$^{Min/+}$ group.

Another intriguing pattern emerged through this study; many of the pathways we consider "canonical" to the progression of cachexia in the male are dysregulated, if they

play a part at all, in the female. We closely examined the IL-6 signaling pathway previously (Chapter 3) [15] For instance, IL-6, which is known to induce MuRF1 and Atrogin-1 during cachexia in the male [20, 60], fails to do so even when IL-6 levels are kept very high. Of course, this in the 15-week mice, where muscle wasting may not yet have begun in earnest. However, when we examine *MuRF1* gene expression between severely cachectic females and 18-week females with IL-6 overexpression, we get a striking result- *MuRF1* expression actually trends lower in the IL-6 overexpression mice (Supplemental Data). AMPK, a key energy-sensing enzyme that plays a central, if paradoxical, role in cachexia development [60] and mitochondrial biogenesis, showed no increase across groups in either the 18-week of 15-week experiment. This is in direct contrast to the male $Apc^{Min/+}$ mouse, where were see a robust induction of AMPK activation during cachexia progression. On the mitochondrial side, severely cachectic males typically have a severe drop in PGC1a expression [14], while we saw a trend toward higher *PGC1α* expression in severely cachectic females. Intriguingly, PGC1α overexpression has been shown to protect from atrophy due to conditions including cachexia [105]. Further, male typically show an increase in *Fis1* expression [14], a marker of a pathway that can lead to mitochondrial fragmentation and mitophagy [14]; here, we see no induction of *Fis1* even in the severely cachectic 18-week mice. These findings point to a more global network of differences between male and female cachectic signaling than simply the IL-6 pathway.

We have thus shown that female cachexia progression can be interrupted and alleviated by the removal of ovaries. This is of interest, as many cell culture and animal models have suggested that estrogen can block IL-6 transcription and downstream

signaling [27, 97, 164]. Additionally, we have shown that sex differences in cachexia extend far beyond the IL-6 signaling pathway. This work raises many important questions: mechanistically, how does OVX affect IL-6 signaling? What are the specific factors at play? What is the mechanism of the synergy between OVX and IL-6 to increase signals that are not increased by either alone. Clearly, future work is needed in each of these areas to achieve a more complete picture of the female response to cachexia.

5.6 Acknowledgements

This work was supported by National Institutes of Health grant # NCI-R01CA121249A501 (JAC), National Institutes of Health Grant P20 RR-017698 from the National Center for Research, and by the USC Behavioral-Biomedical Interface Program, which is a NIGMS/NIH-T32 supported program. Contents of this publication are solely the responsibility of the authors and do not necessarily represent the official views of the NIGMS or NIH.

Table 5.1: Descriptive characteristics of 18-week female C57BL/6 and *Apc*$^{Min/+}$ mice stratified into groups based on body weight change from 15-18 weeks of age. N=43 mice total; remaining ApcMin/+ mice (n=8) not shown fell between cutoff points for "Weight stable" and "Cachectic." B6, C57BL/6; Weight stable, female *Apc*$^{Min/+}$ with <2% body weight loss from peak; Cachectic, female *Apc*$^{Min/+}$ with >9% body weight loss from peak; OVX, ovariectomized at 11 weeks of age; N, number; BW, body weight; w, weeks of age; pg, picograms; ml, milliliter; mg, milligrams; mm, millimeters. * Indicates significant difference from B6 ($p<0.05$); ^ indicates significant difference from weight stable *Apc*$^{Min/+}$; # indicates difference from Cachectic *Apc*$^{Min/+}$. Significance was set at $p<0.05$ for all comparisons.

		Weight stable		
	B6	***Apc*$^{Min/+}$**	**Cachectic *Apc*$^{Min/+}$**	**OVX *Apc*$^{Min/+}$**
N	7	10	8	10
BW at 18w (g)	20.2 ± 0.3	19.9 ± 0.3	17.3 ± 0.6*^	21.0 ± 0.3^#
Inguinal fat (mg)	116.2 ± 9.9	168.3 ± 18.2	3.6 ± 2.5*^	110.9 ± 8.8^#
Tibia length (mm)	16.5 ± 0.1	16.2 ± 0.2	16.2 ± 0.1	16.6 ± 0.1
Hindlimb muscle mass (mg)	297.5 ± 13.1	277.4 ± 5.5	193.8 ± 11.5*^	278.3 ± 9.7#
Hindlimb muscle/Tibia length	18.1 ± 0.8	17.1 ± 0.4*	11.7 ± 0.7*^	16.8 ± 0.5#
Spleen (mg)	87.6 ± 6.3	225.0 ± 20.8*	356.6 ± 35.8*^	222.7 ± 23.2*#
Uterus (mg)	99.9 ± 9.3	63.4 ± 6.4*	25.1 ± 1.6*^	28.2 ± 2.3*^
Heart (mg)	91.3 ± 3.8	97.2 ± 3.4	120.6 ± 6.8*^	108.3 ± 2.6*^
Heart/Tibia length	4.5 ± 0.2	6.0 ± 0.2*	7.5 ± 0.5*^	6.5 ± 0.2*#

Table 5.2: Descriptive characteristics of female ApcMin/+ mice treated by ovariectomy, IL-6 overexpression, or both. Mice were ovariectomized at 11 weeks, electroporated with IL-6 overexpression vector at 13 weeks, and sacrificed at 15 weeks. OVX, ovariectomy; IL-6, interleukin-6; N, number; 15w, 15 weeks of age; BW, body weight; g, grams; mm, millimeters; mg, milligrams; TL, tibia length. * indicates main effect of OVX; # indicates main effect of IL-6; & indicates interaction of OVX x IL-6 (determined by two-way ANOVA). Means with same superscript lowercase letters indicates significant difference between columns (Tukey *post hoc*, $p<0.05$)

	***Apc*$^{Min/+}$**				
	Control	**+IL6**	**OVX**	**OVX + IL-6**	
N	**13**	**10**	**10**	**8**	
15w BW (g)	18.3 ± 0.6^{a}	17.6 ± 0.4^{b}	$21.4 \pm 0.5^{a,b,c}$	18.5 ± 0.9^{c}	*#&
Tibia length (mm)	16.2 ± 0.1	15.9 ± 0.2	16.6 ± 0.1	16.3 ± 0.1	*#
Inguinal fat (mg)	120 ± 29	49 ± 24	85 ± 15	63 ± 21	
Hindlimb muscle mass (mg)	221 ± 15	199 ± 10	248 ± 8	206 ± 17	#
HMM/TL	13.6 ± 0.9	12.5 ± 0.6	14.9 ± 0.5	12.6 ± 1.0	#
% mice estrus cycle present	70%	100%	0%	0%	
Spleen (mg)	197 ± 38	393 ± 47	216 ± 29	304 ± 34	#
Uterus (mg)	$46 \pm 5^{a,b,c}$	29 ± 4^{a}	28 ± 3^{b}	27 ± 3^{c}	*#&
Heart (mg)	93 ± 3	102 ± 6	108 ± 2	109 ± 6	*
Heart/BW	5.2 ± 0.4	5.8 ± 0.4	5.1 ± 0.1	6.1 ± 0.6	#

5.7 Figure Legends

Figure 5.1: Canonical cachexia-related pathways with loss of ovarian function in female *Apc*$^{Min/+}$ mice. A) (Left) Gastrocnemius muscle mass in weight stable and severely cachectic female ApcMin/+ mice. Severely cachectic mice had a significantly different mass than weight stable (p=0.0006). (Right) Gastrocnemius muscle mass in intact and OVX female C57BL/6 and ApcMin/+ mice. There was a trend towards a main effect of genotype (p=0.058); intact B6 significantly differed from intact ApcMin/+ by pre-planned Student's t-test (p=0.016). B) (Left) *MuRF1* gene expression fold change in weight stable and severely cachectic female ApcMin/+ mice. Severely cachectic mice significantly differed from weight stable (p=0.0039). (Right) *MuRF1* gene expression fold change in intact and OVX female C57BL/6 and ApcMin/+ mice. No differences were detected by two-way ANOVA. C) (Left) *Fbxo32* (Atrogin 1) gene expression fold change in weight stable and severely cachectic female ApcMin/+ mice. Severely cachectic mice trended towards a difference from weight stable (p=0.1064). (Right) *Fbxo32* (Atrogin 1) gene expression fold change in intact and OVX female C57BL/6 and ApcMin/+ mice. There was a trend towards an effect of genotype (p=0.068) detected by two-way ANOVA. * indicates significant difference from weight stable. $ indicates significant difference from intact B6. # indicates significant difference from intact ApcMin/+ Significance was set at $p<0.05$.

Figure 5.2: Canonical cachexia-related pathways with overexpression of IL-6 in ovariectomized female *Apc*$^{Min/+}$ mice. A) Gastrocnemius muscle mass (mg) in control, OVX, IL-6 overexpression, and OVX+IL-6 female *Apc*$^{Min/+}$ mice. A main effect of IL-6 overexpression was detected by two-way ANOVA (p=0.044). B) Muscle *MuRF1* gene expression in control, OVX, IL-6 overexpression, and OVX+IL-6 female *Apc*$^{Min/+}$ mice. No significant differences between groups were determined by two-way ANOVA. C) Muscle *Fbxo32* (Atrogin1) gene expression in control, OVX, IL-6 overexpression, and OVX+IL-6 female *Apc*$^{Min/+}$ mice. No significant differences were determines by two-way ANOVA. Significance was set at $p<0.05$.

Figure 5.3: **IL-6 receptor expression with loss of ovarian function in female ApcMin/+ mice.** A) (Left) Muscle *IL6ra* gene expression fold change in weight stable and severely cachectic female ApcMin/+ mice. Severely cachectic mice significantly differed from weight stable (p=0.0387). (Right) Muscle *IL6ra* gene expression fold change in intact and OVX female C57BL/6 and ApcMin/+ mice. No significant differences were determined by two-way ANOVA. B) Muscle IL-6r protein in B6, weight stable, severely cachectic, and OVX ApcMin/+ mice. A difference between groups was determined by one-way ANOVA (p=0.0003); severe is significantly different from B6, weight stable, and OVX groups ($p<0.01$ per comparison, Tukey *post hoc*). C) (Left) Muscle *gp130* gene expression fold change in weight stable and severely cachectic female ApcMin/+ mice. There was a trend towards a difference detected by Student's t-

test (p=0.085). (Right) Muscle *gp130* gene expression fold change in intact and OVX female C57BL/6 and ApcMin/+ mice. No significant differences were determined by two-way ANOVA. D) Muscle gp130 protein in weight stable, severe, and OVX groups. A significant difference between groups was determined by one-way ANOVA (p=0.022); however, no differences between groups were determined by Tukey *post hoc*. * indicates significant difference from weight stable; # indicates significant difference from OVX; $ indicates significant difference from B6. Significance was set at p<0.05 for all measures.

Figure 5.4: IL-6-related downstream signaling with loss of ovarian function in female ApcMin/+ mice. A) Muscle pSTAT3/STAT3 protein in B6, weight stable, severe, and OVX ApcMin/+ groups. A significant difference between groups was determined by one-way ANOVA (p=0.002). Severe is significantly different from B6 and weight stable groups (p<0.01 per comparison, Tukey *post hoc*). B) (Left) Muscle SOCS3 gene expression fold change in weight stable and severely cachectic female ApcMin/+ mice. Severely cachectic mice significantly differed from weight stable (p=0.022). (Right) Muscle SOCS3 gene expression fold change in intact and OVX female C57BL/6 and ApcMin/+ mice. No significant differences were determined by two-way ANOVA. C) Muscle pAMPK/AMPK protein in B6, weight stable, severe, and OVX ApcMin/+ groups. No significant differences between groups were determined by one-way ANOVA. * indicates significant difference from weight stable; $ indicates significant difference from B6. Significance was set at p<0.05 for all measures.

Figure 5.5: IL-6 receptor expression and related downstream signaling with overexpression of IL-6 in ovariectomized female $Apc^{Min/+}$ mice. A) Muscle *gp130* gene expression fold change in control, OVX, IL-6 overexpression, and OVX+IL-6 groups. Two-way ANOVA determined a trend towards main effect of IL-6 (p=0.056) and trend towards interaction of OVX x IL-6 (p=0.064). Pre-planned Student's t-test indicated a significant difference between control ApcMin/+ and sham+ IL-6 group (p=0.043). B) Muscle gp130 protein in control, OVX, IL-6 overexpression, and OVX+IL-6 female $Apc^{Min/+}$ mice. Main effects of OVX (p=0.0003) and IL-6 (p=0.0012) were determined by two-way ANOVA. C) Muscle pSTAT3/STAT3 protein in control, OVX, IL-6 overexpression, and OVX+IL-6 female $Apc^{Min/+}$ mice. A main effect of OVX was determined by two-way ANOVA (p=0.006). D) Muscle *SOCS3* gene expression fold change in control, OVX, IL-6 overexpression, and OVX+IL-6 groups. A trend towards an interaction between OVX x IL-6 was determined by two-way ANOVA (p=0.0553). A trend towards a difference between control and IL-6 + sham groups was determined by Student's t-test (p=0.075). E) Muscle pAMPK/AMPK protein in control, OVX, IL-6 overexpression, and OVX+IL-6 female $Apc^{Min/+}$ mice. No significant differences between groups were determined by two-way ANOVA. * indicates significant difference from control ApcMin/+. Significance was set at p<0.05 for all measures.

Figure 5.6: Mitochondrial biogenesis, dynamics, and function with loss of ovarian function in female ApcMin/+ mice. A) (Left) Muscle PGC1a gene expression fold change in weight stable and severely cachectic female ApcMin/+ mice. There was no difference between the groups (p=0.167). (Right) Muscle PGC1a gene expression in intact and OVX female C57BL/6 and ApcMin/+ mice. No significant differences were detected by two-way ANOVA. B) (Left) Muscle *Mfn1* gene expression fold change in weight stable and severely cachectic female ApcMin/+ mice. There was no difference between the groups (p=0.122). (Right) Muscle *Mfn1* gene expression fold change in intact and OVX female C57BL/6 and ApcMin/+ mice. No differences were detected by two-way ANOVA. C) (Left) Muscle *Fis1* gene expression fold change in weight stable and severely cachectic female ApcMin/+ mice. There was no difference between the groups (p=0.444). (Right) Muscle *Fis1* gene expression fold change in intact and OVX female C57BL/6 and ApcMin/+ mice. D) (Left) Muscle COX activity in weight stable and severely cachectic female ApcMin/+ mice. There was no difference between the groups (p=0.29). (Right) Muscle COX activity in intact and OVX female C57BL/6 and ApcMin/+ mice. A main effect of genotype ($p<0.0001$), a main effect of OVX ($p<0.0001$), and an interaction between the two (p=0.0002) were determined by two-way ANOVA. Tukey *post hoc* determined that the B6 OVX was significantly different from all other groups ($p<0.0001$ for each comparison) and that ApcMin/+ was significantly different from B6 ($p<0.05$). $ indicates significant difference from B6; & indicates significant difference from all other groups. Significance was set at $p<0.05$.

Figure 5.7: Mitochondrial biogenesis, dynamics, and function with overexpression of IL-6 in ovariectomized female *Apc*$^{Min/+}$ mice. A) Muscle PGC1a gene expression fold change in control, OVX, IL-6 overexpression, and OVX+IL-6 groups. No differences were determined by two-way ANOVA. B) Muscle Mfn1 gene expression fold change in control, OVX, IL-6 overexpression, and OVX+IL-6 female Apc$^{Min/+}$ mice. A main effect of Il-6 was determined by two-way ANOVA (p=0.0297). C) Muscle Fis1 gene expression fold change in control, OVX, IL-6 overexpression, and OVX+IL-6 female Apc$^{Min/+}$ mice. No differences were determined by two-way ANOVA. Significance was set at $p<0.05$ for all measures.

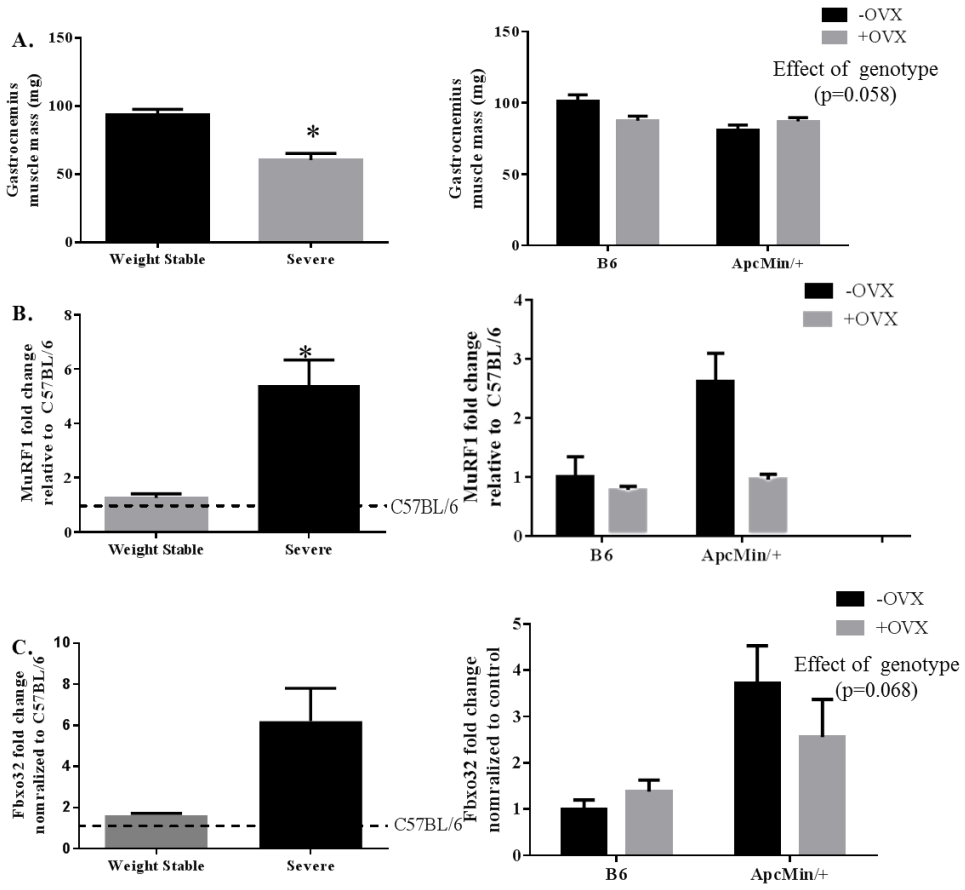

Figure 5.1: Canonical cachexia-related pathways with loss of ovarian function in female *Apc*$^{Min/+}$ mice. A) (Left) Gastrocnemius muscle mass in weight stable and severely cachectic female ApcMin/+ mice. Severely cachectic mice had a significantly different mass than weight stable (p=0.0006). (Right) Gastrocnemius muscle mass in intact and OVX female C57BL/6 and ApcMin/+ mice. There was a trend towards a main effect of genotype (p=0.058); intact B6 significantly differed from intact ApcMin/+ by pre-planned Student's t-test (p=0.016). B) (Left) *MuRF1* gene expression fold change in weight stable and severely cachectic female ApcMin/+ mice. Severely cachectic mice significantly differed from weight stable (p=0.0039). (Right) *MuRF1* gene expression fold change in intact and OVX female C57BL/6 and ApcMin/+ mice. No differences were detected by two-way ANOVA. C) (Left) *Fbxo32* (Atrogin 1) gene expression fold change in weight stable and severely cachectic female ApcMin/+ mice. Severely cachectic mice trended towards a difference from weight stable (p=0.1064). (Right) *Fbxo32* (Atrogin 1) gene expression fold change in intact and OVX female C57BL/6 and ApcMin/+ mice. There was a trend towards an effect of genotype (p=0.068) detected by two-way ANOVA. * indicates significant difference from weight stable. $ indicates significant difference from intact B6. # indicates significant difference from intact ApcMin/+ Significance was set at $p<0.05$.

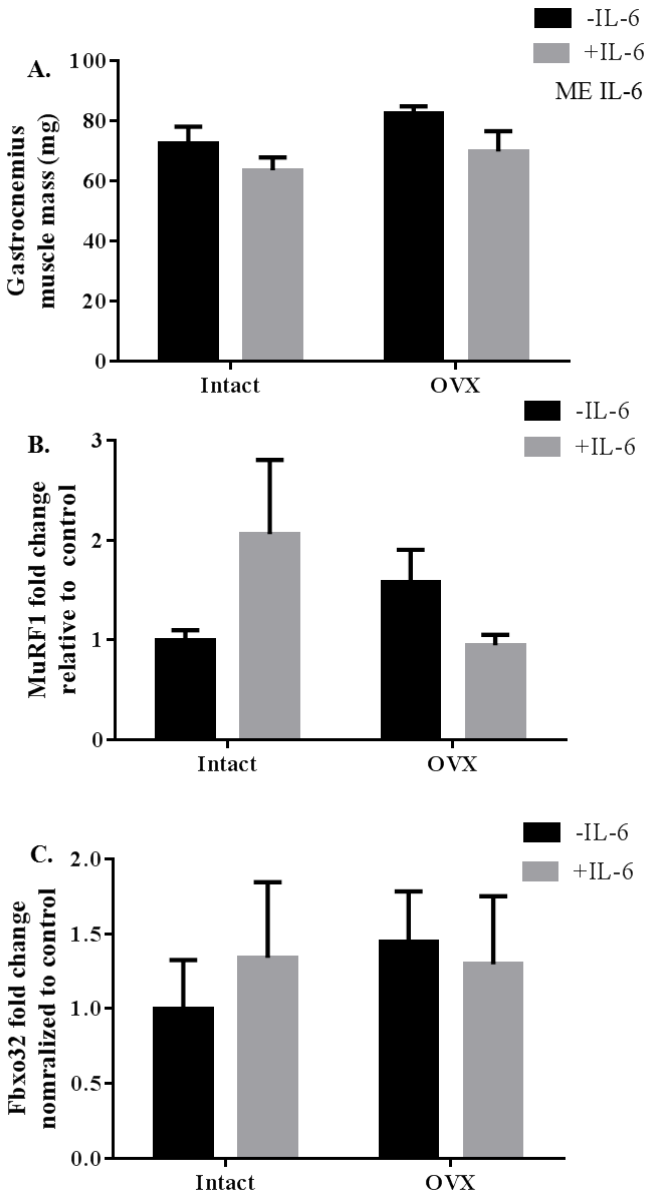

Figure 5.2: Canonical cachexia-related pathways with overexpression of IL-6 in ovariectomized female *Apc*$^{Min/+}$ mice. A) Gastrocnemius muscle mass (mg) in control, OVX, IL-6 overexpression, and OVX+IL-6 female *Apc*$^{Min/+}$ mice. A main effect of IL-6 overexpression was detected by two-way ANOVA (p=0.044). B) Muscle *MuRF1* gene expression in control, OVX, IL-6 overexpression, and OVX+IL-6 female *Apc*$^{Min/+}$ mice. No significant differences between groups were determined by two-way ANOVA. C) Muscle *Fbxo32* (Atrogin1) gene expression in control, OVX, IL-6 overexpression, and OVX+IL-6 female *Apc*$^{Min/+}$ mice. No significant differences were determines by two-way ANOVA. Significance was set at $p<0.05$.

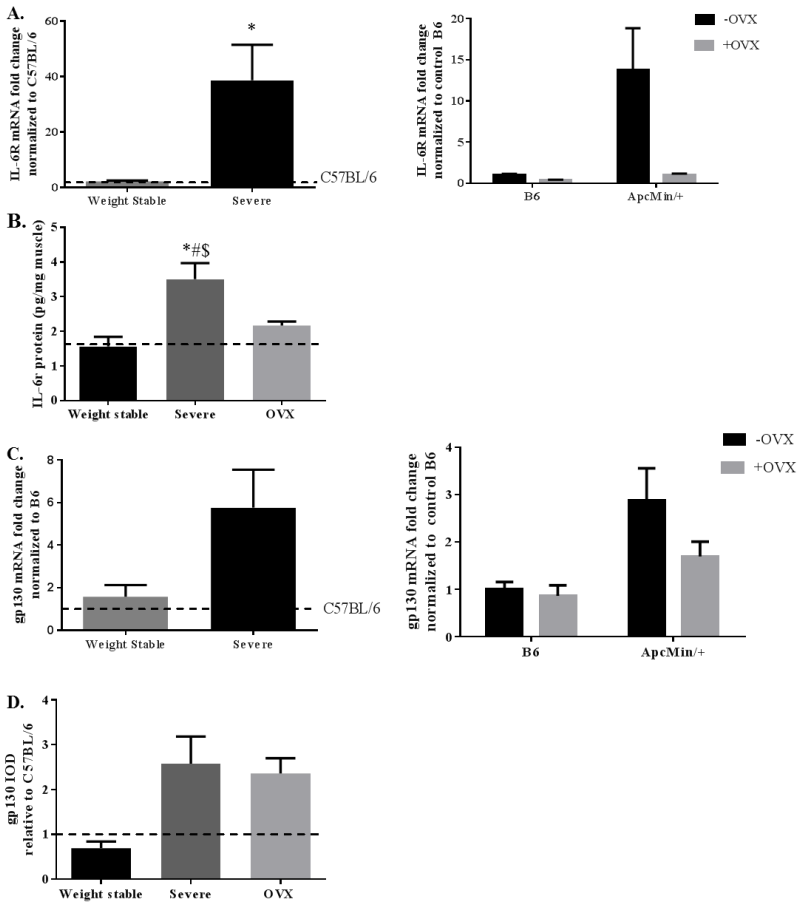

Figure 5.3: **IL-6 receptor expression with loss of ovarian function in female ApcMin/+ mice.** A) (Left) Muscle *IL6ra* gene expression fold change in weight stable and severely cachectic female ApcMin/+ mice. Severely cachectic mice significantly differed from weight stable (p=0.0387). (Right) Muscle *IL6ra* gene expression fold change in intact and OVX female C57BL/6 and ApcMin/+ mice. No significant differences were determined by two-way ANOVA. B) Muscle IL-6r protein in B6, weight stable, severely cachectic, and OVX ApcMin/+ mice. A difference between groups was determined by one-way ANOVA (p=0.0003); severe is significantly different from B6, weight stable, and OVX groups (p<0.01 per comparison, Tukey *post hoc*). C) (Left) Muscle *gp130* gene expression fold change in weight stable and severely cachectic female ApcMin/+ mice. There was a trend towards a difference detected by Student's t-test (p=0.085). (Right) Muscle *gp130* gene expression fold change in intact and OVX female C57BL/6 and ApcMin/+ mice. No significant differences were determined by two-way ANOVA. D) Muscle gp130 protein in weight stable, severe, and OVX groups. A significant difference between groups was determined by one-way ANOVA (p=0.022); however, no differences between groups were determined by Tukey *post hoc*. * indicates significant difference from weight stable; # indicates significant difference from OVX; $ indicates significant difference from B6. Significance was set at p<0.05 for all measures.

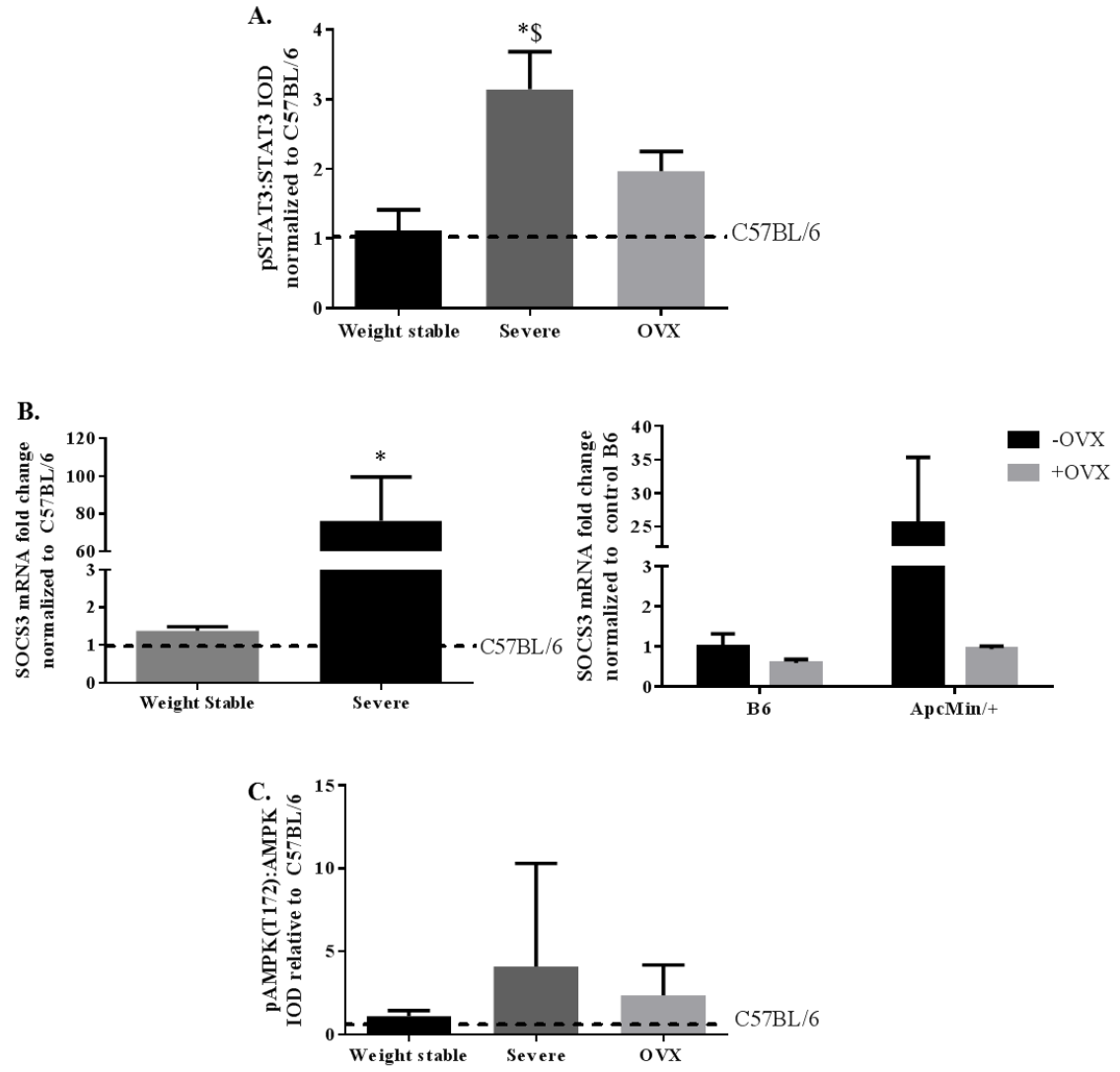

Figure 5.4: IL-6-related downstream signaling with loss of ovarian function in female ApcMin/+ mice. A) Muscle pSTAT3/STAT3 protein in B6, weight stable, severe, and OVX ApcMin/+ groups. A significant difference between groups was determined by one-way ANOVA ($p=0.002$). Severe is significantly different from B6 and weight stable groups ($p<0.01$ per comparison, Tukey *post hoc*). B) (Left) Muscle SOCS3 gene expression fold change in weight stable and severely cachectic female ApcMin/+ mice. Severely cachectic mice significantly differed from weight stable ($p=0.022$). (Right) Muscle SOCS3 gene expression fold change in intact and OVX female C57BL/6 and ApcMin/+ mice. No significant differences were determined by two-way ANOVA. C) Muscle pAMPK/AMPK protein in B6, weight stable, severe, and OVX ApcMin/+ groups. No significant differences between groups were determined by one-way ANOVA. * indicates significant difference from weight stable; $ indicates significant difference from B6. Significance was set at $p<0.05$ for all measures.

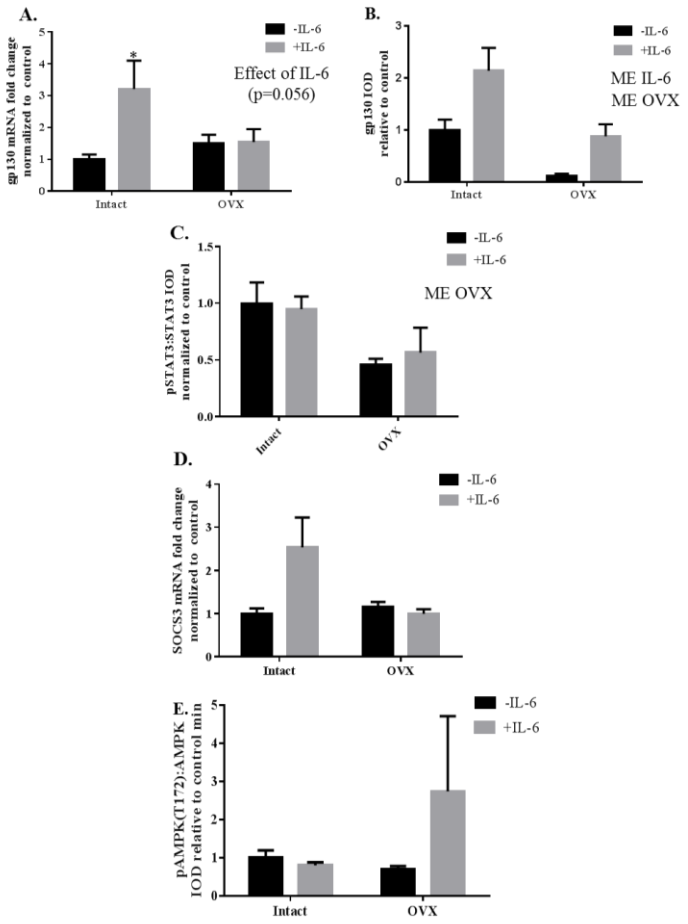

Figure 5.5: IL-6 receptor expression and related downstream signaling with overexpression of IL-6 in ovariectomized female *Apc$^{Min/+}$* mice. A) Muscle *gp130* gene expression fold change in control, OVX, IL-6 overexpression, and OVX+IL-6 groups. Two-way ANOVA determined a trend towards main effect of IL-6 (p=0.056) and trend towards interaction of OVX x IL-6 (p=0.064). Pre-planned Student's t-test indicated a significant difference between control ApcMin/+ and sham+ IL-6 group (p=0.043). B) Muscle gp130 protein in control, OVX, IL-6 overexpression, and OVX+IL-6 female *Apc$^{Min/+}$* mice. Main effects of OVX (p=0.0003) and IL-6 (p=0.0012) were determined by two-way ANOVA. C) Muscle pSTAT3/STAT3 protein in control, OVX, IL-6 overexpression, and OVX+IL-6 female *Apc$^{Min/+}$* mice. A main effect of OVX was determined by two-way ANOVA (p=0.006). D) Muscle *SOCS3* gene expression fold change in control, OVX, IL-6 overexpression, and OVX+IL-6 groups. A trend towards an interaction between OVX x IL-6 was determined by two-way ANOVA (p=0.0553). A trend towards a difference between control and IL-6 + sham groups was determined by Student's t-test (p=0.075). E) Muscle pAMPK/AMPK protein in control, OVX, IL-6 overexpression, and OVX+IL-6 female *Apc$^{Min/+}$* mice. No significant differences between groups were determined by two-way ANOVA. * indicates significant difference from control ApcMin/+. Significance was set at $p<0.05$ for all measures.

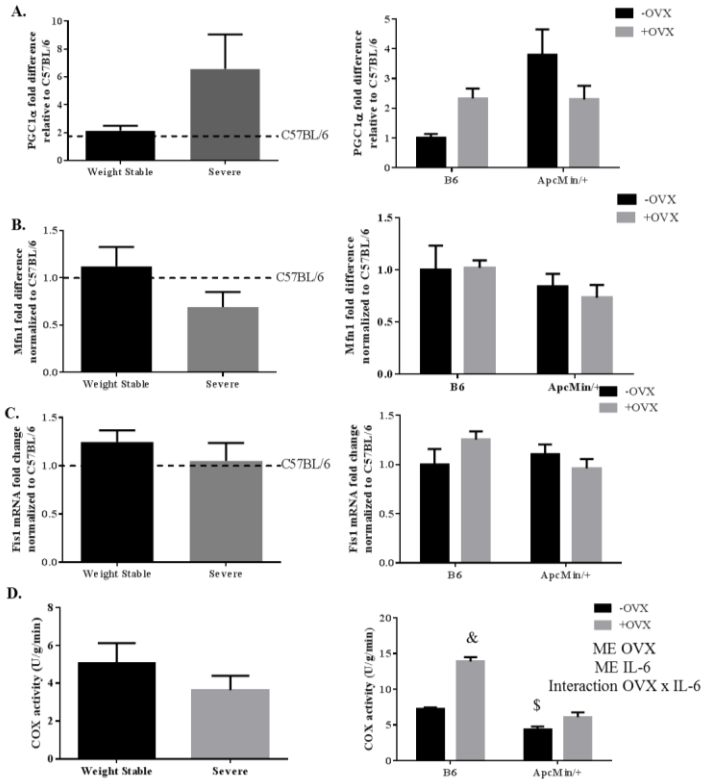

Figure 5.6: Mitochondrial biogenesis, dynamics, and function with loss of ovarian function in female ApcMin/+ mice. A) (Left) Muscle PGC1a gene expression fold change in weight stable and severely cachectic female ApcMin/+ mice. There was no difference between the groups (p=0.167). (Right) Muscle PGC1a gene expression in intact and OVX female C57BL/6 and ApcMin/+ mice. No significant differences were detected by two-way ANOVA. B) (Left) Muscle *Mfn1* gene expression fold change in weight stable and severely cachectic female ApcMin/+ mice. There was no difference between the groups (p=0.122). (Right) Muscle *Mfn1* gene expression fold change in intact and OVX female C57BL/6 and ApcMin/+ mice. No differences were detected by two-way ANOVA. C) (Left) Muscle *Fis1* gene expression fold change in weight stable and severely cachectic female ApcMin/+ mice. There was no difference between the groups (p=0.444). (Right) Muscle *Fis1* gene expression fold change in intact and OVX female C57BL/6 and ApcMin/+ mice. D) (Left) Muscle COX activity in weight stable and severely cachectic female ApcMin/+ mice. There was no difference between the groups (p=0.29). (Right) Muscle COX activity in intact and OVX female C57BL/6 and ApcMin/+ mice. A main effect of genotype ($p<0.0001$), a main effect of OVX ($p<0.0001$), and an interaction between the two (p=0.0002) were determined by two-way ANOVA. Tukey *post hoc* determined that the B6 OVX was significantly different from all other groups ($p<0.0001$ for each comparison) and that ApcMin/+ was significantly different from B6 ($p<0.05$). $ indicates significant difference from B6; & indicates significant difference from all other groups. Significance was set at $p<0.05$.

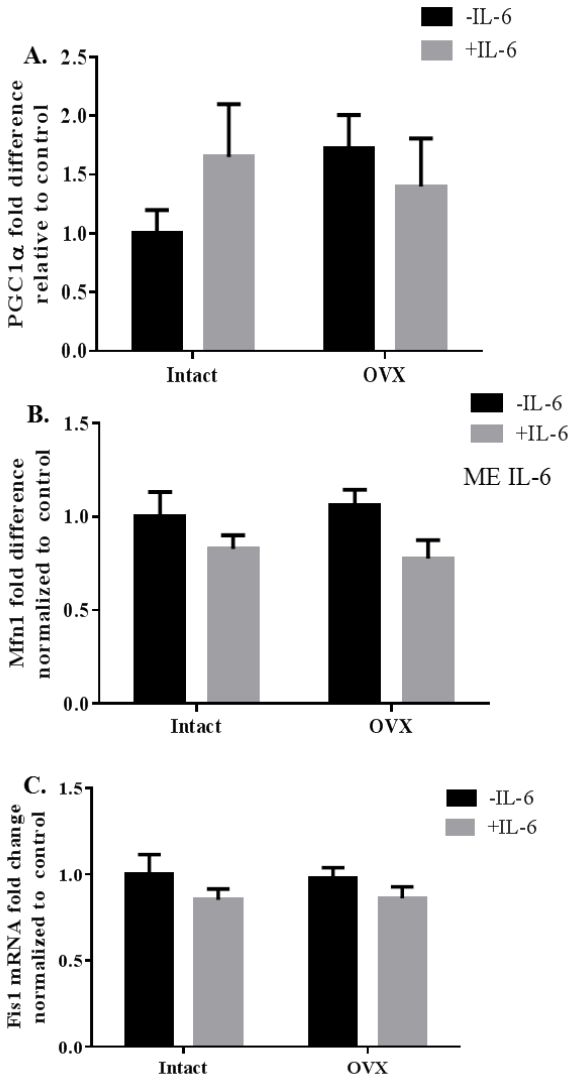

Figure 5.7: Mitochondrial biogenesis, dynamics, and function with overexpression of IL-6 in ovariectomized female *Apc*$^{Min/+}$ mice. A) Muscle PGC1a gene expression fold change in control, OVX, IL-6 overexpression, and OVX+IL-6 groups. No differences were determined by two-way ANOVA. B) Muscle Mfn1 gene expression fold change in control, OVX, IL-6 overexpression, and OVX+IL-6 female Apc$^{Min/+}$ mice. A main effect of Il-6 was determined by two-way ANOVA ($p=0.0297$). C) Muscle Fis1 gene expression fold change in control, OVX, IL-6 overexpression, and OVX+IL-6 female Apc$^{Min/+}$ mice. No differences were determined by two-way ANOVA. Significance was set at $p<0.05$ for all measures.

CHAPTER 6

OVERALL DISCUSSION

The overall purpose of this study was to determine whether ovarian function could alter cachexia progression in female *Apc*$^{Min/+}$ mice through IL-6 signaling and he regulation of skeletal muscle metabolism. Through the completion of these three studies, we have shown that IL-6 signaling during cancer cachexia is differentially regulated in females compared to males, and that ovarian function certainly plays a role in the regulation of said IL-6 signaling. Additionally, ovarian function is very much able to regulate muscle metabolic signaling. Overall, we achieve the purpose of this study and showed that ovarian function has a large role in the regulation of cachexia progression; however, perhaps not the way we had anticipated. The working overall hypothesis for this study was that loss of ovarian function in the female *Apc*$^{Min/+}$ mouse would have aggravated progression of cachexia through altered IL-6 sensitivity, which would increase skeletal muscle dysfunction and lead to aggravated muscle wasting. As we would later find out, "ovarian loss" is not so simple. The loss of ovarian function due to disease, termed "Cycle Absent" in the second study (Chapter 4) turned out to be a very different phenotype from the loss of ovarian function by surgery, as shown by the OVX group of mice in the second and third studies (Chapters 4 and 5). While Cycle Absent mice certainly did have an accelerated progression of cachexia and were the most severely cachectic female *Apc*$^{Min/+}$ mice, including the most severe muscle wasting, the OVX *Apc*$^{Min/+}$ mice surprisingly were alleviated of many cachectic markers. While this could not have been expected at the beginning of these studies, the differences between ovarian dysfunction due to disease and ovarian function loss ovariectomy were important findings (which naturally led to more questions) that had ramifications for cachexia

progression and may one day lead to improved understanding and consideration of the ovary's role in human disease.

This series of studies' legacy may be that it uncovered major differences in signaling between males and females. The first study (Chapter 3) focused on differences in IL-6 signaling, but we found differences in the third study (Chapter 5) as well, in signaling unrelated to IL-6. While the NIH has made strides for the inclusion of female animals in biomedical research, these studies show why is it not sufficient to only examine one sex in complex disease models; further, why the sexes need to be analyzed separately. Had we analyzed males and females together for certain markers in Chapter 3, no change would have been found, but this would have been obscuring the truth. Specifically, it was shown that male $Apc^{Min/+}$ mice have a decrease in SOCS3 protein compared to B6 controls, while female $Apc^{Min/+}$ mice have an increase in SOCS3 protein compared to B6 females (Chapter 3) [15]. This may be a key point of differential regulation between the sexes during cachexia; SOCS3 is a major negative regulator of STAT3 signaling ad may help to explain why, at least initially, females do not experience cachexia progression that is as severe as males. In addition to males having a higher level of circulating IL-6 during cachexia, male $Apc^{Min/+}$ mice have a higher level of muscle IL-6r protein than females. Surprisingly, it was shown that even among B6 animals, males have three-fold higher expression of IL-6R protein in muscle, which may help explain why males seem to be more sensitive to IL-6 signaling. Beyond IL-6 signaling, it was shown in Chapter 5 that severely cachectic females have a trend towards an increase in *PGC1α* gene expression over their weight stable counterparts; we have previously shown that severely cachectic males show a decrease in PGC1α expression

[14]. Additionally, while male ApcMin/+ mice show a strong induction of AMPK with cachexia severity [60], females showed no changes in AMPK activation across severity groups. AMPK is a downstream effector of IL-6 [60], so this may be due to differences in IL-6 signaling and sensitivity between the sexes. While the difference in PGC1α hints at mitochondrial differences, we found several more differences within the mitochondria. While there was no change across female severity groups or even a difference between B6 and *Apc*Min/+ in *Mfn1* gene expression, which plays a key role in mitochondrial fusion, *Apc*Min/+ male show a drastic decrease in this protein [14]. Accordingly, while we see no changes across severity groups or genotype for *Fis1*, a regulator of mitochondrial fission, this protein is drastically induced in severely cachectic $Apc^{Min/+}$ males. The concurrent drop in mitochondrial fusion and increase in fission points to dysregulated mitochondrial dynamics and can lead to increased mitophagy [14]. We see no evidence of this dysregulation in the female however, which may indicate that the mitochondria is not a major factor in the etiology of cachexia-related muscle wasting as it is in the male [14]. Even among basic descriptive characteristics of male and female $Apc^{Min/+}$ mice, it was found that we had to modify classifications for the female. While we have previously classified "severe" males as having lost >20% body weight [14, 60, 106], not a single female $Apc^{Min/+}$ survived to that level of weight loss. Instead, the "severe" classification was modified to >9-10% body weight loss in the female, as these animals were truly sick at this point by multiple measures.

Beyond sex differences, we found striking differences between females with different ovarian statuses. In Chapter 4, female $Apc^{Min/+}$ mice were classified as "Cycle Present" or "Cycle Absent" depending on whether their estrus cycles had ceased

secondary to disease progression. At first glance, it was assumed that "Cycle Absent" ovaries had simply shut down and would show results similar to those of OVX mice. This could not have been further from what the results actually showed. While "Cycle Absent" mice were eventually found to have a phenotype more similar to polycystic ovarian syndrome, including higher ovarian AMH gene expression, lower circulating sIL-6r and lower circulating leptin [42, 67, 151], than to menopausal animals or ovariectomized animals as we had previously assumed, the differences between these mice and OVX mice could not have been further apart. Cycle Absent mice represented the most severe group of female $Apc^{Min/+}$ mice, with all mice that ceased cycling losing more than 9% of their peak body weight (data not shown). Results were most striking when Cycle Absent and OVX were directly compared, as they were with morphological and functional data in Chapter 4. Though, importantly, food intake was the same across all groups from B6 to Cycle Absent $Apc^{Min/+}$ to OVX $Apc^{Min/+}$, Cycle Absent lost a drastic amount of fat and muscle while OVX mice gained weight; this indicates a severe metabolic dysregulation in the Cycle Absent mice. Across functional measures as well, OVX outperformed Cycle Absent mice. Interestingly, Cycle Absent mice showed a definite increase in sensitivity to inflammation independent of IL-6 levels. In our 15-week cohort of mice of which some had IL-6 overexpressed, these animals were unable to induce the inflammation seen in the Cycle Absent mice. Questions remain, however, about the etiology of estrus cycle cessation with disease. While the cessation clearly leads to deleterious outcomes, it is unknown what signaling is involved in causing this ovarian dysfunction. While the majority of women with cachexia secondary to cancer are menopausal [44, 58], many cancers that can lead to cachexia certainly do occur in women

of childbearing age [101]. If this same ovarian dysfunction can happen in humans, this is truly frightening, not to mention a currently unknown effect of cachexia in women.

It would seem, with all the data among these three studies, that ovariectomy is the answer to cachexia in females. This is certainly not what had been hypothesized, but the data is striking. Chapter 4 reveals that OVX *Apc*$^{Min/+}$ mice have higher body weight, stronger muscles, larger muscles, an improved function compared to their ovaries-intact counterparts. Additionally, OVX is associated with a decrease in circulating IL-6 and other circulating inflammatory factors, as well as decreased inflammatory signaling within the muscle which is surprising given estrogen's known anti-inflammatory effects [26, 37]. It is likely, however, that this decrease in inflammatory signaling is contributing to the improved functional and morphological outcomes of these mice. Further, the decreased inflammatory signaling may be related to improved measures in Chapter 5. For instance, OVX ApcMin/+ females have decreased MuRF1 gene expression than their intact counterparts; this could be a downstream effect of lower systemic inflammatory burden. OVX had a main effect across B6 and ApcMin/+ genotypes to decrease gp130 protein expression as well as STAT3 activation; this could effectively slow IL-6 signaling in ApcMin/+ mice to a fraction of what it would be in intact ApcMin/+ mice, having wide-reaching effects as IL-6 signaling leads to several downstream pathways [11], all of which culminate in muscle wasting [11]. Intriguingly, there is some interplay between OVX and IL-6 when IL-6 expression is kept at a constant level, as in our experiment with 15-week mice in Chapters 4 and 5. While 15-week OVX mice continued to grow during the experimental timeframe, as did the 18-week OVX mice, the addition of a constantly higher level of circulating IL-6 blunted this growth, the majority of which was lean mass

(Chapter 4). This same effect was not seen between control ApcMin/+ and sham + IL-6 mice, indicating an interaction between OVX and IL-6 that deserves further exploration.

While this series of studies has answered many important questions and cemented the importance of investigating female animals as well as males, there are many new questions to be answered and much work still to be done. We have successfully shown multiple differences across several pathways where female animals differ from males during cachexia progression, but we are far from uncovering the whole picture. Cachexia even within male animals is still being elucidated piece-by-piece, and this adds another layer of complexity to the discovery of therapeutic targets and the eventual clinical utility of perhaps sex-specific treatments. While the results from OVX mice are striking, it will be important to parse out the specific mechanisms at work. The ovary is a hub of endocrine signaling in the female body, with its two largest exports being estrogen and progesterone. Estrogen has known anti-inflammatory properties [26, 37] and is known to inhibit IL-6 and downstream signaling [25, 27, 37, 92, 97], while its sister progesterone (and its analogs) has been used clinically to increase appetite and relieve some symptoms in cachectic patients [3]. Why, then, does the ablation of these factors along with the ovary lead to improved outcomes?

While there is still much work to be done not only on the further elucidation of cachectic mechanisms and their sex-specific roles, but in discovering therapeutic targets that are not too specific to alleviate the web of complexity that is cancer cachexia, there is reason to be optimistic. While IL-6-specific blockades have had mixed results in clinical trials [12, 126] (possibly due to the enigmatic role of IL-6 in female cachexia?), perhaps insight into the vast differences between the sexes will lead to sex-specific treatments.

Research into both sexes will facilitate this, and upon seeing the optimistic results in OVX *Apc*$^{Min/+}$ mice, perhaps there are helpful lessons to be learned from the ovary, as well.

REFERENCES

1. Farkas J, v.H.S., Kalantar-Zadeh K, Morley JE, Anker SD, Lainscak M, *Cachexia as a major public health problem: Frequent, costly, and deadly.* J Cachexia Saropenia Muscle, 2013. **4**: p. 173-8.
2. Pajak B, O.S., Pijet B, Pijet M, Pogorzelska A, Gajkowska B, Orzechowski A, *Crossroads of cytokine signaling- the chase to stop muscle cachexia.* J Physiol Pharmacol, 2008. **59**(supplement 9): p. 251-64.
3. Suzuki H, A.A., Amitani H, Nakamura N, Inui A, *Cancer cachexia-pathophysiology and management.* J Gastroenterol, 2013. **48**: p. 574-94.
4. Puppa MJ, W.J., Sato S, Cairns M, Baynes JW, Carson JA, *Gut barrier dysfunction in the Apc min/+ mouse model of colon cancer cachexia.* Biochim Biophys Acta, 2012. **1812**(12): p. 1601-6.
5. Puppa MJ, W.J., Velazquez KT, Baltgalvis KA, Sato S, Baynes JW, Carson JA, *The effect of exercise on IL-6 induced cachexia in the Apc min/+ mouse.* J Cachexia Saropenia Muscle, 2012. **3**: p. 117-37.
6. White JP, P.M., Sato S, Gao S, Price RL, Baynes JW, Kostek MC, Matesic LE, Carson JA, *IL-6 regulation on skeletal muscle mitochondrial remodeling during cancer cachexia in the Apc min/+ mouse.* Skeletal Muscle, 2012. **2**(14).
7. Chang S-C, L.J.-K., Lin T-C, Liang W-Y, *Loss of heterozygosity: An independent prognostic factor of colorectal cancer.* World J Gastroenterol, 2005. **11**(6): p. 778-84.
8. Horst D, R.S., Kriegl L, Engel J, Kirchner T, Jung A, *The intreatumoral distribution of beta-catenin is a prognostic marker in colon cancer.* Cancer, 2009. **115**: p. 2063-70.

9. Half E, B.D., Rozen P, *Familial adeomatous polyposis.* Orphanet J Rare Diseases, 2009. **4**(22).

10. Luongo C, M.A., Gledhill S, Dove WF, *Loss of Apc+ in intestinal adenomas from Min mice.* Cancer research, 1994. **54**: p. 5947-52.

11. Bonetto A, A.T., Jin X, Zhang Z, Zhan R, Puzis L, Koniaris LG, Zimmers TA, *JAK/STAT3 pathway inhibition blocks skeletal muscle wasting downstream of IL-6 and in experimental cancer cachexia.* American Journal of Physiology Endocrinology and Metabolism, 2012. **303**(3): p. E410-21.

12. Ando K, T.F., Motojima S, Nakashima K, Kaneko N, Hoshi K, Takahashi K, *Possible role for Tocilizumab, and anti-interleukin-6 receptor antibody, in treating cancer cachexia.* Journal of Clinical Oncology, 2013. **31**(6): p. e69-72.

13. Baltgalvis KA, B.F., Pena MM, Davis JM, Muga SJ, Carson JA, *Interleukin-6 and cachexia in Apc min/+ mice.* American Journal of Physiology Regul Integr Comp Physiol, 2008. **294**(2): p. R393-401.

14. White JP, B.K., Puppa MJ, Sato S, Baynes JW, Carson JA, *Muscle oxidative capacity during IL-6 dependent cancer cachexia.* American Journal of Physiology Regul Integr Comp Physiol, 2011. **300**: p. R201-11.

15. Hetzler KL, H.J., Puppa MJ, Narsale AA, Sato S, Davis JM, Carson JA, *Sex differences in the relationship of IL-6 signaling to cancer cachexia progression.* Biochimica et Biophysica Acta, 2015. **1852**: p. 816-25.

16. Julienne CM, D.J., Goupille C, Pinault M, Berri C, Collin A, Tesseraud S, Couet C, Servais S, *Cancer cachexia is associated with a decrease in skeletal muscle mitochondrial oxidative capacities wirh alteration of ATP production efficiency.* J Cachex Sarco Musc, 2012. **3**: p. 265-75.

17. McClung JM, J.A., Powers SK, Yan Z, *p38 MAPK links oxidative stress to autophagy-related gene expression in cachectic muscle wasting.* Am J Physiol Cell Physiol, 2010. **298**: p. C542-9.

18. Mehl KA, D.J., Berger FG, Carson JA, *Myofiber degeneration/regeneration is induced in the cachectis Apc min/+ mouse.* Journal of Applied Physiology, 2005. **99**: p. 2379-87.

19. Mehl KA, D.J., Clements JM, Berger FG, Pena MM, Carson JA, *Decreased intestinal polyp multiplicity is related to exercise mode and gender in Apc min/+ mice.* Journal of Applied Physiology, 2005. **98**: p. 2219-25.

20. Baltgalvis KA, B.F., Pena MMO, Davis JM, White JP, Carson JA, *Muscle wasting and interleukin-6-induced atrogin1 expression in the cachectic Apc min/+ mouse.* Pflugers Archive, 2009. **457**(5): p. 989-1001.

21. White, J.P., et al., *The regulation of skeletal muscle protein turnover during the progression of cancer cachexia in the Apc(Min/+) mouse.* PLoS One, 2011. **6**(9): p. e24650.

22. White JP, P.M., Narsale A, Carson JA, *Characterization of the male Apc min/+ mouse as a hypogonadism model related to cancer cachexia.* Open Biology, 2013(In press).

23. You S, O.M., Pena MMO, Nassri B, Quiton J, Al-Assad ZA, Liu L, Wood PA, Berger SH, Liu ZJ, Wyatt MD, Price RL, Berger FG, Hrushesky WJM, *Developmental abonormalities in multiple proliferative tissues of Apc min/+ mice.* International J Experimental Pathology, 2006. **87**: p. 227-36.

24. Cho NL, J.S., Carothers AM, Redston M, Bertagnolli MM, *Estrogen receptors alpha and beta and inhibitory modifiers of Apc-dependent tumorigenesis in the proximal colon of Min/+ mice.* Cancer Research, 2007. **67**(5): p. 2366-72.

25. Naugler WE, S.T., Kim S, Maeda S, Kim KH, Elsharkawy AM, Karin M, *Gender disparity in liver cancer due to sex differences in MYD88-dependent IL-6 production.* Science, 2007. **317**: p. 121-4.

26. Nettles KW, G.G., Nowak J, Metivier R, Sharma VB, Greene GL, *CBP is a dosge-dependent regulator of nuclear factor-Kb suppression by the estrogen receptor.* Mol Endocrinol, 2007. **22**(2): p. 263-72.

27. Wang LH, Y.X., Mihalic K, Xiao W, Li D, Farrar WL, *Activation of estrogen receptor blocks interleukin-6-inducible cell growth of human multiple myeloma involving molecular cross-talk between estrogen receptor and STAT3 mediated by co-regulator PIAS3.* J Biol Chem, 2001. **276**(34): p. 31839-44.

28. Bonetto A, A.T., Kunzevitzky, Guttridge DC, Khuri S, Koniaris LG, Zimmers TA, *STAT3 activation in skeletal muscle links muscle wasting and the acute phase response in cancer cachexia.* PLoS One, 2011. **6**(7).

29. Sitnick, M., et al., *Ovariectomy prevents the recovery of atrophied gastrocnemius skeletal muscle mass.* Journal of applied physiology, 2006. **100**(1): p. 286-93.

30. Brown, M., et al., *Estrogen receptor-alpha and -beta and aromatase knockout effects on lower limb muscle mass and contractile function in female mice.* Am J Physiol Endocrinol Metab, 2009. **296**(4): p. E854-61.

31. Swanson HI, W.T., Xie W, Renga B, Zampella A, Distrutti E, Fiorucci S, Kong B, Thomas AM, Guo GL, Narayanan R, Yepuru M, Dalton JT, Chiang JYL, *Role of nuclear receptors in lipid dysfunction and obesity-related diseases.* Drug Metabolism and Disposition, 2012. **41**: p. 1-11.

32. Choi JS, S.J., *Effect of genistein on insulin resistance, renal lipid metabolism, and antioxidative activities in ovariectomized rats.* Nutrition, 2009. **25**: p. 676-85.

33. Wang M, T.B., Reiger KM, Brown JW, Meldrum DR, *17-beta-estradiol decreases p38 MAPK-mediated myocardial inflammation and dysfunction following acute ischemia.* Journal of Molecular and Cellular Cardiology, 2006. **40**: p. 205-12.

34. Chakrabarti S, D.S., *Estradiol modulates tumor necrosis factor-induced endothelial inflammation: role of tumor necrosis factor receptor 2.* Journal of Vascular Research, 2013. **50**(1): p. 21-34.

35. Liu CJ, L.J., Kuo CH, Chu CH, Chen LM, Tsai FJ, Tsai CH, Tzang BS, Kuo WW, Huang CY, *Akt mediates 17beta-estradiol and/or estrogen receptor-alpha inhibition of LPS-induced tumor necrosis factor-alpha expression and myocardial cell apoptosis by suppressing the JNK1/2-NFkB pathway.* Journal of Cellular and Molecular Medicine, 2009. **13**(9B): p. 3655-67.

36. Cossette E, C.I., Tardif K, DonPierre G, Tanguay J-F, *Estradiol inhibits vascular endothelial cells pro-inflammatory activation induced by C-reactive protein.* Molecular and Cellular Biochemistry, 2013. **373**: p. 137-47.

37. Xiao E, X.-Z.L., Ferin M, Wardlaw SL, *Differential effects of estradiol on the adrenocorticotropin responses to interleukin-6 and interleukin-1 in the monkey.* Endocrinology, 2001. **142**(7): p. 2736-41.

38. Barros, R.P., et al., *Muscle GLUT4 regulation by estrogen receptors ERbeta and ERalpha.* Proc Natl Acad Sci U S A, 2006. **103**(5): p. 1605-8.

39. Greising SM, B.K., Kosir AM, Moran AL, Warren GL, Lowe DA, *Estradiol's beneficial effect on murine muscle function is independent of muscle activity.* Journal of Applied Physiology, 2011. **110**: p. 109-15.

40. McClung JM, D.J., Wilson MA, Goldsmith EC, Carson JA, *Estrogen status and skeletal muscle recovery from disuse atrophy.* J Appl Physiol, 2006. **100**: p. 2012-23.

41. Lim J, L.U., *Oxidative damage increases and antioxidant gene expression decreases with aging in the mouse ovary.* Biology of Reproduction, 2011. **84**: p. 775-82.

42. Nikolajuk A, K.I., Karczewska-Kupczewska M, Adamska A, Otziomek E, Wolczynski S, Kinalska I, Gorska M, Straczkowski M, *Serum soluble glycoprotein 130 concentration is*

inversely related to insulin sensitivity in women with polcystic ovary syndrome. Diabetes, 2010. **59**(4): p. 1026-9.

43. Lengyel, E., *Ovarian cancer development and metastasis.* The American journal of pathology, 2010. **177**(3): p. 1053-64.

44. Chen J, I.D., *Estrogen in obesity-associated colon cancer: friend or foe? Protecting postmenopausal women but promoting late-stage colon cancer.* Cancer causes & control : CCC, 2012. **23**: p. 1767-73.

45. Kemik, O., et al., *The relationship among acute-phase response proteins, cytokines and hormones in cachectic patients with colon cancer.* World journal of surgical oncology, 2010. **8**: p. 85.

46. Cannon TY, G.D., Dahlman J, George JR, Lai V, Shores C, Buzkova P, Couch ME, *The effect of altered toll-like receptor 4 signaling on cancer cachexia.* Arch Otolaryngol Head Neck Surg, 2007. **133**(12): p. 1263-9.

47. Greco SH, T.L., Vahle A-K, Rokosh R, Avanzi A, Mahmood SK, Deutsch M, Alothman S, Alqunaibit D, Ochi A, Zambirinis C, Mohaimin T, Rendon M, Levie E, Pansari M, Torres-Hernandez A, Daley D, Barilla R, Pachter HL, Tippens D, Malik H, Boutaajangout A, Wisniewski T, Miller G, *TGFbeta blockade reduces mortality and metabolic changes in a validated murine model of pancreatic cancer cachexia.* PLoS One, 2015. **10**(7): p. e0132786.

48. Talbert EE, G.D., *Impaired regeneration: A roole for the muscle microenvironment in cancer cachexia.* Sem Cell Dev Biol, 2015. **epub before print**.

49. Antunes, D., et al., *Molecular insights into mitochondrial dysfunction in cancer-related muscle wasting.* Biochim Biophys Acta, 2014. **1841**(6): p. 896-905.

50. White JP, R.J., Washington TA, Sato S, Davis JM, Wilson LB, Carson JA, *Overload-induced skeletal muscle extracellular matrix emodelling and myofibre growth in mice lacking IL-6.* Acta Physiologica, 2009. **197**: p. 321-32.

51. Washington TA, W.J., Davis JM, Wlson LB, Lowe LL, Sato S, Carson JA, *Skeletal muscle mass recovery from atrophy in IL-6 knockout mice.* Acta Physiologica, 2011. **202**(4): p. 657-69.

52. Yao X, H.J., Zhong H, Shen N, Faggioni R, Fung M, Yao Y, *Targeting interleukin-6 in inflammmatory autoimmune diseases and cancers.* Pharmacology and Therapeutics, 2014. **141**: p. 125-39.

53. Klover PJ, Z.T., Koniaris LG, Mooney RA, *Chronic exposure to interleukin-6 causes hepatic insulin resistance in mice.* Diabetes, 2003. **52**: p. 2784-9.

54. Shao R, N.M., Karlsson-Lindahl L, Benrick A, Weijdegard B, Lager S, Egecioglu E, Fernandez-Rodriguez J, Gemzell-Danielsson K, Ohlsson C, Jansson J-O, Billig H, *Downregulation of cilia-localized IL-6R alpha by 17beta-estradiol in mouse and human fallopian tubes.* American Journal of Physiology Cell Physiology, 2009. **297**: p. C140-151.

55. Lee SY, B.I., Dulay AT, Ali UA, Zhao G, Abdel-Razeq SS, Bahtiyar MO, Thung SF, Funai EF, Buhimschi CS, *IL-6 trans-signaling system in intra-amniotic inflammation, preterm birth, and preterm premature rupture of the membranes.* Journal of Immunology, 2011. **186**: p. 3226-36.

56. Lo C-W, C.M.-W., Hsiao M, Wang S, Chen C-A, Hsiao S-M, Chang J-S, Lai T-C, Rose-John S, Kuo M-L, Wei L-H, *IL-6 trans-signaling in formation and progression of malignant ascites in ovarian cancer.* Cancer Research, 2011. **71**(2): p. 424-34.

57. O'Brien SM, F.P., Scully P, Landers AMT, Scott LV, Dinan TG, *Impact of gender and menstrual cycle phase on plasma cytokine concentrations.* Neuroimmunomodulation, 2007. **14**: p. 84-90.

58. Syed V, U.G., Mok SC, Ho S-M, *Reproductive hormone-induced STAT3-mediated interleukin-6 action in normal and malignant human ovarian surface epithelial cells.* Journal of the National Cancer Institute, 2002. **94**(8): p. 617-29.

59. Wang Y, v.B.-D.A., Cheon HJ, Yang J, Stark GR, *STAT3 activation in response to IL-6 is prolonged by the binding of the IL-6 receptor to EGF receptor.* Proc Natl Acad Sci, 2013. **110**(42): p. 16975-80.

60. White JP, P.M., Gao S, Sato S, Welle SL, Carson JA, *Muscle mTORC1 suppression by IL-6 during cancer cachexia: a role for AMPK.* American Journal of Physiology Endocrinology and Metabolism, 2012. **304**: p. E1042-52.

61. Redzic JS, K.A., Bahmed K, Dahl KD, Pearson CG, Robinson WA, Robinson SE, Graner MW, Eisenmesser EZ, *Extracellular vesicles secreted from cancer cell lines stimulate secretion of MMP-9, IL-6, TGF-b1 and EMMPRIN.* PLoS One, 2013. **8**(8): p. e71225.

62. Stephens NA, G.C., MacDonald AJ, Tan BH, Galagher IJ, Skipworth RJE, Ross JA, Fearon KCH, Greig CA, *Sexual dimorphism modulates the impact of cancer cachexia on lower limb muscle mass and function.* Clinical Nutrition, 2012. **31**: p. 499-505.

63. Kilgour RD, V.A., Trutschnigg B, Hornby L, Lucar E, Bacon SL, Morais JA, *Cancer-related fatigue: the impact of skeleatl muscle mass and strength in patients with advanced cancer.* J Cachexia Saropenia Muscle, 2010. **1**: p. 177-85.

64. Cosper, P.F. and L.A. Leinwand, *Cancer causes cardiac atrophy and autophagy in a sexually dimorphic manner.* Cancer research, 2011. **71**(5): p. 1710-20.

65. Baehr LM, T.M., Bodine SC, *Muscle hypertrophy is associated with increases in proteasome activity that is independent of MuRF1 and MAFbx expression.* Frontiers in Physiology, 2014.

66. Burney BO, G.J., *Hypogonadism in male cancer patients.* J Cachexia Saropenia Muscle, 2012. **3**(149-55).

67. Mondello P, L.A., Mondello S, Bolignano D, Pitini V, Aloisi C, Buemi M, *Emerging markers of cachexia predict survival in cancer patients.* BMC Cancer, 2014. **14**(828).

68. Abdullah SM, K.A., Leonard D, Das SR, Canham RM, Kamath SA, Vega GL, Grundy SM, McGuire DK, de Lemos JA, *Sex differences in the association between leptin and CRP: Results from the Dallas Heart Study.* Atherosclerosis, 2006. **195**: p. 404-10.

69. Ghazeeri G, A.L., Abbas O, *Immunological differences in women compared with men: Overview and contributing factors.* American Journal of Reproductive Immunology, 2011. **66**: p. 163-9.

70. Zhang D, Z.Y., Wu L, Wang S, Zheng H, Yu B, Li J, *Association of IL-6 gene ploymorphisms with cachexia susceptibility and survival time of patients with pancreatic cancer.* Ann Clin Lab Sci, 2008. **48**(2): p. 113-9.

71. Uri-Belapolsky S, S.A., Eliyahu E, Grossman H, Levi M, Chuderland D, Ninio-Many L, Hasky N, Shashar D, Almog T, Kandel-Kfir M, Harats D, Shalgi R, Kamari Y, *Interleukin-1 deficiency prolongs ovarian lifespan in mice.* Proc Natl Acad Sci U S A, 2014. **111**(34): p. 12492-7.

72. Wu JM, Z.M., Ingram DK, Ottinger MA, *Ovarian aging and menopause: Current theories, hypotheses, and research models.* Experimental Biology and Medicine, 2005. **230**: p. 818-28.

73. Caligoni, *Assessing reproductive status/stages in mice.* Current Protocols in Neuroscience, 2009. **Appendix**: p. 4I.

74. Rolaki A, D.P., Millingos S, Loutradis D, Makrigiannakis A, *Novel trends in follicular development, atresia, and corpus luteum regression: a role for apoptosis.* Reproductive BioMedicine, 2005. **11**(1).

75. Ribas V, N.M., Henstridge DC, Nguyen A-K, Beaven SW, Watt MJ, Hevener EL, *Impaired oxidative metabolism and inflammation are associated with insulin resistance in estrogen receptor alpha-deficient mice.* Physiol Endocrinol Metab, 2010. **298**(2): p. 304-19.

76. Iwasa T, M.T., Kinouchi R, Gereltsetseg G, Murakami M, Munkhzaya M, Altankhuu T, Kuwahara A, Yasui T, Irahara M, *Changes in central and peripheral inflammatory responses to lippolysaccharide in ovariectomized female rats.* Cytokine, 2014. **65**: p. 65-73.

77. Bredfeldt, T.G., et al., *Xenoestrogen-induced regulation of EZH2 and histone methylation via estrogen receptor signaling to PI3K/AKT.* Mol Endocrinol, 2010. **24**(5): p. 993-1006.

78. Martin LA, J.S., Ali S, Marshall C, Dowsett M, *Enhanced estrogen receptor (ER) alpha, ERBB2, and MAPK signal transduction pathways operate during the adaptation of MMCF-7 cells to long-term estrogen deprivation.* J Biol Chem, 2003. **278**(33): p. 30458-68.

79. Yokomaku D, N.T., Numakawa Y, Suzuki S, Matsumoto T, Adachi N, Nishio C, Taguchi T, Hatanaka H, *Estrogen enhances depolarization-induced glutamate release through activation of PI3K and MAPK in cultured hippocampal neurons.* Mol Endocrinol, 2003. **17**(5): p. 831-44.

80. Numakawa T, M.T., Numakawa Y, Richards M, Yamawaki S, Kunugi H, *Protective action of neurotrophic factors and estrogen against oxidative stress-mediated neurodegeneration.* J Toxicol, 2011.

81. Numakawa Y, M.T., Yokomaku D, Taguchi T, Niki E, Hatanaka H, Kunugi H, Numakawa T, *17 beta-estradiol protects cortical neurons against oxidative stress-induced cell death through reduction in the activity of mitogen-activated protein kinase and in the accumulation of extracellular calcium.* Endocrinology, 2007. **148**(2): p. 627-37.

82. Liu H, P.A., Kim JK, *Oestrogen prevents cardiomyocyte apoptosis by suppressing p38 alpha-mediated activation of p53 and by down-regualting p53 inhibition on p38 beta.* Cardiovascular Research, 2010.

83. Wang M, W.Y., Weil B, Abarbanell A, Herrmann J, Tan J, Kelly M, Meldrum DR, *Estrogen receptor beta mediates increased activation of PI3K/Akt signaling and improved myocardial function in female hearts following acute ischemia.* Am J Physiol Regul Integr Comp Physiol, 2009. **296**: p. 972-8.

84. Brown M, N.J., Ferreira A, Bogener JL, Lubahn DB, *Estrogen receptor alpha and beta and aromatase knockout effects on lower limb muscle mass and contractile function in female mice* American Journal of Physiology Endocrinology and Metabolism, 2009. **296**: p. E854-61.

85. Ahtiainen M, P.E., Ronkainen PHA, Alen M, Puolakka J, Kaprio J, Sipila S, Kovanen V, *Age and estrogen-based hormone therapy affect systemic and local IL-6 and IGF-1 pathways in women.* AGE, 2012. **34**: p. 1249-60.

86. Vasconsuelo A, M.L., Boland R, *Participation of HSP27 in the antiapoptotic action of 17 beta-estradiol in skeletal muscle cells.* Cell stress and chaperones, 2010. **15**: p. 183-92.

87. Rogers NH, P.J.I., Strissel KJ, Obin MS, Greenberg AS, *Loss of ovarian function in mice results in abrogated skeletal muscle PPARdelta and FoxO1-mediated gene expression.* Biochem Biophys Res Commun 2010. **392**(1): p. 1-3.

88. Weige CC, A.K., Allred CD, *Estradiol alters cell growth in nonmalignant colonocytes and reduces the formation of preneoplastic lesions in the colon.* Cancer Research, 2009. **69**: p. 9118-24.

89. Press OA, Z.W., Gordon MA, Yang D, Haiman CA, Azuma M, Iqbal S, Lenz H-J, *Gender-related survival differences associated with polymorphic variants of estrogen receptor beta (ERb) in patients with metastatic colon cancer.* Pharmacogenomics J, 2011. **11**(5): p. 375-82.

90. Hartman J, E.K., Lindberg K, Zhao C, Williams C, Strom A, Gustaffson J-A, *Tumor repressive functions of estrogen receptor beta in SW480 colon cancer cells.* Cancer Research, 2009. **69**(15): p. 6100-6.

91. Rondini EA, H.A., Steibel JP, Hursting SD, Fenton JI, *Energy balance modulates colon tumor growth: Interactive roles of insulin and estrogen.* Molecular Carcinogenesis, 2011. **50**(5): p. 370-82.

92. Edwards KM, M.P., *Effects of estrogen versus estrogen and progesterone on cortisol and interleukin-6.* Maturitas, 2008. **61**(4): p. 330-3.

93. Salmassi A, L.S., Hedderich J, Oettinghaus C, Jonat W, Mettler L, *Interaction of Interleukin-6 on human granulosa cell steroid secretion.* Journal of Endocrinology, 2001. **170**: p. 471-8.

94. Tamura K, K.T., Hara T, Takatoshi S, Tohei A, Miyajima A, Seishi T, Kogo H, *Interleukin-6 descreases estrogen production and messenger ribonucleic acid expression encoding aromatase during in vitro cytodifferentiation of rat granulosa cell.* Molecular and Cellular Endocrinology, 2000. **170**: p. 103-111.

95. Nash, M.A., et al., *The role of cytokines in both the normal and malignant ovary.* Endocr Relat Cancer, 1999. **6**(1): p. 93-107.

96. Tringali C, S.T., Silvestri I, Vitale J, Scurati R, Michielon G, Alberti G, Venerando B, *Protective role of 17-beta-estradiol towards IL-6 leukocyte expression induced by intense training in young female athletes.* Journal of Sports Sciences, 2013.

97. Pottratz ST, B.T., Mocharia H, Crabb D, Manolagas SC, *17 beta estradiol inhibits expression of human interleukin 6 promoter reporter constructs by a receptor-dependent mechanism.* Journal of Clinical Investigation, 1994. **93**: p. 944-50.

98. Palanivel R, F.M., Galic S, Honeyman J, Hewitt KA, Jorgensen SB, Steinberg GR, *Reduces Socs3 expression in adipose tissue protects female mice against obesity-induced insulin resistance.* Diabetologia, 2012. **55**: p. 3083-93.

99. Speirs V, K.M., Walton DS, Newton CJ, Desai SB, Atkin SL, *Direct activation of oestrogen receptor alpha by interleukin-6 in primary cultures of breast cancer epithelial cells.* British Journal of Cancer, 2000. **82**(7): p. 1312-6.

100. Azerbaijani BA, S.M., Oskam IC, Nurmio M, Laine T, Tinkanen H, Makinen S, Tanbo TG, Hovatta O, Jahnukainen K, *Effect of previous chemotherapy on the quality of cryopreserved human ovarian tissue in vitro.* PLoS One, 2015 **10**(7): p. e0133985.

101. Sklar, C.A., et al., *Premature menopause in survivors of childhood cancer: a report from the childhood cancer survivor study.* J Natl Cancer Inst, 2006. **98**(13): p. 890-6.

102. D'Eon TM, S.S., Aronovitz M, Obin MS, Fried SK, Greenberg AS, *Estrogen Regulation of of Adiposity and Fuel Partitioning.* J Biol Chem, 2005. **280**(43): p. 35983-91.

103. Enns DL, T.P., *The influence of estrogen on skelestal muscle: Sex matters.* Sports Med, 2010. **40**(1): p. 41-58.

104. Ogawa M, K.T., Harada N, Yamaji R, *Female-specific regulation of skeletal muscle mass by USP19 in young mice.* Journal of Endocrinology, 2015. **225**(3): p. 135-45.

105. Baltgalvis KA, B.F., Pena MM, Davis JM, White JP, Carson JA, *Activity level, apoptosis, and development of cachexia in Apc min/+ mice.* Journal of Applied Physiology, 2010. **109**: p. 1155-61.

106. White JP, B.J., Welle SL, Kostek MC, Matesic LE, Sato S, Carson JA, *The regulation of skeletal muscle protein turnover during the progression of cancer cachexia in the Apc min/+ mouse.* PLoS One, 2011. **6**(9): p. e24650.

107. Cosper PF, L.L., *Cancer causes cardiac atrophy and autophagy in a sexually dimorphic manner.* Cancer Research, 2011. **71**(5): p. 1710-20.

108. Norman K, S.N., Reiss J, Schulzke J, Valentini L, Pirlich M *Effect of sexual dimorphism on muscle strength in cachexia.* J Cachexia Saropenia Muscle, 2012. **3**: p. 111-6.

109. Somasundaram R, H.D., *Chemokines and the microenvironment in neuroectodermal tumor-host interaction.* Seminars in Cancer Biology, 2009. **19**(2): p. 92-6.

110. Tso VK, S.B., Foshaug RR, Churchill TA, Doyle J, Slupsky CM, Fedorak RN, *Meatbolomic Profiles are gender, disease, and timespecific in the interleukin-10 gene-deficient mouse model of inflammatory bowel disease.* PLoS One, 2013. **8**(7): p. e67654.

111. Xing D, N.S., Chen Y-F, Hage F, Oparil S, *Estrogen and mechanisms of vascular protection.* Arteriosclerosis, Thrombosis, and Vascular Biology, 2009. **29**(3): p. 289-95.

112. Scheede-Bergdahl C, W.H., Trutschnigg B, Kilgour RD, Haggarty A, Lucar E, Vigano A, *Is IL-6 the best pro-inflammatory biomarker of clinical outcomes of cancer cachexia?* Clinical Nutrition, 2012. **31**(1): p. 85-8.

113. Kim HJ, K.H., Yun J, Kim KH, Kim SH, Lee S-C, Bae SB, Kim C-K, Lee NS, Lee KT, Park SK, Won JH, Park HS, Hong DS, *Pathophysiological role of hormones and cytokines in cancer cachexia.* J Korean Med Sci, 2012. **27**: p. 128-34.

114. Onesti JK, G.D., *Inflammation based regulation of cancer cachexia.* BioMed Research International, 2014.

115. Mihara M, H.M., Yoshida H, Suzuki M, Shiina M, *IL-6/IL-6 receptor system and its role in physiological and pathological conditions.* Clinical Science, 2012. **122**: p. 143-59.

116. Tzeng HE, T.C., Chang ZL, Su CM, Wang SW, Hwang WL, Tang CH, *Interleukin-6 induces vascular endothelial growth factor expression and promotes angiogenesis through apoptosis signal-regulating kinase 1 in human osteosarcoma.* Biochemical Pharmacology, 2013. **85**(4): p. 531-40.

117. Puppa, M.J., et al., *The effect of exercise on IL-6-induced cachexia in the Apc (Min/+) mouse.* J Cachexia Sarcopenia Muscle, 2011.

118. Hetzler KL, C.B., Shanely RA, Sue H, Kostek MC, *The homeobox gene Six1 alters myosin heavy chain isoform expression in mouse skeletal muscle.* Acta Physiologica, 2013.

119. Puppa MJ, G.S., Narsale AA, Carson JA, *Skeleatl muscle glycoprotein 130's role in Lewis lung carcinoma-induced cachexia.* FASEB journal : official publication of the Federation of American Societies for Experimental Biology, 2014. **28**(2): p. 998-1009.

120. Hardee JP, P.M., Fix DK, Gao S, Hetzler KL, Bateman TA, Carson JA, *The effect of radiation dose on mouse skeletal muscle remodeling.* Radiology and Oncology, 2014. **48**(3): p. 247-56.

121. Steiner JL, D.J., McClellan JL, Guglielmotti A, Murphy EA, *Effects of the MCP-1 synthesis inhibitor bindarit on tumorigenesis and inflammatory markers in the C3(1)/SV40Tag mouse model of breast cancer.* Cytokine, 2014. **66**: p. 60-8.

122. Murphy EA, D.J., McClellan JL, Carmichael MD, *Quercetin's effects on intestinal polyp multiplicity and macrophage number in the Apc min/+ mouse.* Nutrition and Cancer, 2011. **63**(3): p. 421-6.

123. Iwase S, M.T., Saito Y, Nakagawa K, *Steep elevation of blood interleukin-6 (IL-6) associated only with late stage of cachexia in cancer patients.* European cytokine network, 2004. **15**(4): p. 312-6.

124. Argiles JM, L.-S.F., *The role of cytokines in cancer cachexia.* Medicinal Research Reviews, 1999. **19**(3): p. 223-48.

125. Suh S-Y, C.Y., Yeom CH, Kwak SM, Yoon HM, Kim DG, Koh S-J, Park J, Lee MA, Lee YJ, Seo A-R, Ahn H-Y, Yim E, *Interleukin-6 but not tumor necrosis factor-alpha predicts survival in patients with advanced cancer.* Support Care Cancer, 2013. **21**: p. 3071-7.

126. Gandolfi S, G.B., Terzoni D, Civardi G, Cavanna L, *Favorable responses to Tocilizumab in two patients with cancer-related cachexia.* Journal of Pain and Symptom Management, 2013. **46**(2): p. E9-13.

127. Senthil Kumar SPD, S.M., Spicer EG, Goudjo-Ako AJ, Stumph JD, Zhang J, Shi H, *Distinct metabolic effects following short-term exposure of different high-fat diets in male and female mice.* Endocrine Journal, 2014.

128. Bloor ID, S.M., *Sexual dimorphism in white and brown adipose tissue with obesity and inflammation.* Hormones and Behavior, 2014.

129. Mantovani G, M.A., Madeddu C, Serpe R, Massa E, Dessi M, Panzone F, Contu P, *Randomized Phase III Clinical Trial of Five Different Arms of Treatment in 332 patients with cancer cachexia.* The Oncologist, 2010. **15**(2): p. 200-11.

130. Ruzzo A, C.V., Canestrari E, Giacomini E, Santini D, Tonini G, Vincenzi B, Fiorentini G, Magnani M, Graziano F, *Genetic modulation of the interleukin 6 (IL-6) system in patients with advanced gastric cancer: a background for an alternative target therapy.* BMC Cancer, 2014. **14**(357).

131. Carson JA, B.K., *Interleukin-6 as a key regulator of muscle mass during cachexia.* Exerc Sport Sci Rev, 2010. **38**(4): p. 168-176.

132. Batista Jr. ML, O.M., Alcantara PSM, Sandoval R, Peres SB, Neves RX, Silverio R, Maximiano LF, Otoch JP, Seelaender M, *Adipose tissue-derived factors as potential biomarkers in cachectic cancer patients.* Cytokine, 2013. **61**: p. 532-9.

133. Klein C, W.T., Assmus U, Roskams T, Rose-John S, Muller M, Manns MP, Ernst M, Trautwein C, *The IL-6-gp130-STAT3 pathway in hepatocytes triggers liver protection in T cell-mediated liver injury.* Journal of Clinical Investigation, 2005. **115**(4): p. 860-9.

134. Weidle UH, K.S., Eggle D, Kruger A, *Interleukin 6/Interleukin 6 receptor interaction and its role as a therapeutic target for treatment of cachexia and cancer.* Cancer Genomics and Proteomics, 2010. **7**: p. 287-302.

135. Li Y, H.M.-F., Li W-N, Shi A-C, Zhang Y-Y, Wang H-Y, Wang F-X, Li L, Wu T, Ding L, Chen T, Yan W-M, Luo X-P, Ning Q, *SOCS3 expression correlates with severity of inflammation in mouse hepatitis virus strain 3-induced acute liver failure and HBV-ACLF*. Journal of Huazhong University Science and Tehcnology 2014. **34**(3): p. 348-53.

136. Liu X, C.B., Campbell IK, Gauci SJ, Alexander WS, Tonkin BA, Walsh NC, Linossi EM, Nicholson SE, Lawlor KE, Wicks IP, *Supressor of cytokine signaling-3 regulates gp130 cytokine-induced signaling to limit chondrocyte responses during inflammatory arthritis.* Arthritis and Rheumatism, 2014.

137. White GE, C.A., Addley MR, Soilleux EJ, Greaves DR, *Suppressor of cytokine signaling protein SOCS3 expression is increased at sites of acute and chronic inflammation.* Journal of Molecular Histology, 2011. **42**: p. 137-51.

138. Kemik O, S.A., Kemik AS, Hasirci I, Purisa S, Dulger AC, Demiriz B, Tuzun S, *The relationship among acute-phase response proteins, cytokines, and hormones in cachectic patients with colon cancer.* World J Surg Oncol, 2010. **8**(85).

139. Pirlich M, N.K., Lochs H, Bauditz J, *Role of intestinal function in cachexia.* Current Opinions in CLinical Nutrition and Metabolic Care, 2006. **9**: p. 603-6.

140. Maggio M, C.G., Lauretani F, Bandinelli S, Corsi AM, Giallauria F, Guralnik JM, Zuliani G, Cattabiani C, PArrino S, Ablondi F, Dall'Aglio E, Ceresini G, Basaria S, Ferrucci L, *SHBG, sex hormones, and inflammatory markers in older women.* Journal of Clinical Endocrinology and Metabolism, 2011. **96**(4): p. 1053-9.

141. Nikolettos N, A.B., Koster F, Schopper B, Schulz CH, Caglar GS, Efthimiadou A, Pagonopoulou O, Diedrich K, Al-Hasani S, *Cytokine profile in cases with premature elevation of progesterone serum concentrations during ovarian stimulation.* Physiol Res, 2008. **57**: p. 215-224.

142. Wei L-H, C.C.-H., Chen M-W, Rose-John S, Kuo M-L, Chen S-U, Yang Y-S, *The role of IL-6 trans signaling in vascular leakage: Implications for ovarian hyperstimulation syndrome in a murine model.* Journal of Clinical Endocrinology and Metabolism, 2013. **98**(3): p. E472-84.

143. Johnson LNC, S.M., Dillon KE, Lechtenberg L, Schanne A, Gracia CR, *Antimullerian hormone and antral follicle count are lower in female cancer survivors and healthy women taking hormonal contraception.* Fertility and Sterility2014. **102**(3): p. 774-81.

144. Durlinger ALL, G.M., Kramer P, Karels B, Kumar TR, Matzuk MM, Rose UM, de Jong FH, Uilenbroek JTJ, Grootegoed JA, Themmen APN, *Anti-Mullerian hormone attenuates*

the effects of FSH on follicle development in the mouse ovary. Endocrinolgy, 2001. **142**(11): p. 4891-9.

145. Dewailly, D., et al., *The physiology and clinical utility of anti-Mullerian hormone in women.* Hum Reprod Update, 2014. **20**(3): p. 370-85.

146. Tsai VWW, H.Y., Manandhar R, Lee-Ng KKM, Zhang HP, Harriott K, Jiang L, Lin S, Siansbury A, Brown DA Briet SN, *Anorexia/Cachexia of chroonic diseases: A role for the TGFbeta family cytokine MIC-1/GDF15.* J Cachex Sarco Musc, 2012. **3**: p. 239-43.

147. Wakefield LM, H.C., *Beyond TGFbeta: Roles of other TGFbeta superfamily members in cancer.* Nature Reviews Cancer 2013. **13**: p. 328-41.

148. Diakowska D, K.-K.M., Markocka-Maczka K, Diakowski W, Matusiewicz M, Grabowski K, *Circulating leptin and inflammatory response in esophageal cancer, esophageal cancer-related cachexia-anorexia syndrome (CAS), and non-malignant CAS of the alimentary tract.* Cytokine, 2010. **51**: p. 132-7.

149. Loret de Mola, J.R., et al., *Gonadotropins induce the release of interleukin-1 beta, interleukin-6 and tumor necrosis factor-alpha from the human preovulatory follicle.* Am J Reprod Immunol, 1998. **39**(6): p. 387-90.

150. Hannon, P.R., et al., *Di(2-ethylhexyl) phthalate inhibits antral follicle growth, induces atresia, and inhibits steroid hormone production in cultured mouse antral follicles.* Toxicol Appl Pharmacol, 2015. **284**(1): p. 42-53.

151. Chou SH, M.C., *Role of leptin in human reproductive disorders.* J Endo, 2014. **223**(1): p. T49-62.

152. Akyol S, C.S., Purisa S, Aydinli K, *Relationship between lymphocytes, IL-2, and the hormones E2, LH, PRg, and FSH in menopausal and postmenopausal women.* Am J Repro Immunol, 2011. **66**: p. 304-9.

153. Rouach V, K.S., Koch Y, Stern N, Somjen D, *Bone loss in ovariectomized rats: Dominant role for estrogen but apparently not for FSH.* J Cell Biochem, 2011. **112**: p. 128-37.

154. Thompson IR, K.U., *GnRH pulse frequency-dependent differential regulation of LH and FSH gene expression.* Mol Cell Endocrinol, 2014. **385**: p. 28-35.

155. Brauner R, P.S., Bignon-Topalovic J, McElreavy K, Bashamboo A, *Etiology of primary ovarian insufficiency in a series of young girls presenting at a pediatric endocrinology center.* Eur J Pediatr, 2015. **174**: p. 767-73.

156. Silva CA, Y.L., Aikawa NE, Araujo DB, Carvalho JF, Bonfa E, *Autoimmune primary ovarian insufficiency.* Autoimmun Rev, 2014. **13**: p. 427-30.

157. Fourman LT, F.P., *Neuroendocrine causes of amenorrhea- An update.* J Clin Endocrinol metab, 2015. **100**(3): p. 812-24.

158. Tsoli M, S.M., Vanniasinghe AS, Painter A, Zechner R, Clarks S, Robertson G, *Depletion of white adipose tissue in cancer cachexia syndrome is associated with inflammatory signaling and disrupted circadian regulation.* PLoS One, 2013. **9**(3): p. e92966.

159. Yang, Y., et al., *Increased activity of osteocyte autophagy in ovariectomized rats and its correlation with oxidative stress status and bone loss.* Biochem Biophys Res Commun, 2014. **451**(1): p. 86-92.

160. Choi M, C.J.-W., Chaudhari HN, Aseer KR, Mukherjee R, Yun JW, *Gender-dimorphic regulation of skeletal muscle proteins in streptozotocin-induced diabetic rats.* Cellular Physiology and Biochemistry 2013. **31**: p. 408-20.

161. Fujita S, R.B., Bell JA, Cadenas JG, Volpi E, *Basal muscle intracellular amino acid kinetics in women and men.* American Journal of Physiology Endocrinology and Metabolism, 2007. **292**(1): p. E77-83.

162. Marcinko, K. and G.R. Steinberg, *The role of AMPK in controlling metabolism and mitochondrial biogenesis during exercise.* Exp Physiol, 2014. **99**(12): p. 1581-5.

163. Spangenburg, E.E., et al., *Regulation of Physiological and Metabolic Function of Muscle by Female Sex Steroids.* Medicine and science in sports and exercise, 2012.

164. Miyamoto N, M.M., Suzuma I, Suzuma K, Kobayashi K, Honda Y, *Estrogen protects against cellular infiltration by reducing the expressions of e-selectin and IL-6 in endotoxin-induced uveitis.* Journal of Immunology, 1999. **163**: p. 374-9.

165. Baltgalvis, K.A., et al., *Estrogen regulates estrogen receptors and antioxidant gene expression in mouse skeletal muscle.* PLoS One, 2010. **5**(4): p. e10164.

166. Chen Z, Y.I., Galcheva-Gargova Z, Karas RH, Mendelsohn ME, Shaul PW, *Estrogen receptor alpha mediates the nongenomic activation of endothelial nitric oxide synthase by estrogen.* Journal of Clinical Investigation, 1999. **103**(3): p. 401-6.

167. Caligioni, *Assessing reproductive status/stages in mice.* Current Protocols in Neuroscience, 2009. **Appendix**(Appendix-4I).

APPENDIX A

DETAILED METHODS

A.1 Animals

Female *Apc* $^{Min/+}$mice (n=75) and female C57BL/6 mice (n=12) were bred and maintained at the University of South Carolina Animal Resource Facility. *Apc*$^{Min/+}$ mice used were on a C57BL/6 background and were offspring from breeders originally purchased from Jackson Labs (Bar Harbor, ME, USA). Mice were kept on a 12:12h light/dark cycle beginning at 7:00 AM and were given unrestricted access to standard rodent chow (Harlan Teklad Rodent Diet, #8604, Harlan, Indianapolis, IN, USA). Mice were weighed weekly. Food intake was measured at 12 and 18 weeks of age. All experiments were approved by the University of South Carolina's Institutional Animal Care and Use Committee. Mice were sacrificed at 18 or 15 weeks using the following recipe to anesthetize before tissue dissection:

Ketamine	0.11	90 mg/kg BW	**100 mg/ml**
Xylazine	0.09	7 mg/kg BW	**20 mg/ml**
Acepromazine	0.03	1 mg/kg BW	**10 mg/ml**

A.2 Determination of estrus cycling and stage of cycle

Female *Apc* $^{Min/+}$ and C57BL/6 mice had estrus cycling tracked from 10 weeks of age until sacrifice at 18 weeks of age as follows:

1. A sterile cotton swab was dipped in sterile 0.9% saline.
2. The mouse was grasped by the base of the tail, and the cotton swab was gently inserted 0.5 cm into the vagina to collect cells.

3. Cells collected were smeared onto a glass slide (VWR, Radnor, PA, USA) and allowed to dry.
4. Slides were dipped for 5-10 minutes in hematoxylin (Ricca Chemical Company, Arlington, TX, USA), rinsed in deionized water, and allowed to dry.
5. Cell populations were visualized with an Olympus BX41 microscope (Tokyo, Japan) at 100x, and estrus cycle presence and stage were classified based on the observations of Caligoni [73].

A.3 Ovariectomy

Female *Apc* $^{Min/+}$ and C57BL/6 mice were ovariectomized at 11 weeks of age using the following protocol:

1. Mice were anesthetized by ketamine/acepromazine/xylazine.
2. Once anesthetized, the mouse was placed in a prone position on a sterile absorbent pad. The back was shaved from the caudal edge of the ribcage to the base of the tail. The shaved region was then sterilized with betadine (PDI, Orangeburg, NY, USA) and rubbing alcohol (PDI).
3. In a sterile field, using sterilized instruments, a 2-cm dorsal midline incision was made with sterile scissors halfway between the caudal edge of the ribcage and the base of the tail. Fascia was the cleared away by blunt dissection. As second 1-cm long incision was made into the muscle wall.
4. The ovary and surrounding fat pad were extracted through the incision with forceps. A hemostat was closed around the distal oviduct/uterine horn to terminate blood supply to the ovary.

5. Non-absorbable suture (AD Surgical, Sunnyvale, CA) was used to tie off the oviduct, and the ovary was removed. The uterine horn was returned to the peritoneal cavity, and absorbable suture (AD Surgical) was used to close the muscle incision. Wound clips were used to close the skin incision, and the process was repeated on the contralateral side.
6. Mice were placed an a heating pad until they awoke and were given 0.01 mg/kg buprenorphine (Burprenex ©, Reckitt Benckiser Pharmaceuticals, Pendergrass, GA, USA) for pain. Wound clips were removed 7 days after surgery.

A.4 IL-6 overexpression by electroporation

In vivo intramuscular electroporation of an IL-6 plasmid was used to increase circulating IL-6 levels in mice as previously described [117], using the following protocol:

1. The right quadriceps muscle was used to synthesize and secrete exogenous IL-6 into circulation from the injected expression plasmid, and was not used for any analyses in the study. The gastrocnemius muscle used in the study was not subjected to electroporation.
2. Mice were given a 2% mixture of inhalation isoflurane (IsoSol, VEDCO, St. Joseph, Mo, USA) and oxygen (1 L/min) before and during procedure.
3. The right quadriceps area was shaved and cleaned with iodine and ethanol. A small incision (1 cm) was made through the skin and fascia, revealing the muscle.
4. 50 μg of IL-6 plasmid driven by the CMV promoter, or control plasmid (pV1J), suspended in a 50 μl volume of sterile 0.9% saline was slowly injected into the right quadriceps muscle.

5. A series of eight 50 ms, 100 V pulses was used to promote uptake of the plasmid into myonuclei, and the incision was closed with a wound clip.

A.5 Run to Fatigue

At 12, 15, and 18 weeks of age, mice were subjected to a run-to-fatigue treadmill protocol. After 5 minutes of acclimation at 5 meters/minute and 5 minutes of warm-up at 10 m/m, the clock was started when speed was increased to 15 m/m. The treadmill protocol was as follows: 20 minutes at 15 m/m, 20 minutes at 18 m/m, 30 minutes at 20m/m, 30 minutes at 25 m/m, and 28 m/m until all mice stopped. A mouse was considered "fatigued" when it refused to run or could not keep up with the treadmill despite gentle nudging for 1 minute. Time and distance to fatigue were recorded.

A.6 Voluntary cage activity monitor

Place conventional mouse cages (single-housed) in channels. Take the cage card off the cage in order to keep from blocking beams. Make sure the power to the desktop computer and the Opto-3 is on. Under the "Start" menu on the desktop, run the program titled "MultiDeviceSoftware." The program will scan the hardware and make sure all channels (8 total) are connected. Make sure that all channels are enabled. Click on Experiment>Setup. The program will ask whether the user wants to use the default experiment template. Click "No," and choose an old file whose protocol is the same as the experiment planned. Name the new file with channel numbers used and mouse numbers being tested. Once experiment begins, make sure all yellow LED lights (A to D) are flashing on the front of the Opto-M3.

A.7 Dual X-ray absorbiometry (DEXA) Scan

Make sure the DEXA is plugged into the laptop and both machines are on. From the start-up screen of the laptop program, select "Measure QC phantom." Place the quality control phantom mouse in the DEXA to be measured. While phantom is being measured, stand outside of the room. Once DEXA passes QC, it is ready to measure mice. Isoflurane machine should be hooked up to oxygen tank in the room. Turn on oxygen tank and isoflurane meter to 2-2.5%. Place mice in chamber with paper towels lining the bottom. Allow mice to stay in chamber for 5 minutes. Tape nose cone to edge on DEXA scanning region. Place first mouse in DEXA with nose in nose cone. Make sure all legs are spread to sides and within scanning region. Begin scan through laptop prompts. Stand outside of door while scanning is occurring. Afterwards, use manual controls to change region of analysis. Exclude the skull and nose cone from region of interest and press "enter" to get new values. Record all values.

A.8 Grip strength measurement

Grip strength measurements were determined as previously described [5]. Mice underwent 2 sets of 5 forelimb grip strength trials. The first mouse was removed from its cage, held firmly by the base of the tail, and allowed to grasp the top of the grate attached to the force gauge (Chatillon, Largo, FL, USA) with its forepaws. The mouse was firmly pulled down the grate, and forelimb grip strength was recorded in Newtons. The mouse completed the 5 trials of the first set and was returned to its cage. Each mouse tested went through the same procedure for its first trial, and mice were cycled through in the same order for the second trial.

A.9 Fasting glucose

Mice were fasted for five hours prior to blood glucose measurements. Blood glucose measurements were performed using a handheld glucometer (Bayer CONTOUR®, Whippany, NJ, USA) according to the manufacture's instructions.

A.10 Retro-orbital eye bleed

Animals will be fasted for five hours prior to bleeding. Mice will be placed in isoflurane chamber with paper towels lining the bottom. Oxygen tank will be turned on and isoflurane vaporizer will be turned to 2-2.5% . Mice will stay in chamber for 5 minutes. One mouse at a time will be removed and place on an absorbent pad. The mouse will be retrained and a heparinized capillary tube will be gently inserted into the eye socket, anterior to the eyeball. Capillary tube will be gently twisted until blood flow occurs. 1-2 capillary tubes of blood will be collected and place into an Eppendorf tube on ice. Mouse will be returned to home cage and given a subcutaneous injection of 500 µl saline in order to rehydrate. Blood will then be centrifuged at 10,000 rpm for 10 minutes at 4 degrees. Plasma will be pipetted off and added to a new tube. Plasma samples will be kept at -80 degrees until analysis.

A.11 IL-6 ELISA

Use the Biosource KMC0062 kit per manufacturer's instructions. Thaw out plasma samples. Remove the number of 8-well strips required for assay. Reconstitute IL-6 standard and controls according to instructions on vial. Sit at room temperature for 10 minutes. Make a 500 pg/ml standard using 950 ul of standard diluents buffer and 50 ul of

the reconstituted standard. Make a series of 2-fold serial dilutions. Label tubes 250 pg/ml, 125 pg/ml, 62.5 pg/ml, 31.25 pg/ml, 15.7 pg/ml, 7.8 pg/ml, and 0 pg/ml. Add 300 ul of standard diluent buffer to each tube. Make serial dilutions using the 500 pg/ml standard first. Add 100 ul of standards or controls in duplicate to each well and add 50 ul of standard diluents buffer followed by 50 ul of plasma in duplicate to each well. Incubate at room temperature for 2 hours. Dilute wash buffer according to directions and for the appropriate number of wells. Aspirate wells. Wash 4x with wash buffer. Invert plate and tap to dry. Add 100 ul of IL-6 biotin conjugate to each well and incubate at room temperature for 30 min. Aspirate wells. Wash 4x with wash buffer. Invert plate and tap to dry. Prepare HRP-strepavidin according to instructions. Use 10 ul and 10 ml for each strip in the assay. Add 100 ul of the working HRP-strepavidin solution to each well and incubate at room temperature for 30 min. Aspirate wells. Wash 4x with wash buffer. Invert plate and tap to dry. Add 100 ul of the chromagen to each well and incubate at room temperature for 30 min in the dark. Add 100 ul of stop solution. Read on microplate reader at 450 nm.

A.12 Soluble IL-6R Enzyme-linked immunosorbent assay

Soluble IL-6r (sIL-6r) ELISA kit was obtained from MyBioSource (San Diego, CA) and manufacturer's protocol was followed. Briefly, 100 µl of standards and samples were added to wells. 50 µl of conjugate was added to sample in each well, and plate was incubated for 1 hour at 37°C. Plate was washed five times. 50 µl each of Substrate A and B were added to wells. Plate was again incubated at 37°C for 15 minutes until color developed. 50 µl Stop Solution was added to wells, and the plate was immediately read at 450nm on a BioRad iMark plate reader (Carlsbad, CA).

A.13 Leptin Enzyme-linked immunosorbent assay

A commercial mouse leptin ELISA was obtained (Quantikine, R&D Systems, Minneapolis, MN) and manufacturer's instructions were followed. Briefly, standards and samples were added to the pre-coated plate and allowed to incubate for two hours at room temperature. The plate was washed five times and leptin conjugate was added to wells. Plate was allowed to incubate for two hours at room temperature. Again, the plate was washed five times. Substrate Solution was added to wells, and plate was incubated in the dark for thirty minutes at room temperature. Stop Solution was added to wells, and the plate was read at 450 nm on a BioRad iMark plate reader.

A.14 IL-6R ELISA

Muscle IL-6r protein content was determined using a commercial IL-6Ra ELISA (DuoSet, R&D Systems, Minneapolis, MN) as previously described. Briefly, Capture Antibody was used to coat wells of a clear 96-well EIA plate (Costar, Corning, Corning, NY) and allowed to incubate overnight. The second day, plate was blocked for one hour using Reagent Diluent. Plate was washed three times. Standards and samples were added and allowed to incubate for two hours. After washes were repeated, Detection Antibody was added to wells and allowed to incubate for two hours. Washes were repeated and Streptavidin-HRP was added to wells and allowed to incubate for twenty minutes. After washes were repeated, Substrate Solution was added to wells and color was allowed to develop for twenty minutes. Stop Solution was added and plate was read at 450 nm on a BioRad iMark plate reader (Carlsbad, CA).

A.15 Intestinal polyp quantification

Quantification of intestinal polyps was determined as previously described [19]. Briefly, intestinal sections were fixed in formalin at time of sacrifice. At time of analysis, sections were rinsed in deionized water and dipped briefly in 0.1% methylene blue. Polyps from segment 4 were counted under a dissecting microscope; it has been determined that tumor number in segment 4 is representative of total tumor number [122].

A.16 Ovarian Histology

Ovaries were excised from B6, Cycle Present, and Cycle Absent mice and immediately transferred to 4% PFA. Ovaries were mounted in paraffin, sectioned, and stained by hematoxylin and eosin by the University of South Carolina School of Medicine Instrument Resource Facility. Pictures were taken using a Nikon E600 microscope (Nikon, Tokyo, Japan) at 400x and 1000x.

A.17 RNA isolation

Homogenize samples in 1 ml of Trizol on ice (Use new 14 ml Polyproplylen tube). Rinse polytrone with EtOH, then dH2O each homogenization. Transfer homogenate to sterile 1.5 ml tube on ice. Spin samples at max speed for 10 min at 4 °C. Transfer supernatant to a new sterile 1.5 ml tube. Let samples sit at RT for 5 min. Add 200 µl of chloroform. Shake tubes vigorously for 15 s (DO NOT VORTEX). Incubate at RT for 2-3 min. Centrifuge at max for 15 min at 4 °C. Make a new set of 1.5 ml tube. Add 500 µl of

isopropanol each tube. Transfer clear supernatant containing the RNA to a new sterile 1.5 ml tube. Do not disturb protein interface. Vortex tubes. Incubate at RT for 10 min or -20C for overnight to increase precipitation. Centrifuge at max for 15 min at 4 °C. Dump supernatant. Add 1 ml of 75% EtOH (DEPC) to RNA pellet and vortex. Repeat step 15 and 16. Spin at 7500 g (9500 rpm) for 5 min at 4 °C. Dump supernatant and remove remaining liquid with kimwipte. Do not disturb the RNA pellet. Air dry tube upside down for 15 min. Add 15 to 40 µl of DEPC water, depending on pellet size. Pipette up and down to mix. Heat in dry-bath at 60 °C for 10 min. Pipette up and down to mix for at leat 30 times. Read 1.5-2 µl of sample using nano drop at 260 and 280 nm.

RNA concentration = (OD260*40*0.8)/(volume of RNA read in cuvette) OD260/OD280: >1.8 is good; 1.6 to 1.8 is OK; <1.6 is not good.

A.18 cDNA synthesis

Make 10ul of reverse transcriptase cocktail (See ingredients below). Mix with pipette. Spin to collect condensation.

Component	Volume/Reaction (µL)	
	Kit with RNase Inhibitor	Kit without RNase Inhibitor
10X RT Buffer	2.0	2.0
25X dNTP Mix (100 mM)	0.8	0.8
10X RT Random Primers	2.0	2.0
MultiScribe™ Reverse Transcriptase	1.0	1.0
RNase Inhibitor	1.0	—
Nuclease-free H_2O	3.2	4.2
Total per Reaction	10.0	10.0

Measure 1-2ug RNA and volume up to 10ul. Mix samples by pipetting up and down making a 20ul reaction. Place samples in Thermocycler (Program #25, or settings as seen below)

	Step 1	Step 2	Step 3	Step 4
Temperature (°C)	25	37	85	4
Time	10 min	120 min	5 min	∞

A.19 Real-time PCR

Thaw out primers and get master mix out of freezer. Get appropriate number of 8-well tubes and 8-well strips out of bags. Thaw out cDNA (diluted either 1:10 or 1:100 with sdH2O). Make cocktail based on number of samples, plus one negative control, plus one extra sample. You are making 20 ul reactions. Mix by inversion 20x. Spin to collect to bottom of tube.

	1x	10x
2x SYBR Master mix	10.0	100.0
20 uM Primer 1	0.08	0.8
20 uM Primer 2	0.08	0.8
sdH2O	0.84	8.4
	11.0	110.0

Add 11.0 ul of cocktail to each tube. Make sure you are pipetting in 96-well cooling block. Add 9.0 ul of cDNA (1:100 dilution). If measuring mRNA for something that is not very abundant, use 1:10 dilution instead. Pipette up and down to mix about 20 times. Seal 8-wells with 8-strip cap. Set up thermal cycle to default program and add dissociation curve. Set volume to 20 ul. Change number of cycles to 50 if necessary.

A.20 Calculation of real time PCR Ct values

The Ct value is the cycle threshold. This is the cycle number above the set threshold level which is set manually or automatically and the threshold is set above the background. The delta Ct (ΔCt) is the difference in Ct values from the experimental gene from a housekeeping gene (18S, GAPDH, etc.). Take the mean ΔCt values for each group. This data is presented in the manuscript and for statistics. If the data is normally distributed, the ΔCt values can be used for statistics. If the data is not normally distributed, the ΔCt values can be transformed (ex: log transformation). This can be used to run statistics. If the data is transformed for statistics, still present the raw ΔCt values in the manuscript. State in the methods that the data was transformed for statistical purposes. Theoretically, a difference in Ct values by a factor of 1 is a 2-fold change in mRNA. However, since PCR is not 100% efficient, this is only an estimate and the exact change in mRNA is probably a little less than a factor of 2. Therefore, this can only be mentioned in the text of the results or discussion.

A.21 $2^{\wedge -\Delta\Delta CT}$ method

Take the average ΔCT for the control group. Subtract the control group average ΔCT from each individual ΔCT. This is the ΔΔCT. To transform, the equation is $=2^{\wedge -\Delta\Delta CT}$.

A.22 Primers

Find the nMol concentration from the tube, it should be in the range of ~33 nMol. Add TE bx to the tube by a factor of 10. Ex for a 33.20 nMol primer ass 330ul of TE bx. This will result in the primer concentration to be 100uM. Dilute primers to working concentration of 20uM. Do this by combining 20 ul of the 100uM primer with 80 ul of dH20. This is a 1:5 dilution giving you the working 20uM stock. Place the 100uM primer in the appropriate box, most likely Mouse Primers and put the 20uM stock solution in the clear plastic box named 20uM working primers.

A.23 Tissue (protein) homogenization

Make Mueller Buffer (see next page) and store at -20°C. Add 1 mL/100 mg tissue of Mueller Buffer. Prepare diluent buffer (see next page). Half of what you prepared of the Mueller buffer will be added. For example, if you add 200 ul of Mueller buffer for 20 mg of tissue, add 100 ul of diluent buffer. Put the Mueller buffer on ice and have the samples suspended in liquid nitrogen. Have a 1000 mL beaker with deionized H2O and another 1000 mL beaker with weak acid (splash of glacial acetic acid). Also, have a test tube rack with homogenization tubes and some Kim-wipes nearby. Have a 600 mL beaker with ice and a homogenization tube. Also have a beaker for waste. Freeze homogenization tube for 5 seconds in liquid nitrogen. Put the sample in the homogenization tube by inverting the eppendorf tube. If the sample sticks to the side of the eppendorf, flick it with your finger to dislodge it. Immediately add appropriate amount of Mueller buffer to the sample. Homogenize in an up-and-down motion for a few seconds at a time with tube on ice. This prevents heat from accumulating. Also, turn

the homogenizer off and on every few seconds. When the sample is liquefied, use a transfer pipette and put back into original eppendorf. Rinse the transfer pipette with deionized H2O. Rinse the glass probe first with weak acid, dry with Kim-wipe, rinse with deionized H2O, and wipe with Kim-wipe. Rinse the homogenization tube 3 times with weak acid and 3 times with deionized H2O and pour into waste beaker. After all tissues are homogenized, centrifuge the samples for 15 min at 4°C for at 10K rpm. Make a new set of eppendorf tubes. Transfer the supernatant into a new eppendorf tube and add half of original amount of Mueller of diluent buffer. Refreeze the samples at -80 °C for storage.

A.24 Muller and diluent buffer

Mueller Bx	**Stock**	**Desired**	**Volume**	
dH_2O			3.585	mL
Hepes (pH 7.4)	500 mM	50 mM	0.600	mL
Triton-X	100%	0.10%	0.006	mL
EGTA (pH 8.0)	500 mM	4 mM	0.048	mL
EDTA (pH 8.0)	500 mM	10 mM	0.120	mL
$Na_4P_2O_7$	100 mM	15 mM	0.900	mL
β-glycerophosphate	2 M	100 mM	0.300	mL
NaF	500 mM	25 mM	0.300	mL

$NaVO_4$	1 M	5 mM	0.030	mL
Protease inhibitor			0.060	mL
			Total 6.000	mL

Diluent Bx	**Stock**	**Desired**	**Volume**	
Glycerol	100%	50%	1.500	mL
$Na_4P_2O_7$	100 mM	50 mM	1.500	mL
EGTA (pH 8.0)	500 mM	2.5 mM	0.015	mL
β-mercaptoethanol	500 m M	1 mM	0.006	mL
Protease inhibitor			0.030	mL
			Total 3.000	mL

A.25 Bradford protein assay

Dilute BSA from stock to 1 µg/uL working solution. Prepare a 1:5 dilution with deionized H2O of Bio-rad Bradford reagent. You will need 600 µL/sample (in duplicate), plus enough for each standard (in duplicate), and extra for any re-do samples. Put in a glass beaker covered with foil, add a stir bar, cover with Parafilm, and slowly stir. Dilute samples with diluent buffer if necessary. Add 2 µL of samples at the bottom of each well (in duplicate). Add 2, 4, 6, 8 and 10 µL of BSA for standard (in duplicate).

Add 300 µL of Bradford reagent to each well quickly and wait for 15 min in the dark. Place the well plate on the plate reader and read on the spectrophotometer at 595 nm. All absorbance readings need to be within 10% CV in each duplicate. If not, make another standard. Plot average absorbances on a graph with 'protein' on the x-axis and 'absorbance' on the y-axis. CV defined as the ratio of the standard deviation to the mean: CV(%)=(SD/mean)*100

A.26 SDS-PAGE

Make resolving gel: Assemble the glass plates according to the manufacturer's instructions. Fill with water to make sure the mold does not leak. Make correct percentage gel (10 ml per gel) in a 50 or 100 ml beaker. Syringe filter (0.45 µm) all components except for TEMED. Dump out water in mold and use filter paper to dry. Add TEMED to beaker and swirl to mix. Pour gel into mold but leave enough room for comb and 0.5-1 cm. Add 200 ul of isopropanol to top of gel. Wait 20-30 min for gel to solidify. **Make stacking gel:** Make stacking gel (2-3 ml per gel) in a 50 or 100 ml beaker except for TEMED. Dump out unpolymerized acrylamide from resolving gel and use blotting paper to absorb excess isopropanol. Add TEMED to beaker and swirl to mix. Pour stacking gel to top. Insert comb but leave 0.5 to 1 cm of space between bottom of comb and top of resolving gel. Wait 20-30 min for gel to solidify. **Prepare samples:** Boil 2x SDS loading buffer in water bath for 5 minutes. Add 2x SDS loading buffer to individual eppendorf tubes for each sample. Add same amount of protein extract to each eppendorf tube. Cap tubes with boiling cap. Boil samples for 5 minutes in water bath. Let samples sit for at least 30 seconds before removing boiling caps. Briefly centrifuge to collect samples at bottom of tube. **Make running buffer:** Add

800 ml of dH2O and 200 ml of 5x SDS running buffer. **Load the gel:** Connect gels to holder and put into tank. Add running buffer to both inner and outer chambers. Load each sample into each well. Add 10 uL of marker to one lane (not in the middle of the gel). Connect to power supply (black to black and red to red). Run gel at appropriate voltage (160 V for 1 h). Stop when all dye has leaked into the running buffer. **Transfer to membrane:** Presoak membrane in methanol (5 minutes) to enhance the transfer process. Disconnect power and remove gels. Remove one piece of glass and carefully cut away stacking gel and throw away in trash. Use deionized H2O and a spacer to help remove gel into dish with deionized H2O. Put waffle with black side down in tramsfer tray covered in transfer buffer. Put in sponge. Put in blotting paper. Add gel (preferably with marker on right, so when transfer is done, marker will be on the left). Add membrane and smooth out bubbles with spacer. Add blotting paper and smooth out bubbles with spacer. Add sponge and smooth out bubbles with spacer. Close sandwich. Put sandwich in holder (black to black). Put stir bar at bottom of container. Add ice pack. Add transfer buffer. Put holder on stir plate to circulate the running buffer. Quick transfer at 350 mA for 60 min (pack on ice) or transfer overnight 70 mA. **Ponceau Staining**: Use tweezers to remove the membrane and put in a plastic dish with enough Ponceau stain to cover the membrane with protein side up. Shake for 2-3 min and then pour the stain back into the jar. Rinse the membrane with deionized water to destain until the water is not pink. Scan into the computer. Seal membrane in a plastic bag with TBS-T and store in the refrigerator for western blotting or rinse in TBS-T and store in blotting paper at room temperature.

A.27 Western blotting

Put membrane in dish with protein side up. Block membrane in 5% TBST milk for 30 min. Add primary Ab at appropriate dilution in 5% TBST milk. Incubate overnight at 4 °C, 1 h at RT, or 60-90 min at room temperature with gentle rocking. Wash 3 x 5 min with TBST with shaking. Wash 1 x 10 min with TBST with shaking. Add secondary Ab at appropriate dilution in 5% TBST milk Incubate 1 h at RT with gentle rocking. Wash 3 x 5 min with TBST with shaking. Wash 1 x 10 min with TBST with shaking. Make ECL or ECL prime reagent. Remove excess TBST by draining edge of membrane with Kim-wipe. Lay membrane in flat dish. Add ECL (1 min) or ECL prime (5 min) to top of membrane. Remove excess ECL/ECL prime by draining edge of membrane with Kim-wipe. Place membrane face down (protein side down) on piece of plastic wrap. Fold up edges and tape membrane in film cassette face up (protein side up). Put on a piece of film on membrane in the darkroom. To use machine, turn switch from "Standby" to "Run" and the red "Feed film" light will turn on. In dark, open the lid of the developer and feed the film until it catches. You can turn on the light or put in another piece of film when the "Feed Film" light comes on again. Turn machine to "Standby". Mark on film the edges of the membrane and the protein marker with a sharpie.

A.28 Statistical analysis

Chapter 3: All results are reported as means ± SEM. Differences between degrees of cachexia severity were analyzed by one-way ANOVA using Tukey *post hoc* test where appropriate. Differences between sexes and genotypes were determined by two-way ANOVA. Correlations were determined by Pearson's test for correlation. Differences

between 12-14 week and 15-18 week IL-6 treatment groups were determined by Student's t-test. Level of significance was set at 0.05.

Chapter 4: All results are reported as means ± SEM. Differences between B6, Weight stable, Severe, and OVX mice were determined by one-way ANOVA with Tukey *post hoc* where appropriate. Differences between Sham + vector, Sham + IL-6, OVX + vector, and OVX + IL-6 mice were determined by two-way ANOVA with Tukey *post hoc* where appropriate. Level of significance was set at 0.05 for all comparisons.

Chapter 5: All results are reported as means ± SEM. Differences between B6, Cycle Present, and Cycle Absent were analyzed by one-way ANOVA using Tukey *post hoc* where appropriate. Differences between timepoints and ovarian status, were determined by two-way repeated measures ANOVA with Sidak's multiple comparisons test where appropriate. Differences between genotype and ovarian status were determined by two-way ANOVA with Tukey *post hoc* where appropriate. Differences between Cycle Absent and OVX mice were determined by Student's t-test. Differences between Cycle Present, Cycle Absent, and OVX mice were determined by one-way ANOVA with Tukey *post hoc* where appropriate. Differences between Sham + vector, Sham + IL-6, OVX + vector, and OVX + IL-6 mice were determined by two-way ANOVA with Tukey *post hoc* where appropriate. Level of significance was set at 0.05.

APPENDIX B

DOCTORAL DISSERTATION PROPOSAL

THE ROLE OF OVARIAN FUNCTION IN THE PROGRESSION OF CACHEXIA IN THE APCMIN/+ MOUSE

KIMBELL L. HETZLER

DECEMBER 9, 2013

REVISED JANUARY 13, 2014

REVISED APRIL 23, 2015

B.1 Specific Aims

Cachexia is a devastating condition that occurs secondary to several chronic diseases, including AIDS, COPD, chronic renal failure, and many forms of cancer [1]. There is no cure or FDA-approved treatment for cachexia, though it occurs in 30-50% of cancers [1-3] and has an annual mortality rate of 80% [1], underlining the necessity of investigation into its etiology and progression. The most recent definition of cachexia includes an unintentional weight loss of 5% or more secondary to a chronic condition in addition to other symptoms including anemia, fatigue, muscle weakness, increased inflammatory markers and plasma triglycerides, and insulin resistance [1].Though the condition has been well-characterized in the male by our lab and others [4-6, 10, 18-24], almost no research into the condition has taken place in the female. It had long been assumed that the male and female underwent the same pathophysiology leading to cachexia; however, data from our laboratory has shown differences in the response of the male and female (unpublished data). Though both sexes undergo cachexia, data from our lab has shown that the female loses less body weight than the male, and seems to have a differential response to IL-6 from the male [20]. Cachectic male and female *Apc* $^{min/+}$ mice have similar plasma IL-6 levels (unpublished data). However, induced overexpression of IL-6 in the male abrogates the cachectic response [5, 6, 20], but has no effect in the female. There is no increase in STAT3 signaling in the female *Apc* $^{min/+}$ mouse with overexpression of IL-6 (unpublished data), indicating that something is blocking this pathway. Importantly, it has been shown that estrogen, specifically 17β-estradiol, can block STAT3 signaling [27].

Ovarian function plays a major role in the health and disease outcomes of females. The role of estrogen, in particular, in the health of both males and females has come into focus in the past decade. Body composition is regulated in part by estrogen signaling, and it has been shown that the ablation of such has a significant deleterious impact on regulation of muscle and fat mass [29-32]; this dysregulation has potentially dire consequences when coupled with the innate dysregulation of cachexia. Estrogen has well-documented benefits against inflammation [33-35], particularly IL-6 [36, 37], that may provide some benefit to the female during the onset and progression of cancer cachexia. In addition, the relatively recent discovery of estrogen receptors α and β in skeletal muscle has led to new insight into estrogen's benefits to skeletal muscle mass and strength [30, 38, 39]. Specifically, estrogen is necessary for recovery from atrophy [29, 40]. Preliminary data from our lab shows that estrous cycling, which normally occurs in the C57BL/6 mouse until around 14 months of age [41], ceases during the progression of cancer cachexia in the female *Apc* $^{min/+}$ mouse, which indicates interplay between the ovary and cachexia.

IL-6 plays a role in the normal cyclic signaling of the ovary [42], but can lead to pathology of the ovary when dysregulated [42, 43]. This supports the hypothesis that there is interplay between ovarian function and IL-6. This, together with the known inhibition of IL-6/STAT3 signaling by estrogen [27] provides the rationale for this study. The novelty of this study arises from it being, to my knowledge, the first study to specifically look at mechanisms of cachexia in the female *Apc* $^{min/+}$ mouse, as well as the first study to investigate a potential role of estrogen signaling.

The *overall purpose* of the proposed study is to determine if ovarian function can alter cachexia progression in the female *Apc* $^{min/+}$ mouse through IL-6 signaling and the regulation of skeletal muscle metabolism. The *working hypothesis* of the proposed study is that loss of ovarian function in the female *Apc* $^{min/+}$ mouse causes abrogated progression of cachexia through altered IL-6 sensitivity, which increases skeletal muscle metabolic dysfunction and leads to increased skeletal muscle loss. Outcomes related to the specific aims of the study include body composition, in vivo functional capacity, abnormal blood biochemistry, tissue IL-6 signaling, and disrupted skeletal muscle metabolism.

In order to prove the proposed study's overall hypothesis three specific aims are proposed.

Specific Aims

Aim 1. Determine if ovarian function in female *Apc* $^{min/+}$ mice regulates specific components of cachexia progression.

Aim 2. Determine if IL-6 regulation of cachexia progression is regulated by ovarian function in the female *Apc* $^{min/+}$ mouse.

Aim 3. Determine whether cachexia-induced skeletal muscle metabolic dysfunction is regulated by ovarian function in the female *Apc* $^{min/+}$ mouse.

B.2 Research Design

Aim 1. Determine if ovarian function in female *Apc* $^{min/+}$ mice regulates specific components of cachexia progression.

Overall Design: Aim 1 will determine whether there is an association between ovarian function and the extent of cachexia progression in the female *Apc* $^{min/+}$ mouse. The *working hypothesis* of this aim is that normal ovarian function will protect against the

progression of cachexia, including body composition changes, functional deficits, and abnormal blood biochemistry. This aim consists of 2 experiments. Experiment 1.1 is a time course experiment and will examine cachexia progression in mice with normal and abnormal ovarian function at the early (15 week) and late (18 week) stages of cachexia. Normal and abnormal ovarian function will be categorized using daily estrous cycling data primarily, with verification from plasma estrogen levels taken over the time course. Experiment 1.2 will examine the effect of ovariectomy on the progression of cachexia at the early (15 week) and late (18 week) stages of cachexia. Outcomes from this aim will relate ovarian function to **changes in body composition, whole body function, and blood biochemistry** in ovaries-intact and ovariectomized mice at early cachexia (15 week) and cachexia (18 week) timepoints.

Experiment 1.1: Determine if abnormal ovarian function during the time course of cachexia progression in ovaries-intact female *Apc* $^{min/+}$ mice is associated with changes in body composition, functional deficits, and abnormal blood biochemistry.

Hypothesis 1.1: Normal ovarian function will be associated with less severe changes in body composition, functional deficits, and abnormal blood biochemistry than irregular ovarian function in the female *Apc* $^{min/+}$ mouse.

Design: Female *Apc* $^{min/+}$ mice will be followed from 10 weeks of age to sacrifice at 15 weeks (early stage cachexia, n=12) or sacrifice at 18 weeks (late stage cachexia, n=12). Abnormal ovarian function will be classified by continuous measurement of estrous cycling and verified by plasma estrogen levels from blood taken at 12, 14, 16, and 18 weeks of age. Additional measurements will include ovarian mRNA expression of

estrogen and progesterone at 15-week and 18-week endpoints. Body composition outcomes will comprise body fat percentage and lean mass percentage determined by DEXA as well as total body weight loss at 12, 14, 16, and 18 weeks. Functional outcomes will comprise volitional grip strength, run-to-fatigue time, food intake, and cage activity at 12, 14, 16, and 18 weeks. Blood biochemistry outcomes will comprise hematocrit (for determination of anemia), plasma insulin levels, and plasma triglyceride levels at 12, 14, 16, and 18 weeks.

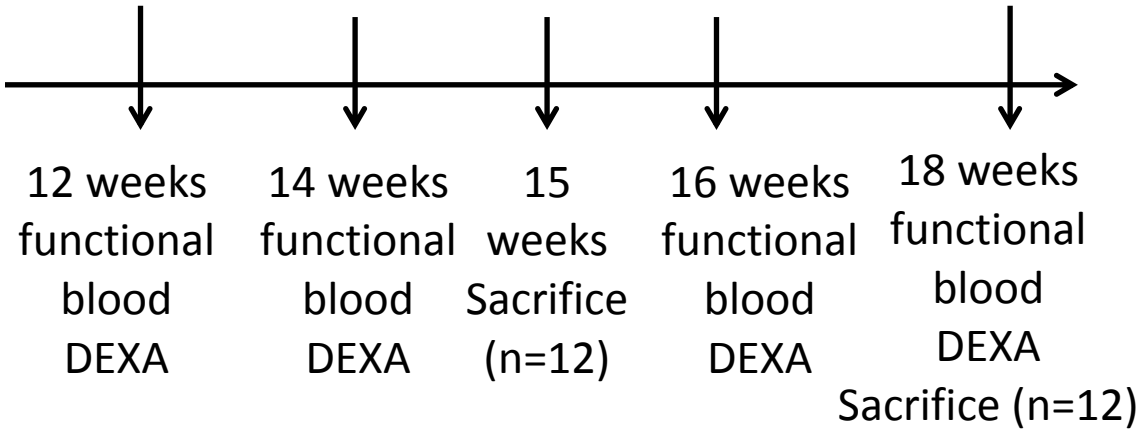

Expected Outcomes Outcomes from this experiment will relate ovarian function to body composition, functional outcomes, and biochemical measures over time. Specifically, ovarian function will be categorized as "normal" or "abnormal" by daily measurement of estrous cycling. Additionally, ovarian endocrine function will be examined by plasma estrogen levels at 12, 14, 16, and 18 weeks, and estrogen/progesterone mRNA from ovaries at 15 and 18 week timepoints. Body composition will comprise changes over time from 12 weeks (pre-cachexia) to 18 weeks (late stage cachexia) in percentage body fat and weight loss. These will be compared between normal and abnormal ovarian function

groups during early stage cachexia (15 week) and late stage cachexia (18 week). Functional outcomes will comprise volitional grip strength, run to fatigue time, food intake, and cage activity. Changes over time from 12-18 weeks in these outcomes will be compared between normal and abnormal ovarian function groups during early stage cachexia (15 week) and late stage cachexia (18 week). Abnormal blood biochemistry outcomes will comprise hematocrit (for determination of anemia), plasma insulin levels, and plasma triglyceride levels. Changes over time from 12-18 weeks in these outcomes will be compared between normal and abnormal ovarian function groups during early stage cachexia (15 week) and late stage cachexia (18 week)..

Experiment 1.2: Determine if <u>ablation of ovarian endocrine function (ovariectomy)</u> in the female *Apc* $^{min/+}$ mouse regulates components of cachexia progression, including changes in body composition, functional deficits, and abnormal blood biochemistry.

Hypothesis 1.2: Ovariectomy will lead to more severe progression of cachexia, including greater body composition changes, greater functional deficits, and more severe blood biochemical abnormalities in the female *Apc* $^{min/+}$ mouse.

Design: Female *Apc* $^{min/+}$ mice and female C57BL/6 mice will be ovariectomized (OVX) at 11 weeks of age and will be followed until sacrifice at 15 weeks (early stage cachexia, n=8 *Apc*$^{min/+}$, n=4 B6) or sacrifice at 18 weeks (late stage cachexia, n=8 *Apc* $^{min/+}$, n=4 B6). Mice from experiment 1.1 will be used as control for ovariectomy. Body weight will be tracked weekly. Body composition will be determined by DEXA at 12, 14, 16, and 18 weeks of age. Measurement of function including grip strength, run to fatigue

time, food intake, and cage activity will be taken at 12, 14, 16, and 18 weeks of age. Blood for determination of anemia as well as determination of plasma estrogen, insulin, and triglycerides will be collected at 12, 14, 16, and 18 weeks of age. It is expected that plasma estrogen will be depleted within 2 weeks of ovariectomy.

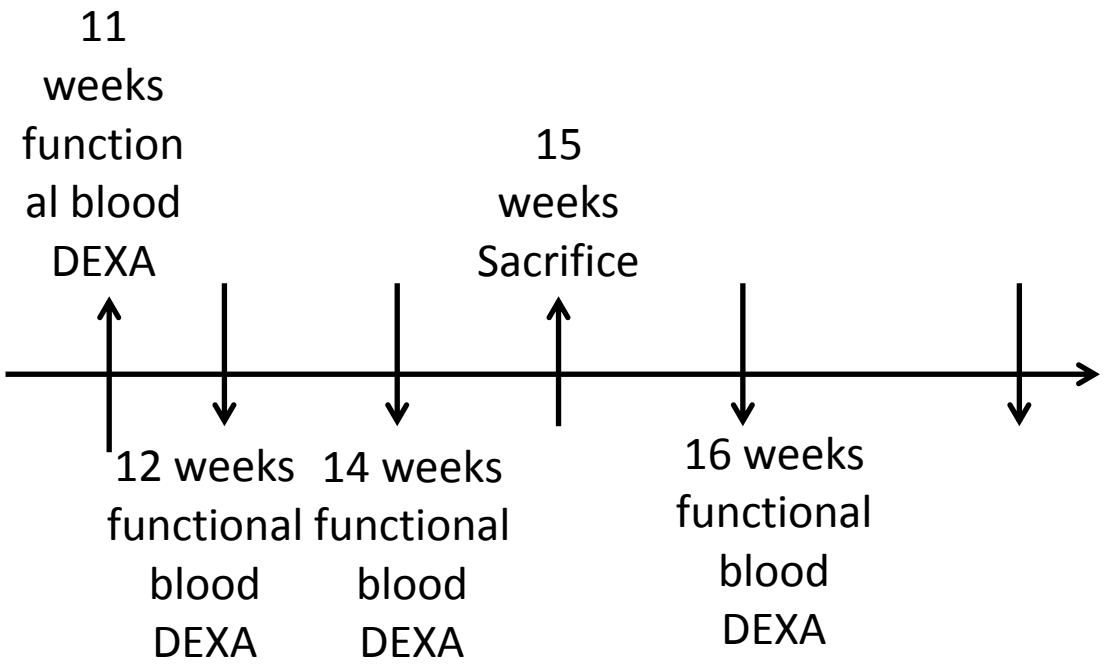

Expected Outcomes: To stratify by ovarian function, we will compare ovariectomized (OVX) and intact (SHAM) mice. Outcomes will include measurements of body composition, function, and circulating blood biochemistry over the time course of the experiment. Mice from Experiment 1.1 with the addition of intact female B6 (n=4) mice will serve as controls for the effects of ovariectomy. Ovariectomized B6 controls will be crucial to control for the changes in body composition that can occur after ovariectomy. Ovarian function outcomes will comprise measurement of estrous cycling in intact mice, and plasma estrogen levels to verify efficacy of ovariectomy in OVX mice. Body

composition outcomes will comprise changes over time from 12 weeks (pre-cachexia) to 18 weeks (late stage cachexia) in percentage body fat and weight loss. These will be compared between OVX and SHAM groups during early stage cachexia (OVX-15 weeks vs. SHAM-15 weeks) and during late stage cachexia (OVX-18 weeks vs. SHAM-18 weeks). Functional outcomes will comprise volitional grip strength, run to fatigue time, food intake, and cage activity. Changes over time from 12-18 weeks in these outcomes will be compared between OVX and SHAM groups during early stage cachexia (OVX-15 weeks vs. SHAM-15 weeks) and during late stage cachexia (OVX-18 weeks vs. SHAM-18 weeks). Abnormal biochemistry outcomes will comprise hematocrit (for determination of anemia), plasma insulin levels, and plasma triglyceride levels. Changes over time from 12-18 weeks in these outcomes will be compared between OVX and SHAM groups during early stage cachexia (OVX-15 weeks vs. SHAM-15 weeks) and late stage cachexia (OVX-18 weeks vs. SHAM-18 weeks).

Overall Aim 1 Interpretation:

Differences seen in Experiment 1.1 between mice with normal and abnormal ovarian function will indicate that cessation of normal estrous cycling alters the progression of cachexia in female *Apc* $^{min/+}$ mice.

More severe changes in body composition including greater loss of body fat percentage and body weight in mice with abnormal ovarian function will indicate that normal ovarian function is protective of body composition.

More severe loss of volitional strength or cage activity in mice with abnormal ovarian function will indicate that normal ovarian function can protect from these deficits

during the progression of cachexia, though it will not be possible to say through this experiment whether this is due to effects of ovarian signaling in the muscle.

A lower run-to-fatigue time in mice with abnormal ovarian function will indicate that normal ovarian function protects endurance, though it will not be possible to say through this experiment whether this is due to effects on oxidative capacity of the muscles or systemic factors.

Lower food intake in mice with abnormal ovarian function will indicate that normal ovarian function protects appetite during cachexia, possibly relating to body weight maintenance.

More severe anemia in mice with abnormal ovarian function will indicate that normal ovarian function is protective against this process during cachexia progression.

Increased insulin levels in mice with abnormal ovarian function will indicate that normal ovarian function is protective against insulin resistance during cachexia progression.

Higher triglyceride levels in mice with abnormal ovarian function will indicate that normal ovarian function is protective against the dysregulation of lipid metabolism during cachexia progression.

Differences seen in Experiment 1.2 between OVX and SHAM mice will indicate that lack of ovarian function alters the progression of cachexia in female *Apc* $^{min/+}$ mice.

More severe changes in body composition including greater loss of body fat percentage and body weight in OVX mice will indicate that ovarian function is protective of body composition.

More severe loss of volitional strength or cage activity in OVX mice will indicate that ovarian function can protect from these deficits during the progression of cachexia, though it will not be possible to say through this experiment whether this is due to effects of ovarian signaling in the muscle.

A lower run-to-fatigue time in OVX mice will indicate that ovarian function protects endurance, though it will not be possible to say through this experiment whether this is due to effects on oxidative capacity of the muscles or systemic factors.

Lower food intake in OVX mice will indicate that ovarian function protects appetite during cachexia, possibly relating to body weight maintenance.

More severe anemia in OVX mice will indicate that ovarian function is protective against this process during cachexia progression. Increased insulin levels in OVX mice will indicate that ovarian function is protective against insulin resistance during cachexia progression.

Higher triglyceride levels in OVX mice will indicate that ovarian function is protective against the dysregulation of lipid metabolism during cachexia progression.

Aim 2. Determine if IL-6 regulation of cachexia progression is regulated by ovarian function in the female *Apc* $^{min/+}$ mouse.

Overall Design: Aim 2 will determine whether the response to endogenous and overexpressed IL-6 levels is altered by the loss of ovarian function in ovaries-intact and ovariectomized female *Apc* $^{min/+}$ mice. The *working hypothesis* of this aim is that endogenous IL-6 levels will increase in the absence of ovarian function, and response to IL-6 will be abrogated in the absence of ovarian function. This aim consists of 3

experiments. Experiment 2.1 will examine the relationship of circulating IL-6 and downstream tissue signaling in mice with normal and abnormal ovarian function at the early (15 week) and late stages of cachexia (18 week). Experiment 2.2 will examine the relationship between circulating IL-6 and downstream tissue signaling in ovariectomized and intact mice at the early (15 week) and late stage cachexia (18 week). Experiment 2.3 will examine the effect of overexpressed IL-6 on cachexia progression in ovariectomized and intact mice. Outcomes from this aim will relate ovarian function to circulating IL-6 levels and tissue IL-6 signaling in ovaries-intact and ovariectomized mice at early cachexia (15 week) and cachexia (18 week) timepoints, as well as in ovariectomized mice with overexpressed IL-6 levels at 15 weeks.

Experiment 2.1: Determine if the loss of ovarian function in ovaries-intact female *Apc* $^{min/+}$ mice regulates circulating IL-6 levels and IL-6 signaling in cachexia target tissues during the progression of cachexia.

Hypothesis 2.1: Endogenous circulating IL-6 levels and tissue-level IL-6 signaling, including STAT3 activity, AMPK activity, and p38 activity, will increase with dysregulation of ovarian function during the progression of cachexia in the female *Apc* $^{min/+}$ mouse.

Design: The same cohort of mice used in Experiment 1.1 will be used to complete this experiment. Female *Apc* $^{min/+}$ mice will be followed from 10 weeks of age to sacrifice at 15 weeks (early stage cachexia, n=12) or sacrifice at 18 weeks (late stage cachexia, n=12). Body weight will be tracked weekly and estrous cycling will be determined daily.

Blood for determination of plasma estrogen and IL-6 will be collected at 12, 14, 16, and 18 weeks of age.

Expected Outcomes This experiment will relate ovarian function to endogenous IL-6 levels over time and tissue-level downstream signaling in cachexia target tissues including liver, muscle and fat during early cachexia (15 weeks) and cachexia (18 weeks). Specifically, ovarian function will be categorized as "normal" or "abnormal" based on daily estrous cycle measurements as in Experiment 1.1. Secondarily, plasma estrogen levels at 12, 14, 16, and 18 weeks of age will be measured and ovarian estrogen and progesterone mRNA from 15 and 18 week timepoints will be measured. IL-6 levels will be determined from plasma taken at 12, 14, 16, and 18 weeks and will be compared between mice with normal and abnormal ovarian function during early stage cachexia (15 week) and late stage cachexia (18 week). Tissue-level signaling downstream of IL-6 will be determined in cachexia target tissues including liver, skeletal muscle, and fat. Markers of signaling pathways downstream of IL-6 will include p-STAT3/STAT3, p-AMPK/AMPK, p-p65/p65, p-p38/p38, and gp130. Levels of these proteins will be compared between mice with normal and abnormal ovarian function during early stage cachexia (15 week) and late stage cachexia (18 week).

Experiment 2.2: Determine if the <u>ablation of ovarian function (ovariectomy)</u> in female *Apc* $^{min/+}$ mice regulates circulating IL-6 levels and IL-6 signaling in cachexia target tissues during the progression of cachexia.

Hypothesis 2.2: Ovariectomy will cause increased endogenous circulating IL-6 levels and abrogation of tissue-level IL-6 signaling in the female *Apc* $^{min/+}$ mouse, including increased STAT3 activity, AMPK activity, and p38 activity.

Design: The same cohort of mice used in Experiment 1.2 will be used in this experiment. Female *Apc* $^{min/+}$ mice and female C57BL/6 mice will be ovariectomized (OVX) at 11 weeks of age and will be followed until sacrifice at 15 weeks (early stage cachexia, n=12 *Apc*$^{min/+}$, n=4 B6) or sacrifice at 18 weeks (late stage cachexia, n=12 *Apc* $^{min/+}$, n=4 B6). Blood for determination of plasma estrogen and IL-6 will be collected at 12, 14, 16, and 18 weeks of age. It is expected that plasma estrogen will be depleted within 2 weeks of ovariectomy. Mice from experiment 2.1 will be used as intact controls.

Expected Outcomes Outcomes from this experiment will relate presence of ovarian function (OVX versus SHAM) to endogenous IL-6 levels over time and downstream signaling in cachexia target tissues including liver, skeletal muscle, and fat during early stage cachexia (15 weeks) and late stage cachexia (18 weeks), using animals from Experiment 2.1 and intact female B6 (n=4) mice as controls. Specifically, ovarian function will be stratified as OVX or SHAM. Blood taken at 14 weeks will be used to measure plasma estrogen levels in order to verify efficacy of ovariectomy in OVX mice. IL-6 levels will be determined from plasma taken at 12, 14, 16, and 18 weeks and will be compared between OVX and SHAM groups during early cachexia (OVX-15 weeks vs. SHAM-15 weeks) and during cachexia (OVX-18 weeks vs. SHAM-18 weeks). Signaling downstream of IL-6 will be determined in cachexia target tissues including liver, skeletal muscle, and fat. Markers of signaling pathways downstream of IL-6 will include p-STAT3/STAT3, p-AMPK/AMPK, p-p65/p65, p-p38/p38, and gp130. Levels of these

proteins will be compared between OVX and SHAM groups during early cachexia (OVX-15 weeks vs. SHAM-15 weeks) and during cachexia (OVX-18 weeks vs. SHAM-18 weeks).

Experiment 2.3: Determine if the ablation of ovarian function (ovariectomy) alters the cachectic response to IL-6 overexpression in the female *Apc* $^{min/+}$ mouse.

Hypothesis 2.3: Ovariectomy will cause abrogated IL-6 induction of cachexia in the female *Apc* $^{min/+}$ mouse.

Design: Female *Apc* $^{min/+}$ mice will be followed from 10 weeks of age to sacrifice at 15 weeks of age. N=32 mice total; n=16 will undergo ovariectomy (OVX) and n=16 will undergo sham surgery (SHAM) at 11 weeks of age. Two weeks will be allowed for hormone washout; n=16 (n=8 OVX and n=8 sham) mice will then undergo IL-6 overexpression by electroporation at 13 weeks of age, with the remainder of mice being electroporated with a control vector. Functional measurements including grip strength, run to fatigue, food intake, and cage activity will be taken at 11 and 15 weeks of age. Blood will be taken at 13 and 15 weeks to verify efficacy of ovariectomy and IL-6 overexpression as well as to measure plasma estrogen (in intact mice), insulin, and triglycerides. Functional measurements including grip strength, run to fatigue, activity monitoring, and food intake will be completed at 11 weeks and 15 weeks of age.

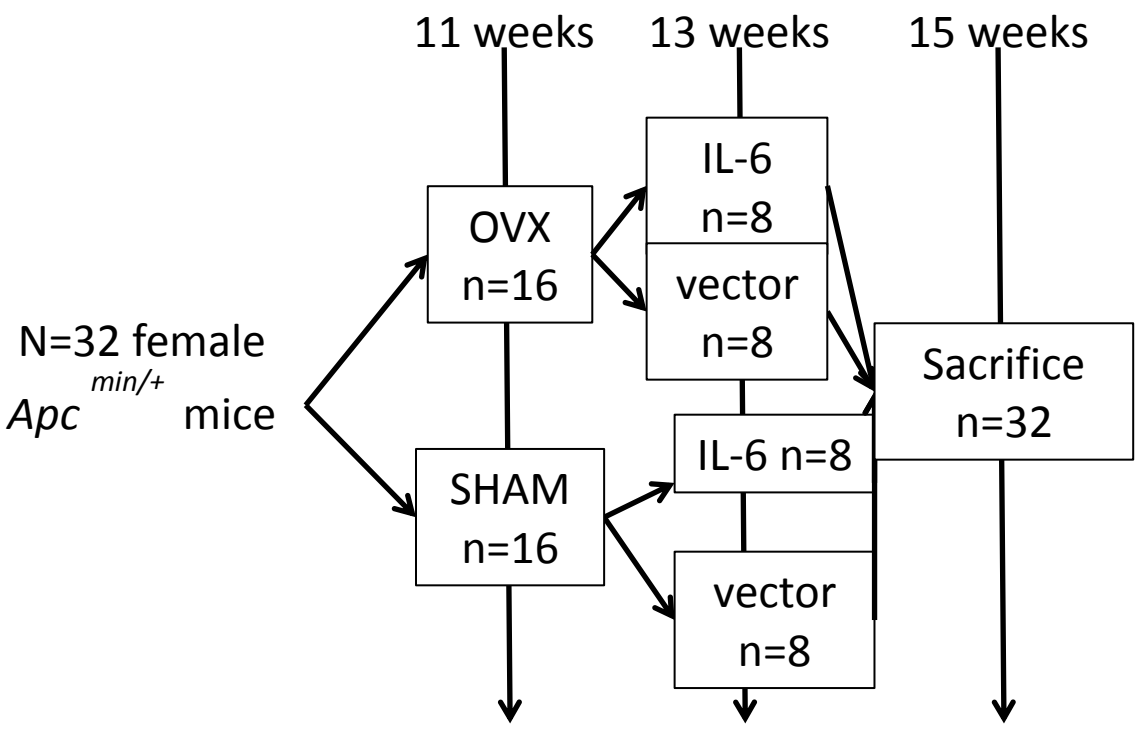

Expected Outcomes This experiment will relate presence of ovarian function to whole-body function and tissue-level IL-6 signaling in cachexia target tissues including liver, skeletal muscle, and fat in mice with IL-6 systemically overexpressed. Measurement of plasma IL-6 levels at 15 weeks will verify overexpression. Functional outcomes including grip strength, run to fatigue, cage activity, and food intake will be compared between OVX and SHAM mice overexpressing IL-6 (OVX-IL-6 versus SHAM-IL-6) and between OVX mice overexpressing IL-6 or a control vector (OVX-IL-6 versus OVX-vector). Expression of p-STAT3/STAT3, p-AMPK/AMPK, p-p65/p65, p-p38/p38, and gp130 will be measured in liver, skeletal muscle, and fat. Levels of these proteins will be compared between OVX and SHAM mice overexpressing IL-6 (OVX-IL-6 versus SHAM-IL-6) and between OVX mice overexpressing IL-6 or a control vector (OVX-IL-6 versus OVX-vector).

Overall Aim 2 Interpretation.

Differences seen in Experiment 2.1 between mice with normal and abnormal ovarian function will indicate whether cessation of normal ovarian function during the progression of cachexia alters sensitivity to IL-6 in female *Apc* $^{min/+}$ mice.

An increase in circulating IL-6 levels in mice with abnormal ovarian function compared to mice with normal ovarian function will indicate that normal ovarian function suppresses IL-6 levels during the progression of cachexia in female *Apc* $^{min/+}$ mice.

An increase in the ratio of pSTAT3/STAT3 expression in liver, skeletal muscle, or fat in mice with abnormal ovarian function compared to mice with normal ovarian function will indicate that normal ovarian function suppresses the STAT3 pathway in this tissue.

An increase in the ratio of pAMPK/AMPK expression in liver, skeletal muscle, or fat in mice with abnormal ovarian function compared to mice with normal ovarian function will indicate that normal ovarian function suppresses the AMPK pathway in this tissue.

An increase in the ratio of pp65/p65 expression in liver, skeletal muscle, or fat in mice with abnormal ovarian function compared to mice with normal ovarian function will indicate that normal ovarian function suppresses the NfκB pathway in this tissue.

An increase in the ratio of pp38/p38 expression in liver, skeletal muscle, or fat in mice with abnormal ovarian function compared to mice with normal ovarian function will indicate that normal ovarian function suppresses the p38/MAPK pathway in this tissue.

An increase in gp130 expression in liver, skeletal muscle, or fat in mice with abnormal ovarian function compared to mice with normal ovarian function will indicate that normal ovarian function suppresses the ability of that tissue to respond to IL-6. It will be important to note whether these differences in signaling occur in the presence or absence of an increase in circulating IL-6 with abnormal ovarian function, as this could provide or eliminate a potential mechanism for this action.

Differences seen in Experiment 2.2 between OVX mice and intact mice will indicate whether lack of ovarian function during the progression of cachexia alters sensitivity to IL-6 in female *Apc* $^{min/+}$ mice.

An increase in circulating IL-6 levels in OVX mice compared to mice with ovarian function will indicate that ovarian function suppresses IL-6 levels during the progression of cachexia in female *Apc* $^{min/+}$ mice.

An increase in the ratio of pSTAT3/STAT3 expression in liver, skeletal muscle, or fat in OVX mice compared to mice with ovarian function will indicate that ovarian function suppresses the STAT3 pathway in this tissue.

An increase in the ratio of pAMPK/AMPK expression in liver, skeletal muscle, or fat in OVX mice compared to mice with ovarian function will indicate that ovarian function suppresses the AMPK pathway in this tissue.

An increase in the ratio of pp65/p65 expression in liver, skeletal muscle, or fat in OVX mice compared to mice with ovarian function will indicate that ovarian function suppresses the NfκB pathway in this tissue.

An increase in the ratio of pp38/p38 expression in liver, skeletal muscle, or fat in OVX mice compared to mice with ovarian function will indicate that ovarian function suppresses the p38/MAPK pathway in this tissue.

An increase in gp130 expression in liver, skeletal muscle, or fat in OVX mice compared to mice with ovarian function will indicate that normal ovarian function suppresses the ability of that tissue to respond to IL-6. It will be important to note whether these differences in signaling occur in the presence or absence of an increase in circulating IL-6 with abnormal ovarian function, as this could provide or eliminate a potential mechanism for this action.

Functional differences seen in Experiment 2.3 between OVX-IL-6 and SHAM-IL-6 groups will indicate whether ovarian function protects against the abrogated functional deficits caused by overexpression by IL-6 that are seen in the *Apc* $^{min/+}$ male mouse [5, 6, 20].

Signaling differences seen in Experiment 2.3 will be interpreted similarly to those in Experiment 2.2, but with an interesting caveat. Differences in signaling between OVX-IL-6 and SHAM-IL-6 groups will indicate whether intact ovarian function protects against abrogated downstream signaling, even in the presence of overexpressed IL-6. Differences between OVX-IL-6 and OVX-vector groups will indicate whether IL-6 is able to further abrogate inflammatory signaling beyond the effects of ovariectomy in female *Apc* $^{min/+}$ mice.

Aim 3. Determine whether cachexia-induced skeletal muscle metabolic dysfunction is regulated by ovarian function in the female *Apc* $^{min/+}$ mouse.

Overall Design: Aim 3 will determine whether ovarian function is associated with the dysregulation of skeletal muscle metabolism including protein turnover and mitochondrial function seen with cachexia in the female *Apc* $^{min/+}$ mouse. The *working hypothesis* of this aim is that intact ovarian function is protective against protein turnover dysregulation and mitochondrial dysfunction. This aim consists of 3 experiments. Experiment 3 .1 will examine skeletal muscle protein turnover and mitochondrial dysfunction in mice with normal and abnormal ovarian function at the early (15 week) and late (18 week) stage of cachexia. Experiment 3.2 will examine skeletal muscle protein turnover and mitochondrial dysfunction in ovariectomized and intact mice at the early (15 week) and late (18 week) stage of cachexia. Experiment 3.3 will examine skeletal muscle protein turnover and mitochondrial dysfunction in ovariectomized and intact mice with systemically overexpressed IL-6. Outcomes from this aim will relate ovarian function to markers of protein turnover and mitochondrial function in ovaries-intact and ovariectomized mice at early cachexia (15 week) and cachexia (18 week) timepoints, as well as in ovariectomized mice with overexpressed IL-6 levels.

Experiment 3.1: Determine if the loss of ovarian function during the progression of cachexia in ovaries-intact female *Apc* $^{min/+}$ mice is associated with skeletal muscle metabolic dysfunction, including the regulation of protein turnover and mitochondrial function.

Hypothesis 3.1: Dysregulation of skeletal muscle protein turnover, including increased degradation and decreased synthesis; and mitochondrial function, including decreased mitochondrial content, increased turnover, and decreased oxidative capacity, will be abrogated by the cessation of normal ovarian endocrine function during the progression of cachexia in ovaries-intact female *Apc* $^{min/+}$ mice.

Design: The same cohort of mice used in Experiments 1.1 and 2.1 will be used for this experiment. Female *Apc* $^{min/+}$ mice will be followed from 10 weeks of age to sacrifice at 15 weeks (early stage cachexia, n=8) or 18 weeks (late stage cachexia, n=8). Body weight will be tracked weekly and estrous cycling will be determined daily. Blood for determination of plasma estrogen will be collected at 12, 14, 16, and 18 weeks of age. Muscle for analysis will be dissected at time of sacrifice.

Expected Outcomes This experiment will relate ovarian function to muscle protein turnover (synthesis and degradation) and mitochondrial function (content, turnover, and oxidative capacity). Specifically, ovarian function will be categorized as "normal" or "abnormal" based on daily measurement of estrous cycling, with verification by plasma estrogen levels from blood taken at 12, 14, 16, and 18 weeks of age and estrogen/progesterone mRNA from ovaries at 15 and 18 week endpoints. Muscle protein synthesis outcomes will include p-Akt/Akt and mTOR. These outcomes will be compared between mice with normal and abnormal ovarian function during the early

stage (15 weeks) and late stage (18 weeks) of cachexia. Muscle protein degradation outcomes will include pFoxO3/FoxO3, Atrogin1, MuRF1, and ubiquitin. These outcomes will be compared between mice with normal and abnormal ovarian function during the early stage (15 weeks) and late stage (18 weeks) of cachexia. Mitochondrial content outcomes will include cytochrome C and TFAM. These outcomes will be compared between mice with normal and abnormal ovarian function during the early stage (15 weeks) and late stage (18 weeks) of cachexia. Markers of mitochondrial turnover will include Fis1 and Mfn1, and markers of oxidative capacity will include COX IV activity. These outcomes will be compared between mice with normal and abnormal ovarian function during the early stage (15 weeks) and late stage (18 weeks) of cachexia. All muscle outcomes will be measured in soleus (oxidative) and tibialis anterior (TA; glycolytic) muscle from mice at early cachexia (15 week) and cachexia (18 week) timepoints. Oxidative and glycolytic muscle will both be analyzed to determine differential cachexia response; it is expected that glycolytic muscle is more susceptible to effects of cachexia.

Aim 3.2: Determine if the ablation of ovarian function (ovariectomy) alters skeletal muscle metabolic regulation, including protein turnover and mitochondrial function, during the progression of cachexia in the female *Apc* $^{min/+}$ mouse

Hypothesis 3.2: Dysregulation of protein turnover, including increased degradation and decreased synthesis; and mitochondrial function, including decreased mitochondrial content, increased turnover, and decreased oxidative capacity, will be abrogated by ovariectomy in female *Apc* $^{min/+}$ mice.

Design: The same cohort of mice used in Experiments 1.2 and 2.2 will be used for this experiment. Female *Apc* $^{min/+}$ mice and female C57BL/6 mice will be ovariectomized (OVX) at 11 weeks of age and will be followed until sacrifice at 15 weeks (early stage cachexia, n=8 *Apc*$^{min/+}$, n=4 B6) or 18 weeks (late stage cachexia, n=8 *Apc* $^{min/+}$, n=4 B6). Mice from Experiment 3.1 will be used as intact controls for this experiment. Blood for determination of plasma estrogen will be collected at 12, 14, 16, and 18 weeks of age. It is expected that plasma estrogen will be depleted within 2 weeks of ovariectomy.

Expected Outcomes: Outcomes from this aim will relate presence of ovarian function (OVX versus SHAM) to muscle protein turnover (synthesis and degradation) and mitochondrial function (content, turnover, and oxidative capacity), using animals from experiment 3.1 and intact female B6 mice as controls. Muscle protein synthesis outcomes will include p-Akt/Akt and mTOR. These outcomes will be compared between OVX mice and intact mice during the early stage (15 weeks) and late stage (18 weeks) of cachexia. Muscle protein degradation outcomes will include pFoxO3/FoxO3, Atrogin1, MuRF1, and ubiquitin. These outcomes will be compared between OVX mice and intact mice with during the early stage (15 weeks) and late stage (18 weeks) of cachexia. Mitochondrial content outcomes will include cytochrome C and TFAM. These outcomes will be compared between OVX mice and intact mice during the early stage (15 weeks) and late stage (18 weeks) of cachexia. Markers of mitochondrial turnover will include Fis1 and Mfn1, and markers of oxidative capacity will include COX IV activity. These outcomes will be compared between OVX mice and intact mice during the early stage (15 weeks) and late stage (18 weeks) of cachexia. All muscle outcomes will be measured in soleus (oxidative) and tibialis anterior (TA; glycolytic) muscle from mice at early

cachexia (15 week) and cachexia (18 week) timepoints. Oxidative and glycolytic muscle will both be analyzed to determine differential cachexia response; it is expected that glycolytic muscle is more susceptible to effects of cachexia.

Experiment 3.3: Determine if the ablation of ovarian function (ovariectomy) alters IL-6 overexpression regulation of skeletal muscle metabolism in the female *Apc* $^{min/+}$ mouse.

Hypothesis 3.3: Ovariectomy will cause abrogated dysregulation of protein turnover, including increased degradation and decreased synthesis, and mitochondrial function, including decreased mitochondrial content, increased turnover, and decreased oxidative capacity, in response to overexpression of IL-6 in the female *Apc* $^{min/+}$ mouse.

Experiment 3.3: The same cohort of mice used in Experiment 2.3 will be used in this experiment. Female *Apc* $^{min/+}$ mice will be followed from 10 weeks of age to sacrifice at 15 weeks of age. N=32 mice total; n=16 will undergo ovariectomy (OVX) and n=16 will undergo sham surgery (SHAM) at 11 weeks of age. Two weeks will be allowed for hormone washout; n=16 (n=8 OVX and n=8 sham) mice will then undergo IL-6 overexpression by electroporation at 13 weeks of age, with the remainder of mice being electroporated with a control vector. Blood will be taken at 13 and 15 weeks to verify efficacy of ovariectomy and IL-6 overexpression.

Outcomes Outcomes from this aim will relate presence of ovarian function (OVX versus SHAM) to muscle protein turnover (synthesis and degradation) and mitochondrial function (content, turnover, and oxidative capacity), in the presence or absence of IL-6 overexpression. Mice will be categorized as OVX or SHAM based on ovariectomy

status. Blood taken at 14 weeks will verify efficacy of ovariectomy in OVX mice. Measurement of plasma IL-6 levels will verify overexpression. Muscle protein synthesis outcomes will include p-Akt/Akt and mTOR. These outcomes will be compared between OVX mice with and without IL-6 overexpression (OVX-IL-6 and OVX-vector), and between groups of mice with IL-6 overexpression (SHAM-IL-6 and OVX-IL-6). Muscle protein degradation outcomes will include pFoxO3/FoxO3, Atrogin1, MuRF1, and ubiquitin. These outcomes will be compared between OVX mice with and without IL-6 overexpression (OVX-IL-6 and OVX-vector), and between groups of mice with IL-6 overexpression (SHAM-IL-6 and OVX-IL-6). Mitochondrial content outcomes will include cytochrome C and TFAM. These outcomes will be compared between OVX mice with and without IL-6 overexpression (OVX-IL-6 and OVX-vector), and between groups of mice with IL-6 overexpression (SHAM-IL-6 and OVX-IL-6). Markers of mitochondrial turnover will include Fis1 and Mfn1, and markers of oxidative capacity will include COX IV activity. These outcomes will be compared between OVX mice with and without IL-6 overexpression (OVX-IL-6 and OVX-vector), and between groups of mice with IL-6 overexpression (SHAM-IL-6 and OVX-IL-6). All muscle outcomes will be measured in soleus (oxidative) and tibialis anterior (TA; glycolytic) muscle from mice at early cachexia (15 week) and cachexia (18 week) timepoints. Oxidative and glycolytic muscle will both be analyzed to determine differential cachexia response; it is expected that glycolytic muscle is more susceptible to effects of cachexia.

Overall Aim 3 Interpretation

Differences seen in Experiment 3.1 between mice with normal and abnormal ovarian function will indicate whether cessation of normal ovarian function during the progression of cachexia alters regulation of skeletal muscle metabolism in female *Apc* $^{min/+}$ mice.

A decrease in the pAkt/Akt ratio or mTOR in mice with abnormal ovarian function compared to mice with normal ovarian function will indicate that normal ovarian function protects protein synthesis in muscle during the progression of cachexia in female *Apc* $^{min/+}$ mice.

An increase in muscle protein degradation outcomes in mice with abnormal ovarian function compared to mice with normal ovarian function will indicate that normal ovarian function suppresses these pathways in skeletal muscle.

A decrease in mitochondrial content outcomes in mice with abnormal ovarian function compared to mice with normal ovarian function will indicate that normal ovarian function protects mitochondrial content.

An increase in the proteins levels of mitochondrial turnover markers in mice with abnormal ovarian function compared to mice with normal ovarian function will indicate that normal ovarian function regulates mitochondrial turnover.

A decrease in COX IV activity in mice with abnormal ovarian function compared to mice with normal ovarian function will indicate that normal ovarian function protects oxidative capacity in skeletal muscle.

Differences seen in Experiment 3.2 between OVX mice and intact mice will indicate whether lack of ovarian function during the progression of cachexia alters skeletal muscle metabolism in female *Apc* $^{min/+}$ mice.

A decrease in the pAkt/Akt ratio or mTOR in OVX mice compared to mice with ovarian function will indicate that normal ovarian function protects protein synthesis in muscle during the progression of cachexia in female *Apc* $^{min/+}$ mice.

An increase in muscle protein degradation outcomes in OVX mice compared to mice with ovarian function will indicate that ovarian function suppresses these pathways in skeletal muscle.

A decrease in mitochondrial content outcomes in OVX mice compared to mice with ovarian function will indicate that ovarian function protects mitochondrial content.

An increase in the proteins levels of mitochondrial turnover markers in OVX mice compared to mice with ovarian function will indicate that ovarian function regulates mitochondrial turnover.

A decrease in COX IV activity in OVX mice compared to mice with ovarian function will indicate ovarian function protects oxidative capacity in skeletal muscle.

Differences seen in Experiment 3.3 between OVX mice with and without IL-6 overexpression, and between intact and OVX mice with IL-6 overexpression, will determine the effect of ovariectomy on IL-6 induced effects on skeletal muscle metabolism during cachexia progression in female *Apc* $^{min/+}$ mice.

A decrease in the pAkt/Akt ratio or mTOR in OVX mice overexpressing IL-6 compared to SHAM mice with IL-6 overexpression will indicate that ovarian function regulates IL-6's effect on this pathway.

An increase in muscle protein degradation outcomes in OVX mice overexpressing IL-6 compared to SHAM mice with IL-6 overexpression will indicate that ovarian function regulates IL-6's effect on these pathways.

A decrease in mitochondrial content outcomes in OVX mice overexpressing IL-6 compared to SHAM mice with IL-6 overexpression will indicate that ovarian function regulates IL-6's effect on mitochondrial content.

An increase in the proteins levels of mitochondrial turnover markers in OVX mice overexpressing IL-6 compared to SHAM mice with IL-6 overexpression will indicate that ovarian function regulates IL-6's effect on mitochondrial turnover.

A decrease in COX IV activity in OVX mice overexpressing IL-6 compared to SHAM mice with IL-6 overexpression will indicate that ovarian function regulates IL-6's effect on oxidative capacity in skeletal muscle.

B.3 Power Analysis

Experiment 1.1, 2.1, 3.1: Female *Apc* $^{min/+}$ mice will be followed from 10 weeks of age to sacrifice at 15 weeks (early stage cachexia) or sacrifice at 18 weeks (late stage cachexia). Abnormal ovarian function will be classified by continuous measurement of estrous cycling and verified by plasma estrogen levels from blood taken at 12, 14, 16, and 18 weeks of age. Additional measurements will include ovarian mRNA expression of estrogen and progesterone at 15-week and 18-week endpoints. Body composition

outcomes will comprise body fat percentage and lean mass percentage determined by DEXA as well as total body weight loss at 12, 14, 16, and 18 weeks. Functional outcomes will comprise volitional grip strength, run-to-fatigue time, food intake, and cage activity at 12, 14, 16, and 18 weeks. Blood biochemistry outcomes will comprise hematocrit (for determination of anemia), plasma insulin levels, and plasma triglyceride levels at 12, 14, 16, and 18 weeks.

Two-tailed Student's t-tests: abnormal-15 vs. normal-15; normal-18 vs. abnormal-18

alpha = 0.05; effect size = 0.5; power= 0.8 ' n= 6 per group (12 per timepoint)

http://euclid.psych.yorku.ca/datavis/online/power/index.html

Effect size based on findings in Puppa et al. 2011 with male *Apc* $^{min/+}$ mice over a similar time course [4].

Experiment 1.2, 2.2, 3.2: Female *Apc* $^{min/+}$ mice and female C57BL/6 mice will be ovariectomized (OVX) at 11 weeks of age and will be followed until sacrifice at 15 weeks (early stage cachexia) or 18 weeks (late stage cachexia). Mice from experiment 1.1 will be used as control for ovariectomy. Body weight will be tracked weekly. Body composition will be determined by DEXA at 12, 14, 16, and 18 weeks of age. Measurement of function including grip strength, run to fatigue time, food intake, and cage activity will be taken at 12, 14, 16, and 18 weeks of age. Blood for determination of anemia as well as determination of plasma estrogen, insulin, and triglycerides will be collected at 12, 14, 16, and 18 weeks of age. It is expected that plasma estrogen will be depleted within 2 weeks of ovariectomy.

2x2 ANOVA: genotype X treatment (B6-SHAM, B6-OVX, MIN-SHAM, MIN-OVX at each timepoint)

Preplanned t-tests: MIN-OVX vs. MIN-SHAM at each timepoint, MIN-OVX vs. B6-OVX

alpha = 0.05; effect size = 0.75; power= 0.8 ‘ n= 8 per group

http://euclid.psych.yorku.ca/datavis/online/power/index.html

Effect size based on findings in Spangenburg et al. 2012 comparing muscle outcomes in OVX and SHAM mice [163].

Experiment 2.3, 3.3: Female *Apc* $^{min/+}$ mice will be followed from 10 weeks of age to sacrifice at 15 weeks of age. Half will undergo ovariectomy (OVX) and half will undergo sham surgery (SHAM) at 11 weeks of age. Two weeks will be allowed for hormone washout; half of each treatment group (OVX or SHAM) will then undergo IL-6 overexpression by electroporation at 13 weeks of age, with the remainder of mice being electroporated with a control vector. Functional measurements including grip strength, run to fatigue, food intake, and cage activity will be taken at 11 and 15 weeks of age. Blood will be taken at 13 and 15 weeks to verify efficacy of ovariectomy and IL-6 overexpression as well as to measure plasma estrogen (in intact mice), insulin, and triglycerides. Functional measurements including grip strength, run to fatigue, activity monitoring, and food intake will be completed at 11 weeks and 15 weeks of age.

2x2 ANOVA: surgery x vector (OVX-IL-6, OVX-vector, SHAM-IL-6, SHAM-vector)

Preplanned t-tests: OVX-IL-6 vs. OVX-vector; OVX-IL-6 vs. SHAM-IL-6

alpha = 0.05; effect size = 0.75; power= 0.8 ‘ n= 8 per group

http://euclid.psych.yorku.ca/datavis/online/power/index.html

Effect size based on findings in Baltgalvis et al. 2009 regarding IL-6 overexpression in male *Apc* $^{min/+}$ mice [20]

B.4 Limitations, Pitfalls, and Alternatives

-Effects of ovariectomy: Ovariectomy has wide-reaching effects on whole-body metabolism and body composition [29, 39, 163, 165], even when performed in wildtype mice. Therefore, a wildtype (B6) group of mice has been added to experiments involving ovariectomy, in order to control for these effects.

-Effects of ovariectomy on IL-6 overexpression: Prior to this study, IL-6 overexpression has never been performed in an ovariectomized mouse. Though there is ample evidence of estrogen’s effects on IL-6 [27, 36, 92], it is impossible to know what the effects will be *in vivo* until this experiment is carried out. Therefore, it is a distinct possibility that ovariectomy will have no additive effect with IL-6 overexpression in the female *Apc* $^{min/+}$ mouse. However, this experiment is still worthwhile and would still garner valuable information in this case. It would be beneficial to know that ovarian function is not suppressing IL-6 in the model of cancer cachexia so that other avenues could be explored.

-Other options for ablation of ovarian function: Because ovariectomy carries so many side effects in the female mouse, it is possible that the results from experiments involving ovariectomy will be difficult to interpret. Should this become a problem during the course of this work, there are options for chemical intervention in place of this operation. ICI 182,780 is an inhibitor of estrogen receptors α and β that is available commercially and has been widely used to explore the effects of estrogen and estrogen deficiency in mice [166]. However, the ovary produces hormones besides estrogen, so this alternative approach would slightly alter the focus of this research.

B.5 Preliminary Data

Table B1. Body weight, tibia length and gonadal fat mass of wild-type and *Apc* $^{Min/+}$ mice. Table B1 demonstrates body weights at 14 weeks (pre-cachexia) and 20 weeks (cachexia), tibial length, gonadal fat, and percent of gonadal fat lost in the female and male *Apc* $^{min/+}$ mouse compared to wild type mice. Male and female *Apc* $^{min/+}$ each undergo cachexia, though the female does not exhibit the weight loss seen in the male.

			Body weight (g)		Tibial length	Gonadal fat	Gonadal fat / tibia	% of gonadal
	Group	N	14 week	20 week	(mm)	(mg)		fat loss vs. Wt.
Male	Wt	5	26.5 ± 0.8	28.4 ± 0.9	17.4 ± 0.1	638 ± 80	36.8 ± 4.8	-
	Min	6	24.3 ± 0.3	22.1 ± 1.0	17.1 ± 0.1	78 ± 29	4.5 ± 1.7	88%
Female	Wt	6	19.8 ± 0.4	21.4 ± 0.4	17.1 ± 0.1	238 ± 20	14.0 ± 1.2	-
	Min	9	18.9 ± 0.7	18.8 ± 0.6	16.5 ± 0.2	47 ± 26	2.8 ± 1.5	80%

Table B2. Changes in plasma IL-6 concentration during the development of cachexia. Table B2 demonstrates endogenous plasma IL-6 levels in male and female *Apc* $^{min/+}$ mice at 14 weeks (pre-cachexia) and 20 weeks (cachexia).

			Plasma IL-6 (pg/ml)	
	Group	N	14 weeks	20 weeks
Male	Wt	5	0 ± 0	0 ± 0
	Min	5	5.5 ± 2.4	38.6 ± 16.7
Female	Wt	5	0 ± 0	0 ± 0
	Min	5	1.5 ± 1.5	11.0 ± 4.5

Table B3. Changes in plasma IL-6 concentration in female *Apc* $^{min/+}$ mice after 2 weeks of IL-6 over-expression. Table B3 demonstrates that electroporation of and IL-6 overexpression vector is sufficient to increase circulating levels of IL-6 in the female *Apc* $^{min/+}$ mouse.

		Plasma IL-6 (pg/ml)	
Group	N	Pre	Post
Wt	6	0 ± 0	126.2 ± 19.1
Min	5	1.5 ± 1.5	95.2 ± 34.0

Table B4. The effect of IL-6 over-expression and exercise on body weights, growth, food consumption and voluntary physical activity in female wild-type and *Apc*$^{Min/+}$ mice. Table B4 demonstrates that there are no significant differences between vector-treated female *Apc* $^{min/+}$ mice and female *Apc* $^{min/+}$ mice with IL-6 overexpressed from 12-14 weeks of age with respect to body weight loss, food consumption, or cage activity.

	C57BL/6				ApcMin/+			
	CC Vector	CC IL-6	Ex Vector	Ex IL-6	CC Vector	CC IL-6	Ex Vector	Ex IL-6
N	5	6	6	4	4	5	5	6
BW 12 weeks	21.0 ± 0.3	20.6 ± 0.4	19.4 ± 0.3	20.6 ± 0.4	20.0 ± 0.7	18.3 ± 0.9	17.1 ± 1.1	17.2 ± 0.3
BW/TL 12 weeks	1.20 ± 0.02	1.20 ± 0.02	1.20 ± 0.01	1.10 ± 0.03	1.20 ± 0.04	1.10 ± 0.04	1.10 ± 0.06	1.10 ± 0.02
BW 14 weeks	21.2 ± 0.3	21.2 ± 0.4	20.7 ± 0.2	21.2 ± 0.4	20.3 ± 0.6	18.1 ± 1.5	17.6 ± 1.7	18.0 ± 0.2
BW/TL 14 weeks	1.20 ± 0.02	1.30 ± 0.03	1.20 ± 0.01	1.20 ± 0.02	1.20 ± 0.03	1.20 ± 0.08	1.10 ± 0.10	1.10 ± 0.01
Tibia length (mm)	17.1 ± 0.1	16.9 ± 0.1	16.9 ± 0.1	16.8 ± 0.1	16.6 ± 0.1	16.5 ± 0.2	16.1 ± 0.3	16.2 ± 0.1
Plasma IL-6 (pg/ml)	0.0 ± 0.0	126.2 ± 19.1	0.0 ± 0.0	116.8 ± 16.6	1.5 ± 1.5	95.2 ± 34.0	14.0 ± 10.6	94.2 ± 19.1
14-week Food Consumption (g/g)	0.16 ± 0.01	0.15 ± 0.02	0.20 ± 0.02	0.16 ± 0.02	0.19 ± 0.03	0.18 ± 0.04	0.15 ± 0.02	0.17 ± 0.02
14-week Physical Activity counts	10323 ± 1566	12533 ± 2049	9154 ± 1546	7017 ± 1764	5769 ± 1773	3189 ± 718	7054 ± 3353	4668 ± 1854

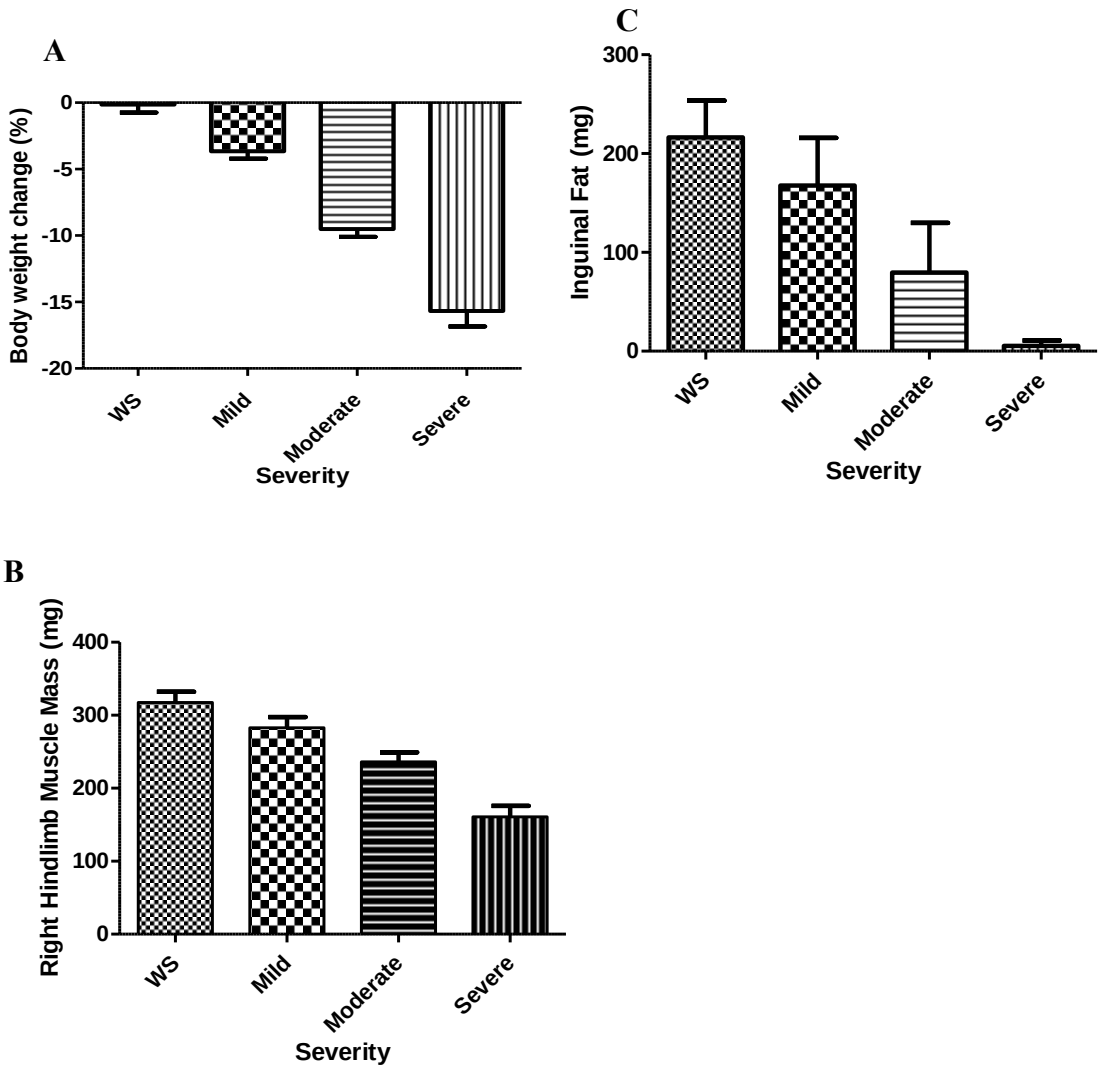

Figure B1 demonstrates that, in the female *Apc* $^{min/+}$ mouse (n=24), **A**) Average body weight loss (%) increases with increasing cachexia severity ($p<0.0001$) **B)** Average right hindlimb muscle weight (mg) decreases with increasing severity of cachexia ($p<0.0001$) **C)** Average inguinal fat mass (mg) decreases with increasing cachexia severity ($p=0.0089$).

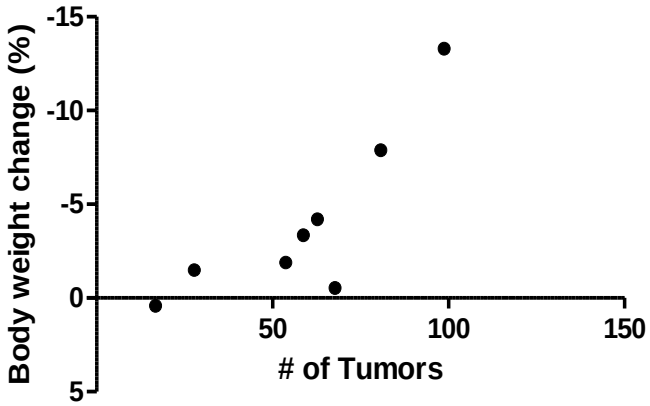

Figure B2 demonstrates that in the female *Apc* $^{min/+}$ mouse, intestinal polyp (tumor) count is correlated with percent body weight loss (n=8) (p=0.01).

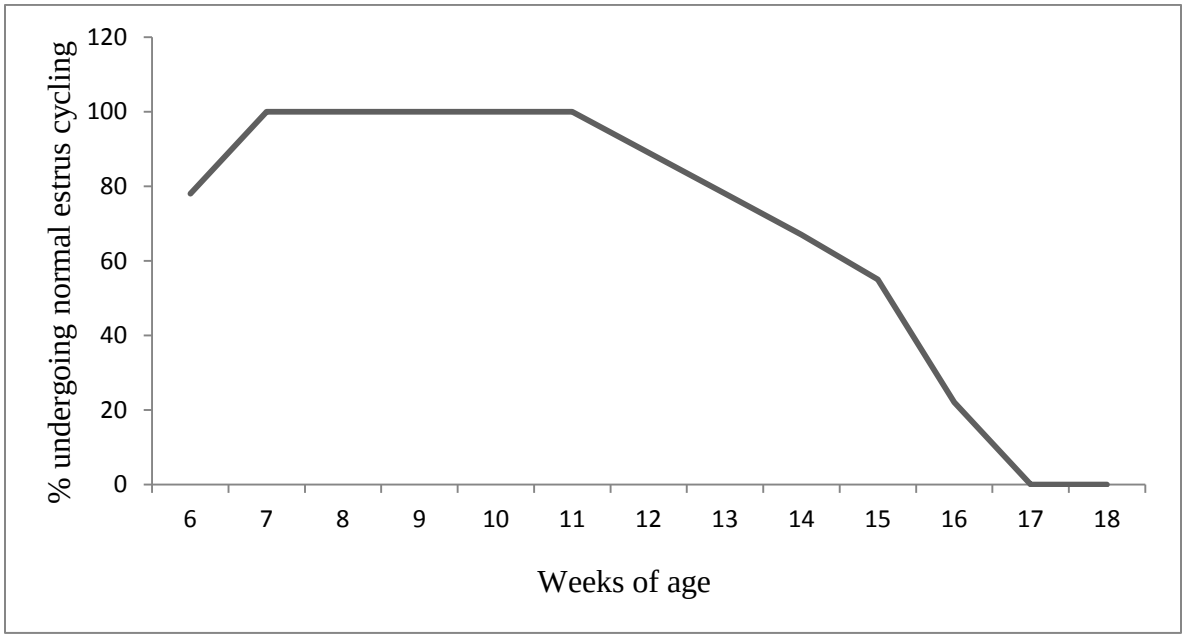

Figure B3 demonstrates percent of female *Apc* $^{min/+}$ mice that continue to undergo normal estrus cycling as cancer and cachexia progress. All mice begin normal cycling by 8 weeks of age, the normal age of sexual maturation in C57BL/6 mice [167]. Mice begin to withdraw from normal cycling at ~11 weeks of age. By 17 weeks of age, all female *Apc* $^{min/+}$ mice have ceased cycling (n=9).

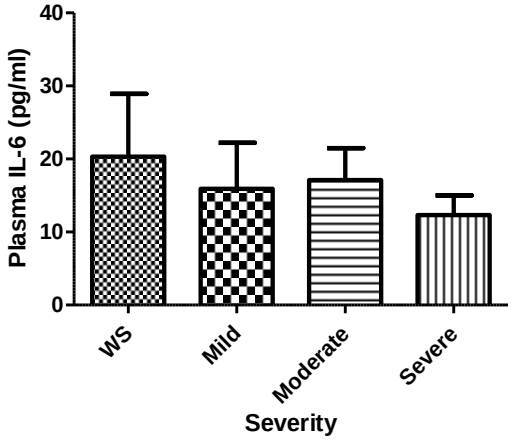

Figure B4 demonstrates that in the female *Apc* $^{min/+}$ mouse, there is no relationship between endogenous plasma IL-6 level and cachexia severity at 18 weeks of age (n=24).

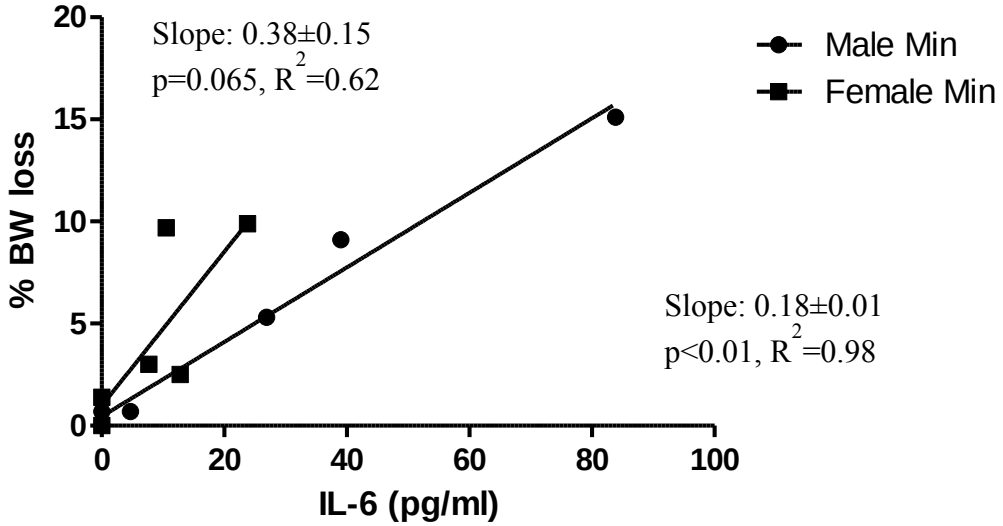

Figure B5 demonstrates that though circulating IL-6 levels are comparable in the male (n=6) and female (n=4) *Apc* $^{min/+}$ mouse, the female may show a blunted body weight loss response compared to the male.

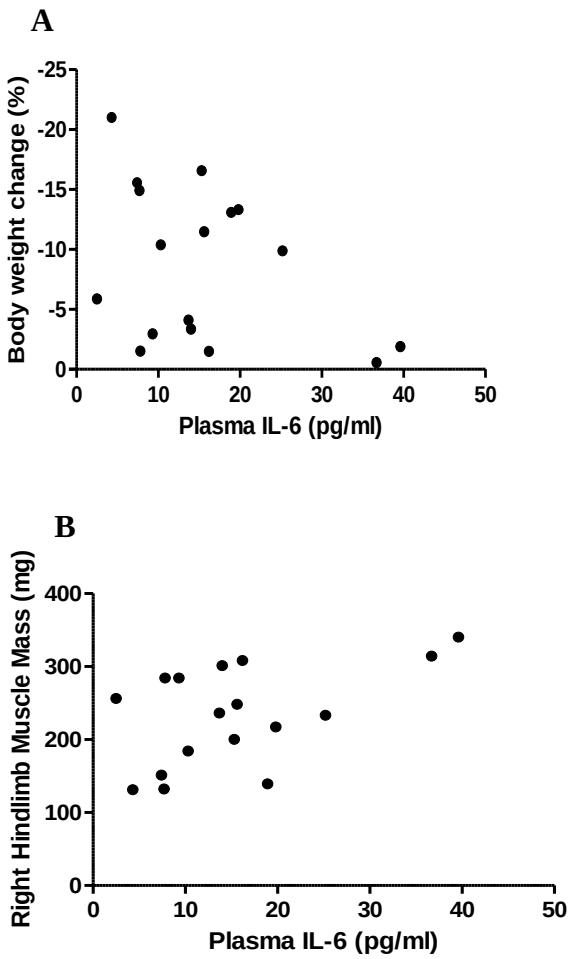

Figure B6 demonstrates that **A)** there is no relationship between body weight change and circulaing IL-6 levels in the female *Apc* $^{min/+}$ mouse (n=24); however, interestingly, **B)** there is a significant relationship between circulating plasma IL-6 levels and increasing hindlimb muscle mass (n=24 (p=0.03).

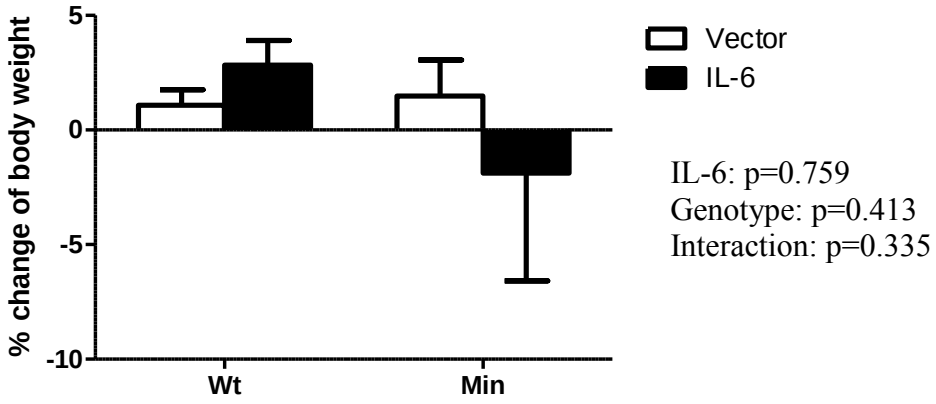

Figure B7 demonstrates that there is no relationship between IL-6 overexpression and body weight loss in the female *Apc* $^{min/+}$ mouse.

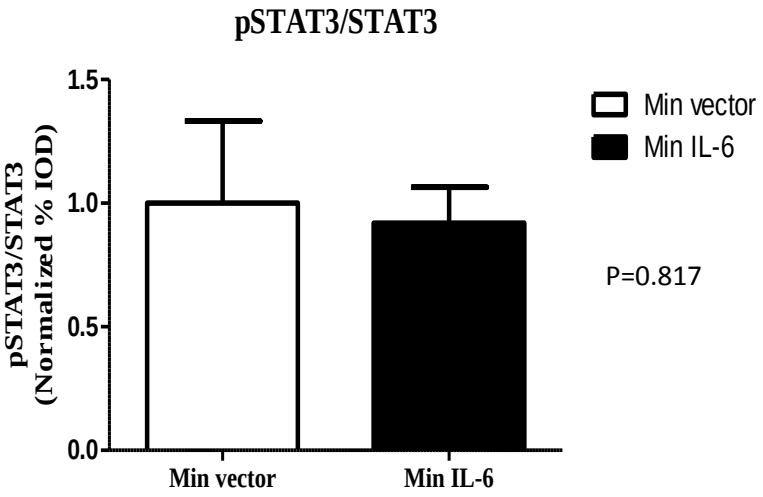

Figure B8 shows that there is no difference in STAT3 signaling between female *Apc* $^{min/+}$ mice treated with IL-6 overexpression (n=5) and vector-treated mice (n=4).

APPENDIX C

RAW DATA

Sac Data 18 weeks Group	Mouse #	Body weight	Peak BW	BW loss from peak	% BW change from peak
Intact-18	**3376**	19.2	19.2	0	0.00%
Intact-18	**3427**	19.4	19.4	0	0.00%
Intact-18	**3509**	19.1	19.1	0	0.00%
Intact-18	**3518**	19.4	19.4	0	0.00%
PFOVX ctrl	**4236**	20.5	20.6	0.1	-0.49%
Intact-18	**3519**	18.9	19	0.1	-0.53%
Intact-18	**3352**	21.2	21.4	0.2	-0.93%
Intact-18	**3346**	19.4	19.6	0.2	-1.02%
Intact-18	**3587**	20.1	20.4	0.3	-1.47%
Intact-18	**3345**	18.9	19.4	0.5	-2.58%
Intact-18	**3392**	21.7	22.3	0.6	-2.69%
Intact-18	**3344**	19.1	19.7	0.6	-3.05%
Intact-18	**3428**	18.4	19.6	1.2	-6.12%
Intact-18	**3511**	19.5	20.9	1.4	-6.70%
Intact-18	**3382**	18.7	20.1	1.4	-6.97%
Intact-18	**3424**	18.7	19.5	0.8	-4.10%
PFOVX ctrl	**4233**	19.3	21.2	-1.9	-8.96%
PFOVX ctrl	**4228**	17	18.7	-1.7	-9.09%
Intact-18	**3434**	16.7	18.4	1.7	-9.24%
Intact-18	**3510**	17.6	19.4	1.8	-9.28%
Intact-18	**4111**	19.7	22.1	2.4	-10.86%
Intact-18	**3429**	17.7	20.5	2.8	-13.66%
Intact-18	**3435**	15.8	18.4	2.6	-14.13%
PFOVX ctrl	**4234**	14.3	17.7	-3.4	-19.21%

Week of cycle end	Fasting Glucose	Tibia length	R Sol	L sol	R Plant	L Plant	R Gas	L Gas	R TA	L TA
YES	129	15.9	7	7	11	12	91	90	32	41
YES	159	16.2	7	7	21	16	97	91	38	33
		16.7	7	6	14	11	81	88	30	31
	104	16	7	6	16	12	95	86	34	36
		15.3	7	5	12	14	105	81	22	33
	185	16.4	7	7	10	14	95	86	27	35
YES	137	16.5	7	5	12	13	99	94	27	24
YES	136	16.1	7	5	9	10	83	89	28	35
		17	8	7	11	10	96	78	39	32
YES	131	16.4	5	7	11	11	93	92	30	25
YES	106	16	11	9	15	15	103	100	31	39
YES	104	16.4	5	6	8	11	82	81	31	31
YES	117	16.2	8	5	13	18	92	82	31	35
		17.1	6	11	10	12	81	85	28	37

YES	165	16.2	6	6	13	10	85	79	21	32
14		16.1	6	10	17	14	90	70	19	25
15		16.4	5	7	9	13	64	69	21	24
15		15.8	7	1	11	10	49	60	17	18
15.15	108	16	7	6	12	12	67	65	28	27
14.75		16.8	6	9	11	7	62	50	20	21
15.5		16.2	7	6	10	11	66	70	28	20
14.15	220	16.5	10	10	16	22	78	72	20	33
15.5	139	16.1	6	6	9	10	45	56	23	24
14.75		15.7	3	3	6	5	41	49	19	17

R EDL	L EDL	R Quad	R RF	L Quad	L RF	TRMW	TMRW/TL	Liver	Spleen	Uterus
5	7	128	63	119	64	274	17.2	973	270	85
6	7	129	70	122	70	298	18.4	966	127	73
9	10	125	60	122	60	266	15.9	846	190	53
5	8	132	63	109	47	289	18.1	1013	330	56
5	9	109	59	130	63	260	17.0	1318	247	36
7	6	132	61	122	44	278	17.0	1048	258	65
9	6	132	70	133	69	286	17.3	1130	248	49
4	4	119	63	126	55	250	15.5	1110	270	38
6	7	108	54	121	66	268	15.8	1206	132	87
8	11	117	62	123	51	264	16.1	892	155	47
12		190	96	147	72	362	22.6	874	82	88
8	7	85	51	119	57	219	13.4	1030	245	41
8	7	125	62	123	50	277	17.1	1105	270	40
9	10	115	61	112	60	249	14.6	1203	559	41
7	3	95	60	88	55	227	14.0	940	259	50
6	4	95	46	82	33	233	14.5	1485	497	32
3	3	87	48	90	49	189	11.5	1609	432	21
4	4	72	40	80	43	160	10.1	1432	380	29
5	7	99	50	96	45	218	13.6	1086	365	32
4	6	78	46	66	37	181	10.8	811	294	24
8	4	93	38	87	33	212	13.1	1325	516	21
6	5	108	58	87	42	238	14.4	1026	408	27
10	7	85	56	80	49	178	11.1	912	249	28
5	5	61	37	66	33	135	8.6	1063	209	19

Ute+ovs	Heart	Heart:BW	heart:tibia	Mes Fat	Epi Fat	TF	Lymph	IL-6	Total tumors
107	101	5.26	6.35	131	162	293	32	10	
88	99	5.10	6.11	122	122	244	40		
72	85	4.45	5.09	103	149	252	41	56.7	
71	80	4.12	5.00	90	130	220	35	4.9	

61	117	5.71	7.65	184	175	359	21	15.8	
83	96	5.08	5.85	93	162	255	32	37.7	
63	104	4.91	6.30	269	307	576	37	15.4	13
58	90	4.64	5.59	172	191	363		7.1	3
113	107	5.32	6.29	167	95	262	49	0	
58	85	4.50	5.18	123	283	406	37	44	
110	99	4.56	6.19	248	293	541	34	144	
57	88	4.61	5.37	126	192	318	30	16	5
55	100	5.43	6.17	90	90	180	39	0	
58	99	5.08	5.79	161	81	242	33	233	
57	96	5.13	5.93	108	122	230	35	32.6	
40	122	6.52	7.58	111	0	111	36	68.2	
31	139	7.20	8.48	159	10	169	45	21.4	
41	147	8.65	9.30	222	0	222	32	17.4	
44	102	6.11	6.38	103	0	103	31	124	7
35	88	5.00	5.24	73	0	73		72.4	
29	121	6.14	7.47	262	19	281	30	66.6	
36	115	6.50	6.97	88	0	88	25	23.5	
37	125	7.91	7.76	195	0	195	23	96.9	15
27	128	8.95	8	91	0	91	26	17.4	

OVX-18		**F1**		21.9	23.9	2	-8.37%		
OVX-18		**F2**		21.3	22	0.7	-3.18%		
OVX-18		**F3**		21.3	22.2	0.9	-4.05%		
OVX-18		**F4**		22.9	23.5	0.6	-2.55%		
OVX-18		**F5**		21.3	23.6	2.3	-9.75%		
OVX-18		**3713**		19.8	21	1.2	-5.7%		
OVX-18		**3954**		20	20	0	0.0%		
OVX-18		**3955**		20.4	20.4	0	0.0%		
OVX-18		**3960**		19.5	20	0.5	-2.5%		
OVX-18		**3962**		21.1	21.1	0	0.0%		
B6-18					**3464**	19.5	19.7	-0.2	-1.0%
B6-18					**3465**	20.6	21	-0.4	-1.9%
B6-18					**3467**	20.5	21.4	-0.9	-4.2%
B6-18					**3596**	20.4	20.4	0	0.0%
B6-18					**3606**	21.4	21.4	0	0.0%
B6-18					**3607**	19.5	19.5	0	0.0%
86	4.41	4.4102564			252	72	324	25	0
98	4.76	4.7572816			134	101	235	23	0
110	5.37	5.3658537			136	136	272	28	0
92	4.51	4.5098039				144	144		0

83	3.88	3.8785047				0
81	4.15	4.1538462		119	119	0

B6 OVX 18	3716	21.7	21.7	0	0%
B6 OVX 18	3879	19.6	20	-0.4	-2%
B6 OVX 18	3961	22.9	23.3	-0.4	-2%
B6 OVX 18	3963	21.5	21.9	-0.4	-2%
B6 OVX 18	3964	23.8	23.8	0	0%

16	6	8	12	10	79	82	34	30
16	8	7	11	12	94	90	37	36
16.8	7	7	13	10	93	88	42	40
17	8	8	10	11	91	92	38	30

6	6	102	58	113	42	239	14.9375	956	57	20
8	9	133	75	128	67	291	18.1875	1260	107	28
8	8	131	75	123	65	294	17.5	1061	94	47
11	7	120	70	123	65	278	16.352941	1087	99	27

101	5.15306122	6.3125		166	166		48.9
114	4.97816594	7.125	146	184	330	46	280
107	4.97674419	6.3690476	124	155	279	49	0
124	5.21008403	7.2941176	163	389	552	42	104

Tumor Counts-18 weeks

Group	Mouse #	Cycle?	% BW loss	Segment 1	Segment 2	Segment 3	Segment 4	Colon	Total
Intact-18	3424	NO	**4%**	0	7	15	35	3	**60**
Intact-18	3429	NO	**12%**	1	5	12	22	2	**42**
Intact-18	3434	NO	**9%**	3	5	31	36	1	**76**
Intact-18	3435	NO	**14%**	3	10	55	34	4	**106**
Intact-18	4111	NO		5	22	55	67	3	**152**
Intact-18	3510	NO	**9%**	9	22	47	17	2	**97**
Intact-18	4228	NO		8	10	14	9	1	**42**
Intact-18	4233	NO		0	21	4	9	1	**35**
Intact-18	4234	NO		5	8	34	38	1	**86**
			9.6%	**3.7777778**	**12.222222**	**29.666667**	**29.666667**	**2**	**77.333**
			3.8%	**3.3**	**7.3**	**19.5**	**18.1**	**1.1**	**37.8**
			1.7%	**1.2**	**2.6**	**6.9**	**6.4**	**0.4**	**13.4**
Intact-18	3344		**3%**	0	0	0	0	5	**5**
Intact-18	3345		**3%**	3	2	1	1	0	**7**
Intact-18	3427		**0%**	2	2	4	1	1	**10**
Intact-19	3346								
Intact-18	3352	**1%**	1	2	0	0	0	**3**	

Intact-18	3376	**4%**	2	0	2	8	1	**13**
Intact-18	3382	**7%**	2	5	6	0	2	**15**
Intact-18	3392	**4%**	3	0	0	2	7	**12**
Intact-18	3428	**6%**	2	30	21	5	0	**58**
Intact-18	4236		2	2	8	3	1	**16**
Intact-18	3509		3	3	1	1	0	**8**
Intact-18	3511		4	2	4	5	0	**15**
Intact-18	3518		2	0	2	1	0	**5**
Intact-18	3519		2	0	5	0	3	**10**
		3.5%	**2.2**	**3.7**	**4.2**	**2.1**	**1.5**	**13.6**
		2.3%	**1.0**	**8.0**	**5.7**	**2.5**	**2.2**	**14.0**
		0.8%	**0.3**	**2.8**	**2.0**	**0.9**	**0.8**	**4.9**

OVX-18	F2		-3.2%	1	5	6	2	0	13
OVX-18	F3		-7.4%	4	0	0	0	2	6
OVX-18		3962	0.0%	3	6	19	9	1	39
OVX-18		3960	-2.5%	2	2	14	12	2	32
OVX-18		3955	0.0%	4	9	18	10	0	41
OVX-18		3954	0.0%	5	5	28	12	2	52
			-2.2%	**3.2**	**4.5**	**14.2**	**7.5**	**1.2**	**30.5**
			2.9%	**1.5**	**3.1**	**10.0**	**5.2**	**1.0**	**17.6**
			1.2%	**0.6**	**1.3**	**4.1**	**2.1**	**0.4**	**7.2**

15 WEEK TUMOR DATA

Group	Mouse #	Segment 1	Segment 2	Segment 3	Segment 4	Colon	Total	Large
Intact-15	3847	2	3	0	0	0	**5**	3
Intact-15	3852	5	1	2	7	1	**16**	8
Intact-15	3826	5	4	3	7	0	**19**	11
Intact-15	3980	14	19	55	43	0	**131**	41
Intact-15	3979	7	9	18	13	0	**47**	13
Intact-15	3850	1	1	4	2	0	**8**	5
Intact-15	3981	5	15	16	57	1	**94**	34
Intact-15	3984	3	18	36	16	1	**74**	36
		5.3	**8.8**	**16.8**	**18.1**	**0.4**	**49.3**	**18.9**
		4.0	**7.6**	**19.6**	**20.7**	**0.5**	**46.3**	**15.4**
		1.4	**2.7**	**6.9**	**7.3**	**0.2**	**16.4**	**5.5**
sham+IL-6	4136	10	12	11	24	0	**57**	27
sham+IL-6	4137	4	9	30	11	3	**57**	18

sham+IL-6	337	0	8	20	14	1	**43**	18
sham+IL-6	338	0	4	6	11	0	**21**	10
sham+IL-6	4045	0	0	0	0	0	**0**	0
sham+IL-6	822	3	3	5	2	1	**14**	9
sham+IL-6	823	5	5	13	2	2	**27**	14
sham+IL-6	4135	2	0	2	0	1	**5**	4
		3.0	**5.1**	**10.9**	**8.0**	**1.0**	**28.0**	**12.5**
		3.2	**4.0**	**9.4**	**8.0**	**1.0**	**20.8**	**8.1**
		1.1	**1.4**	**3.3**	**2.8**	**0.4**	**7.4**	**2.9**
OVX+vector	4054	0	0	0	0	0	**0**	0
OVX+vector	4042	0	0	0	1	0	**1**	1
OVX+vector	4043	5	2	1	0	0	**8**	5
OVX+vector	3855	1	0	1	3	0	**5**	3
OVX+vector	3878	4	4	2	12	0	**22**	10
		2.0	**1.2**	**0.8**	**3.2**	**0.0**	**7.2**	**3.8**
		2.1	**1.6**	**0.7**	**4.5**	**0.0**	**7.9**	**3.5**
		0.7	**0.6**	**0.3**	**1.6**	**0.0**	**2.8**	**1.3**
OVX+IL-6	4159	7	0	16	10	1	**34**	14
OVX+IL-6	4148	2	11	2	3	0	**18**	9
OVX+IL-6	3886	2	4	1	2	0	**9**	4
OVX+IL-6	3892	2	4	2	0	0	**8**	4
		3.3	**4.8**	**5.3**	**3.8**	**0.3**	**17.3**	**7.8**
		2.2	**4.0**	**6.2**	**3.8**	**0.4**	**10.4**	**4.1**
		0.8	**1.4**	**2.2**	**1.3**	**0.2**	**3.7**	**1.5**

COX ACTIVITY

min OVX	-4.1		B6	0		min OVX	-3.2		min intact	-2.7	
3877	**Time**	Abs	3606	**Time**	Abs	F2	**Time**	Abs	3392	**Time**	Abs
	0	0.176		**0**	0.201		**0**	0.209		**0**	0.163
	10	0.17		**10**	0.174		**10**	0.202		**10**	0.158
	20	0.165		**20**	0.173		**20**	0.2		**20**	0.156
	30	0.158		**30**	0.165		**30**	0.188		**30**	0.157
	40	0.154		**40**	0.165		**40**	0.184		**40**	0.151
	50	0.154		**50**	0.163		**50**	0.179		**50**	0.148
	Abs/min	0.033		**Abs/min**	0.084		**Abs/min**	0.042		**Abs/min**	0.021
	dilution	20		**dilution**	20		**dilution**	20		**dilution**	20

	vol sample	0.005		**vol sample**	0.012		**vol sample**	0.006		**vol sample**	0.0054
	U/g/min	6.6484		**U/g/min**	7.358		**U/g/min**	7.05128		**U/g/min**	3.91738
B6	-1.02		B6	-4.21		min OVX	-7.4		min intact	-14.1	
3464	**Time**	Abs	3467	**Time**	Abs	F3	**Time**	Abs	3435	**Time**	Abs
	0	0.183		**0**	0.179		**0**	0.184		**0**	0.191
	10	0.169		**10**	0.173		**10**	0.173		**10**	0.185
	20	0.157		**20**	0.163		**20**	0.163		**20**	0.182
	30	0.147		**30**	0.167		**30**	0.168		**30**	0.171
	40	0.145		**40**	0.167		**40**	0.153		**40**	0.17
	50	0.138		**50**	0.156		**50**	0.149		**50**	0.166
	Abs/min	0.078		**Abs/min**	0.048		**Abs/min**	0.063		**Abs/min**	0.036
	dilution	20		**dilution**	20		**dilution**	20		**dilution**	20
	vol sample	0.0111		**vol sample**	0.008		**vol sample**	0.019		**vol sample**	0.0094
	U/g/min	7.0785		**U/g/min**	6.044		**U/g/min**	3.34008		**U/g/min**	3.85784
min intact	-9.28		min OVX	-9.7		min intact	-6.1		min intact	-9.2	
3510	**Time**	Abs	F5	**Time**	Abs	3428	**Time**	Abs	3434	**Time**	Abs
	0	0.213		**0**	0.222		**0**	0.193		**0**	0.161
	10	0.208		**10**	0.219		**10**	0.188		**10**	0.156
	20	0.2		**20**	0.203		**20**	0.185		**20**	0.157
	30	0.178		**30**	0.195		**30**	0.17		**30**	0.149
	40	0.178		**40**	0.185		**40**	0.168		**40**	0.151
	50	0.174		**50**	0.186		**50**	0.159		**50**	0.15
	Abs/min	0.039		**Abs/min**	0.057		**Abs/min**	0.024		**Abs/min**	0.012
	dilution	20		**dilution**	20		**dilution**	20		**dilution**	20
	vol sample	0.0091		**vol sample**	0.008		**vol sample**	0.0065		**vol sample**	0.0083
	U/g/min	4.3171		**U/g/min**	7.177		**U/g/min**	3.71936		**U/g/min**	1.45637
min intact	-12.2		min OVX	-8.4		B6	0		min OVX	-5.7	
3429	**Time**	Abs	F1	**Time**	Abs	3607	**Time**	Abs	3713	**Time**	Abs
	0	0.194		**0**	0.175		**0**	0.246		**0**	0.153
	10	0.188		**10**	0.168		**10**	0.24		**10**	0.148
	20	0.182		**20**	0.16		**20**	0.229		**20**	0.143
	30	0.174		**30**	0.155		**30**	0.225		**30**	0.139
	40	0.167		**40**	0.146		**40**	0.22		**40**	0.14
	50	0.164		**50**	0.142		**50**	0.22		**50**	0.136
	Abs/min	0.036		**Abs/min**	0.04		**Abs/min**	0.051		**Abs/min**	0.03

				n	5		**n**			**n**	
	dilution vol sample U/g/min	20 0.0075 4.8352		**dilution vol sample U/g/min**	20 0.009 5.037		**dilution vol sample U/g/min**	20 0.0118 4.3537		**dilution vol sample U/g/min**	20 0.0047 6.42974
min intact	**-1**		B6	**0**		min OVX	**0**		B6 OVX	**0**	
3346	**Time**	ABS	3596	**Time**	Abs	3954	**Time**	ABS	3716	**Time**	ABS
	0	0.26		**0**	0.192		**0**	0.222		**0**	0.259
	10	0.26		**10**	0.175		**10**	0.22		**10**	0.248
	20	0.245		**20**	0.152		**20**	0.209		**20**	0.24
	30	0.24		**30**	0.148		**30**	0.213		**30**	0.243
	40	0.24		**40**	0.147		**40**	0.208		**40**	0.24
	50	0.238		**50**	0.144		**50**	0.203		**50**	0.23
	Abs/min	0.045		**Abs/min**	0.12		**Abs/min**	0.039		**Abs/min**	0.057
	dilution vol sample U/g/min	20 0.0096 4.7218		**dilution vol sample U/g/min**	20 0.0133 9.1588		**dilution vol sample U/g/min**	20 0.0058 6.7734		**dilution vol sample U/g/min**	20 0.0073 7.86542
min intact	**0**		min intact	**0**		min OVX	**0**		min intact	**-2.6**	
3427	**Time**	Abs	3518	**Time**	ABS	3962	**Time**	ABS	3345	**Time**	ABS
	0	0.146		**0**	0.272		**0**	0.239		**0**	0.288
	10	0.139		**10**	0.255		**10**	0.231		**10**	0.279
	20	0.136		**20**	0.254		**20**	0.228		**20**	0.27
	30	0.137		**30**	0.254		**30**	0.224		**30**	0.26
	40	0.137		**40**	0.25		**40**	0.22		**40**	0.248
	50	0.135		**50**	0.25		**50**	0.211		**50**	0.242
	Abs/min	0.03		**Abs/min**	0.054		**Abs/min**	0.033		**Abs/min**	0.054
	dilution vol sample U/g/min	20 0.0054 5.5963		**dilution vol sample U/g/min**	20 0.005 11.333		**dilution vol sample U/g/min**	20 0.005 6.64835		**dilution vol sample U/g/min**	20 0.0085 6.39948
B6 OVX	**-5.5**		min intact	**0**		min OVX	**-2.5**		min intact	**-3.5**	
3964	**Time**	ABS	3509	**Time**	ABS	3960	**Time**	ABS	3344	**Time**	ABS
	0	0.187		**0**	0.192		**0**	0.144		**0**	0.234
	10	0.184		**10**	0.189		**10**	0.131		**10**	0.227
	20	0.168		**20**	0.175		**20**	0.118		**20**	0.222
	30	0.16		**30**	0.178		**30**	0.12		**30**	0.226

	40	0.158		**40**	0.175		**40**	0.11		**40**	0.22
	50	0.152		**50**	0.175		**50**	0.102		**50**	0.22
	Abs/min	0.057		**Abs/min**	0.051		**Abs/min**	0.078		**Abs/min**	0.036
	dilution	20		**dilution**	20		**dilution**	20		**dilution**	20
	vol sample	0.0064		**vol sample**	0.016		**vol sample**	0.0192		**vol sample**	0.0137
	U/g/min	8.9715		**U/g/min**	3.251		**U/g/min**	4.09226		**U/g/min**	2.64699
min intact	**-0.5**		min intact	**-0.9**		min OVX	**0**		min intact	**-1.5**	
3519	**Time**	ABS	3352	**Time**	ABS	3955	**Time**	ABS	3587	**Time**	ABS
	0	0.324		**0**	0.288		**0**	0.282		**0**	0.315
	10	0.311		**10**	0.26		**10**	0.258		**10**	0.293
	20	0.303		**20**	0.256		**20**	0.254		**20**	0.273
	30	0.304		**30**	0.213		**30**	0.255		**30**	0.263
	40	0.298		**40**	0.191		**40**	0.25		**40**	0.267
	50	0.3		**50**	0.19		**50**	0.25		**50**	0.249
	Abs/min	0.063		**Abs/min**	0.096		**Abs/min**	0.084		**Abs/min**	0.126
	dilution	20		**dilution**	20		**dilution**	20		**dilution**	20
	vol sample	0.0199		**vol sample**	0.005		**vol sample**	0.0181		**vol sample**	0.0144
	U/g/min	3.189		**U/g/min**	20.15		**U/g/min**	4.67488		**U/g/min**	8.8141
B6 OVX	**-5.5**		min intact	**-6.7**		B6 OVX	**-1.8**		min intact	**-1.5**	
3879	**Time**	ABS	3511	**Time**	ABS	3963	**Time**	ABS	3151	**Time**	ABS
	0	0.278		**0**	0.32		**0**	0.256		**0**	0.31
	10	0.248		**10**	0.301		**10**	0.257		**10**	0.308
	20	0.248		**20**	0.3		**20**	0.238		**20**	0.3
	30	0.224		**30**	0.285		**30**	0.222		**30**	0.304
	40	0.212		**40**	0.284		**40**	0.22		**40**	0.301
	50	0.222		**50**	0.27		**50**	0.214		**50**	0.297
	Abs/min	0.09		**Abs/min**	0.06		**Abs/min**	0.054		**Abs/min**	0.03
	dilution	20		**dilution**	20		**dilution**	20		**dilution**	20
	vol sample	0.0032		**vol sample**	0.014		**vol sample**	0.0081		**vol sample**	0.0127
	U/g/min	28.331		**U/g/min**	4.317		**U/g/min**	6.71551		**U/g/min**	2.37951
B6 OVX	**-1.7**										
3961	**Time**	ABS									
	0	0.309									
	10	0.293									
	20	0.29									

30	0.288
40	0.279
50	0.279
Abs/min	0.057
dilution	20
vol sample	0.005 7
U/g/min	10.07 3

RT-PCR 15 WEEK

mouse	Treatment	IL-6 Ct	18s Ct	Dct	DDct	fold change	Normalized
787		35.46	15.50667	19.95333	0.937	0.522	0.482
789		34.295	15.393	18.902	-0.114	1.082	0.999
813		33.65	15.11	18.54	-0.476	1.391	1.284
814		33.705	15.413	18.292	-0.724	1.652	1.524
3826		34.815	15.423	19.392	0.376	0.770	0.711
150		33.26	15.30	17.967	-1.049	2.069	1.910
337		29.503	15.983	13.52	-5.496	45.125	41.651
338		32.49	15.513	16.977	-2.039	4.109	3.793
822		34.886	15.616	19.27	0.254	0.838	0.774
823		34.426	15.406	19.02	0.004	0.997	0.920
3747		32.65	15.323	17.327	-1.689	3.224	2.976
4045		33.363	15.27	18.093	-0.923	1.896	1.750
4135		35.21	15.563	19.647	0.631	0.646	0.596
4136		33.986	15.44667	18.53933	-0.477	1.391	1.284
4137		33.0066	15.336	17.6706	-1.345	2.541	2.345
159		33.31	15.296	18.014	-1.002	2.003	1.848
161		32.893	15.21	17.683	-1.333	2.519	2.325
162		34.023	15.373	18.65	-0.366	1.289	1.189
3854		34.436	15.483	18.953	-0.063	1.045	0.964
3855		31.675	15.216	16.459	-2.557	5.884	5.431
3878		31.43	15.23	16.20	-2.812	7.022	6.481
4042		34.87	15.45	19.42	0.403	0.756	0.698
4043		34.31	15.39	18.92	-0.093	1.066	0.984
4054		34.51	15.25	19.26	0.243	0.845	0.780

160	[redacted]	33.41	15.20	18.21	-0.809	1.752	
168		33.45	15.31	18.13	-0.883	1.844	1.702
176		26.29	15.60	10.68	-8.334	322.659	297.814
3657		34.65	15.37	19.28	0.264	0.833	0.769
3886		36.15	15.34	20.81	1.793	0.289	0.266
3892		33.84	15.36	18.48	-0.532	1.446	1.334
4148		28.97	16.68	12.29	-6.726	105.849	97.699
4159		35.32	15.32	20.00	0.984	0.506	0.467

		IL-6r	GAPDH				
mouse	Treatment	Ct	Ct	Dct	DDct	fold change	Normalized
787	[redacted]	28.14	24.12	4.02	0.614	0.653	0.477
789		30.215	24.775	5.44	2.034	0.244	0.178
813		28.115	24.515	3.6	0.194	0.874	0.638
814		28.06	25.4	2.66	-0.746	1.677	1.224
3826		28.025	25.3	2.725	-0.681	1.604	1.170
3847		28.235	24.31	3.925	0.519	0.698	0.509
3950		26.76	25.47	1.29	-2.116	4.336	3.163
3979		28.235	24.645	3.59	0.184	0.880	0.642
3980		23.27	28.13	-4.86	-8.266	307.885	224.590
150		28.22	23.67	4.55	1.144	0.453	0.330
337		22.815	25.83	-3.015	-6.421	85.702	62.516
338		24.695	24.475	0.22	-3.186	9.102	6.640
822		26.125	25.005	1.12	-2.286	4.878	3.558
823		26.065	23.8	2.265	-1.141	2.206	1.609
3747		22.16	26.025	-3.865	-7.271	154.477	112.685
4045		25.945	24.875	1.07	-2.336	5.050	3.684
4135		27.12	24.135	2.985	-0.421	1.339	0.977
4136		25.96	24.23	1.73	-1.676	3.196	2.331
4137		24.74	24.36	0.38	-3.026	8.147	5.943
159		28.71	23.505	5.205	1.799	0.287	0.210
161		28.51	24.015	4.495	1.089	0.470	0.343
162		26.545	24.52	2.025	-1.381	2.605	1.900
3854		27.61	23.085	4.525	1.119	0.460	0.336

3855		26.315	23.895	2.42	-0.986	1.981	1.445
3878		26.54	24.39	2.15	-1.261	2.397	1.749
4042		25.29	25.52	-0.23	-3.631	12.391	9.039
4043		26.04	25.60	0.44	-2.966	7.815	5.701
4054		24.55	24.22	0.33	-3.076	8.434	6.152
160		27.77	24.16	3.61	0.204	0.868	0.633
168		27.71	24.25	3.46	0.054	0.963	0.703
176		24.48	24.09	0.39	-3.021	8.119	5.922
3657		26.19	23.51	2.68	-0.731	1.660	1.211
3886		27.02	24.52	2.50	-0.906	1.874	1.367
3892		25.84	23.84	2.00	-1.411	2.660	1.940
4148		24.56	25.40	-0.84	-4.251	19.044	13.892
4159		28.35	24.16	4.19	0.784	0.581	0.424

		TGFb	18s				
mouse	Treatment	Ct	Ct	Dct	DDct	fold change	Normalized
787		29.42	15.183	14.237	0.434	0.740	0.688
789		29.81	15.18	14.63	0.827	0.564	0.524
813		29.315	15.136	14.179	0.376	0.770	0.716
814		29.605	15.483	14.122	0.319	0.801	0.745
3826		28.21	15.34	12.87	-0.933	1.909	1.775
3847		28.556	15.523	13.033	-0.770	1.705	1.585
3950		29.663	16.09	13.573	-0.230	1.172	1.090
3979		29.036	15.25	13.786	-0.017	1.012	0.941
3980		29.343	15.55	13.793	-0.010	1.007	0.936
150		30.16	15.37	14.785	0.982	0.506	0.471
337		28.653	15.86	12.793	-1.010	2.013	1.872
338		29.756	15.47	14.286	0.483	0.715	0.665
822		29.345	15.533	13.812	0.009	0.993	0.924
823		29.315	15.396	13.919	0.116	0.922	0.858
3747		29.38	15.323	14.057	0.254	0.838	0.779
4045		29.745	15.355	14.39	0.587	0.666	0.619
4135		29.753	15.62	14.133	0.330	0.795	0.739
4136		29.296	15.433	13.863	0.060	0.959	0.892
4137		27.533	15.326	12.207	-1.596	3.022	2.810
159		29.14	15.405	13.735	-0.068	1.048	0.974
161		29.31	15.463	13.847	0.044	0.970	0.902
162		28.75	15.635	13.115	-0.688	1.611	1.498
3854		30.03	15.296	14.734	0.931	0.524	0.488

3855		28.506	15.34	13.166	-0.637	1.555	1.446
3878		28.32	15.45	12.87	-0.929	1.903	1.770
4042		29.42	15.53	13.89	0.091	0.939	0.873
4043		30.03	15.65	14.38	0.572	0.672	0.625
4054		28.61	15.40	13.21	-0.593	1.508	1.402
160		28.19	15.27	12.91	-0.890	1.853	1.723
168		28.82	15.28	13.54	-0.259	1.196	1.112
176		28.62	15.46	13.17	-0.636	1.554	1.445
3657		29.32	15.37	13.95	0.142	0.906	0.842
3886		28.96	15.30	13.66	-0.143	1.104	1.026
3892		28.16	15.30	12.86	-0.939	1.917	1.782
4148		28.44	16.76	11.68	-2.123	4.355	4.049
4159		30.16	15.65	14.52	0.712	0.610	0.567

		TLR4	GAPDH				
mouse	Treatment	Ct	Ct	Dct	DDct	fold change	Normalized
787		26.14	23.24	2.9	0.507	0.704	0.549
789		27.76	23.315	4.445	2.052	0.241	0.188
813		25.695	23.97	1.725	-0.668	1.589	1.240
814		26.125	24.52	1.605	-0.788	1.727	1.347
3826		25.86	24.57	1.29	-1.103	2.148	1.676
150		29.02	23.83	5.19	2.797	0.144	0.112
337		25.975	26.14	-0.165	-2.558	5.889	4.595
338		25.945	24.64	1.305	-1.088	2.126	1.659
822		27.035	24.99	2.045	-0.348	1.273	0.993
823		26.745	23.89	2.855	0.462	0.726	0.566
3747		26.08	26.03	0.05	-2.343	5.074	3.959
4045		27.135	25.07	2.065	-0.328	1.255	0.979
4135		28.805	24.505	4.3	1.907	0.267	0.208
4136		26.285	24.235	2.05	-0.343	1.268	0.990
4137		24.875	24.05	0.825	-1.568	2.965	2.313
159		27.525	23.635	3.89	1.497	0.354	0.276
161		27.205	24.325	2.88	0.487	0.714	0.557
162		26.57	24.825	1.745	-0.648	1.567	1.223
3854		27.75	23.5	4.25	1.857	0.276	0.215
3855		26.47	24.085	2.385	-0.008	1.006	0.785
3878		26.81	24.39	2.42	0.022	0.985	0.768
4042		31.66	25.12	6.54	4.147	0.056	0.044
4043		27.09	25.35	1.75	-0.648	1.567	1.223

4054	[redacted]	25.69	24.06	1.63	-0.763	1.697	1.324
160		26.85	24.19	2.66	0.262	0.834	0.651
168		26.57	24.25	2.32	-0.073	1.052	0.821
176		26.05	24.09	1.96	-0.433	1.350	1.053
3657		27.67	23.51	4.16	1.762	0.295	0.230
3892		26.46	23.84	2.62	0.227	0.854	0.667
4148		25.91	25.40	0.51	-1.883	3.688	2.878
4159		28.08	24.16	3.92	1.527	0.347	0.271

APPENDIX D

PERMISSION TO REPRINT

CHAPTER 3

RightsLink

Copyright Clearance Center

Thank You For Your Order!

Dear Ms. Kimbell Hetzler,

Thank you for placing your order through Copyright Clearance Center's RightsLink service. Elsevier has partnered with RightsLink to license its content. This notice is a confirmation that your order was successful.

Your order details and publisher terms and conditions are available by clicking the link below:
http://s100.copyright.com/CustomerAdmin/PLF.jsp?ref=1d1fbdf0-66f5-43fd-a510-9c745aa82233

Order Details
Licensee: Kimbell L Hetzler
License Date: Jun 19, 2015
License Number: 3652680800365
Publication: Biochimica et Biophysica Acta (BBA) - Molecular Basis of Disease
Title: Sex differences in the relationship of IL-6 signaling to cancer cachexia progression
Type Of Use: reuse in a thesis/dissertation
Total: 0.00 USD

To access your account, please visit https://myaccount.copyright.com.

Please note: Online payments are charged immediately after order confirmation; invoices are issued daily and are payable immediately upon receipt.

To ensure that we are continuously improving our services, please take a moment to complete our customer satisfaction survey.

B.1:v4.2

ELSEVIER LICENSE
TERMS AND CONDITIONS

Oct 21, 2015

This is a License Agreement between Kimbell L Hetzler ("You") and Elsevier ("Elsevier") provided by Copyright Clearance Center ("CCC"). The license consists of your order details, the terms and conditions provided by Elsevier, and the payment terms and conditions.

All payments must be made in full to CCC. For payment instructions, please see information listed at the bottom of this form.

Supplier	Elsevier Limited The Boulevard,Langford Lane Kidlington,Oxford,OX5 1GB,UK
Registered Company Number	1982084
Customer name	Kimbell L Hetzler
Customer address	921 Assembly Street COLUMBIA, SC 29208
License number	3652680800365
License date	Jun 19, 2015
Licensed content publisher	Elsevier
Licensed content publication	Biochimica et Biophysica Acta (BBA) - Molecular Basis of Disease
Licensed content title	Sex differences in the relationship of IL-6 signaling to cancer cachexia progression
Licensed content author	Kimbell L. Hetzler,Justin P. Hardee,Melissa J. Puppa,Aditi A. Narsale,Shuichi Sato,J. Mark Davis,James A. Carson
Licensed content date	May 2015
Licensed content volume number	1852
Licensed content issue number	5
Number of pages	10
Start Page	816
End Page	825
Type of Use	reuse in a thesis/dissertation

Portion	full article
Format	electronic
Are you the author of this Elsevier article?	Yes
Will you be translating?	No
Title of your thesis/dissertation	The Role of Ovarian Function on cancer cachexia progression in the female Apc Min/+ mouse
Expected completion date	Oct 2015
Estimated size (number of pages)	300
Elsevier VAT number	GB 494 6272 12
Permissions price	0.00 USD
VAT/Local Sales Tax	0.00 USD / 0.00 GBP
Total	0.00 USD